Contribution of the endothelial protein CLEC14A to the pathogenesis of liver disease and liver cancer

by

Joanne Marie O'Rourke

A thesis submitted to the University of Birmingham for the degree of DOCTOR OF PHILOSOPHY

School of Immunology and Immunotherapy,

College of Medicine and Dentistry

University of Birmingham

2024

UNIVERSITY OF
BIRMINGHAM

University of Birmingham Research Archive

e-theses repository

This unpublished thesis/dissertation is copyright of the author and/or third parties. The intellectual property rights of the author or third parties in respect of this work are as defined by The Copyright Designs and Patents Act 1988 or as modified by any successor legislation.

Any use made of information contained in this thesis/dissertation must be in accordance with that legislation and must be properly acknowledged. Further distribution or reproduction in any format is prohibited without the permission of the copyright holder.

Abstract

The endothelium is a crucial component of the liver microenvironment. Hepatic sinusoidal endothelial cells (HSEC) that line the liver sinusoids form a unique specialised microvasculature. I investigated the expression of CLEC14A in the human liver and described how it is upregulated on sinusoidal endothelium in hepatocellular carcinoma (HCC). It can also be found on larger vessels supplying HCC and in bridging fibrosis in chronic liver disease. Flow-based adhesion assays with HSEC revealed that CLEC14A mediates the adhesion of neutrophils and in vitro angiogenesis studies revealed that CLEC14A promotes the migration and tube formation of HSEC.

I have evaluated CLEC14A as a serum biomarker in HCC, however, the detection of CLEC14A in the serum of cirrhotic non-HCC patients limits its value as a HCC surveillance tool in this cohort. I have shown that low shear stress upregulates CLEC14A on HSEC and CLEC14A is also upregulated by hypoxia and these conditions have the opposite effect on Multimerin 2, a ligand of CLEC14A. I have also narrowed down the region of Multimerin 2 where it interacts with CD248 showing that it is at a distinctly different site from where VEGF binds MMRN2.

I have presented digital spatial profiling data that support a role for CLEC14A in HCC tumour angiogenesis and suggest it may also influence the recruitment of natural killer cells. In addition, high CLEC14A expression is associated with poor tumour differentiation and vascular invasion. This work has indicated that CLEC14A is a novel target in pathological angiogenesis in liver disease and HCC, and also contributes to the immune microenvironment in liver disease.

Dedication

Dedicated to the memory of Rita O'Rourke, an exemplar of kind-heartedness, graciousness and fortitude.

Acknowledgements

I would like to thank Professor Shishir Shetty and Professor Roy Bicknell for the opportunity to work in their laboratories and for their guidance and patience during my fellowship.

I have been very fortunate to work alongside Dr Victoria Heath and thank her for her unwavering kindness and encouragement in the Bicknell laboratory. I am also grateful to Dr Marco Rink for introducing me to molecular cloning, Dr Margaret Goodall for guiding me through monoclonal antibody production, Dr Jamie Webster from the protein expression facility for sharing his invaluable knowledge and experience with protein production; and consultant histopathologist Dr Owen Cain for an extremely useful review of immunohistochemistry.

I am also very grateful to Dr Gary Reynolds, Brian Bempong, Dr Zsuzanna Nagy, Dr Kelly Hunter, Joe Flint, Dr Georgiana Neag, Dr Daniel Patten, Dr Alex Wilkinson and Janine Youster, for their instrumental technical support during this project.

This fellowship was made possible by support from CRUK and the Wellcome Trust translational development fund. I am also very appreciative to the patients and staff from the Birmingham Liver Unit at the Queen Elizabeth Hospital for tissue and serum samples.

Finally, I would like to thank my amazing family, friends, hepatology and gastroenterology colleagues for their never-ending support throughout my career.

Table of Contents

1 INTRODUCTION 1

1.1 BACKGROUND 1

1.2 HUMAN LIVER 2

1.2.1 Liver architecture 2
1.2.2 Liver cell populations 3
1.2.3 Liver vasculature 7
1.2.4 Liver function 7

1.3 LIVER DISEASE 10

1.3.1 Acute liver disease 10
1.3.2 Chronic liver diseases 11
1.3.3 Development of hepatocellular carcinoma 12

1.4 THE LIVER'S IMMUNE ENVIRONMENT 21

1.4.1 Liver resident leucocytes 24
1.4.2 The immune microenvironment in acute liver disease 37
1.4.3 The immune microenvironment in chronic liver disease and the development of fibrosis 38
1.4.4 The immune microenvironment in hepatocellular carcinoma 42

1.5 ANGIOGENESIS 52

1.5.1 Normal angiogenesis 52
1.5.2 Angiogenesis in liver disease 54
1.5.3 Tumour angiogenesis 56

1.6 LEUCOCYTE RECRUITMENT 60

1.6.1 Classical leucocyte adhesion cascade 61
1.6.2 Recruitment via liver sinusoidal cells 66
1.6.3 Leucocyte recruitment in HCC 68

1.7 TUMOUR ENDOTHELIAL MARKERS 69

1.7.1 Tumour endothelial markers in hepatocellular carcinoma 69
1.7.2 Targeting the tumour vasculature 70

1.8 C-TYPE LECTIN DOMAIN GROUP 14 FAMILY 70

1.8.1 CLEC14A and interaction with MMRN2 70
1.8.2 CD93 73
1.8.3 CD248 74
1.8.4 Thrombomodulin 74

1.9 HYPOTHESIS AND AIMS 75

2 MATERIALS AND METHODS 76

2.1 HUMAN LIVER TISSUE AND SERUM 76

2.2 COMMONLY USED SOLUTIONS 76

2.3 PRIMARY ANTIBODIES 77

2.4 SECONDARY ANTIBODIES 78
2.5 RECOMBINANT PROTEINS 78
2.6 MOLECULAR BIOLOGY 79
2.6.1 Oligonucleotides 79
2.6.2 Plasmids 80
2.6.3 Cloning methods 81
2.6.4 Gibson cloning into pcDNA3 Fc plasmid 83
2.7 CELL CULTURE 83
2.7.1 HEK293T 83
2.7.2 Isolation and cell culture of liver sinusoidal endothelial cells 84
2.7.3 Stimulation of primary LSEC cultures 85
2.7.4 General cell culture, passaging and storage 85
2.7.5 SiRNA transfections 85
2.7.6 Plasmid transfections 86
2.8 BIOCHEMISTRY 87
2.8.1 Cell lysis, SDS-PAGE, western blotting 87
2.8.2 Far western blotting 88
2.9 PROTEIN EXPRESSION AND PURIFICATION 88
2.10 CELL AND TISSUE STAINING 89
2.10.1 Immunohistochemical staining of paraffin tissue 89
2.10.2 Immunofluorescent staining of paraffin 90
2.10.3 Immunofluorescent staining of cells 90
2.11 SERUM SAMPLE COLLECTION 90
2.12 QUANTITATIVE PCR 91
2.13 HSEC EXPOSURE TO HYPOXIA 91
2.14 ANGIOGENESIS ASSAYS 91
2.14.1 Matrigel assay 91
2.15 ENDOTHELIAL CELL MIGRATION ASSAY 92
2.16 ISOLATION OF HUMAN NEUTROPHILS 92
2.17 FLOW CYTOMETRY 92
2.17.1 Neutrophil static adhesion assays. 93
2.17.2 Neutrophil flow assays. 93
2.18 MONOCLONAL ANTIBODY GENERATION 95
2.18.1 Screening Rat test bleeds for antibody production. 96
2.18.2 Haemagglutination assay for supernatants of clones 96
2.18.3 Isotype determination 97
2.19 CLEC14A ELISA 97
2.20 DIGITAL SPATIAL PROFILING 98
2.21 STATISTICAL ANALYSIS 98

2.22 ILLUSTRATIONS 99

3 THE EXPRESSION OF CLEC14A AND MMRN2 IN HUMAN HEPATIC TISSUE 100

3.1 INTRODUCTION 100

3.1.1 Cancer genome atlas interrogation for CLEC14A, CD93, MMRN2 expression in hepatocellular carcinoma and association with clinical outcomes 101

3.2 THE EXPRESSION OF CLEC14A, IN NORMAL AND DISEASED LIVER TISSUE BY IMMUNOHISTOCHEMISTRY 103

3.2.1 CLEC14A in normal liver 105
3.2.2 CLEC14A in chronic liver disease 107
3.2.3 CLEC14A in hepatocellular carcinoma 111

3.3 CLEC14A EXPRESSION IN HSEC 122

3.3.1 Dual staining of CLEC14A with endothelial cell markers 122
3.3.2 Protein quantification of CLEC14A in HSEC 124

3.4 MULTIMERIN 2 AND CD248 EXPRESSION 127

3.5 CD248 BINDING TO MMRN2 131

3.6 SUMMARY OF EXPRESSION STUDIES 134

4 EVALUATION OF CLEC14A AS A POTENTIAL SERUM BIOMARKER 137

4.1 INTRODUCTION AND AIMS. 137

4.2 RESULTS 139

4.2.1 Serum CLEC14A and AFP for each HCC Barcelona Stage 139
4.2.2 Serum CLEC14A and AFP in fibrosis, cirrhosis and HCC 142
4.2.3 Tumour characteristics and serum CLEC14A and AFP. 146
4.2.4 Correlation of laboratory values to CLEC14A for all cohorts of patients 148
4.2.5 Detectable serum CLEC14A HCC and effect on recurrence and transplant-free survival 149
4.2.6 CLEC14A serum values and expression in HCC tissue 151

4.3 CLEC14A RNA EXPRESSION IN DIFFERENT TUMOUR TYPES 153

4.4 DISCUSSION 155

5 CHAPTER 5: THE REGULATION OF CLEC14A AND MMRN2 IN LIVER SINUSOIDAL ENDOTHELIAL CELLS 159

5.1 RESPONSE TO CYTOKINE STIMULATION 160

5.2 RESPONSE TO HYPOXIA 164

5.3 RESPONSE TO SHEAR STRESS 166

5.4 DISCUSSION 170

6 INVESTIGATING THE FUNCTIONAL ROLE OF CLEC14A IN HSEC 172

6.1 SI RNA KNOCKDOWN OF CLEC14A 174

6.2 ANGIOGENESIS ASSAYS 174

6.2.1 Endothelial cell migration 174
6.2.2 HSEC tubule formation in Matrigel 177

6.3 LEUCOCYTE ADHESION ASSAYS 181

6.4 NEUTROPHIL ADHESION IN THE STATIC CONDITION FOLLOWING PRECONDITIONING WITH FLOW 182

6.4.1 Recombinant CLEC14A binding to neutrophils 191
6.4.2 The effect of CD93 and MMRN2 knock down on CLEC14A expression in HSEC. 198
6.4.3 Summary of functional studies 199

7 CHAPTER 7: GENERATION OF MONOCLONAL ANTIBODIES TO HUMAN MMRN2 495-674 204

7.1 INTRODUCTION 204

7.1.1 Screening of immune response in rat serum by ELISA 205
7.1.2 Screening of hMMRN2 positive hybridoma clones by ELISA 207

7.2 ELISA TO EVALUATE ABILITY TO BLOCK CLEC14A -MMRN2 INTERACTION 208

7.3 SUMMARY OF MONOCLONAL ANTIBODY PRODUCTION 210

8 CHAPTER 8: TRANSCRIPTOMIC DIGITAL SPATIAL PROFILING OF HIGH AND LOW CLEC14A EXPRESSING HEPATOCELLULAR CARCINOMA TISSUE 212

8.1 INTRODUCTION 212

8.2 TISSUE PREPARATION OVERVIEW 214

8.3 DATA PROCESSING 219

8.4 STATISTICAL ANALYSIS 225

8.5 RESULTS 225

8.5.1 Exploration of the data 225
8.5.2 Differences in CLEC14A expression by region of the tumour 235
8.5.3 Correlation studies 239
8.5.4 Clinical data 255
8.5.5 Pathway analysis 261

8.6 DISCUSSION 267

8.6.1 General overview 267
8.6.2 Using DSP to learn more about CLEC14A 268

9 CHAPTER 9: DISCUSSION AND FUTURE WORK 273

9.1 OVERVIEW 273

9.2 SUMMARY OF MAIN FINDINGS 275

9.3 LIMITATIONS OF STUDIES 280

9.4 TRANSLATIONAL ASPECTS OF THE WORK 280

10 APPENDICES 282

10.1 APPENDIX 1. DATA FROM VOLCANO PLOTS SHOWING DIFFERENTIAL GENE EXPRESSION BETWEEN TUMOUR, NON-TUMOUR AND PERI-TUMOUR REGIONS. 282

10.2 APPENDIX 2. DATA FROM VOLCANO PLOT SHOWING DIFFERENTIAL GENE EXPRESSION FOR CLEC14A HIGH VS CLEC14A LOW EXPRESSING CASES. 297

11 REFERENCES..... 300

List of Tables

Table 1. The Eastern Cooperative Oncology Group (ECOG) Scale. 18
Table 2. A selection of international HCC surveillance strategies. Guidelines from the UK, Europe and America and a summary of their main recommendations for surveillance for HCC. 20
Table 3. Innate lymphocytes in the healthy adult liver. Table summarising the main groups of innate lymphocytes in the liver, their effector molecules and proposed roles in liver disease. 30
Table 4. T-cell subsets and their associated function. 34
Table 5. Chemokines and their receptors relevant to liver pathology. 39
Table 6. Immune cell populations found in HCC. 43
Table 7. Anti-angiogenic therapy for HCC. 60
Table 8. Commonly used solutions. 77
Table 9. Primary antibodies.. 78
Table 10. Secondary antibodies.. 78
Table 11. Recombinant proteins used during the project. 79
Table 12. List of oligonucleotides used for sequencing reactions. Oligonucleotide sequences are displayed 5' to 3'. 79
Table 13. Construction of plasmids from PCR products. 80
Table 14. Restriction digest components. 81
Table 15. Reagent quantities for plasmid transfections. 86
Table 16. Summary of patient demographics, laboratory tests and tumour markers. 118
Table 17. Summary of Clinicopathological Characteristics. 119
Table 18. Summary of patient demographics, laboratory tests and tumour markers. 144
Table 19. CLEC14A and AFP values based on tumour characteristics. 147
Table 20. Correlation between laboratory values and CLEC14A for the whole patient cohort. 148
Table 21. Correlation values for genes associated with angiogenesis in tumour areas. ..243
Table 22. Correlation values for genes associated with angiogenesis in non-tumour areas. 245
Table 23. Correlation values for genes associated with angiogenesis in peri-tumour areas. 246
Table 24. Genes associated with a neutrophil degranulation signature and correlation with CLEC14A expression in tumour regions. 249
Table 25. Cell abundance scores correlated with CLEC14A normalised counts in tumour tissue. 251
Table 26. Cell abundance scores correlated with CLEC14A normalised counts in non-tumour tissue. 252
Table 27. Cell abundance scores correlated with CD31 normalised counts in tumour tissue. 253
Table 28. Cell abundance scores correlated with CD34 normalised counts in tumour tissue. 254
Table 29. Summary of patient demographics, laboratory results and tumour characteristics for CLEC14A high expression and CLEC14A low expression. 256
Table 30. Correlations between laboratory values and CLEC14A normalised counts. ..257
Table 31. Size and number of HCC tumours and correlation with CLEC14A expression. 257
Table 32. Gene enrichment analysis using g:profiler. 264

List of Figures

Figure 1. Schematic representation of the structure of the hepatic lobule.. 3
Figure 2. Human Liver Cell Populations.....6
Figure 3. The main cells of the tumour microenvironment......14
Figure 4. Summary of systemic treatments for HCC and mechanism of action. 15
Figure 5. BCLC staging, treatment recommendations and prognosis.....16
Figure 6. Immune Cells of the Liver. 23
Figure 7. Main mechanisms for CTLA4 and PD1 inhibiting T cell responses. 50
Figure 8. Chemokines in HCC.....52
Figure 9. Angiogenesis.....54
Figure 10. The leucocyte adhesion cascade. 62
Figure 11. CLEC14A-MMRN2-CD248 interaction.. 72
Figure 12. Neutrophil flow assay set-up.....94
Figure 13. TCGA data for CLEC14A, MMRN2, CD93 and CD248 expression and relationship to overall survival. 102
Figure 14. Structures found in a normal liver.....105
Figure 15. Second example: Expression of CLEC14A in normal human liver. 106
Figure 16. Expression of CLEC14A in autoimmune hepatitis 107
Figure 17. Expression of CLEC14A in A) Alcoholic liver disease, B) Non-alcoholic fatty liver disease 108
Figure 18. Expression of CLEC14A in Primary biliary cholangitis. 109
Figure 19. Expression of CLEC14A in Primary biliary cholangitis. 110
Figure 20. Expression of CLEC14A in a case of HCC with patchy CLEC14A sinusoidal positivity. 111
Figure 21. Expression of CLEC14A in a case of HCC with diffuse sinusoidal staining. 112
Figure 22. Expression of CLEC14A in hepatocellular carcinoma and adjacent non-tumour cirrhotic tissue.....113
Figure 23. Chronic liver disease tissue cases and CLEC14A expression. 115
Figure 24. HCC tumour tissue and adjacent non-tumour CLEC14A expression. 116
Figure 25. Tumour CLEC14A expression and tumour characteristics.....120
Figure 26. Probability of survival/recurrence based on tissue CLEC14A protein expression. 121
Figure 27. CLEC14A expression on cultured HSEC.....123
Figure 28. HSEC isolated from HCC tissue and non-tumour tissue. 124
Figure 29. Western blot of HSEC lysate probed for CLEC14A. 125
Figure 30. Western blot of HSEC lysates probed for CLEC14A. 126
Figure 31. Western blot demonstrating CLEC14A binds MMRN2 in HSEC.....127
Figure 32. Multimerin 2 tissue expression in HCC and chronic liver disease. 128
Figure 33. CD248 expression in a fibrotic human liver.....129
Figure 34. Co-localisation of CLEC14A, MMRN2 and CD248 in tumours.....130
Figure 35. Western blot demonstrating that recombinant CD248 binds MMRN2. 132
Figure 36. CLEC14A serum values according to Barcelona tumour staging. 140
Figure 37. AFP serum values with tumour stage. 141
Figure 38. A dot plot of individual CLEC14A values in the fibrosis, cirrhosis and HCC cohorts.....145
Figure 39. Kaplan Meier curves for recurrence and transplant free survival by serum AFP or serum CLEC14A level. 150
Figure 40. HCC cases with matched CLEC14A serum values and tissue CLEC14A immunohistochemistry. 152

Figure 41. CLEC14A RNA expression in different tumour types. 154
Figure 42. CLEC14A mRNA expression in HSEC in response to inflammatory stimuli. 161
Figure 43. CLEC14A mRNA expression in HSEC in response to cytokine stimulation. 162
Figure 44. CLEC14A mRNA expression in HSEC in response to growth factors. 163
Figure 45. CLEC14A, MMRN2 and CD93 expression in response to hypoxia. 165
Figure 46. CLEC14A, MMRN2 and CD93 expression in response to shear stress. 168
Figure 47. The effect of delayed tissue fixation on CLEC14A expression in liver tissue. 169
Figure 48. Reactome pathways associated with the top 1000 genes that correlate positively with CLEC14A in liver tissue. 173
Figure 49. CLEC14A knockdown in HSEC. 174
Figure 50. Representative images for the wound scratch assay. 175
Figure 51. Wound scratch assay % closure following CLEC14A knockdown. 176
Figure 52. Example of HSEC matrigel tubule formation assay. 177
Figure 53. Matrigel tubule formation assay CLEC14A KD vs control representative images. 179
Figure 54. Matrigel tubule formation assay, number of tubules at 6, 12, 18 and 24 hours. 180
Figure 55. Adhesion and transmigration of neutrophils under static conditions following preconditioning of HSEC with either low or high shear stress. 183
Figure 56. siRNA knockdown of CLEC14A and neutrophil adhesion under static conditions. 184
Figure 57. siRNA knockdown of CLEC14A and neutrophil adhesion under flow. 186
Figure 58. Neutrophil flow assays with HSEC in the presence of CLEC14A monoclonal antibodies CRT1, CRT2, CRT3. 187
Figure 59. Neutrophil flow assays with HSEC in the presence of CLEC14A monoclonal antibodies CRT4 and CRT5. 188
Figure 60. HSEC incubation with monoclonal antibodies CRT1-5. 189
Figure 61. Recombinant CLEC14A interacting with neutrophils. 192
Figure 62. HCC case with high neutrophil infiltration. 194
Figure 63. HCC case example with just a couple of areas of neutrophil infiltration. 195
Figure 64. 4 HCC cases with minimal neutrophil infiltrate. 196
Figure 65. Immunofluorescence images of CLEC14A and neutrophil elastase. 197
Figure 66. PBMCs express MMRN2. 198
Figure 67. The effect of knock down of CD93 and MMRN2 on CLEC14A expression. 199
Figure 68. MMRN2 495-674-Fc antigen used for immunisation. 205
Figure 69. Test bleeds from immunised rats immunised with hMMRN2 495-674-Fc. 206
Figure 70. Elisa to test supernatant from clone 305 for antibody response to antigen coated plates. 207
Figure 71. Testing monoclonal antibodies for the ability to block the CLEC14A -MMRN2 interaction. 209
Figure 72. The region of MMRN2 that binds CLEC14A (530-624) contains many highly conserved regions. 210
Figure 73. Summary of the main processes for the DSP experiment. 217
Figure 74. Examples of selection of regions of interest for DSP. 218
Figure 75. Line plot showing sequencing metrics. 220
Figure 76. Line plots showing 2 ROIs where sequencing likely failed. 222
Figure 77. Example box plots for a gene count pre and post-normalisation. 224
Figure 78. PCA plot for the whole cohort. 227

Figure 79. PCA plots for individual cases.....228
Figure 80. Volcano plots showing differential gene expression between tumour, non-tumour and peri-tumour regions.....229
Figure 81. Exploration of DSP data looking at immune markers.....230
Figure 82. Exploration of the data looking at immune markers and vascular invasion.231
Figure 83. Box plots showing CLEC14A gene expression in 2 cohorts: CLEC14A low expressing tumours and CLEC14A high expressing tumours based on protein staining by immunohistochemistry. 233
Figure 84. CLEC14A expression A) across whole cohort, B) CLEC14A high only cases. 234
Figure 85. CLEC14A expression in peripheral and central regions of tumours. 236
Figure 86. The most central and peripheral CLEC14A counts for each tumour. 237
Figure 87. Profiling CLEC14A expression across a tumour.....238
Figure 88. Correlation graphs for CLEC14A vs CD34, PECAM1, CD4 and CD8.....241
Figure 89. Correlation matrix for genes associated with angiogenesis in tumour areas. 242
Figure 90. Correlation matrix for genes associated with angiogenesis in non-tumour areas. 244
Figure 91. CLEC14A expression in tumours vs tumour differentiation.....259
Figure 92. CLEC14A expression in tumours vs vascular invasion.....260
Figure 93. Volcano plot showing differential gene expression for CLEC14A high vs CLEC14A low expressing cases.....262
Figure 94. Biological systems over-represented in CLEC14A high tumours. 265
Figure 95. Voronoi pathway visualisation.....266

List of abbreviations used

AA Amino acids

AIH Autoimmune hepatitis

ALD Alcoholic liver disease

Ang Angiopoietins

APCs Antigen Presenting Cells

BCLC Barcelona Clinic Liver Cancer

bFGF Basic Fibroblast Growth Factor

bFGFR Basic Fibroblast Growth Factor Receptor

BSA Bovine serum albumin

cNK cells Conventional Natural Killer Cells

CTLDs C-type lectin-like domains

DAMP Damage Associated Molecular Patterns

DCs Dendritic Cells

ECL Enhanced Chemi-Luminescence

ECM Extracellular Matrix

ECOG Eastern Cooperative Oncology Group

ELISA Enzyme-linked immunosorbent assay

EMT Epithelial-Mesenchymal Transition

FAP Fibroblast associated protein

FC Flow Cytometry

FCS Fetal calf serum

FGF Fibroblast growth factor

G-MDSCs Granulocytic Myeloid-Derived Suppressor Cells

HA Hyaluronan

HAT Hyoxanthine-aminopterin-thymidine

HBV Hepatitis B virus

HCC Hepatocellular Carcinoma

HCV Hepatitis C virus

HDL High-Density Lipoprotein

HEK Human embryonic kidney

HFE Gene linked to haemochromatosis

HGF Hepatocyte growth factor

HIFs Hypoxia-Inducible Factors

HIF-1α Hypoxia-inducible factor-1α

HSCs Hepatic Stellate Cells

HSEC Human sinusoidal endothelial cells

HUVEC Human umbilical vein endothelial cells

ICAM-1 Intercellular adhesion molecule-1

IF Immunofluorescence

IHC Immunohistochemistry

ILCs Innate Lymphoid Cells

iNKT Invariant Natural Killer T

IP Immunoprecipitation

LDL Low-Density Lipoprotein

LFA-1 Lymphocyte function-associated antigen-1

LTi Lymphoid tissue-inducer

MAC-1 Macrophage-1 antigen

MADCAM-1 Mucosal vascular adhesion cell adhesion molecule-1

MAIT Mucosal-Associated Invariant T cells

MAMP Microbial Associated Molecular Patterns

MCP-1 Monocyte Chemoattractant Protein 1

MDSC Myeloid Derived Suppressor Cells

MHC Major Histocompatibility Complex

MMRN2 Multimerin-2

NAFLD Non-Alcoholic Fatty Liver Disease

NASH Non-alcoholic steatohepatitis

NCPH Non-cirrhotic portal hypertension

NF-κB Nuclear Factor Kappa-Light-Chain-Enhancer of Activated B Cell

NK Natural Killer

NKT Natural Killer T cell

NL Normal liver

NO Nitric oxide

NT Nucleotide

PBC Primary biliary cholangitis

PBMCs Peripheral blood mononuclear cells

PBS Phosphate buffered saline

PDGF Platelet Derived Growth Factor

PEI Polyethylenimine

PRR Pattern Recognition Receptors

PSGL-1 P-selectin glycoprotein ligand-1

qPCR Quantitative Polymerase Chain Reaction

RES Reticuloendothelial System

RHBDL2 Rhomboid-Like Protein 2

RIN RNA Integrity Number

ROS Reactive Oxygen Species

RTC Rat tail collagen

SABR Stereotactic Ablative Radiotherapy

SDS-PAGE Sodium Dodecyl Sulphate Polyacrylamide Gel

TACE Transarterial Chemoembolisation

TAM Tumour-associated macrophages

Tc Cytotoxic T cells

TCGA The Cancer Genome Atlas

TILs Tumour Infiltrating Lymphocytes (TILS)

TLRs Toll-like receptors

Treg Regulatory T cell

TSLP Thymic Stromal Lymphopoietin

VCAM-1 Vascular Cell Adhesion Molecule-1

VEGF Vascular Endothelial Growth Factor

VEGFR2 VEGF-A receptor

WB Western blot

1

1 Introduction

1.1 Background

The role of the vasculature in pathological angiogenesis and in the modulation of the immune microenvironment in the human liver is explored in this thesis. There is a focus on CLEC14A, a member of the C-type lectin domain (CTLD) group 14 family. In this chapter, I discuss the structure of the human liver and the distinct microenvironments encountered in different disease states. The burden of chronic liver disease continues to increase worldwide, and we have seen an increased incidence of HCC which is associated with significant morbidity and mortality. I explore the dysregulation of angiogenesis in chronic liver disease and HCC and our current understanding of the mechanisms of leucocyte recruitment. I then provide an overview of known tumour markers in hepatocellular carcinoma and finish with a review of the CTLD group 14 family.

1.2 Human liver

1.2.1 Liver architecture

The liver is located in the right upper quadrant of the abdomen and is the largest solid organ in the human body. Traditionally we think of the liver as having four lobes: the left and right main lobes and the smaller caudate and quadrate lobes. It can be macroscopically subdivided into segments based on blood supply. Histologically it has functional units called lobules, first identified in 1665 by Weppler (Malarkey et al., 2005). Lobules consist of a central vein (branch of the hepatic vein) in the centre surrounded by 4-6 portal areas, and they have a hexagonal shape **Figure 1**.

Within a lobule, hepatocytes are arranged in lines, and between these lie a thin fenestrated endothelium called a sinusoid. At the corners of the hexagon, you find a portal vein branch, a hepatic artery branch and a bile duct branch; this triad is also referred to as the portal triad. Blood flows from branches of the hepatic artery and portal vein across the lobule and drains via the central vein (Moro-Sibilot et al., 2016), draining into the inferior vena cava.

Within the liver, the alternative organisation of hepatocytes defines zones 1-3. These zones are classified according to oxygen supply. Zone 1 encircles the portal triad, where oxygenated blood from the hepatic artery branches enters. Zone 3 is found centrally, and here oxygenation is lower. Zone 2 is located between zones 1 and 3.

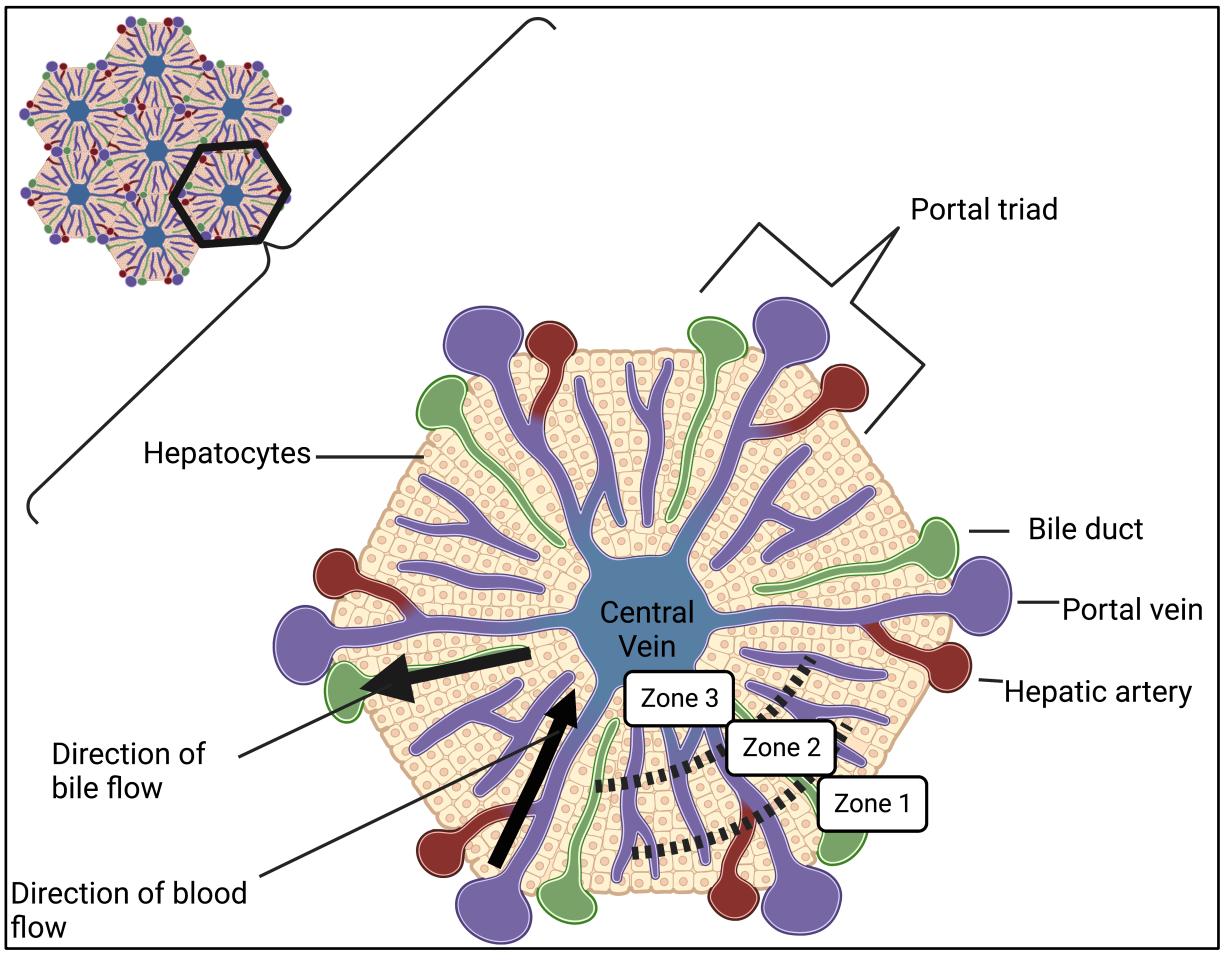


Figure 1. Schematic representation of the structure of the hepatic lobule. The outer zone receives blood with more oxygen than the tissue in the inner zone.

1.2.2 Liver cell populations

The main cell types that make up the liver, parenchymal and non-parenchymal cells, are shown in **Figure 2**. Hepatocytes, the primary liver cells, compose about 60% of the liver and are capable of producing acute-phase proteins, expressing

innate immune receptors and presenting antigens. (Jenne and Kubes, 2013). Hepatocytes, therefore, have a pivotal role in maintaining immunotolerance. Hepatocyte surfaces face the sinusoid and space of Disse, the canaliculus or a neighbouring hepatocyte.

The sinusoids consist of endothelial cells, hepatic stellate cells, Kupffer cells, and Natural Killer (NK) cells (50% of hepatic NK cells reside within the sinusoids) and form a functional unit. Sinusoids are lined by endothelium which is different from other vessels because it does not have a regular basement membrane. Sinusoidal endothelial cells have small pores called fenestrae and act like a filter between the sinusoid and the space of Disse; they are capable of endocytosis and have many receptors. The fenestrae facilitate the diffusion of macromolecules from flowing blood to the hepatocytes. On the blood-flowing side of sinusoids are Kupffer cells and NK cells. Kupffer cells are macrophages and there are more in periportal areas (Kolios et al., 2006). Hepatic NK cells are lymphocytes attached to the sinusoidal surface and are capable of cytotoxicity against tumour and virus-infected hepatocytes (Wisse et al., 1997).

Hepatic stellate cells lie within the space of Disse and make contact with parenchymal cells and several sinusoids via their cytoplasmic projections. Hepatic stellate cells store vitamin A and when activated become collagen-producing myofibroblasts. Hepatocytes synthesise and secrete bile into bile canaliculi between adjacent hepatocytes. This intralobular canalicular network drains into canals of Hering, which connect via short bile ductules to the larger terminal bile ducts within the portal tracts. Cholangiocytes are bile duct epithelial cells that line

the extrahepatic and intrahepatic bile ducts. Cholangiocytes differ in their properties depending on which level of bile duct they arise and cilia on cholangiocytes can serve as mechano and chemosensors (Masyuk et al., 2008), and chronic liver diseases can affect specific areas of the biliary tree.

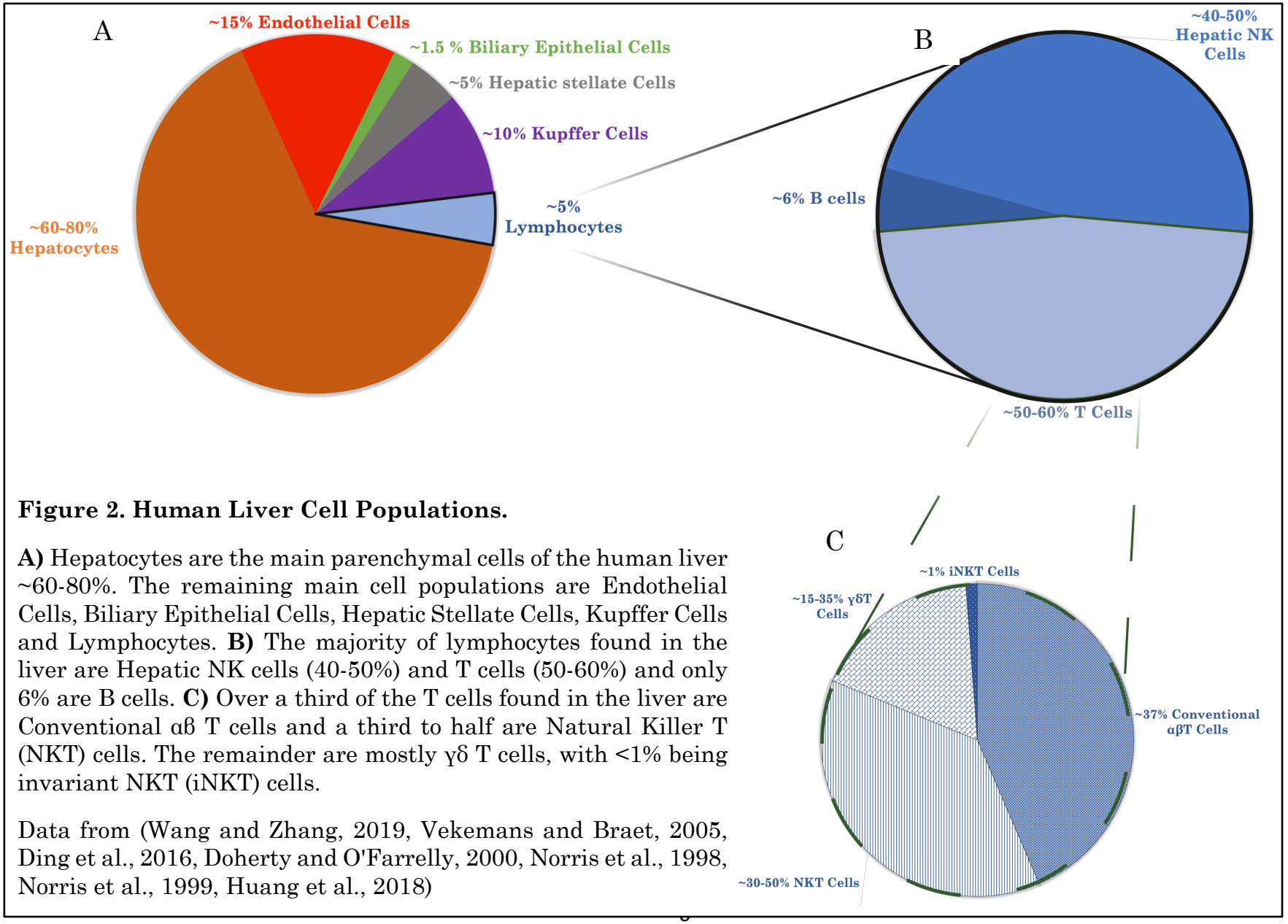


Figure 2. Human Liver Cell Populations.

A) Hepatocytes are the main parenchymal cells of the human liver ~60-80%. The remaining main cell populations are Endothelial Cells, Biliary Epithelial Cells, Hepatic Stellate Cells, Kupffer Cells and Lymphocytes. **B)** The majority of lymphocytes found in the liver are Hepatic NK cells (40-50%) and T cells (50-60%) and only 6% are B cells. **C)** Over a third of the T cells found in the liver are Conventional αß T cells and a third to half are Natural Killer T (NKT) cells. The remainder are mostly γδ T cells, with <1% being invariant NKT (iNKT) cells.

Data from (Wang and Zhang, 2019, Vekemans and Braet, 2005, Ding et al., 2016, Doherty and O'Farrelly, 2000, Norris et al., 1998, Norris et al., 1999, Huang et al., 2018)

1.2.3 Liver vasculature

The liver is a highly vascular organ that receives a quarter of our cardiac output. It has a dual blood supply; the main hepatic artery supplies just over a quarter of the inflow, and the portal vein the remainder (Abdel-Misih and Bloomston, 2010). The hepatic artery and portal vein blood supply meets in the hepatic sinusoids. Liver sinusoids have slow-flowing blood at a low pressure, which augments endothelial and immune cell interactions with flowing blood. Hepatic anatomy can be divided into eight segments based on portal bifurcations known as the Couinaud model (Skandalakis et al., 2004). Each segment has its own vascular inflow and outflow, which permits targeted therapies such as arterial embolisation or surgical resection if one of these segments is affected by cancer.

The complex flow architecture in the hepatic circulation needs to facilitate controlled blood delivery because flow pressure alterations can impact liver regeneration (Fisher et al., 1954).

1.2.4 Liver function

The liver is the largest solid organ in the human body and has many crucial functional roles. The liver receives blood from the gastrointestinal tract via the portal vein and therefore receives both macro and micronutrients from the intestines and plays a role in modifying these into usable forms or storage. The liver synthesises bile, enabling the absorption of lipids from the intestines. There is also a crucial role in glucose metabolism, immune regulation, protein and amino acid metabolism, and detoxification (Trefts et al., 2017).

1.2.4.1 Lipid metabolism

The liver is critical for lipid and lipoprotein metabolism. The liver is the most active site for cholesterol synthesis, deriving cholesterol from the intestine in chylomicron remnants. This cholesterol can enter plasma membranes and metabolic pathways or is excreted in bile; cholesterol is a precursor of bile acids and steroid hormones. Bile is, therefore, an essential route for cholesterol excretion. Lipoproteins are essential for facilitating the circulation and metabolism of lipids.

1.2.4.2 Bile acid synthesis

Bile acid synthesis occurs in the liver and is regulated by the quantity of bile acid returning to the liver via the enterohepatic circulation, negative feedback control. Bile acids are conjugated and excreted from the liver into the small intestine to facilitate fat digestion and absorption. In the terminal ileum, 95% of bile acids are reabsorbed and reach the liver via the enterohepatic circulation.

1.2.4.3 Amino acid metabolism

Amino acid metabolism is another vital function of the liver. Amino acids are derived from the diet or tissue breakdown and metabolised by many pathways. The liver plays an essential role in amino acid homeostasis, determining which are released systemically or utilised by the liver for essential compounds, for example, in gluconeogenesis (Paulusma et al., 2022). In liver failure or portal hypertension, where the liver is bypassed, converting ammonia (a product of amino acid

deamination) to urea is reduced resulting in neurological disturbances (Aldridge et al., 2015).

1.2.4.4 Production of plasma proteins

The liver produces plasma proteins, including albumin, fibrinogen, α1-antitrypsin, haptoglobin, caeruloplasmin, ferritin, transferrin and several coagulation factors. Cytokines stimulate the production of some of these from the hepatocyte and inhibit others, contributing to fluctuations in concentrations in response to inflammation. The most abundant protein produced by the liver is albumin, which is reduced in advanced chronic liver disease states (Pain et al., 1978).

1.2.4.5 Carbohydrate metabolism

As eluded to earlier, the liver is essential for carbohydrate metabolism. The liver is capable of glycogen synthesis and storage predominantly in the perivenous hepatocytes. It is also capable of glucose release and production via glycogenolysis and gluconeogenesis, initially in the periportal hepatocytes. In liver failure blood glucose can be low, and in chronic liver disease, the contribution of carbohydrates to energy production is reduced (Schneeweiss et al., 1990).

1.2.4.6 Immune Regulation

Finally, the liver has a very distinct immune regulation, and this immune microenvironment is discussed further in section 1.4. As described previously, the liver is continually exposed to nutrient-rich blood from the gastrointestinal tract

and contains bacterial degradation products. However, this does not result in organ damage from immune activation and inflammation. The immune function of the liver promotes tolerance instead of active responses to the antigens encountered locally. These functions are the result of coinhibitory receptors and immunosuppressive mediators.

1.3 Liver disease

Liver disease can be considered a spectrum of hepatic states. Liver inflammation and hepatocyte injury can be acute and fully resolve with no significant sequelae, with full restoration of the liver parenchyma and function. If the inflammation is chronic it can lead to distortion of the architecture of the liver and fibrosis ensues; in advanced cases, the fibrosis progresses to cirrhosis. In this state, you can see many changes, including increased extracellular matrix production, the formation of cirrhotic nodules, and changes to the liver vasculature, including neo-angiogenesis (Fernandez et al., 2009).

1.3.1 Acute liver disease

Acute inflammation of the hepatic parenchyma is called acute hepatitis. It is generally referred to as acute if the inflammation lasts less than six months (Schaefer and John, 2022). The most common cause is a viral infection which can be hepatotropic like Hepatitis A to E and non-hepatotropic like Epstein-Barr virus (Ryder and Beckingham, 2001). Many non-infectious insults can also cause acute liver inflammation. This includes medication (prescription, non-prescription and

herbal remedies); immunologic, for example, autoimmune hepatitis; secondary to biliary tract abnormality; pregnancy-related, for example, acute fatty liver of pregnancy; ischaemic injury, for instance, in cardiogenic shock; seronegative phenomenon and many others. The most worrisome event is when acute liver inflammation causes acute liver failure, which may necessitate a liver transplant in severe cases.

1.3.2 Chronic liver diseases

Damage to the liver can be caused by many agents, as previously discussed. When this persists, it results in chronic inflammation. This can lead to fibrosis and, finally, the architecture of the liver becoming distorted with the development of cirrhosis. The most common aetiologies of chronic liver disease and liver cirrhosis vary by region of the world and have changed over the years with advances in treatment for viral hepatitis and, conversely, a deterioration in diet and lifestyle in many Western countries. In the developed world, the most common causes are alcoholic liver disease, non-alcoholic fatty liver disease (NAFLD), chronic viral hepatitis B and C and haemochromatosis. Sadly, chronic liver disease is associated with significant morbidity and mortality, and rates appear to be rising in Western countries (Cheemerla and Balakrishnan, 2021).

As fibrosis develops, there is an element of reversibility, but as it progresses to advanced stages and the development of cirrhosis, the liver architecture remains abnormal. However, liver function can improve with the right interventions in some cases. Fibrosis is the deposition of extracellular matrix (ECM), the liver's

response to injury. In chronic liver injury, Hepatic stellate cells (HSCs) are activated into proliferative fibrogenic myofibroblasts, laying down ECM and releasing cytokines and other leucocyte-recruiting mediators. The pattern of liver fibrosis can vary by aetiology; for example, hepatotropic viruses cause portal expansion, periportal fibrosis and bridging (septal) fibrosis; in alcoholic liver disease and NAFLD, we can see fibrosis in a centrilobular perivenular distribution and sinusoidal fibrosis.

Chronic liver disease may have no or non-specific symptoms when the liver is in a 'compensated state'. The most common complications and manifestations, which sadly may be at the initial diagnosis of chronic liver disease, are portal hypertension (resistance of portal blood flow) with the development of varices (dilated veins at risk of rupture) and ascites (abnormal accumulation of fluid in the abdomen); hepatocellular insufficiency manifesting as jaundice or hepatic encephalopathy (a neuropsychiatric condition secondary to accumulation of detrimental products of metabolism) and the development of primary liver cancer in the form of hepatocellular carcinoma (HCC).

1.3.3 Development of hepatocellular carcinoma

Liver cancer is now a common cancer worldwide and a leading cause of cancer-related deaths (Bray et al., 2018). Primary liver cancer includes HCC, making up greater than 80% of cases globally (El-Serag and Rudolph, 2007). In England, over a ten-year period to 2009, HCC incidence increased from 0.63 per 100,000 to 2.48

per 100000 (Konfortion et al., 2014). Although we have surveillance programs for HCC, survival is less than 20% in this cancer (Altekruse et al., 2012).

Most HCCs develop on a background of cirrhosis, and the incidence of cirrhosis is increasing; 90% of cases occur in this setting (Sherman, 2010). It is predicted that by 2040 each year 1.4 million people may be diagnosed, an increase of 55%, and 56.4% more people than in 2020 may die from liver cancer (Rumgay et al., 2022). NAFLD is becoming a common aetiology of HCC in Western countries (Estes et al., 2018), and together with alcohol, it is a significant problem in Western populations. The risk attributable to the hepatitis C virus is decreasing thanks to the sustained virological response achieved with antiviral drugs. HBV infection accounts for over 50% of cases in Asia and Africa but only a fifth of cases in the Western world (Global Burden of Disease Liver Cancer et al., 2017). However, vaccination against hepatitis B has made some impact.

The pathophysiology of the development and progression of HCC has yet to be fully understood. Genetics, the microenvironment and the aetiology and severity of the underlying liver disease will govern the initial hepatocyte malignant transformation. Hanahan et al. described how a tumour is not just made up of proliferating tumour cells and described how multiple cell types are essential for a tumour to thrive. The collective term used to describe this is the 'tumour microenvironment' (Hanahan and Weinberg, 2011). The cross-talk between different cell types in this environment is pivotal in tumourigenesis, facilitating the critical processes of angiogenesis, invasion and metastases, evading immune destruction and generating tumour-promoting inflammation. **Figure 3** outlines

the main cells which make up the tumour microenvironment (Hanahan and Weinberg, 2011).

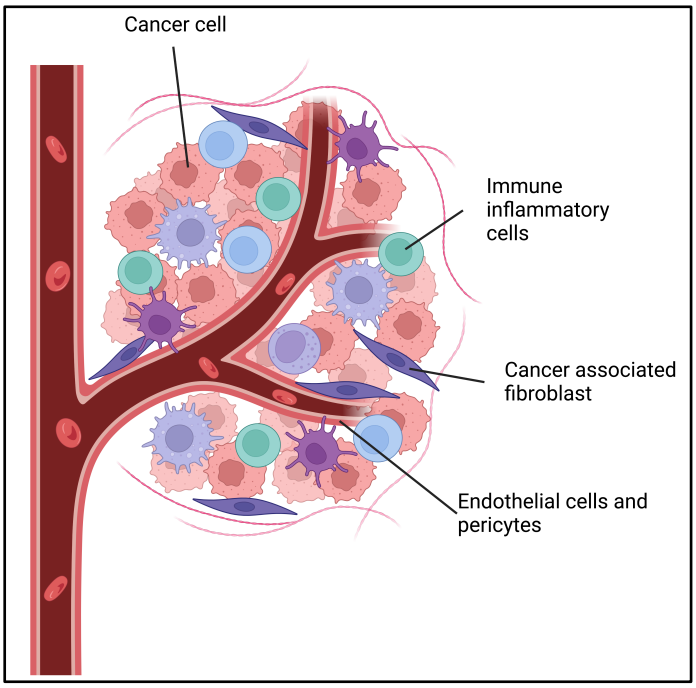


Figure 3. The main cells of the tumour microenvironment. An overview of the key cell populations found in the tumour microenvironment. Adapted from (Hanahan and Weinberg, 2011).

Hepatic resection and liver transplantation have been the mainstay of treatment for patients with HCC. With the selection of suitable patients within well-defined and restrictive criteria, the outcomes for liver transplantation are excellent, with a five-year survival of more than 70% (Mazzaferro et al., 2011). Non-surgical treatments for early-stage HCC include loco-regional therapy with radiofrequency or microwave ablation with curative potential. For intermediate-stage HCC, transarterial chemoembolisation (TACE) is commonly used and, in recent years, stereotactic ablative radiotherapy (SABR). There has been a progression in the arsenal of systemic treatments available to treat HCC. Available options include

tyrosine kinase inhibitors, immune checkpoint inhibitors and other monoclonal antibodies inhibiting angiogenesis pathways. A summary of systemic treatments and their mechanisms of action is shown in **Figure 4.** Checkpoint blockade as a single treatment modality only benefits a few patients with HCC. However, when these are combined with VEGF inhibition or tyrosine kinase inhibitors, a more inflammatory environment develops, and the response to checkpoint inhibitors escalates. It enhances Dendritic cells (DCs) and cytotoxic T cells and inhibits Tumour-associated macrophages (TAMs), Regulatory T cells (T_{regs}) and Myeloid-derived suppressor cells (MDSCs) (Llovet et al., 2021).

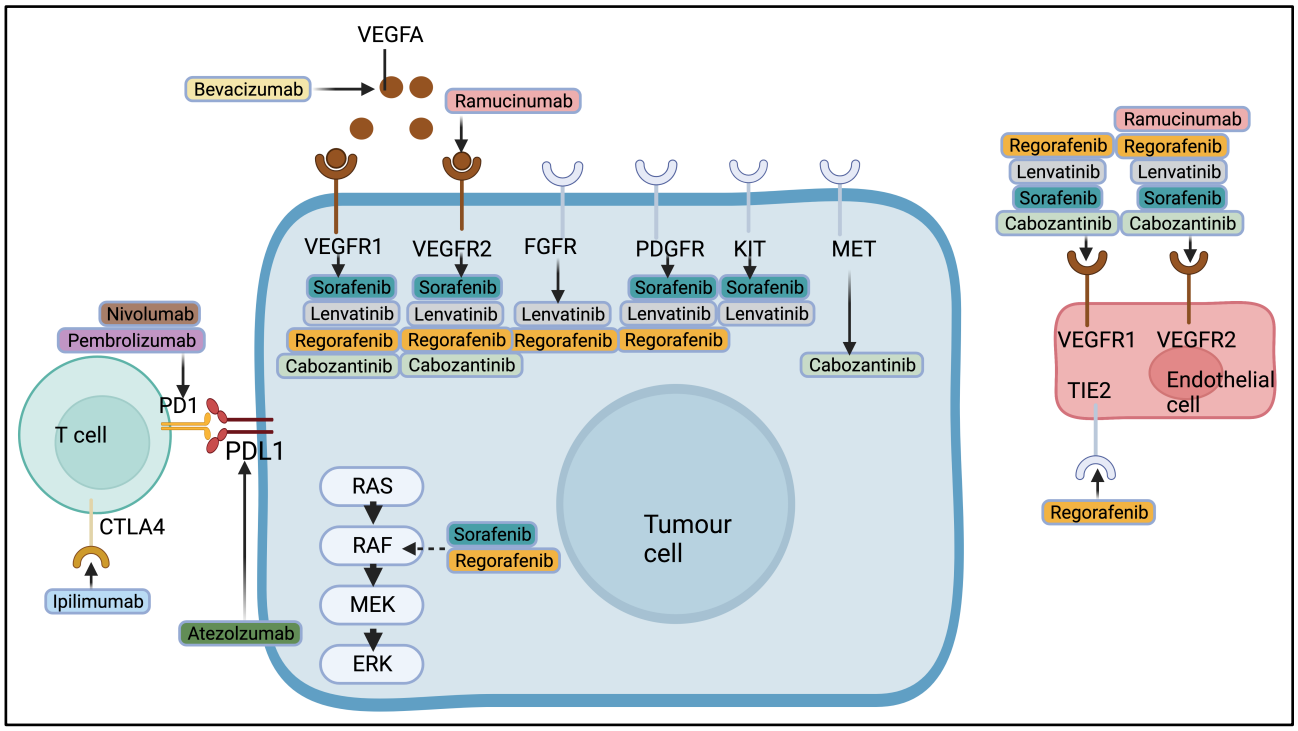
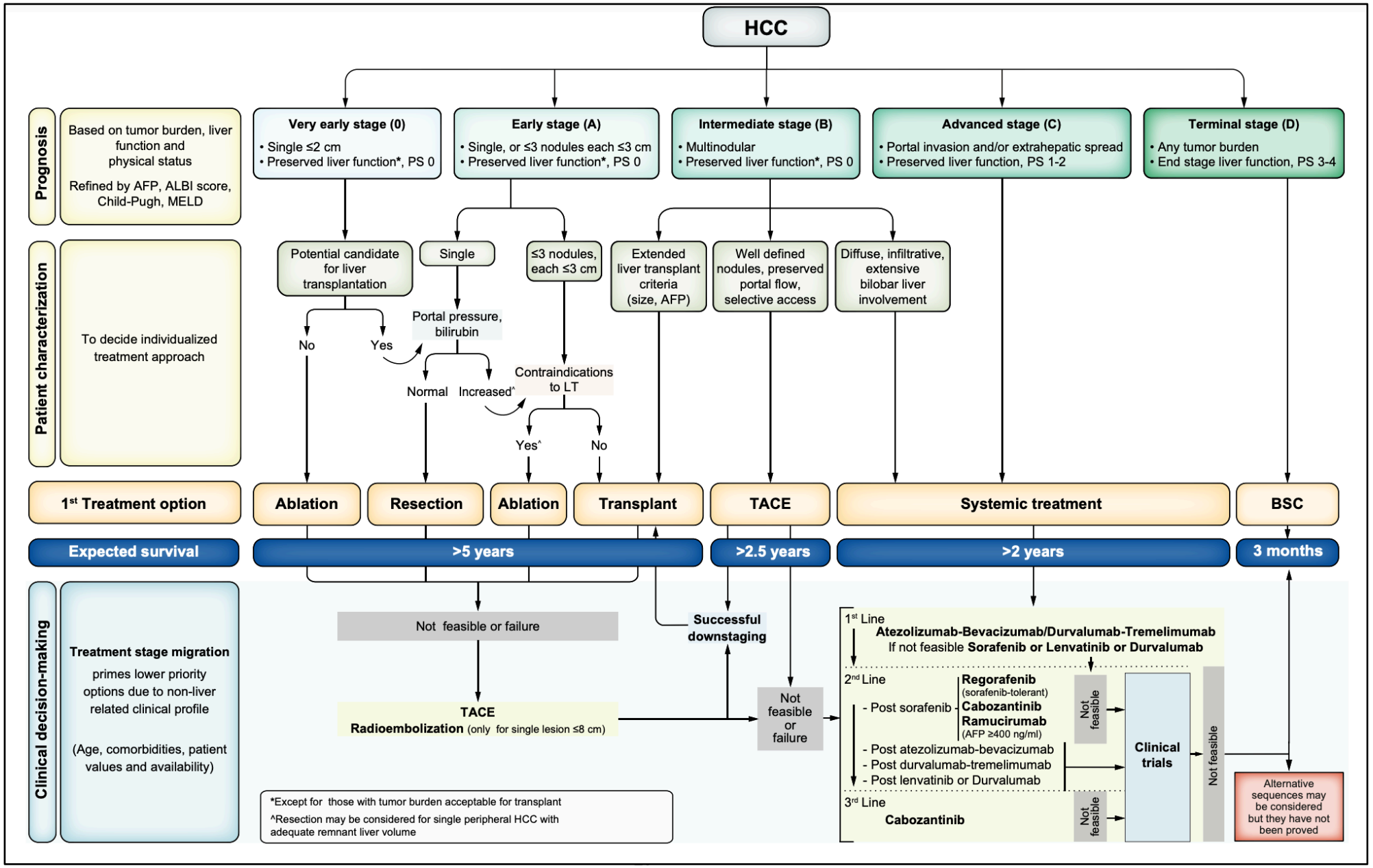


Figure 4. Summary of systemic treatments for HCC and mechanism of action. Adapted from (Llovet et al., 2021)

One limitation of various treatments is that HCC develops predominantly on the background of cirrhosis, and treatment may precipitate decompensation and a deterioration in health that increases mortality. Treatment is recommended according to the tumour stage and the Barcelona Clinic Liver Cancer (BCLC) staging system shown in **Figure 5**. Performance status (PS) is a scale to grade daily functionality, and the BCLC staging system incorporates the Eastern Cooperative Oncology Group (ECOG) scale shown in **Table 1**.

Next Page

Figure 5. BCLC staging, treatment recommendations and prognosis. It shows median survival related to first-line treatment recommendations for each stage. AFP alpha-fetoprotein; ALBI albumin-bilirubin; BCLC Barcelona Clinic Liver Cancer; BSC best supportive care; ECOG-PS, Eastern Cooperative Oncology Group-performance status; LT liver transplantation; MELD model of end-stage liver disease; TACE transarterial chemoembolisation. Taken from (Reig et al., 2022)


HCC
Prognosis
Based on tumor burden, liver function and physical status
Refined by AFP, ALBI score, Child-Pugh, MELD
Very early stage (0)
• Single ≤2 cm
• Preserved liver function*, PS 0
Early stage (A)
• Single, or ≤3 nodules each ≤3 cm
• Preserved liver function*, PS 0
Intermediate stage (B)
• Multinodular
• Preserved liver function*, PS 0
Advanced stage (C)
• Portal invasion and/or extrahepatic spread
• Preserved liver function, PS 1-2
Terminal stage (D)
• Any tumor burden
• End stage liver function, PS 3-4
Patient characterization
To decide individualized treatment approach
Potential candidate for liver transplantation
Single
≤3 nodules, each ≤3 cm
Extended liver transplant criteria (size, AFP)
Well defined nodules, preserved portal flow, selective access
Diffuse, infiltrative, extensive bilobar liver involvement
No
Yes
Portal pressure, bilirubin
Normal
Increased^
Contraindications to LT
Yes^
No
1st Treatment option
Ablation
Resection
Ablation
Transplant
TACE
Systemic treatment
BSC
Expected survival
>5 years
>2.5 years
>2 years
3 months
Clinical decision-making
Treatment stage migration
primes lower priority options due to non-liver related clinical profile
(Age, comorbidities, patient values and availability)
Not feasible or failure
Successful downstaging
TACE
Radioembolization (only for single lesion ≤8 cm)
Not feasible or failure
1st Line
Atezolizumab-Bevacizumab/Durvalumab-Tremelimumab
If not feasible Sorafenib or Lenvatinib or Durvalumab
2nd Line
- Post sorafenib
Regorafenib
(sorafenib-tolerant)
Cabozantinib
Ramucirumab
(AFP ≥400 ng/ml)
Not feasible
- Post atezolizumab-bevacizumab
- Post durvalumab-tremelimumab
- Post lenvatinib or Durvalumab
3rd Line
Cabozantinib
Not feasible
Clinical trials
Not feasible
Alternative sequences may be considered but they have not been proved
*Except for those with tumor burden acceptable for transplant
^Resection may be considered for single peripheral HCC with adequate remnant liver volume

Grade	ECOG Performance Status
0	Fully active, able to carry on all pre-disease performance without restriction
1	Restricted in physically strenuous activity but ambulatory and able to carry out work of a light or sedentary nature, e.g., light house work, office work
2	Ambulatory and capable of all selfcare but unable to carry out any work activities; up and about more than 50% of waking hours
3	Capable of only limited selfcare; confined to bed or chair more than 50% of waking hours
4	Completely disabled; cannot carry on any selfcare; totally confined to bed or chair
5	Dead

Table 1. The Eastern Cooperative Oncology Group (ECOG) Scale.

The Eastern Cooperative Oncology Group (ECOG) Scale. First published in 1982 and used to describe a patient's functional status. (Oken et al., 1982)

Patients with early-stage disease are considered for ablation modalities, surgical resection and liver transplantation. Those with intermediate-stage disease are considered for TACE, and those with advanced disease are considered for systemic treatments. In cases of liver resection, TACE and systemic therapies are used in those with preserved liver function, predominantly Child-Pugh A cirrhosis.

When considering treatment modalities for HCC, it is clear that the most effective strategies are those designed to target early HCC. Therefore it is crucial that patients with cirrhosis are identified, which can be challenging in compensated disease if there are no symptoms and normal blood parameters. Once cirrhosis has been diagnosed, patients should enter a surveillance programme. Sadly many patients still present with advanced HCC at the same time as their cirrhosis is first diagnosed.

Surveillance as a secondary prevention strategy for HCC is now well established. A meta-analysis showed that surveillance improved survival because tumours are detected earlier and amenable to curative treatment modalities. HCC surveillance with ultrasonography in cirrhotic patients should be performed every six months. This interval has been shown to improve survival compared to the annual surveillance (Santi et al., 2010). Still, from a randomised control trial, there is no advantage to increasing surveillance to every three months in the case of ultrasonography (Trinchet et al., 2011).

Ultrasound scan forms the mainstay of surveillance in most guidelines; there is a lack of validated tumour markers available for this cancer, and better biomarkers

are urgently needed. The most commonly used biomarker is AFP, which features in guidelines but will miss 40% of cancers (Daniele et al., 2004). A summary of some of the international guidelines on surveillance is summarised in **Table 2.**

Guideline	Recommendation	Reference
NICE UK	• Ultrasound with or without AFP every 6 months in cirrhosis. • Ultrasound and AFP in patients with significant fibrosis and HBV. • Consider in METAVIR stage less than F2 or Ishak stage less than 3 if older than 40, family history of HCC and HBV DNA is >20000 IU/ml	(Ahmadzadeh et al., 2009, NICE, 2017)
EASL Europe	• Ultrasound every 6 months in Child Pugh A and B cirrhosis and Child Pugh C if a transplant candidate. • Current biomarkers are suboptimal for routine surveillance. • Survey select non-cirrhotic HBV patients at intermediate/high risk of HCC determined by PAGE (evidence low, recommendation weak) • Survey non-cirrhotic F3 patients, regardless of aetiology maybe considered (evidence low, recommendation weak)	(EASL, 2018)
AASLD	• Ultrasound with or without AFP every 6 months for those with Child Pugh A and B cirrhosis or Child Pugh C if a transplant candidate. • Non-cirrhotic with chronic hepatitis B and a family history of HCC should also undergo surveillance.	(Marrero et al., 2018)

Table 2. A selection of international HCC surveillance strategies. Guidelines from the UK, Europe and America and a summary of their main recommendations for surveillance for HCC.

In the UK we frequently combine six monthly ultrasounds with AFP. It is known that ultrasound is very operator dependent and in addition, it can be technically

challenging in patients with obesity. AFP is the only validated biomarker in use, and it has been shown to increase the sensitivity for detecting HCC to 63% compared to 45% in early-stage HCC (Tzartzeva et al., 2018). There is still, however, an unmet need for robust biomarkers with high sensitivity and specificity for the early detection of HCC.

1.4 The liver's immune environment

The liver contains a large and diverse population of resident immune cells. The gut-derived nutrients and molecules from gut microflora which the liver is continuously exposed to, need to be tolerated by the liver. Conversely, the liver must also be poised to remove hazardous stimuli like infection, cancer or autoimmunity. Therefore the liver is constantly in a state of regulated homeostatic inflammation.

A heterogeneous population of phagocytic cells in tissues are essential for the clearance of bacteria, toxins, and exogenous antigens, known as the mononuclear phagocyte system (Goel and Eapen, 2022). The term reticuloendothelial system (RES) considers the proximity of macrophages and endothelial cells, which reside next to each other. Liver sinusoidal endothelial cells can also remove macromolecules and nanoparticles by endocytosis (Smedsrod et al., 1990).

The liver is capable of both innate and adaptive immune responses. The innate response lacks antigen specificity, and adaptive mechanisms are antigen-specific. Examples of the effector cells of the innate immune system include neutrophils,

macrophages, NK cells and NKT cells, and examples of adaptive cells are T lymphocytes and B lymphocytes. A summary of cells most relevant to the liver immune system is summarised in **Figure 6** Adapted from (Goel and Eapen, 2022, Freitas-Lopes et al., 2017)

.

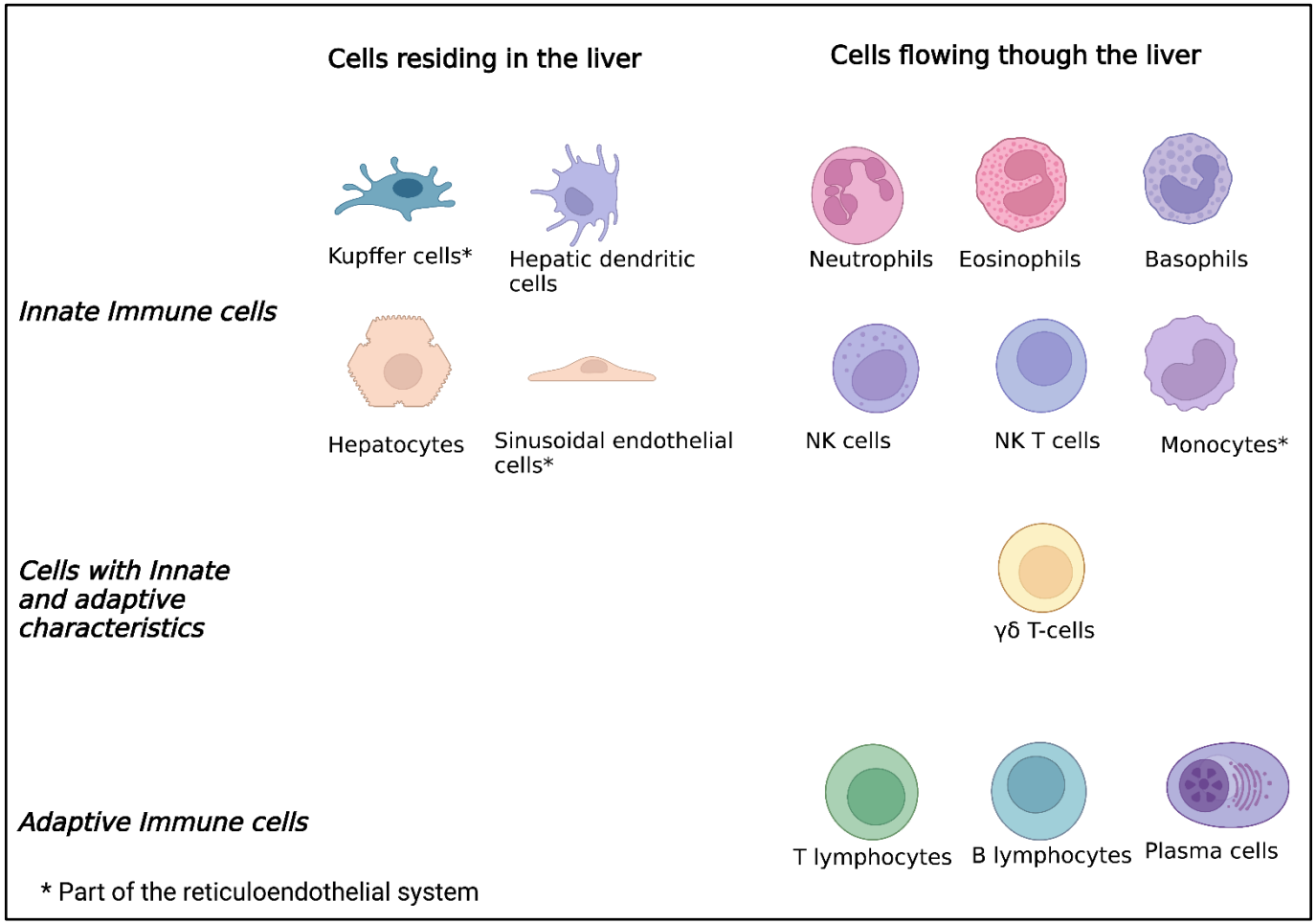


Figure 6. Immune Cells of the Liver.

Adapted from (Goel and Eapen, 2022, Freitas-Lopes et al., 2017)

1.4.1 Liver resident leucocytes

The liver is enriched with innate leucocytes including liver dendritic cells (DCs) and macrophages which facilitate effective antigen presentation activating adaptive immune responses. NK cells and NK T cells are lymphocytes that are prevalent in the liver, and along with γδ T cells, Kupffer cells and myeloid-derived suppressor cells, these liver resident cells are prevalent around the liver sinusoids.

1.4.1.1 Kupffer cells

The largest population of hepatic macrophages are Kupffer cells, forming the lining of the liver sinusoids. They were first described in 1876 by Karl Wilhelm von Kupffer but twenty years later, they were identified as macrophages (Wake et al., 1989). Pattern recognition receptors (PRR) expressed by Kupffer cells bind to microbial-associated molecular patterns (MAMPs) and damage-associated molecular patterns (DAMPs) arriving into the liver, and upon binding, these MAMPs and DAMPs are phagocytosed and degraded by Kupffer cells and hepatocytes which also express PRRs. This protects from excessive immune activation. In addition, they express complement receptors and Fc receptors to facilitate rapid phagocytic activity and production of inflammatory cytokines and play a role in immune regulation, tissue repair, and liver regeneration (Elsegood et al., 2015).

1.4.1.2 Dendritic cells

DCs can be found in the healthy liver. They are antigen-presenting cells (APCs) and can induce immune responses within the liver. They are predominantly found

subcapsular and around central veins (Prickett et al., 1988). They express Major Histocompatibility Complex (MHC) class II and can capture, process and present antigens through their interaction with T cells, initiating immune responses rather than directly killing pathogens. In homeostasis, these cells are immature and tolerogenic; they interact with and can phagocytose particles and form MCH class II-peptide complexes (ten Broeke et al., 2013). In chronic inflammation, mature DCs have a proinflammatory phenotype (Mendez-Sanchez et al., 2021).

1.4.1.3 Myeloid-derived suppressor cells

Myeloid-derived suppressor cells (MDSCs) are found in healthy livers but expand in disease states (Nagaraj et al., 2009). They produce immunosuppressive molecules and can suppress T-cell activation. This ability to inhibit the immune response in pathological conditions (Gabrilovich and Nagaraj, 2009) is a source of ongoing research.

1.4.1.4 Lymphocytes

The frequencies of hepatic T cell subpopulations vary between individuals. However, even in non-diseased states, abundant lymphoid cells highlight their importance in immune haemostasis in healthy individuals. There are resident hepatic lymphocytes and lymphocytes in the circulation that infiltrate the liver and then mature and differentiate in the liver; distinguishing between the two is challenging. Cytokines within the liver can induce expansion of T cell populations, and we have known for some time that in pathological conditions increased

production of cytokines affects the function and phenotype of local lymphoid cells and also increase recruitment from peripheral circulating blood (Yoong et al., 1999, Leite-De-Moraes et al., 1998). In a normal human liver, 65% of all lymphocytes consist of NK cells, T cells expressing NK molecules (NKT) and γδ T cells (Doherty and O'Farrelly, 2000). NK cells are innate lymphoid cells; NKT cells and γδ T cells bridge innate and adaptive immune mechanisms.

1.4.1.4.1 Innate lymphocytes

The dominant presence of innate immune cells supports the ability of the liver to respond promptly to a range of threats, and they are essential players in liver immune surveillance. These hepatic innate populations are significant cytokine producers influencing innate and adaptive responses. Innate lymphocytes (ILCs) are a group of cells that include NK cells and several subgroups of ILCs, resident in the liver parenchyma, that can recognise infection, damage and cancer cells and are primed to recognise and respond rapidly. The predominant innate immune cell type is the NK cell. NK cells are classified as innate immune cells but influence innate and adaptive responses. Many hepatic NK cells in the liver confirm that the liver is primed to be mounting tolerogenic responses in health (Mikulak et al., 2019).

In 2013 Spit et al. proposed that ILCs be categorised into three groups to simplify the complex nomenclature used to describe these cells, with sometimes multiple names for one cell type. The classification proposed was based on the cytokines they produce and the transcription factors their development and function depend

on (Spits et al., 2013). Group 1 ILCs were defined by the ability to make IFNγ and the inability to produce T_H2 and T_H17 cell-associated cytokines. The primary example in this group is the NK cell. NK cells have cytotoxic activities and once activated produce large quantities of IFNγ. The liver contains an NK cell subset with phenotypic and functional differences from conventional NK (cNK) cells. They are found to be localised within the hepatic sinusoids (Hudspeth et al., 2016).

Group 2 ILCs produce T_H2 cell-associated cytokines when stimulated by IL25, IL33 and thymic stromal lymphopoietin (TSLP). Group 2 ILCs are predominantly found in the lung and are rare in the liver, approximately 5% of all ILCs (Kim et al., 2016). However, there has been increased interest in Group 2 ILCs in acute and chronic liver disease in recent years. One study demonstrated an inflammatory role for ILC2s, which amplify immune-mediated hepatitis by recruiting eosinophils in murine immune-mediated hepatitis (Neumann et al., 2017). It has been shown that IL-33 is elevated in the serum of a cohort of patients with cirrhosis compared to controls. In a mouse model, IL-33 was needed for advanced hepatic fibrosis in vivo, and the effects were related to the activation and expansion of ILC2s (McHedlidze et al., 2013). The production of cytokines IL-17A and IL-22 characterises group 3 ILCs. Group 3 liver ILCs are involved in the progression or amelioration of some liver diseases despite their rarity in the liver. Depending on the disease, the microenvironment dictates the beneficial or detrimental effect of IL-22 (Cobleigh and Robek, 2013). Given that Group 3 ILCs are the primary source of IL-22, they may contribute to liver disease. For example, during HBV infection, IL-22 was found to increase the recruitment of immune cells and exacerbate the

fibrosis (Zhao et al., 2014). In contrast, IL-22 was protective from alcohol-related liver damage via STAT3 activation (Ki et al., 2010). In addition to innate lymphoid cell groups 1, 2 and 3, there are also mucosal-associated invariant T cells (MAITs) (Walker et al., 2013, Kurioka et al., 2016). The innate lymphocytes in the adult healthy liver are summarised in **Table 3**, together with their main effector molecule and function.

Cell Group	Cell Subset	Effector molecules	Role in Liver disease
ILC group 1	NK	Perforin, Granzyme B, IFNγ	• NK cells can directly eradicate infected cells or tumour cells (Morvan and Lanier, 2016). • Resolving fibrosis by directly killing activated hepatic stellate cells (Radaeva et al., 2006). • Defective function and reduced numbers of NK cells in HCC (Cai et al., 2008)
	ILC1	IFNγ, TNFα, GM-CSF, Perforin, Granzyme B	• Liver ILC1s express the cytotoxic molecules (Tang et al., 2016). • Function in liver diseases is not fully understood but have a role in protecting against acute liver injury (Nabekura et al., 2020).
ILC group 2	ILC2	IL-5, IL-13	• Promote disease progression in autoimmune hepatitis (Neumann et al., 2017). • Profibrotic function of hepatic ILC2s in chronically inflamed liver tissue (McHedlidze et al., 2013). • May contribute to the progression of cholangiocarcinoma (Nakagawa et al., 2017).
ILC group 3	ILC3	IL-17A, IL-22,	• Rare population of cells • Increased in steatohepatitis models and may reduce liver damage (Hamaguchi et al., 2021).
Innate – Like T lymphocytes	iNKT (Type I NKT cell)	TNFα, IFNγ, IL-4, IL-10, IL-13, IL-17A, GM-CSF	• Protective during the acute phase of liver injury and detrimental role in chronic conditions (Zeissig et al., 2017)
	Non-iNKT (Type II NKT cell)	IFNγ IL-13	• Display a proinflammatory cytokine profile in patients with AIH (Sebode et al., 2019) • Inhibit the action of iNKT cells in liver inflammation mouse models (Halder et al., 2007, Maricic et al., 2015) • May protect from liver fibrosis in human via Il-22(Paquin-Proulx et al., 2018)

	γδT	IFNγ, TNFα, IL-17A, Perforin. Granzym B	• Protective functions of IL-17^{+} γδ T cells via NKT cell inhibition in immune-mediated liver diseases (Zhao et al., 2011). • γδ T cells might contribute to HCV-triggered liver injury (Tseng et al., 2001). • Antiviral immune response seen and subsequent clearance of viruses (Hou et al., 2013). • May contribute to anti-tumoral immune responses (Devaud et al., 2013). • Thought to promote fibrosis progression through activation of hepatic stellate cells (Zou et al.) (Meng et al., 2012). • Role in the anti-fibrotic pathway in hepatic inflammation by alleviate the inflammatory reaction (Hammerich et al., 2014)
	MAIT	IL-17, IFNγ	• Proposed defensive role against a range of bacteria, fungi and viruses via rapid production of IFNγ and IL-17 (Kurioka et al., 2016). • May drive bile duct damage in chronic inflammation (Afford et al., 2001).

Table 3. Innate lymphocytes in the healthy adult liver. Table summarising the main groups of innate lymphocytes in the liver, their effector molecules and proposed roles in liver disease. (Adapted from (Chen and Tian, 2021)

1.4.1.4.2 Adaptive lymphocytes

The liver is primed for an adaptive immune response; it can expeditiously recruit distinct populations of immune cells. It can be considered to have two main arms mediated by B cells or T cells. Due to its unique blood supply, the liver is the first point of contact for antigens in the gastrointestinal tract. Although it has the ability to mount an aggressive response in most circumstances, it remains tolerant. In a healthy liver, the resident cells of the liver suppress the adaptive immune response in part due to the expression of anti-inflammatory cytokines, for example, hepatocyte-derived IL-10 (Stijlemans et al., 2020, Safadi et al., 2004).

1.4.1.4.2.1T cell lymphocytes

There are CD4+ and CD8+ positive T cells; and γδ T cells which play a role in adaptive and innate immunity. CD4+ T cells can be divided into subtypes, including Th1, Th2, Th17, and follicular helper T cells that enhance innate and adaptive immunity and immunosuppressive Tregs. CD8+ T cells consist of two groups, cytotoxic T cells (Tc), also known as killer T cells and CD8+ Tregs, which can inhibit Th cells. γδ T cells can phagocytosis, destroy tumour cells, and play a role in immune regulation by suppressing CD8+ T cells (Shuai et al., 2016).

On recognition of antigens complexed with MHC class I (CD8+ cytotoxic T cells) or class II (CD4+ helper T cells), they can undergo clonal expansion. High numbers of T cells are cytotoxic and can efficiently secrete inflammatory cytokines such as TNFα, INF γ and IL-2 (Rowell et al., 1997).

Studies comparing the populations of T cells found in the liver compared to peripheral blood are very informative. In the peripheral blood, 70% of T cells are conventional single positive CD4+CD8- and CD8+CD4- αß T cells, but in the liver, it is less than 40%. The CD4+ to CD8+ cells ratio is also reversed in the liver, and up to 90% express CD8. We also find double negative T cells in the liver and double positive for CD4 and CD8 and CD8 cells that lack the ß chain (CD8 α+ ß-) (Doherty and O'Farrelly, 2000). There are hepatic T lymphocytes with limited diversity TCRs, which share profiles with NK cells and are referred to as NKT cells. These cells represent, on average, a third of all liver CD3+ cells but only 2% in the peripheral blood (Norris et al., 1999), and although expressing TCRs, they are considered part of the innate arm of the immune system.

A summary of T-cell groups, main secreted effector molecules and function is found in **Table 4**, taken from (Shuai et al., 2016)

1.4.1.4.2.2B Lymphocytes

B cell populations are also found in the healthy liver, making up approximately 8% of lymphocytes (Norris et al., 1998). Functions include the production of cytokines, which can be pro-inflammatory or anti-inflammatory, antigen presentation for activating T cells and antibody production (Patel et al., 2021). CD20+ B cells have been seen to localise in liver sinusoids near the portal tracts. Moro-sibilot et al. showed that the human liver contains naïve and memory B cells and IgA-producing plasma cells. Some of these were directed against gut microbiota (Moro-Sibilot et al., 2016). It has been published that B cell biology is changed in many chronic

liver disease conditions; however, studies on this population of lymphocytes are limited (Patel et al., 2021)

T-cell group	Subset	Main Effector Molecules Secreted	Function
CD4 T-cells	Th1	IFN-γ, IL-2, TNF-α	• Activation of CD8 T cells • Induction of Ig class switching to complement-fixing antibodies • Cell-mediated and delayed-type hypersensitivity responses
	Th2	IL-4, IL-5, IL-9, IL-10, IL-13 and IL-25	• Induction of Ig class switching to IgG1 and IgE • Role in antibody-dependent cell-mediated cytotoxicity • Role in allergic responses • Suppression of Th1 cells and Th17 cells
	Th17	IL-17, IL-21, IL-22, IFN-γ	• Suppression of Treg cell function
	Tfh	IL-21, IL-4	• B-cell proliferation and differentiation and maturation in lymphatic tissue • Activation of CD8 T cells
	Treg	IL-10 and TGF-ß	• Inhibit Th17 proliferation and secretion of IL-17 Suppression of proliferation of CD4 CD25(-) T cells, CD8 T cells and their secretion of IFN-γ • Suppression of innate immunity
CD8 T-cells	Tc	Granzymes, perforin, IFN-γ, TNF-α, IL-4, IL-5, IL-9, IL-10, IL-13, IL-17 and IL-21	• Cytotoxicity against tumours and intracellular pathogens • Promotion of Th2-mediated allergy • Role in autoimmunity
	CD8 Treg	Secretion of granzymes, perforin, TGF-ß and IL-10	• Suppression of the proliferation of Th cells • Suppression of immunity in response to infection
γδ T-cells	γδ T-cells	Secretion of IL-10, IL-17, IL-22, TNF-α and IFN-γ	• Suppression of CD8 T cells • Phagocytosis of bacteria • Cytotoxic against hepatic tumours • Induction of hepatocyte apoptosis • Limit hepatic inflammation and fibrosis

Table 4. T-cell subsets and their associated function. (Taken from (Shuai et al., 2016)

1.4.1.5 Neutrophils

Neutrophils are the largest leucocyte population in peripheral blood and are a major effector cell of innate immunity. They have a short half-life of less than one day but can survive over five days in some circumstances (Pillay et al., 2010). Neutrophils are not overtly present in a healthy liver but accumulate in infection and inflammation. Under the influence of cytokines and chemotactic stimuli, neutrophils migrate from the peripheral blood to an inflammatory focus (Freitas-Lopes et al., 2017). Upon arrival, neutrophils are capable of phagocytosis, the release of DNA extracellular traps and can secrete granules containing proteolytic enzymes, bactericidal proteins, metalloproteinases and lysozymes (Faurschou and Borregaard, 2003). Although classically known for their role in killing bacteria, neutrophils are also pivotal in non-bacteria-related liver damage. One study induced a sterile thermal liver injury and demonstrated that neutrophils penetrated the injury site, dismantled injured vessels, and created channels for vascular regrowth (Wang et al., 2017). It is well documented that neutrophil infiltration during inflammation generates oxidative stress and leads to hepatocyte death by producing reactive oxygen species (ROS). This can include sterile injury, drug injury, and ischaemic injury, in addition to insults from bacteria and viruses. The nature of the injury and inflammation influences how neutrophils are recruited and the molecules on LSEC that are up or down-regulated. In sterile conditions, neutrophils can extravasate to reach the site of inflammation, and in bacterial insults, they can arrest and remain within the sinusoids to assist with trapping microbial invaders (McDonald et al., 2012). It is

thought that the binding of neutrophils to the sinusoids is mediated by CD44, at least in the case of LPS exposure, and this phenomenon is not seen in $CD44^{-/-}$ mice (McDonald et al., 2008). In LPS exposure, there was also downregulation of MAC-1, preventing extravasation of neutrophils into the liver, where they could cause significant tissue damage (Menezes et al., 2009). In a model using poxvirus as the pathogen, the arrest was mediated by MAC-1 (Jenne et al., 2013).

The other side of neutrophils is that they are essential in tissue repair. Neutrophils can regulate a macrophage phenotype switch from a proinflammatory to a reformative type (Yang et al., 2019). During extravasation into liver tissue, neutrophils release MMPs, MMP-8 and MMP-9 have been shown to reduce collagen accumulation and, therefore, fibrosis progression promoting repair (Saijou et al., 2018). The most abundant MicroRNA in neutrophils is MicroRNA-223, and it is thought that this is key to the resolving effector function of neutrophils transforming macrophages into a reparative phenotype (Calvente et al., 2019). Neutrophils share some of their phenotypic markers with MDSCs. Granulocytic myeloid-derived suppressor cells (G-MDSCs) in the circulation are enriched in cancer patients and are sometimes referred to as 'low-density neutrophils' (Lecot et al., 2019).

In summary, neutrophils, like many other immune cells, are a complex, multi-faceted imperative host defence from microbes and sterile insults and can cause inflammation and significant tissue damage while trying to protect the host in acute and chronic settings. However, they are also key in resolving inflammation and facilitating tissue repair.

1.4.2 The immune microenvironment in acute liver disease

The mechanisms governing acute liver injury vary depending on the aetiology. There are three possible outcomes following acute injury: full resolution; progression to chronic liver disease, if the insult continues; or acute liver failure can result. Acute liver failure occurs when hepatocyte death exceeds hepatocyte regeneration with rapid loss of liver function, and it can be the result of direct hepatocyte damage from the initiating insult or immune-mediated liver injury. In acute liver injury, the innate immune response is activated more promptly than adaptive immunity.

In addition to activating leucocyte populations recruited to the site, a fibrotic response is designed to protect hepatocytes. This is regulated by cytokines and growth factors released by leucocytes; they frequently include TNFα, IL6, PDGF and TGFß (Michalopoulos, 2007), and we see the activation of HSCs and ECM production. Macrophages can then produce mediators to increase metalloproteinases to resolve the injury (Duarte et al., 2015). The liver has the ability to fully recover after injury driven by inflammatory mediators and growth factors. For example, in IL-6 deficient mice, there is impaired liver regeneration (Cressman et al., 1996). TNF alpha is significantly elevated in the livers of patients with acute liver injury and correlates with lymphocyte accumulations, and additionally increased KCs (Zou et al., 2009). However, IL-6 and IL-10 can down-regulate TNFα in acute liver failure (Louis et al., 1997, Cressman et al., 1996).

KCs are pivotal in releasing IL-6 and TNFα, promoting hepatocyte proliferation. KCs can be stimulated by neutrophils recruited to the liver (Selzner et al., 2003), triggering liver regeneration. KCs capable of phagocytosis can release cytokines that influence other immune cells and contribute to the degree of damage that occurs (Szabo et al., 2007).

In hepatocyte necrosis neutrophils are rapidly recruited, potentiating tissue damage. Neutrophils will extravasate to contact hepatocytes in the presence of chemotactic signals, leading to neutrophil activation, which in turn leads to intracellular oxidative stress and eventually cell death; infiltration by neutrophils is often an early response to tissue damage (Liu et al., 2006).

Monocytes and macrophages secrete large quantities of pro-inflammatory cytokines and can trigger adaptive immune responses. NK cells have potent cytotoxic capability, and hepatic NK cells can influence T-cell responses and even directly cause hepatocyte death (Ochi et al., 2004). NK T cells are also critical cells capable of driving acute liver injury via IL-4 and IFNγ (Tiegs, 2007).

Overall the initial mechanism of acute liver injury is driven by the innate immune system and is complex, aetiology-specific, and many cell types participate.

1.4.3 The immune microenvironment in chronic liver disease and the development of fibrosis

As previously described, liver injury leads to activation of the innate immune system and HSC activation, and when it persists, it leads to fibrosis as ECM is deposited. Hepatocyte and cholangiocyte death can directly activate HSCs or via

cytokines released by immune cells, including ILCs, Kupffer cells, Th17 cells and monocytes. Many cytokines are produced in the liver, and macrophages are predominant producers (Maher, 2001). It is well established that HSCs are activated via TGFß1, the most profibrotic cytokine; TGFß stimulates the synthesis of ECM proteins (Xu et al., 2016). In NASH, liver injury triggers Kupffer cells to release IL-1ß, which activates HSCs (Miura et al., 2010). In addition, ROS generated from liver injury stimulates HSCs to produce collagen I (Gandhi, 2012). Platelet-derived growth factor (PDGF) produced by macrophages in addition to other cells is also considered to be fibrogenic (Kocabayoglu et al., 2015), stimulating HSC proliferation, promoting collagen production and deposition and transforms HSCs into myofibroblasts.

Cytokine production and the proportions can vary depending on the aetiology of the injury; chemokine pathways are also critical in the recruitment of leucocytes. The CC- and CXC- receptor families have vital roles in regulating inflammation in the liver. Chemokines influence many cells, including hepatocytes, endothelial cells, immune cells and HSCs. The chemokines and receptors involved again vary depending on the liver disease aetiology, as summarised by (Marra and Tacke, 2014) shown in **Table 5.**

(Next Page)

Table 5. Chemokines and their receptors relevant to liver pathology. (Taken from(Marra and Tacke, 2014)

Chemokine	Main receptor(s)	Target cells	Role in liver disease/ disease relevance
CCL1	CCR8	Monocytes/macrophages	Fibrosis
CCL2	CCR2	Monocytes/macrophages , HSCs	Initiation of inflammation, fibrosis, NAFLD/NASH
CCL3	CCR1, CCR5	NK, Th1, CD8	HCV, HBV, NAFLD/NASH, fibrosis
CCL4	CCR1, CCR5	NK, Th1, CD8	HCV, HBV, NAFLD/NASH, fibrosis
CCL5	CCR1, CCR5	NK, Th1, CD8	HSCs HCV, HBV, NAFLD/NASH, fibrosis
CCL17	CCR4	Treg	HCV
CCL19	CCR7	CD8 T, DCs	HCV
CCL20	CCR6	γδ T, Th17, HSCs	Cholestatic, HCV, alcohol, fibrosis
CCL21	CCR7	CD8 , DCs	HCV, fibrosis
CCL22	CCR4	Treg	HCV
CCL25	CCR9	Monocytes/macrophages , HSCs	Fibrosis
CXCL1	CXCR2	Neutrophils, monocytes	Initiation of inflammation, alcohol
CXCL2	CXCR2	Neutrophils, monocytes	Initiation of inflammation, alcohol
CXCL5	CXCR2	Neutrophils	Alcohol, fibrosis
CXCL6	CXCR1, CXCR2	Neutrophils, monocytes	Alcohol
CXCL8	CXCR1, CXCR2	Neutrophils, monocytes	Initiation of inflammation, alcohol, HBV
CXCL9	CXCR3	NK, Th1, Th17	HCV, fibrosis
CXCL10	CXCR3	NK, Th1, Th17, HSCs	Cholestatic, HCV, HBV, fibrosis
CXCL11	CXCR3	NK, Th1, Th17	HCV, fibrosis
CXCL12	CXCR4, CXCR7	HSCs, LSECs, HCCs	Fibrosis, regeneration, HCC
CXCL13	CXCR5	B cells	HCV
CXCL16	CXCR6	NKT cells	HCV, fibrosis
CX3CL1	CX3CR1	Monocytes/macrophages	HCV, fibrosis

The innate and adaptive immune systems have essential roles in developing liver fibrosis. The phenotype of macrophages determines fibrosis progression or resolution of the injury. In inflammatory stimuli, macrophages can differentiate into either M1 or M2 phenotype. M1 leads to the release of pro-inflammatory cytokines, progressing inflammation and fibrosis development; in contrast, M2 are anti-inflammatory in their function (Wang et al., 2021a). NK cells can also protect against fibrosis by mediating the destruction of activated HSCs (Krizhanovsky et al., 2008). NKT cells increase in liver inflammation, and the cytokines they produce can also drive fibrosis. We see the expansion of DCs, normally key for tolerance in the liver, in fibrosis, and they can stimulate NK cells, T cells and HSCs in murine studies (Connolly et al., 2009).

From the adaptive immune system perspective, Th1 lymphocytes are considered antifibrotic due to cytokines such as IFNγ that they produce, and Th2 are profibrotic and capable of producing drivers of fibrosis such as IL-4. Therefore, the ratio of these two subtypes of cells can impact whether there is a predominant state of anti- or pro-fibrotic stimuli (Wynn, 2004). IL-17 is secreted by Th17 cells and neutrophils and is profibrogenic stimulating HSC (Hammerich et al., 2011).

Regarding the role of B cells, evidence from B cell-deficient mice suggests that they are also crucial in the development of fibrosis, and liver fibrosis was attenuated in the absence of B cells (Novobrantseva et al., 2005).

1.4.4 The immune microenvironment in hepatocellular carcinoma

HCC is an inflammation-associated cancer that can be infiltrated by innate and adaptive immune cells. However, the number of infiltrating cells and cell types varies between tumours of the same type. It would seem logical that a high inflammatory infiltrate would be a good thing and represents the host's attempt to halt the tumour progression. Still, although there may be anti-tumour effects, immune infiltration can augment the microenvironment to favour tumour growth. This can be in the form of providing the tumour with signals required for the proliferation of tumour cells, promoting angiogenesis, and degrading the ECM to facilitate invasion and distal metastases. Overall it has been established that immune infiltrates are associated with a better prognosis (Wada et al., 1998). Promoting the tumorigenic microenvironment is multifactorial, arising from cellular stress, epigenetic modifications, mitochondria changes and senescence. For example, in viral hepatitis from HBV and HCV, the liver injury progresses due to the host's immune response (Knolle and Thimme, 2014). DAMPS from hepatocyte death lead to chronic inflammation, increased proinflammatory cytokines and HCC development. Similarly, in alcohol-related liver disease, hepatic steatosis leads to the death of hepatocytes and increased DAMPS, activating the innate immune system and driving inflammation and fibrosis, leading to increased HCC risk. In summary, innate and adaptive immune responses are essential for eliminating malignant cells, but this anti-tumour response is impaired in chronic liver disease.

In recent years the treatment options for HCC have changed with the introduction of immunotherapy. The main immune cells in HCC are T lymphocytes, and we still use the term infiltrating lymphocytes implying that these are normal circulating cells which enter the tumour. Several other types of immune cells are found in HCC, discussed in the following sections on the innate and adaptive immune systems in HCC. The immune cell populations found in HCC and whether they exacerbate or ameliorate the progression of HCC are shown in **Table 6** below.

Cell type	HCC
CD8+ T cells	↑↓
CD4+ effector T cells	↑↓
Treg cells	↑
B cells	↑↓
KCs or monocytes	↑
NKT cells	↓
NK cells	↓
HSCs	↑
DCs	↑
Neutrophils	↑

Table 6. Immune cell populations found in HCC.

Arrows indicate whether the immune cell type exacerbates (upward arrow) or ameliorates (downward arrow) the progression of HCC. (taken from (Ringelhan, 2018)

1.4.4.1 The innate immune system in HCC

KCs and monocytes, as mentioned previously, are activated in liver inflammation. KCs can promote HCC by producing IL-6 (Kong et al., 2016) and ROS (Yuan et al., 2017). Endogenous DCs may exacerbate HCC because of their ability to increase immune tolerance (Ouyang et al., 2016). DCs have also been used as a therapeutic agent in HCC (Chen et al., 2018). M2 Macrophages promote progression, metastases (Dong et al., 2019), and their interaction with T lymphocytes also promotes progression (Kuang et al., 2010).

NK cells recognise tumour cells due to the low expression of MHC I and can then exhibit cytotoxicity and promote inflammation via cytokine release. High NK cells in tumours are associated with increased survival in HCC (Wu et al., 2020). However, it is described that NKs in tumours don't always have this effect and prognosis is also linked to the microenvironment of a particular tumour and the influence of the tumour cells' ability to inhibit NK function (Bozward et al., 2021). Tregs can also inhibit NK function via TGFß or IL-2 (Juengpanich et al., 2019, Ghiringhelli et al., 2005).

DCs are important APCs, but when function is impaired, they may play a role in tumour escape from the immune system. They can activate specific T -cells to have an anti-tumour role and also activate innate immune effector cells. This is why the DC vaccine was pursued as a potential immunotherapy (Palmer et al., 2009), and the reduced function of DCs has been documented in HCC (Kakumu et al., 2000).

NKT cells are increased in the liver in cirrhosis and HCC. Still, their role in HCC needs to be clarified, and they appear to be able to promote tumour growth and

have anti-tumour functionality (Bandyopadhyay et al., 2016). NK cells have been studied more, and in addition to their anti-fibrosis role via their ability to affect macrophage phenotypes, they also have an anti-tumour role. It has been shown that in HCC, their function seems to diminish, and NK cell dysfunction develops with inactive and immature NK cells (Zhang et al., 2017).

The effect of fibrosis on liver resident immune cells, which generally survey and protect from cancer cells, may lead to cancer development. NK cells have diminished function in chronic liver disease (Kawarabayashi et al., 2000, Zhang and Friedman, 2012), and normally NK cells would induce apoptosis of tumour cells detected as part of their function in tumour surveillance because tumour cells lack MHC class I expression (Dhatchinamoorthy et al., 2021). NK cells also express the NKG2D receptor; NKG2D ligands have deficient expression levels in normal cells but are upregulated in damaged or transformed cells. Therefore, the upregulation of NKG2D ligands by tumour cells is another mechanism by which NK cells can mediate the lysis of tumour cells (Diefenbach et al., 2001).

Neutrophil infiltration is common in alcoholic steatohepatitis and is also seen in NASH (Cho and Szabo, 2021). They are reported to contribute to fibrosis by activating HSCs (Ibusuki et al., 2013). In the context of HCC, the importance of their role has yet to be fully established, and opinions are conflicting about their relevance. They are said to be associated with a poor prognosis in HCC (Li et al., 2017). They can support tumour growth, angiogenesis and metastatic progression by producing HGF, VEGF and MMP9 (Xu et al., 2014). In HCC, neutrophils are also reported to help recruit macrophages and Treg cells (Zhou et al., 2016).

In recent years MDSCs have drawn increasing attention in HCC research, and consideration has been given to whether they could be a potential therapeutic target. A recent meta-analysis found that increased MDSC levels correlate with poor prognosis in HCC (Zhang et al., 2019a). We know that MDSCs can reduce innate and adaptive immune responses; therefore, reduced anti-tumour responses would be anticipated.

1.4.4.2 The adaptive immune system in HCC

In NASH, there is evidence that activated CD8+T cells drive liver damage but also have a role in anti-tumour surveillance. Activated T cells produce mitogenic cytokines linked to promoting HCC (Haybaeck et al., 2009, Finkin et al., 2015). The primary tumour infiltrating lymphocytes (TILS) in HCC are CD8+ T cells, and large numbers correlate with improved survival (Endig et al., 2016). This suggests that the role of CD8+T cells differs in chronic liver disease and HCC scenarios. A lack of CD4+ T cells and increased Treg cells correlates with poor survival in HCC (Fu et al., 2013). Cytotoxic T (CD8+) cells are key mediators of immunity against tumours. It has been shown that many CD8+ T cells are dysfunctional (Zheng et al., 2017). It is thought that this dysfunction may be under the regulation of Treg cells, and higher numbers of Treg cells infiltrating the tumour are associated with worse outcomes (Langhans et al., 2019).

Forkhead box protein P3 (FoxP3) is a marker of Treg cells that can suppress immune responses in HCC, and high FoxP3 expression has been associated with a poor prognosis (Lin et al., 2013, Huang et al., 2012). A meta-analysis looking at

data in different types of tumours found in HCC and gastric cancer survival was lower in high FoxP3+ T cell infiltration and recurrence high, but in colorectal cancer, high infiltrates were associated with better survival (Huang et al., 2014). High tumour infiltrating lymphocytes (TILs) have been associated with better prognosis in a meta-analysis (Yao et al., 2017). This, however, was contradicted by another meta-analysis which found that high CD3+ T lymphocytes in the tumour centre were associated with poorer outcomes (Ding et al., 2018).

Cytotoxic T cells are CD8+; in cancer, high levels are usually associated with a better prognosis. High numbers of CD8+ T lymphocytes in HCC have been reported to be associated with improved survival (Ding et al., 2018). In HCC, the number of CD8+ T cells is lower than in the distal non-tumour tissue (Yarchoan et al., 2017), and within the tumour numbers are lower centrally compared to the margins (Sun et al., 2015), perhaps due to suppression of migration by Tregs (Fu et al., 2007). Another study looking at HCC in the setting of NASH found that CD8+ T cells with elevated PD-1 expression, exhausted effector cells, led to accelerated tumour growth (O'Leary, 2021).

CD4+ T cells can differentiate into many subsets depending on the stimulus. (Takeuchi and Saito, 2017) and lower numbers are found in more advanced HCC (Fu et al., 2013).

Combination therapy with anti-PD-1 and anti-VEGF antibodies is now the first line treatment for advanced HCC with a response rate of 30% (Cheng et al., 2022). A healthy immune system needs to be able to differentiate between tumour cells and normal cells. In the case of T cells, antigens are recognised by the T cell

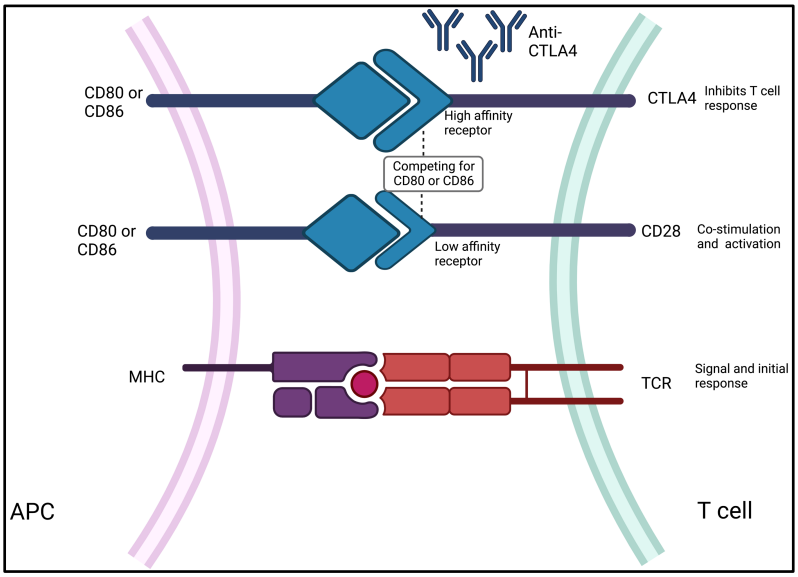
receptor, and there are immune checkpoints to keep this process under tight regulation and prevent autoimmunity. However, this system can be dysfunctional in tumours, making them resistant to the effects of the immune system. The idea of blocking immune checkpoints means a full immune response can occur. Immune system inhibitory ligands and receptors are commonly overexpressed in the tumour microenvironment. CTLA4 antibodies were one of the first immunotherapies in cancer to have FDA approval following the initial concept by James Allison (Leach et al., 1996) , who later received The Nobel prize for his work. CTLA4 is expressed in T cells, where it regulates T cell activation. When an antigen is recognised, CD28 signalling amplifies and T cells are activated; CTLA4 counteracts this receptor and they share the same ligands CD80 and CD86. CTLA4 competes with CD28 and can inhibit T cell activation (Parry et al., 2005). CTLA4 also prevents CD80 and CD86 from engaging CD28. CTLA4 is expressed by activated CD8+ effector T cells and CD4+ T cells, reducing helper T-cell activity and Tregs enhancing their immune suppression capabilities (Buchbinder and Desai, 2016).

PD1 limits T cell activity, and expression increases once cells are activated. PD1 is expressed on tumour lymphocytes, including Tregs, in many solid organ tumours (Li et al., 2022). Increased Tregs are found in many tumours, and blockade of the PD1 pathway will suppress their function. The ligands for PD1 are PDL1 and PD2. PD1 can also be found on activated B cells and NK cells; blockade of PD1 enhances effector T-cell and NK cell activity, and antibody production. In cancer and viral hepatitis high levels of PD1 expression are found, which leads to the exhaustion of

antigen-specific T cells and PD1 blockade reduces this (Feray and Lopez-Labrador, 2019, Lee et al., 2015).

PD1 expression on CD8+ T cells is reported to be a marker of their exhausted state in tumours (Ahmadzadeh et al., 2009). PD1 ligands are commonly upregulated on the tumour cell surface. PD1 blockade can enhance the effector functions of lymphocytes in the tumour micro-environment because lymphocyte function is inhibited when PD1 encounters its ligand PDL1. It should be noted that PDL1 expression in HCC tumours is associated with a worse overall survival (Gao et al., 2009). Two mechanisms are thought to increase the expression of PDL1 in tumours; one is a response to IFNγ, and the second is aberrant oncogenic signalling pathways (Cha et al., 2019). The overall effect is that up-regulation of PDL1 leads to inhibitory receptors being engaged in lymphocytes and creating an immunosuppressive environment. Hopefully, we will see more therapeutic opportunities and the potential for multiple blockades of these immunosuppressive checkpoints in the coming years. It seems logical that PD1 pathway blockade will only be useful in tumours expressing high levels of PDL1. The principle mechanism of action of CTLA4 and PD1 is illustrated in **Figure 7**.

A)



B)

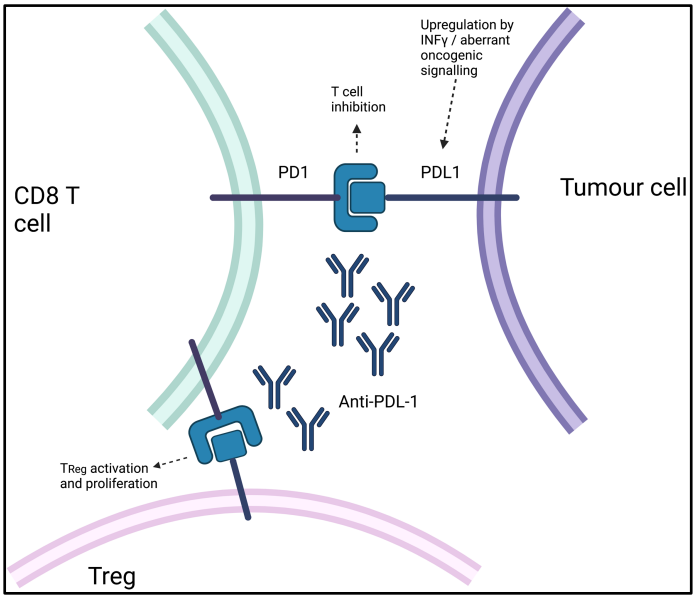


Figure 7. Main mechanisms for CTLA4 and PD1 inhibiting T cell responses.

A) The MHC-antigen complex activates the TCR. Co-stimulation by CD28 bound to one of its ligands is required for activation. The same ligands can also bind CTLA4, which inhibits T cell responses and CTLA4 possesses a higher affinity for these ligands than CD28. Immunotherapy targeting CTLA4 enhances T cell activity.

B) PD1 is highly expressed on tumour lymphocytes. Its ligand PDL1 is upregulated on many tumour cells and engagement supresses T cell function. PD1 is highly expressed on Tregs and in the presence of its ligands can be activated inhibiting immune responses. Anti-PDL1 can therefore enhance CD8 T cell activity and reduce the effects of immunosuppressive Tregs.

The role of B cells is not fully understood, but it is hypothesised that the proximity of T cells and B cells in HCC tumours has functional significance and may control the growth of tumours (Garnelo et al., 2017). The evidence is conflicting, but a study by Zhang et al. supported the idea that increased B cells have an anti-tumour effect and B cells correlate with improved survival (Zhang et al., 2019b). However, in one murine study infiltrating B cells correlated with more aggressive tumours and poor outcomes(Faggioli et al., 2018).

1.4.4.3 Chemokines in the HCC Microenvironment

Chemokines make an important contribution to hepatocellular carcinoma progression and influence angiogenesis, leucocyte trafficking and the expansion of tumour cells. A summary of some of the important chemokines in HCC and their contributions is shown in **Figure 8**.

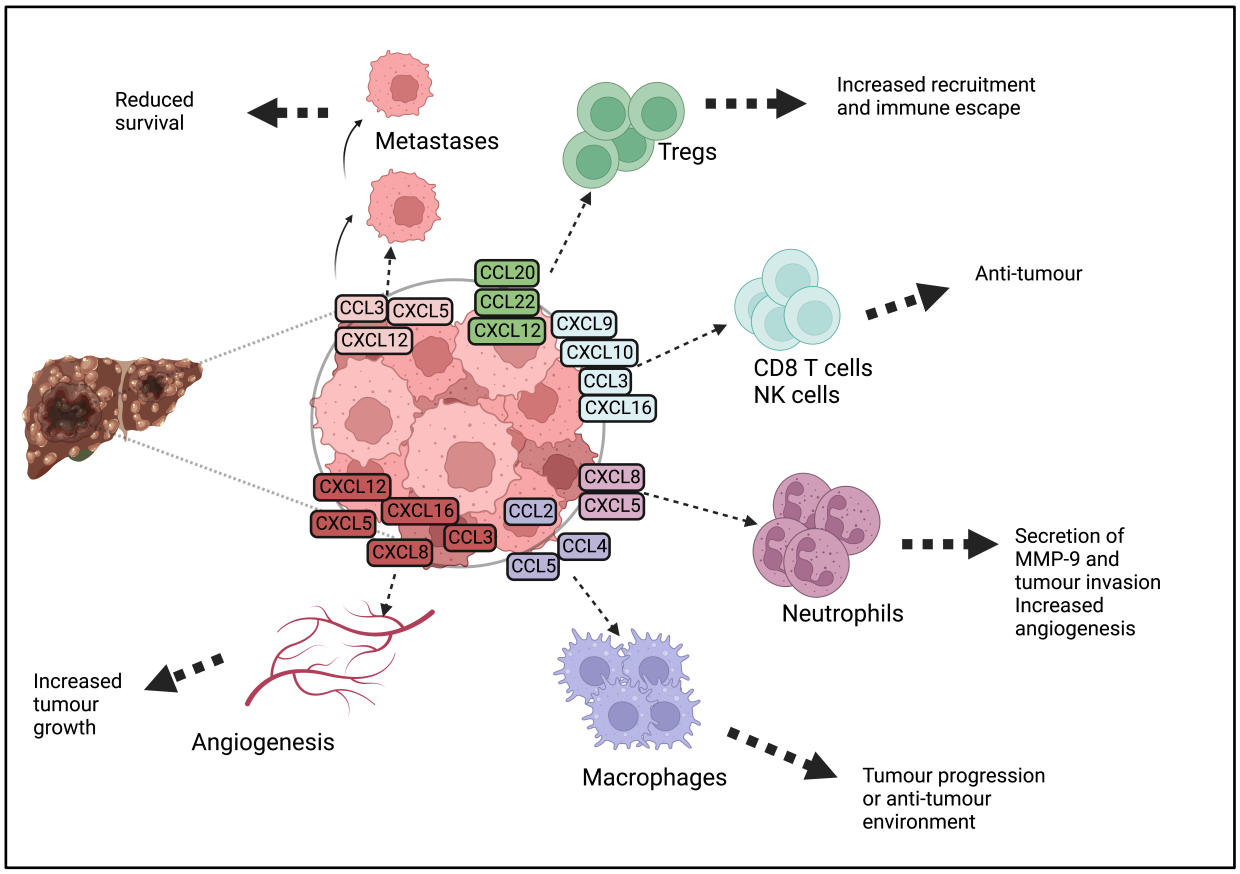


Figure 8. Chemokines in HCC.

Chemokines in HCC can regulate leucocyte trafficking, which in the case of T cells and NK cells, has an anti-tumour effect. The recruitment of regulatory T cells leads to immune evasion and tumour progression. Recruited macrophages can lead to an anti-tumour environment or facilitate immune evasion. Neutrophils secrete MMP-9, and this promotes tumour invasion and angiogenesis. Chemokines can also contribute directly to the behaviour of tumour cells, promoting metastases. (Adapted from (Marra and Tacke, 2014), incorporating (Ghanem et al., 2014, Liang et al., 2015, Xiong et al., 2022, Xue et al., 2021, Zhang et al., 2016, Nie et al., 2021, Yuan et al., 2010).

1.5 Angiogenesis

1.5.1 Normal angiogenesis

Angiogenesis is the expansion and remodelling of the vascular network. Normal vasculature is usually quiescent in adults but is transiently active and considered a normal physiological process, such as wound healing or female reproductive

cycles. It should be a structured and tightly regulated process that balances pro-angiogenic and anti-angiogenic factors. Factors secreted include Vascular Endothelial Growth Factor (VEGF), Fibroblast Growth Factor (FGF), angiopoietins (Ang) and Platelet-Derived Growth Factor (PDGF). Two examples of pathological angiogenesis are diabetic retinopathy and solid organ tumours. Tumours continually sprout vessels to support the growth of tumours, and the process of angiogenesis is continually 'switched on' (Hanahan and Folkman, 1996). Hypoxia-inducible factor-1α (HIF-1α) regulates the expression and release of vascular endothelial growth factor (VEGF-A), initiating the angiogenesis process (Saponaro et al., 2013). Therefore, the proangiogenic growth factor VEGF-A is secreted in response to a hypoxic environment. Endothelial cells exposed to high concentrations of VEGF-A become tip cells, leading the developing sprout through the ECM. Filopodia, which extend from tip cells, secrete proteolytic enzymes to create a pathway through the ECM, and filopodia possess VEGF-A receptors (VEGFR2) which facilitate alignment with the VEGF-A gradient (Gerhardt et al., 2003). The contraction of actin in filopodia directs the tip cell towards the stimulus. Cells proliferate behind a tip cell endothelial stalk to form a capillary, enabling the capillary sprout to elongate. Tip cells from two or more sprouts can converge and fuse, creating a continuous lumen through which blood can flow. For the capillaries to be stable ECM is deposited, and pericytes are recruited (Adair and Montani, 2010). This process is summarised in **Figure 9**.

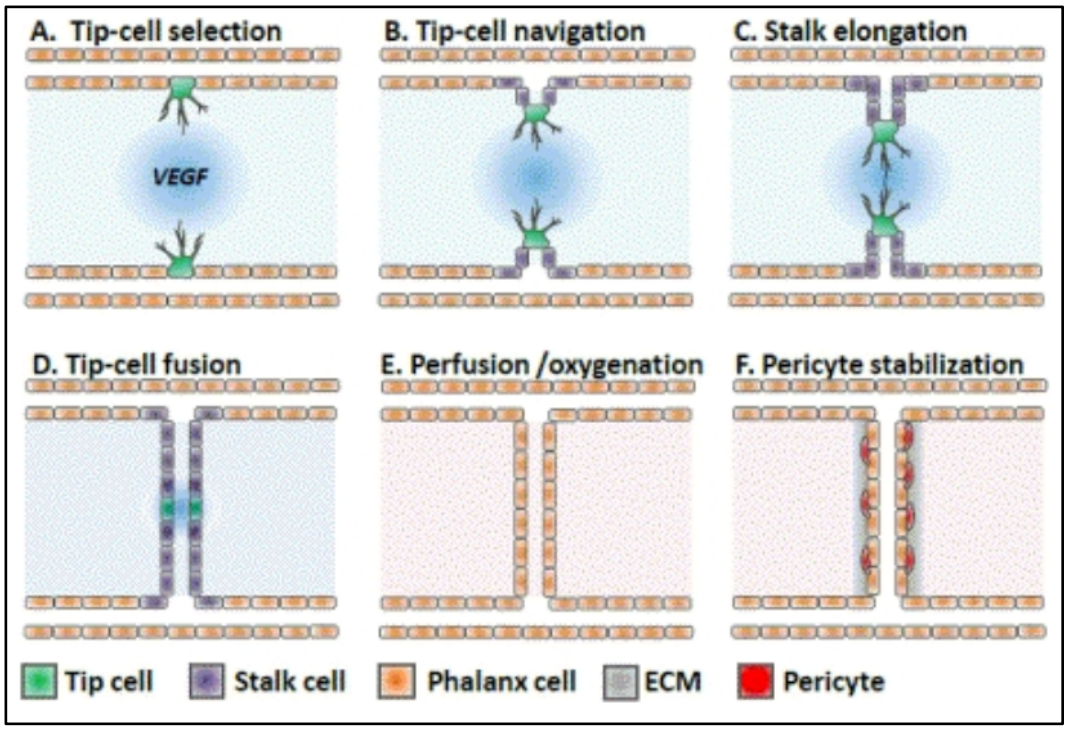


Figure 9. Angiogenesis.

VEGF secretion in response to hypoxia initiates endothelial cells to become tip cells (A) which sprout and elongate (B/C). Tips cells then fuse, generating a lumen for blood flow (D/E). Pericytes then stabilise the newly formed vessel (F). (Taken from Adair and Montani, 2010)

1.5.2 Angiogenesis in liver disease

Endothelial cells will proliferate when exposed to specific growth factors. These can be secreted from endothelial cells or other cells in the microenvironment, including leucocytes, HSCs and hepatocytes. This is predominantly through VEGF. The VEGF promotor contains hypoxia-inducible factors (HIFs), and we know that hypoxia and inflammation are the main drivers of pathological angiogenesis (Ramakrishnan et al., 2014). In inflammation, vascular permeability increases and many leucocytes are recruited via chemokines.

Liver fibrosis is associated with pathological angiogenesis and sinusoidal remodelling. Hypoxia is a common finding as fibrosis progresses, as fibrotic septa and capillarisation of the sinusoids impair oxygen diffusion. This hypoxia, along with HIFs, acts as a pro-angiogenic stimulus. However, pathological angiogenesis and immaturity of vessels can disrupt standard tissue repair, and fibrosis progresses (Zhang et al., 2015). Activated HSCs promote angiogenesis by producing VEGF and angiopoietin-1, and blocking these reduce the fibrosis (Taura et al., 2008, Yoshiji et al., 2003). CCXCL8, CXCL9, CXCL10 and CXCL12, which can also stimulate angiogenesis in liver fibrosis, are also produced by HSCs (Strieter et al., 2005).

Monocyte-derived macrophages can propagate hepatic inflammation and fibrosis. These CCL-2-dependent infiltrating macrophages have been shown to promote angiogenesis (Ehling et al., 2014). HSCs in hypoxia conditions also regulate angiogenesis by increased production of VEGF (Dirscherl et al., 2020).

Examples of pathological angiogenesis are in viral hepatitis C, where there is increased expression of VEGF and HGF and increased Nitric oxide (NO), leading to vasodilatation. Increases in HGF can lead to a decrease in VE-cadherin important for intercellular contacts. A study by Xalcedo et al. compared patients with and without HCV and found an association with severity of inflammation and the level of VEGF in the serum providing a link with angiogenesis (Salcedo et al., 2005). In PBC it has also been observed that there is increased expression of VEGF, Ang-1, Ang-2 and their receptors; and in AIH new vessels were observed in inflamed portal tracts (Medina et al., 2005).

1.5.3 Tumour angiogenesis

For a tumour to grow, it requires active proliferation and the availability of nutrients, oxygen and the removal of waste products to support this. Tumours, therefore, require a blood supply and it is proposed that in the initial stages this is via existing vasculature (Donnem et al., 2013). Then cells promote pathological blood supply to support aberrantly proliferating tumour cells. Tumour vessels are structurally distinct from normal blood vessels; they are disordered and lack an intact basement membrane (Sund et al., 2004) .

Judah Folkman published in 1971 that tumour growth is angiogenesis-dependent (Folkman, 1985). Although it was back in 1794 that John Hunter suggested that vascularity and metabolic requirements are proportional (Adair and Montani, 2010). It has been shown that neovascularisation must occur for a tumour to grow beyond 2-3 mm (Gimbrone et al., 1972). Vessel structure is different in tumours when compared to healthy tissues. A disordered network of fragile vessels develops, and vessel diameters can vary along with the width of the junctions (Helmlinger et al., 1997). The mural cell coverage of endothelial cells in tumours has also been observed to differ depending on the tumour type. It is reported that tumour-associated pericytes have a role in stabilising vessels; in other reports, they are seen to be more loosely attached, making vessels leakier (Jain, 2003). The role of these tumour-associated pericytes and pericyte-like cells around tumour endothelial cells and their origin and function has yet to be fully understood. There has been debate over the presence of pericytes in abnormal tumour vasculature,

but it is now believed that they are present but loosely associated in most tumours (Raza et al., 2010).

Anti-angiogenic therapy is one of the systemic treatments available for the highly vascular tumour HCC. VEGF is the most well-known angiogenic factor. VEGF is very important in tumour angiogenesis as well as normal angiogenesis. Many tumours secrete VEGF, which has been associated with increased density of blood vessels in tumours (Brodsky et al., 2007). VEGF-A is important for angiogenesis and binds to VEGFR 1, 2 and 3; Bevacizumab is a VEGF-A antibody used in the treatment of cancer. VEGF gene expression can be upregulated by hypoxia and oncogene signalling. VEGF ligands can be sequestered in the extracellular matrix and released by degrading proteases (Kessenbrock et al., 2010). VEGF inhibition limits angiogenesis and reduces tumour growth (Borgstrom et al., 1996). Tumours can be poorly vascularised, and necrotic areas develop from poor oxygenation. It has been found that levels of VEGF are increased by hypoxia in HCC cells, and in tissue samples, levels were highest adjacent to necrotic areas (von Marschall et al., 2001). VEGF also increases vascular permeability (Kohn et al., 1992), which is advantageous to tumour cells facilitating dissemination.

Fibroblast growth factors 1,2,4 and 8 have been researched for their role in angiogenesis in HCC. FGF2 is the one that has been most studied and promotes angiogenesis, and it can upregulate VEGF in murine models (Yoshiji et al., 2002). It has been shown that FGF2 overexpression leads to increased tumour growth. This can be suppressed by a VEGFR2 monoclonal antibody implying the effects of FGF2 are mediated by its effects on VEGF (Yoshiji et al., 2002). FGFs bind to

heparin sulfate and it's binding sites of FGFR and activate intracellular tyrosine kinases (Loo et al., 2001). Heparinase also promotes angiogenesis by directly stimulating endothelial cells and mediating the release of heparin sulfate-bound bFGF from the ECM (Vlodavsky et al., 2000). Heparinase induces endothelial invasion and is associated with developing metastases (Vlodavsky et al., 2006).

Angiopoietins (Ang), important in normal angiogenesis, have also been implicated in tumour angiogenesis. Ang-1 stabilises new vessels and Ang-2 antagonises Ang-1 (Maisonpierre et al., 1997). Ang-2 increases in tumour vessels compared to normal blood vessels and contributes to vessel weakness (Moon et al., 2003). Ang proteins interact with Tie receptors (also tyrosine kinase receptors), and over-expression of Ang-2 compared to Ang-1 has been found in HCC (Mitsuhashi et al., 2003).

The PDGF/PDGFR complex is important in tumour induced angiogenesis (Raica and Cimpean, 2010), and it has been suggested that Neuropilin-1 (NRP-1), which co-localises with PDGF receptor-ß, promotes HCC progression (Xu et al., 2018).

It is no wonder that antiangiogenic therapy has been important in the repertoire of anti-cancer research and treatment regimens. Anti-angiogenic therapy may act by destroying tumour blood vessels and, therefore, leads to shrinkage of the tumour. Another theory is that it normalises tumour vessels (Jain, 2005). The rationale for combining immunotherapy with an anti-angiogenic therapy is that reducing tumour vasculature and creating hypoxia in the tumour leads to increased PD-L1, suppressing immune responses and, therefore, combined with

immune checkpoint therapy is advantageous. A summary of positive phase 3 trials of anti-angiogenic therapy in HCC is shown in **Table 7.**

Drug	Indication	Mechanism of action	Clinical Trials	Date of FDA approval	Date of NICE approval
Sorafenib	Unresectable HCC	Multi-kinase inhibitor targeting VEGFRs, PDGFR and Raf kinases.	SHARP trial and Asia-Pacific trial	2007	2017
Levatinib	Unresectable HCC	Multi-kinase inhibition of VEGFRs, FGFRs, RET, KIT and PDGFR.	REFLECT trial 2018	2018	2018
Regorafenib	HCC previously treated with Sorafenib	Tyrosine kinase inhibitor targeting VEGFRs, Tie-2, PDGFß, FGFRs and RET.	RESORCE trial 2017	2017	2018
Cabozantinib	HCC previously treated with Sorafenib	Tyrosine kinase inhibitor targeting MET, AXL and VEGFR-2	CELESTIAL trial 2018	2019	2022
Ramucirumab	HCC previously treated with Sorafenib	Monoclonal antibody blocking the action of	REACH-2 trial 2019	2019	N/A

	and AFP >400	VEGFR-2 inhibiting the VEGF axis			
Bevacizumab (In combination with Atezolizumab)	Unresectable HCC with no prior systemic treatment	Monoclonal antibody that blocks VEGF-A. (Used in combination with an anti-PD-L1 antibody)	IMbrave150 trial 2020	2020	2020

Table 7. Anti-angiogenic therapy for HCC. Anti-angiogenic therapies with positive Phase III trial results for HCC, including indication for use, main mechanism of action, the landmark clinical trial and dates of FDA and NICE approval. Adapted from (Moawad et al., 2020) (Zhu et al., 2020).

1.6 Leucocyte recruitment

The endothelium has an important role in modulating immune cell recruitment. In tumours, it has been established that the recruitment of high numbers of TILs correlates with better outcomes (Fridman et al., 2012). Immune cells are recruited into tissues from blood vessels. It is a multi-step, finely regulated process that includes the phases of rolling, activation, adhesion, crawling, and migration of immune cells (Ley et al., 2007) . Migration to the periphery must then negotiate endothelial, pericyte and basement membrane barriers (Barreiro et al., 2002).

As previously discussed, immune cells play essential roles in normal and pathological states. Recruiting immune cells to the site where they are required involves interactions between the individual leucocyte and the endothelial cell layer. This section discusses the mechanism of adhesion and migration through

the endothelium, the roles other cells play in recruiting leucocytes to their destination in general and then specific to the liver environment.

1.6.1 Classical leucocyte adhesion cascade

Leucocyte recruitment is a sequence of steps (**Figure 10**) facilitated by multiple adhesion molecules expressed on the surface of endothelial cells and ligands expressed by the migrating cells. The changes in endothelial cells depend on the circumstances and microenvironment that lead them to mediate recruitment actively. The term 'activated endothelium' describes the primed endothelium for this purpose. The stimuli for this activation include proinflammatory cytokines or bacterial endotoxins; examples include TNF-α, IL-1ß, IFNγ and lipopolysaccharides (Hunt and Jurd, 1998). Without this stimulation, the endothelium is not adhesive. A multi-step cascade process can be generalised for most leucocytes, **Figure 10**. Leucocyte interaction with the endothelium was first described in the nineteenth century by Dutrochet and Wagner (Dutrochet, 1824, Wagner, 1839). Still, the mechanisms facilitating this process have only been described and expanded in the last few decades. Key mediators include integrins, selectins, chemokines, and their receptors.

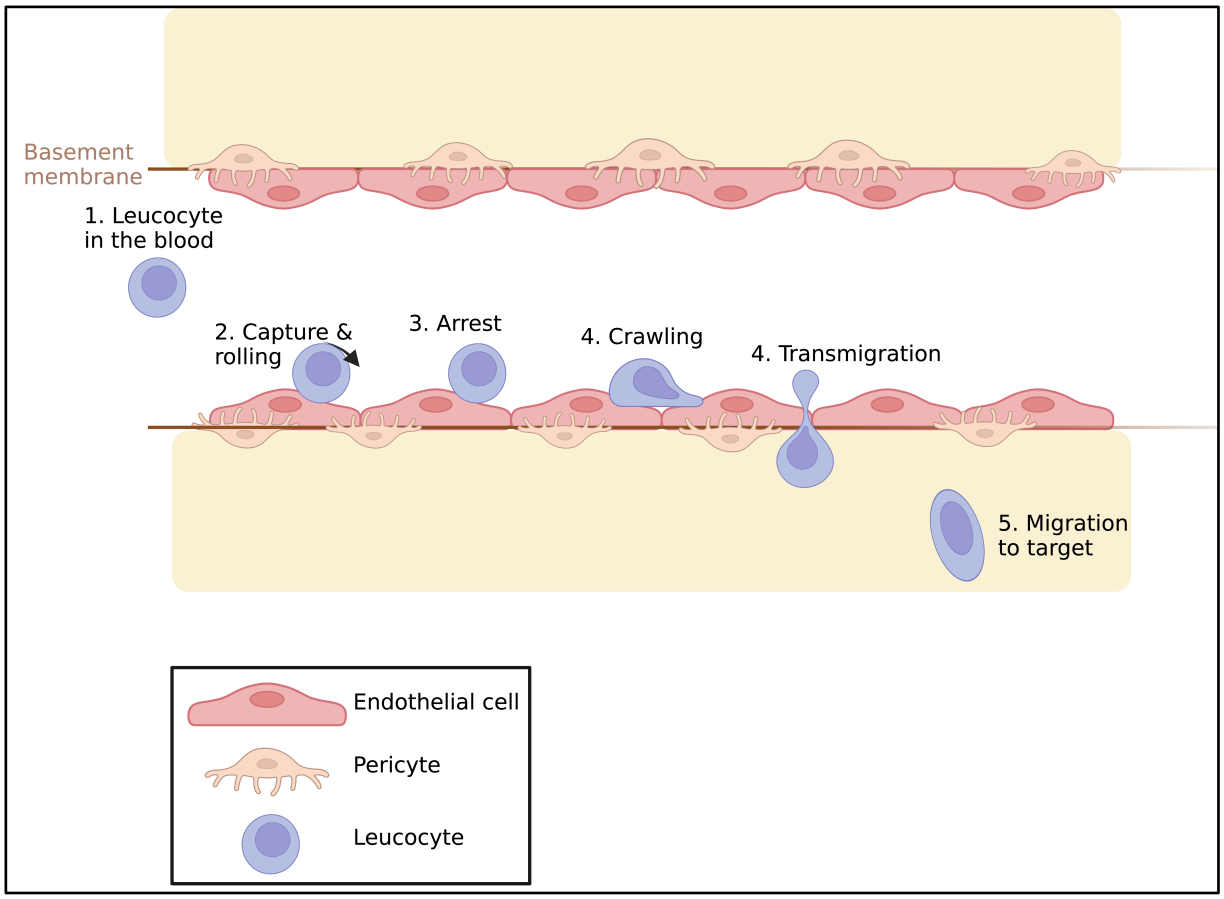


Figure 10. The leucocyte adhesion cascade.

1) Leucocytes in the blood are captured by activated endothelium and express adhesion molecules. 2) Leucocyte rolling is mediated by the expression of selectin ligands. 3) Arrest and firm adhesion are induced when integrins on the leukocyte bind to Intercellular adhesion molecule – 1 (ICAM-1) on the activated endothelium. 4) Further integrin-mediated adhesion strengthening and spreading and crawling followed by transmigration which can be paracellular or transcellular. 5) Cells then migrate into the tissue

1.6.1.1 Rolling

Leucocytes flowing in the blood initially slow, termed rolling, by tethering to the endothelium. L-selectin, P-selectin and E-selectin mediate rolling, endothelial cells express E-selectin and P-selectin once stimulated, and leucocytes express L-selectin. Adhesion and rolling steps are mediated by E and P selectins on the endothelium and their leucocyte receptors; L-selectin, P-selectin glycoprotein ligand-1 (PSGL-1), CD44, CD43 and E-selectin (Zarbock et al., 2011). This rolling step is reversible; cells can detach and continue in the blood flow unless the rolling is followed by arrest. PSGL-1 is a ligand for all three selectins, and PSGL-1 interaction with L-selectin allows adherent leucocytes to capture further leucocytes. It has been shown that rolling cells detach when flow ceases because L-selectin and P-selectin require a shear stress (Finger et al., 1996, Lawrence et al., 1997). The rolling nature of the cell is because of bonds forming and then being broken.

Integrins also have a role in rolling as well as mediating firm adhesion. Cell lines expressing α4ß7 integrin roll on recombinant Mucosal vascular adhesion cell adhesion molecule-1 (MADCAM1) (Berlin et al., 1995) and lymphocytes can roll on recombinant Vascular cell adhesion molecule-1 (VCAM-1) via α4ß1 (VLA4) integrin (Alon et al., 1995). VLA4-dependent rolling is particularly important for monocytes and T cells. In murine models, activated endothelial cells expressed E-selectin and increased ICAM-1, leading to a slow rolling (Kunkel and Ley, 1996).

Secondary capture is when adherent leucocytes facilitate the capture of other leucocytes, and you see the rolling of several cells in a line mediated by PSGL and L-selectin (Alon et al., 1996).

1.6.1.2 Adhesion

Integrins are important for leucocyte adhesion. The $ß_2$ integrin family consists of different heterodimers, each with a common ß subunit and a distinct α subunit and ligand; Lymphocyte function-associated antigen-1 (LFA-1) ($\alpha_L ß_2$), and Macrophage-1 antigen (Mac-1) ($\alpha_M ß_2$) are common examples. B2 integrins are exclusive to leucocytes, but they have different expression patterns. LFA-1 is expressed on all leucocytes, and Mac-1 is expressed mainly on myeloid cells. LFA-1 binds limited ligands such as ICAM 1-5, but Mac-1 can bind at least 40 different ligands, including ICAMs (Fagerholm et al., 2019).

VCAM-1, on the endothelium, is activated in the presence of pro-inflammatory signals, and it recognises leukocyte VLA4 and α4ß7 integrins mediating adhesion. ICAM-1 is expressed on endothelium and leucocytes, and inflammatory mediators increase levels. ICAM-1 binds to leucocyte integrins and can bind to LFA-1 and Mac-1 (Ala et al., 2003). Stable adhesion is when the leucocytes arrest on the endothelium, followed by flattening.

In an inflammatory setting, cytokines activate the endothelium to express adhesion molecules, and the endothelium also produces chemokines. Chemokines promote leucocyte arrest from the rolling state, promoting integrin conformational changes and increasing affinity, and leucocyte integrins then bind to ICAM1 or

VCAM1 on endothelial cells. Chemokine signalling can regulate distinct integrins in specific leucocyte populations, assisting specific interactions (Mitroulis et al., 2015).

1.6.1.3 Crawling and trans-endothelial migration

Leucocytes can crawl on the endothelium and then begin the migration process through the endothelium. Crawling relies on leucocyte ß1 and ß2 integrins binding to ICAM-1 and VCAM-1, respectively. Neutrophils and monocytes crawl along the endothelium via MAC-1 and ICAM-1 until they reach preferred sites for paracellular transmigration. If crawling is inhibited, cells may travel transcellular instead of paracellular (Phillipson et al., 2006). Once adhered, transmigratory cups have been observed, which are rich in ICAM-1 and VCAM-1. In inflammation, endothelial cells can alter how junctional molecules function to favour migration; for example, VE-cadherin may be reduced at the site. Molecules which may actively promote migration include Platelet and endothelial cell adhesion molecule-1 (PECAM-1), ICAM-1, ICAM-2, Endothelial cell adhesion molecule (ESAM) and junctional adhesion molecules (JAMS). The endothelial-cell junctional molecule ESAM appears to mediate neutrophil rather than T-cell migration (Wegmann et al., 2006).

1.6.1.4 Complete transmigration

Complete transmigration is most commonly via the paracellular route but can also be via the transcellular route. Transcellular migration of leucocytes is via

membrane protrusions into endothelial cells (Muller, 2011). Once migrated through the endothelial cell layer, cells must penetrate the basement layer and pericyte sheath.

1.6.2 Recruitment via liver sinusoidal cells

The classical leucocyte recruitment cascade applies to some micro vasculatures, including skeletal muscle, skin and mesentery. Still, the recruitment mechanism in hepatic sinusoidal vasculature is distinct in structure and functionality. Many experimental models looking at the recruitment cascade in vitro use HUVEC stimulated mainly with TNFα and then perfused with leucocytes; neutrophils are commonly used in many studies. Intravital microscopy has changed opinions on some of the initial recruitment mechanisms in the liver. For example, it was observed that in the sinusoids, adhesion could occur without the observation of rolling, and it can be independent of selectins (Wong et al., 1997).

In the liver, 50% of lymphocytes in an in vitro study took the transcellular route (Shetty et al., 2011). Intracellular crawling has also been noted by this group, where lymphocytes crawl from within one endothelial cell into another endothelial cell under the influence of INFγ (Patten et al., 2017).

There are several chemokines in the liver endothelium relevant to chronic liver diseases. For leucocyte adhesion, chemokines and chemoattractants on the endothelium are important, particularly CC and CXC chemokines and their sinusoid receptors (Oo et al., 2010).

As previously described, the liver microvasculature is unique and is composed of fenestrated endothelium. In the liver sinusoids, some lymphocytes are recruited by classical integrin pathways; others use non-classical, i.e., non-integrin mechanisms. The low shear flow within hepatic sinusoids means reduced selectin-dependent attachment and rolling (Wilkinson et al., 2020). Therefore, this specialised endothelium has different adhesion molecules than non-liver postcapillary venules. There is less E-selectin, P-selectin and VCAM-1 but high ICAM-1 and VAP-1. The leucocyte adhesion cascade has been described in many organs and endothelial types. In liver disease, non-classical molecules are important in leucocyte recruitment; these examples are now discussed.

VAP-1 is one example that facilitates adhesions and migration and is upregulated in inflamed livers. VAP-1 is expressed by endothelial cells and facilitates lymphocyte recruitment, and it can be upregulated in response to inflammation (McNab et al., 1996). Activation of VAP-1 leads to escalated expression of inflammatory proteins such as CXCL8 and ICAM-1, increasing lymphocyte adhesion. This phenomenon has been observed using endothelial cells from the liver but not in HUVEC (Lalor et al., 2007).

We also see the importance of scavenger receptors for leucocyte adhesion in the liver (Patten and Shetty, 2018); an example is Stabilin-1 which is involved in Treg recruitment across sinusoidal endothelium. Stabilin-1 is upregulated in LSEC in the presence of HGF (Shetty et al., 2011).

CD44 is found in many cell types, and activated lymphocytes increase the expression of CD44 and can then adhere to endothelium. The ligand is hyaluronan

(HA), and activated T cells have been shown to roll on HA-coated plates (DeGrendele et al., 1996). Neutrophils express a lot of CD44, and mice lacking CD44 on neutrophils could not recruit neutrophils (Mohamadzadeh et al., 1998). Sinusoidal endothelial cells express other receptors for HA, including stabilin-2 (Falkowski et al., 2003).

In many vascular beds, the ß2 integrin is important for the firm adhesion of many leucocytes. This is not believed to be as critical in liver sinusoids but is in post-sinusoidal venules. One group showed that TNFα mediated adhesion was dependent on ICAM-1 in post-sinusoidal vessels, but this was not apparent in sinusoids. In contrast, Il-1 mediated adhesion depended on ICAM in both situations (Patrick et al., 2007).

1.6.3 Leucocyte recruitment in HCC

The endothelial cell phenotype also plays a critical role in leucocyte recruitment in the tumour microenvironment. There is evidence that endothelial cells adapt according to their microenvironment and display plasticity. A study on Murine HCC endothelial cells demonstrated that the cells were capable of reverting to a more 'normal' phenotype when isolated and incubated in vitro (Salnikova et al., 2013).

In HCC, there is a well described CD8+, CD68+,FoxP3+ infiltrate, and high expression of PD-L1 on LSEC correlates with CD8+ T cells and survival (Ihling et al., 2019). The distinct immune populations found within HCC are likely the result of interactions between circulating leucocytes and the different endothelium found

in HCC. Yoong et al. showed that HCC contains more T cells than colorectal metastases in the liver. They also found that ICAM-1 and VAP-1 on tumour endothelium in HCC were highly expressed and that T cells bound readily to HCC endothelium but not the endothelium found in colorectal metastases (Yoong et al., 1998).

The molecules expressed by LSEC are, therefore, critical in determining the nature of the immune microenvironment of the liver and highlight the active role of LSEC in liver inflammation, acute disease, chronic liver disease and HCC.

1.7 Tumour endothelial markers

1.7.1 Tumour endothelial markers in hepatocellular carcinoma

Cancer cells proliferate, and hypoxaemia develops if insufficient oxygen supports continued growth. Therefore many angiogenic factors are upregulated. Examples include HIF, VEGFA, PDGF and Ang2, which facilitate the angiogenic switch to the 'on' position (Carmeliet and Jain, 2000). As previously discussed, endothelial cells are generally quiescent. In the presence of angiogenic signals from an environment of hypoxaemia, endothelial cells become activated. They are also influenced by inflammation, for example, TNF and interleukins, to facilitate immune cell trafficking. It has been previously reported that they can return to quiescence once the activation stimulus has been removed, and therefore, they are functionally plastic. Some specific genes are unique and upregulated in endothelial cells found in tumours, tumour endothelial markers (St Croix et al., 2000). We also know that the adhesion molecules on endothelial cells are different in tumours

compared to healthy organs, and tumour endothelial cells have been noted to up-regulate stem cell markers CD34, CD61, and CD105 (Sievert et al., 2014).

1.7.2 Targeting the tumour vasculature

It is accepted that anti-cancer targets should not be restricted to targeting the tumour cells but that targeting the tumour microenvironment can also be effective. When looking at targets in tumours, it is vital to understand the expression and function of any prospective candidates outside the tumour, which may predispose to side effects.

1.8 C-type lectin domain group 14 family

There is a superfamily of proteins containing C-type lectin-like domains (CTLDs). A loop-in loop structure characterises the CTLD, and a second-long loop is involved in the Ca2+-dependent carbohydrate binding (Zelensky and Gready, 2005). The type 14 C-type lectin family has 4 members: CLEC14A, CD93, CD248 and thrombomodulin. All 4 members have been linked to blood vessels (Zhuang et al., 2011).

1.8.1 CLEC14A and interaction with MMRN2

CLEC14A is a 490 amino acid transmembrane protein. CLEC14A is over-expressed by tumour endothelium, regulates sprouting angiogenesis (Noy et al., 2015), mediates endothelial cell-to-cell adhesion (Rho et al., 2011), and is localised at the cell membrane. Filopodia extensions are observed when CLEC14A is overexpressed in human embryonic kidney 293 T cells (HEK293T) (Bocci et al.,

2019). The ligand for CLEC14A has been identified as MMRN2, confirmed using SILAC based proteomics (Zanivan et al., 2013). A monoclonal antibody raised against CLEC14A, blocked CLEC14A-MMRN2 binding and inhibited endothelial tube formation and sprouting (Noy et al., 2015). Multiple tissue microarrays have previously shown CLEC14A overexpression on tumour vessels in multiple solid tumours, including HCC (Mura et al., 2012). CLEC14A is also cleaved and can be detected in the serum. This utility is yet to be explored using CLEC14A as a biological marker of tumour behaviour, responses to treatment and outcomes. CLEC14A is cleaved by rhomboid-like protein 2 (RHBDL2), and this shedding inhibits angiogenesis (Noy et al., 2016). It is postulated that this may form part of a regulatory mechanism where cleaved CLEC14A competes for MMRN2 with cell membrane-bound CLEC14A limiting endothelial cell migration and sprouting.

MMRN2 (Endoglyx-1) is found along blood vessels close to endothelial cells in normal and tumour vasculature and contributes to blood vessel homeostasis (Lorenzon et al., 2012). Levels have been shown to increase in tumour angiogenesis, and overexpression leads to decreased pericyte coverage in tumour vessels (Lorenzon et al., 2012). Soluble MMRN2 has antiangiogenic activity (Noy et al., 2016), and in vivo, overexpression halted the development of tumour-associated vessels and impaired tumour growth (Colladel et al., 2016). However, the function of MMRN2 and its mechanism of action has not been extensively studied. We know that MMRN2 is also the ligand for CD248 and VEGF (Khan et al., 2017, Colladel et al., 2016), but the significance is yet to be elucidated; however, it may be that MMRN2 is playing a regulatory role in tumour angiogenesis.

Khan et al. identified that the extracellular matrix protein MMRN2 and CLEC14A are expressed by endothelial cells only, while CD248 expression is limited to stromal pericytes and fibroblasts. All three are upregulated in the tumour microenvironment. Previous studies have focused on blocking the CLEC14A-MMRN2 interaction even though CLEC14 and CD248 can bind MMRN2 simultaneously (**Figure 11**).

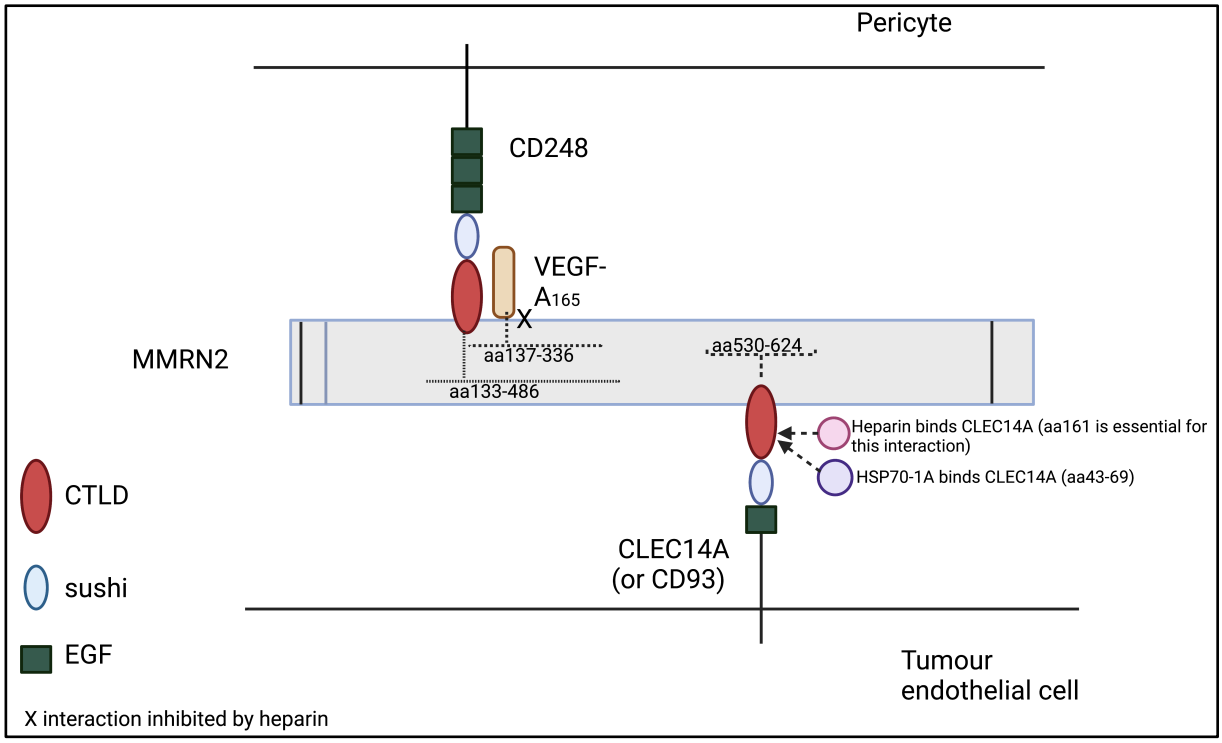


Figure 11. CLEC14A-MMRN2-CD248 interaction. Multimerin is a ligand for CD248, CLEC14A, CD93 and VEGF-A$_{165}$. CLEC14A is also capable of binding Heparin and HSP70-1A. Adapted from ((Khan et al., 2017, Colladel et al., 2016, Sandoval et al., 2020).

Interestingly it has also been demonstrated that VEGF binds to MMRN2, adding another layer to this angiogenic signature (Colladel et al., 2016). However, the

significance of these interactions and how they impact on each other to date is not fully understood.

1.8.2 CD93

The predominant site for CD93 expression is on the endothelium and it has been demonstrated to be one of the key regulators in tumour angiogenesis in a range of solid organ tumours (Masiero et al., 2013). CD93 has also been found to be expressed on neutrophils, monocytes and stem cells, and it can be shed, and a soluble form of the ectodomain has been detected in human serum (Bohlson et al., 2005). CD93 has been described as having anti-inflammatory effects. In a mouse model of peritonitis, there was an increase in neutrophil and monocyte infiltration in the $CD93^{-/-}$ mice and a reduced vascular integrity (Greenlee-Wacker et al., 2011). In a pancreatic ductal adenocarcinoma mouse model, blockade of CD93 normalises vasculature and improves immunotherapy responses. The study also looked at the effect of CD93 blockade on immune cell infiltration and found increases in CD4+, CD8+ T cells and increased NK and NKT cells in the tumours but a reduction in MDSCs (Sun et al., 2021).

Interestingly inflammatory mediators, TNF and LPS, have been shown to promote monocyte CD93 cleavage (Bohlson et al., 2005).

1.8.3 CD248

CD248 (also known as TEM1 or Endosialin) was historically thought to be expressed by endothelial cells, but this is now known to be inaccurate, and tumour-associated pericytes and fibroblasts express it. CD248 is minimally expressed in healthy tissues (Lax et al., 2007). CD248 is increased in pericytes during active angiogenesis and tumour development (Bagley et al., 2008). It is increasingly recognised that fibroblasts and pericytes are essential components of the tumour microenvironment, but our knowledge is still evolving. It has been shown that tumour-associated fibroblasts affect migration and the invasion of tumour cells (Boire et al., 2005, Christian et al., 2008). It is suggested that CD248 leads to dynamic vascular remodelling, and it has been observed in the CD248 knockout that the quantity of small vessels is increased. However, invasiveness is reduced, and fewer metastases are seen (Nanda et al., 2006). A phase one study of a CD248 monoclonal antibody showed that tumour stability was observed in 56% of patients (Diaz et al., 2015), although the mechanism has not been fully elucidated. Our knowledge to date all points to a critical role for CD248 expressing primary tumour pericytes and fibroblasts in facilitating metastatic dissemination and supports CD248 as a promising therapeutic target (Viski et al., 2016).

1.8.4 Thrombomodulin

Thrombomodulin is found predominantly on vascular endothelium and is a natural anti-coagulant factor preventing thrombosis. It has also been found to be

expressed by platelets, monocytes, macrophages and neutrophils (Conway et al., 1992). Thrombomodulin has been shown to have anti-inflammatory activity (Conway et al., 2002) and soluble thrombomodulin has been detected in human serum (Zycinska et al., 2009).

1.9 Hypothesis and aims

This thesis was to test the hypothesis that CLEC14A is involved in angiogenesis and modulates the immune microenvironment in chronic liver disease and HCC.

Aims

1) Describe the expression of CLEC14A in normal liver tissue, cirrhosis and HCC.
2) Identify what regulates the expression of CLEC14A in hepatic sinusoidal endothelial cells.
3) Determine if CLEC14A influences angiogenesis in the hepatic sinusoidal endothelium.
4) Investigate if CLEC14A affects the recruitment of leucocytes across HSEC

2

2 Materials and Methods

2.1 Human liver tissue and serum

I obtained liver tissue from tumour resections or diseased livers from the liver transplant programme or from donor tissue that was not utilised. Tissue and serum was obtained with prior patient consent and with ethical approval in place. REC reference 06/Q2702/61 and 06/Q2707/182.

2.2 Commonly used solutions

Name	Constituents
Phosphate buffered saline (PBS)	140 mM NaCl, 10 mM Na2HPO4, 2.7 mM KCl and 1.76 mM KH2PO4, pH 7.4
Phosphate buffered saline TWEEN (PBST)	140 mM NaCl, 10 mM Na2HPO4, 2.7 mM KCl and 1.76 mM KH2PO4, pH 7.4, 0.1% (v/v) TWEEN
Tris-acetate-EDTA (TAE)	40 mM Tris, 20 mM acetic acid, 1 mM EDTA
2x SDS-PAGE sample buffer (reducing)	100 mM Tris-HCl pH 6.8, 4% (w/v) SDS, 20% (v/v) glycerol, 0.2% (w/v) bromophenol blue, 200mM ß-mercaptoethanol
2x SDS-PAGE sample buffer (non-reducing)	100 mM Tris-HCl pH 6.8, 4% (w/v) SDS, 20% (v/v) glycerol, 0.2% (w/v) bromophenol blue
Resolving gel	97.5 mM Tris pH 8.8, 0.025% SDS, 0.001% ammonium persulphate, 0.001% TEMED, with 6-18% polyacrylamide

Stacking gel	Stacking gel was made up of 15.8 mM Tris pH 6.8, 0.013% SDS, 5% polyacrylamide, 0.001% ammonium persulphate and 0.001% TEMED.
Stacking gel buffer	125 mM Tris-HCl pH 6.8, 0.1% (w/v) SDS
Resolving gel buffer	375 mM Tris-HCl pH 8.8, 0.1% (w/v) SDS
Western blot transfer buffer	25 mM Tris, 187.2 mM glycine, 20% methanol
2x NP40 lysis buffer	2% (v/v) NP40, 20mM Tris pH7.5, 300 mM NaCl, 2 mM EDTA and 0.02% Na azide. Protease inhibitor cocktail (100x) added just before use (Thermo fisher #78430)

Table 8. Commonly used solutions.

2.3 Primary antibodies

Antibody	Manufacturer	Species raised in	Application (concentration or dilution)
CLEC14A polyclonal	R&D	Sheep	WB (0.1 µg/mL) IHC/IF (10 µg/mL)
Multimerin-2 polyclonal	Abcam	Rabbit	WB (0.2 µg/mL)
Multimerin-2 Clone H572	Thermoscientific	Mouse	IF (10µg/ml)
CD248 IgG1	BD Biosciences	Mouse	IHC/IF (100 µg/mL) WB (0.5 µg/mL)
Anti-human CD31 monoclonal (clone JC70A)	Dako	Mouse	IHC/IF (1.29 µg/mL)
Neutrophil Elastase	Thermoscientific	Rabbit	IHC/IF (5µg/ml)
Beta-actin AC-15	Sigma	Mouse	WB (1µg/ml)
CLEC14A (CRT1)	Internal	Mouse	IF (10µg/ml)
CLEC14A (CRT2)	Internal	Mouse	IF (10µg/ml)
CLEC14A (CRT3)	Internal	Mouse	IF (10µg/ml)
CLEC14A (CRT4)	Internal	Mouse	IF (10µg/ml)
CLEC14A (CRT5)	Internal	Mouse	IF (10µg/ml)

Table 9. Primary antibodies. Listed with manufacturer details, species raised in and concentration for each application. Western blot (WB), immunofluorescence (IF), immunohistochemistry (IHC).

2.4 Secondary antibodies

Antibody	Manufacturer & catalogue number	Species raised in	Concentration for each application
Anti-mouse HRP	Dako	Goat	WB (1:5000)
Anti-rabbit HRP	Vector labs	Goat	IHC – ready to use
Anti-mouse HRP	Vector labs	Goat	IHC – ready to use
Anti-sheep HRP	R&D	Donkey	WB (0.2µg/ml) IHC (1µg/ml)
Anti-human Fc HRP	Sigma (#A0170)	Goat	WB (2 µg/mL) ELISA (1µg/mL
Anti-Rat HRP	DAKO (#P0450)	Rabbit	ELISA 1 in 5000
Anti-His HRP	Sigma	Mouse	WB (0.2 µg/mL) ELISA (0.1µg/ml)
Anti-Rabbit HRP	Abcam	Goat	WB (0.2 µg/mL)
Anti Sheep FITC	Thermofisher	DOnkey	FC (10µg/ml)

Table 10. Secondary antibodies. Listed with manufacturer details, species raised in and concentration used for each application. Western blot (WB), immunofluorescence (IF), immunohistochemistry (IHC), enzyme-linked immunosorbent assay (ELISA) flow cytometry (FC).

2.5 Recombinant proteins

Protein	**Source**	**Expression system**
Human CLEC14A-ECD-Fc	R&D	
Human CLEC14A -ECD – Fc (R161)	Donated by Heath Laboratory	

Human MMRN2 FL – His	pHL-AviTag^3 Plasmid Bicknell Laboratory stock	HEK 293T
Human MMRN2 134-486 His	pHL-AviTag^3 Plasmid Bicknell Laboratory stock	HEK 293T
Human MMRN2 487-820 His	pHL-AviTag^3 Plasmid Bicknell Laboratory stock	HEK 293T
Human MMRN2 134-350 His	pHL-AviTag^3 Construct made during project	HEK 293T
Human MMRN2 495-674 – His	pHL-AviTag^3 Plasmid Bicknell Laboratory stock	HEK 293T
Human MMRN2 495-674 - Fc	pcDNA3 Construct made during project	HEK 293T

Table 11. Recombinant proteins used during the project.

Source details and whether the protein was purchased, donated or expressed in HEK293T.

2.6 Molecular Biology

2.6.1 Oligonucleotides

Oligonucleotides were ordered from Eurogentec and reconstituted in nuclease-free water at a concentration of 100 µM.

Oligo. No	**Plasmids Sequenced**	**Oligonucleotides used for sequencing reactions 5' to3'**
Jo1	pHL-AviTag^3 F	TTCTTTTTCCTACAGCTCCTGG
Jo2	pHL-AviTag^3 R	AATGATTTGCCCTCCCATATGT
Jo19	pcDNA3 Fc MMRN2 495-674 Fc R	ATGAGGGTGTCCTTGGGTTTTG
T7	pcDNA3 Fc MMRN2 495-674 Fc F	TAATACGACTCACTATAGGG

Table 12. A- List of oligonucleotides used for sequencing reactions. Oligonucleotide sequences are displayed 5' to 3'.

Oligo. No	Description of oligonucleotide	Sequence 5' to3'
Jo7	MMRN2 134-350 FW	TAGTAGACCGGTGATTCCATGGCAATCCCTGA
Jo8	MMRN2 134-350 RV	TAGTAG GGTACCATTGGTCCCTGGGGCCT
Jo9	MMRN2 351-487 FW	TAGTAGACCGGTGGCAGTCTGGTGTTGGCAACG
Jo10	MMRN2 351-487 RV	TAGTAG GGTACCCTTGATGAGGTCGGCATG
Jo11	MMRN2 495-674 FW	AACGGCCGCCAGTGTGCTGGAATTCGCCACCATGGGGATCCTTCCCAGC
Jo25	MMRN2 495-674 RV	CTCACTCGATGAAGAACCGCGGCCGCCCGGCCGCGGGGGCTCCG

Table 12. B- List of oligonucleotides used for the construction of plasmids.

2.6.2 Plasmids

Plasmids were constructed by restriction enzyme digest and ligation reactions or Gibson assembly reactions

Oligo. No.	Plasmid Cloning Final construct	Cloning method	Source plasmid (s)
Jo7 & Jo8	pHLAvitag MMRN2 134-350	Restriction using Agel and Kpnl restriction sites	pHLAvitag MMRN2 134-487
Jo9 & Jo10	pHL Avitag MMRN2 351-487	Restriction using Agel and Kpnl restriction sites	pHLAvitag MMRN2 134-487
Jo11 & Jo 25	pcDNA3 Fc MMRN2 495-674 Fc	Gibson using restriction sites NotI and EcoRI	pHLAvitag MMRN2 495-674 His and empty pcDNA3

Table 13. Table 13. Construction of plasmids from PCR products.

Displaying the primers used, details of parent plasmid and final construct created.

2.6.3 Cloning methods

2.6.3.1 Plasmid cloning, by restriction enzyme digest, into pHL-Avitag3

PCR amplification of the insert gene was performed using primers with restriction sites as listed above. Q5 High fidelity DNA polymerase (NEB) used for PCR to minimise mutations as per manufacturers instructions. The PCR product was purified using QIAquick PCR purification kit (Qiagen). Restriction digests were then set up for

- PCR product – using the entire PCR reaction
- Recipient plasmid – 1µg of recipient plasmid

Restriction digest

Component	50µ Reaction
DNA	1µg
10 x NEB Buffer 1.1	5µl (1x)
AgeI	10 units
KpnI	10 units
Nuclease free water	To 50µl
Mix gentle using pipette. Incubate for 1 hour at 37°C	

Table 14. Restriction digest components.

The digested DNA was then run on a 1% (w/v) agarose (Bioline) gel dissolved in 1xTAE buffer with the addition of SYBR safe DNA gel stain (Invitrogen). The samples, after being mixed with 6x loading dye (Thermo Scientific) were loaded

and run at 100V for 30 minutes. The Generuler kb DNA ladder (Thermo Scientific) was run alongside to check the appropriate DNA size. A UV transilluminator was used to visualise the DNA on the gel, and DNA was cut out using a scalpel. The QIAquick Gel Extraction Kit (Qiagen) was used to extract the DNA from the gel as per the manufacturer's instructions.

To ligate the insert into the recipient plasmid, a 3:1 insert:vector ratio was used; they were combined in an eppendorf with T4 DNA ligase (NEB) following the manufacturer's instructions. For bacterial transformation, 1-2µl of the ligation reaction was combined with Bioline alpha-select bronze efficiency chemically competent cells per manufacturer's instructions. Then the reaction was diluted to 1ml in LB medium (Thermo Scientific) and put on a shaker for 60 minutes at 37°C. 200µl of cell transformation mixture was then spread on an LB agar plate containing the appropriate antibiotic (ampicillin) and incubated overnight at 37°C. For colony screening the next day, 5 clones were picked and each put into 50µl H2O, gently mixed and 20µl placed at 95°C for 10 minutes to lyse and then centrifuged for 3 minutes (the other 30µl was saved for a starter culture if clone correct). 2µl of supernatant was used for the PCR, which was performed using a primer from within the insert and one from the vector backbone to check the insert and orientation. Correct clones were placed in 120ml LB media and left overnight at 37° on a shaker. The next day a glycerol stock was made from 8ml of overnight culture centrifuged at x5000g for 5 minutes. After removing the supernatant, the pellets were resuspended using 750µl LB media and 250µl of autoclaved 20% glycerol and stored at -80 °C. With the remaining overnight culture, a commercial

miniprep kit (Sigma) was used following the manufacturer's instructions to isolate DNA to send for sequencing to confirm the construct was correct. DNA was submitted to Source Biosciences for sequencing, and alignments were checked using Benchling software.

2.6.4 Gibson cloning into pcDNA3 Fc plasmid

PCR of the insert was performed as described before using primers listed in **Table 12B** followed by purification and DpnI digest of PCR product. A restriction site double digest of the vector using the technique described previously was performed. The fragment and digested vector were run on an agarose gel, excised, and gel extraction was performed. The concentration of DNA was checked using the Nanodrop 1000 spectrophotometer. For Gibson the following ratios were used: 0.03pmol of vector and 0.06pmol of insert.

- Pmols = (weight in ng) x 1000/ (base pairs x 650 daltons)

The NEB HiFi DNA Assembly protocol was followed as per the manufacturer's instruction.

2.7 Cell Culture

All cell culture was carried out in a laminar flow hood under sterile conditions.

2.7.1 HEK293T

After testing for mycoplasma using the Lookout®Mycoplasma PCR Detection Kit (Sigma Aldrich MP0035), Human Embryonic Kidney 293T (HEK293T) cells were cultured in Dulbecco's modified Eagle's medium (DMEM) (Thermo Scientific), with 10% foetal calf serum (FCS) (GIBCO Life Technologies), 4 mM L-glutamine (Life

Technologies), 100 U/ml penicillin and 100 µg/ml streptomycin (Life Technologies) to make complete DMEM (cDMEM).

2.7.2 Isolation and cell culture of liver sinusoidal endothelial cells

1cm^3 tissue was finely diced and digested with 0.2% collagenase Type 1A (Sigma, UK) for 1 hour in a shaking incubator at 37°C. The tissue was then passed through a 70µm filter, and the cell suspension was washed three times by centrifugation at 300 x g for 5 minutes, followed by purification by density gradient centrifugation over Percoll™ (Amersham Biosciences). Negative magnetic selection with mouse HEA-125 antibody (50µg/ml, 1:10 Progen Biotec) and Dyna beads conjugated with goat anti-mouse antibody (Invitrogen) was used to remove biliary epithelial cells followed by positive selection of endothelial cells using anti-human CD31 coated Dyna beads (Invitrogen). The cells were cultured in human endothelial cell medium (Gibco) supplemented with 2mM L-glutamine, 100U/ml penicillin and 100µg/ml streptomycin (Sigma), 10% Human serum, 10ng/ml of VEGF (Peprotech) and 10ng/ml of hepatocyte growth factor (HGF (Peprotech), initially in a T25 flask coated in 1% rat tail collagen (RTC) (Corning) at 37°C. Following the positive selection of endothelial cells with CD31 described above, the remaining supernatant was collected and pelleted. The pellet was washed in PBS and then resuspended in FCS 10% v/v in DMEM and penicillin, streptomycin and L-glutamine (PSG) at the above mentioned concentrations.

2.7.3 Stimulation of primary LSEC cultures

Cytokines and growth factors were added to confluent HSEC at 10µg/ml concentrations for 24 hours before RNA extraction and qPCR. Stimulants were obtained from Peprotech except for LPS (Sigma).

2.7.4 General cell culture, passaging and storage

Cells were cultured on tissue culture plastic plates or flasks at 37°C in a humidified 5% CO_2 incubator and passaged as required. To detach cells, they were washed in PBS, and trypsin was added (TrypLE x1 Invitrogen), followed by incubation at 37°C until detached. Media was then added to the cells and pelleted by centrifugation. The pellet was resuspended in media and transferred to a new coated tissue culture vessel. If storage was required, pelleted cells were resuspended in freezing media consisting of 10% DMSO in FCS (Sigma) transferred to cryovials and placed in a MrFrosty™ (Wessington Cryogenics, UK) at -80°C for 24 hours, then the next day they were transferred to liquid nitrogen for long term storage. When needed again, cells were resuspended in warm media, and viability was checked with a trypan blue stain.

2.7.5 SiRNA transfections

SiRNA for CLEC14A knockdowns were purchased from Thermo Scientific. D1 – Assay ID 129879 and D2- Assay ID 129880. 175,000 cells were seeded onto RTC coated 6-well plates and incubated for 24 hours. Cells were washed in PBS, and 800µl of

OptiMEM (Gibco) was added. 1µl of 20µM siRNA was added to 167.5µl of OptiMEM, and 3µl of RNAiMAX lipofectamine (Invitrogen) was mixed with 27µl OptiMEM. Both mixtures are kept at room temperature for 10 minutes. The 30µl mix, with lipofectamine, is added to the siRNA and flicked and incubated for 10 minutes. This is then added to the cells. No antibiotics are used. After 48 hours, assays are performed, and knockdown is confirmed using western blotting.

2.7.6 Plasmid transfections

Plasmids made were transfected into HEK293T cells using polyethylenimine (PEI) (1mg/ml) (Sigma-Aldrich). The ratio of DNA to PEI was 1:4. Cells were plated at quantities specified below in cDMEM, and the next day DNA was added to Opti-MEM vortexed and incubated for 10 minutes at room temperature, then added to HEK293T cells. See the table below for reagent quantities depending on plate size.

Plate size	**Cells plated**	**Media Volume**	**Opti-mem**	**DNA**	**PEI**
6-well	$3x10^5$	2ml	100µl	1µg	4µl
6cm	$1x10^6$	3ml	300µl	3µg	12µl
10cm	$3x10^6$	10ml	1ml	9µg	36µl
15cm	$6x10^6$	20ml	2ml	18µg	72µl

Table 15. Reagent quantities for plasmid transfections.

Transfected HEK293T cells were washed in PBS then scraped and pelleted. NP40 lysis buffer (eg 500 µl for a confluent 10cm plate of cells) was added with protease inhibitors and vortexed for 1 minute followed by incubation on ice for 30 minutes.

The mixture was then centrifuged at maximum speed at 4°C for 15 minutes and supernatant removed and stored at 20°C.

2.8 Biochemistry

2.8.1 Cell lysis, SDS-PAGE, western blotting

Protein samples were separated by sodium dodecyl sulphate polyacrylamide gel electrophoresis (SDS-PAGE). Gels were made in mini gel cassettes (Thermo Scientific) using a resolving and a stacking gel **Table 8**. The gels were then run at 70mV through the stacking gel followed by 120 mV for 2 hours, and samples were transferred to PVDF membranes in a transfer buffer for 2 hours run at 30 mV in a 4°C cold room. PVDF membranes were then blocked in 5% (w/v) milk in PBST for 1 hour at room temperature. Primary antibodies were incubated at concentrations indicated in **Table 9** overnight at 4°C followed by washing 5 times in PBST for 5 minutes per wash. The membranes were then incubated for 1 hour at room temperature with secondary antibodies **Table 10** conjugated with HRP, followed by washing as above. HRP was detected using enhanced chemi-luminescence (ECL) using Amersham ECL western blotting detection reagent (GE Healthcare) as per manufacturer's instructions and imaged using a LI-COR Odyssey imager.

2.8.2 Far western blotting

Far western blotting involved incubating PVDF membranes for 1 hour with the Fc fused CD248-Extracellular domain (2 µg/mL). The protein tag was detected with HRP-linked antibody incubation (anti-Fc HRP).

2.9 Protein expression and purification

HEK239T cells were plated in 15 cm (x10) tissue culture dishes and grown to confluency in cDMEM. HEK293T cells were then transfected using PEI, as described previously. The following day media was then replaced with Opti-MEM and cultured for three days, then replaced with fresh Opti-MEM until around one litre was obtained. PMSF crystals and 1 mM EDTA were added to inhibit proteases in the cultured medium. All collected media was filtered using 0.2 µm vacuum filters, and all purification was carried out at 4°C. The cultured medium was then loaded onto a column containing 500µl of appropriate beads (protein A or Nickle NTA, depending on the tag of interest) at 1 ml per minute and then beads washed with 200 mL of PBS. Fc-bound proteins were eluted with 100 mM sodium citrate pH 3.0 or 0.1M glycine PH 2.2, then immediately neutralised by adding 1M Tris pH 9.0 (100 µL per 1000 µL). For His tagged proteins, 250mM imidazole PBS was used for elution.

2.10 Cell and tissue staining

2.10.1 Immunohistochemical staining of paraffin tissue

Paraffin-embedded sections were placed in xylene for 3 minutes (x3), alcohol for 3 minutes (x3) and then water for 3 minutes (x2). 10ml of high pH antigen unmasking solution (Vector Laboratories) was added to 1 litre of distilled water and placed in a microwave at high power for 10 minutes. The slides were added and returned to the microwave for another 30 minutes, followed by 10 minutes of cooling down before cold water was slowly added to cool the slides. The slides were washed in PBS with 0.1% tween (PBST) for 5 minutes. Endogenous peroxidase activity was inhibited by incubating the slides in 0.3% H_2O_2 in methanol for 30 minutes, followed by washing in water. A wax pen was used to draw around the tissue, and 2% casein was used for blocking for 20 minutes. Primary antibodies were added for 1 hour in a humidity chamber on a rocker, followed by washing in PBST for 5 minutes x3. A secondary antibody was added for 30 minutes, followed by washing x3. Vector VIP substrate kit was then added for 5 minutes. Sections were washed in water for 5 minutes, stained with Mayer's haematoxylin for 30 seconds, and rinsed in water. Slides were then placed in alcohol for three minutes x 3, xylene for three minutes x 3, and then DPX mount was used with a cover slip, and slides were left to dry overnight. Slides were imaged using a Zeiss Axio slide scanner and visualised in Zen imaging software.

2.10.2 Immunofluorescent staining of paraffin

As above but samples were protected from light, Hoechst was used for nuclei staining and fluorescent immunomount (Yunusova et al.) was used with the glass cover slips.

2.10.3 Immunofluorescent staining of cells

For staining HSEC, cells were grown in IBIDI chambers on rat tail collagen. Primary antibodies were added at 37°C for 30 minutes before washing in PBS media, followed by fixation in 4% paraformaldehyde for 15 minutes. Cells were blocked with 10% goat serum and secondary antibodies, and Hoechst was added for 30 minutes at room temperature and protected from light before washing in PBST and imaging. Cells were imaged using the confocal LSM510 microscope. If internalisation of the antibody was suspected, the primary antibody was incubated on ice for 15 minutes before washing and fixation.

2.11 Serum sample collection

Samples were collected from patients with hepatocellular carcinoma (pre-treatment), liver cirrhosis or liver fibrosis after consent was obtained. Samples were collected in gold-top tubes containing a serum separator and were immediately centrifuged at 2000g for 10 minutes. The serum was then stored at -80 °C.

2.12 Quantitative PCR

Analysis of mRNA expression was performed by using TaqMan Gene expression assays with FAM-labelled probes (Applied Biosystems, UK). GAPDH was used as the housekeeping gene. The cycle threshold value (Ct) for the gene of interest was normalised against the housekeeping gene, and relative expression was calculated using the $2^{-\Delta\Delta Ct}$ method. For the reaction Taqman 2x master mix (Applied Biosystems) was used at a final concentration of x1 together with 20x assay mix (applied biosystems) at x0.5, 100µg/ml of cDNA and made up to 10µl.

2.13 HSEC exposure to hypoxia

Confluent HSEC in a 6-well plate were left either in a standard incubator in normoxia conditions or a hypoxic chamber (RS Mini Galaxy incubator, Wolf laboratories, UK) with an oxygen content of 2%, for 24 hours.

2.14 Angiogenesis assays

2.14.1 Matrigel assay

PBS was added to a 12 well plate and then removed. Matrigel was thawed overnight on ice in a cold room and 70µl added to each well. After 5 minutes in the incubator 160,000 HSEC were added to each well and placed in the Cell IQ and images captured every hour for 24 hours. Images were analysed using the ImageJ 'Angiogenesis Analyzer' plugin and the number of meshes per image was recorded.

2.15 Endothelial cell migration assay

HSEC were seeded into a 6 well plate, 200,000 cells per well. The following day a scratch was created down the centre of each well using a pipette tip. The plate was immediately placed into the Cell IQ and images captured every hour for 24 hours. The scratch area was analysed at each time point as percentage closure, areas were quantified using ImageJ (NIH, Maryland, USA).

2.16 Isolation of human neutrophils

Histopaque (HP) 1199 and 1077 (Sigma) are warmed to room temperature for 30 minutes. 2.5ml of HP 1119 is added to a 15ml tube, and 2.5ml of HP 1077 is gently pipetted on top. 5ml of blood is gently added to the surface and then spun at 500g for 45 minutes with the break off. Peripheral blood mononuclear cells (PBMCs) are removed first to minimise contamination, followed by neutrophils. 10 ml of PBS without Ca/Mg (Gibco) is added to the neutrophils. The neutrophils are spun at 500g for 5 minutes and resuspended to 1 ml, and cells are counted. Cells are kept at room temperature and used immediately for assays.

2.17 Flow cytometry

Neutrophils or PBMCs were incubated with MADCAM-1- FC (R&D), CLEC14A-ECD-Fc (R&D) or human Fc (Sigma) alone, which had been fluorescently labelled with Invitrogen Zenon™ Human IgG Labelling Kit. If no Fc tag, ie cells were

incubated with CLEC14A-ECD, then cells were fixed and stained with anti-CLEC14A primary and anti-sheep FITC secondary antibody. Following incubations, cells were washed in PBS (without Ca/Mg) (Gibco). Samples were run on a Cyan flow cytometer, and results were analysed using Flow Jo software.

2.17.1 Neutrophil static adhesion assays.

Neutrophils were added to confluent HSEC, which had been stimulated with TNF 10µg/ml for 24 hours. The neutrophils (100,000/ml) were left on the HSEC for 5 minutes in RPMI containing Ca/Mg (Gibco) before being removed, and images were then captured for analysis.

2.17.2 Neutrophil flow assays.

An Ibidi µ-slide VI 0.4 channel slide (Thistle Scientific, UK) was coated in RTC by injecting 30µl into each channel and incubating for 2 hours at 37 °C followed by washing in PBS. HSEC from a T75 flask were dissociated in trypsin-EDTA, washed in PBS and placed in complete media at a concentration of $3x10^6$ cells per ml. 30µl of media was then added to each Ibidi channel. Cells were left to adhere for 1 hour before the media was topped up. Once confluent cells were stimulated with TNF 10µg/ml for 24 hours. Neutrophils were flowed over the HSEC at a concentration of 500,000 neutrophils per ml at 0.05Pa for 5 minutes at 37°C. Neutrophils were kept in RPMI free from Ca/Mg until being added to media containing Ca/Mg at the start of each lane run. After 5 minutes of flow the HSEC

were washed with 3 minutes of flowing media. Adherent neutrophils were captured by phase-contrast Olympus IX50 inverted microscope (Olympus). Adherent neutrophils appeared phase bright, and those that had transmigrated phase dark. If CRT antibodies vs Isotype control were being tested, the antibodies were added to the HSEC at 20µg/ml along with Fc receptor block 30 minutes before the flow assay. The flow assay set-up in shown in **Figure 12**.

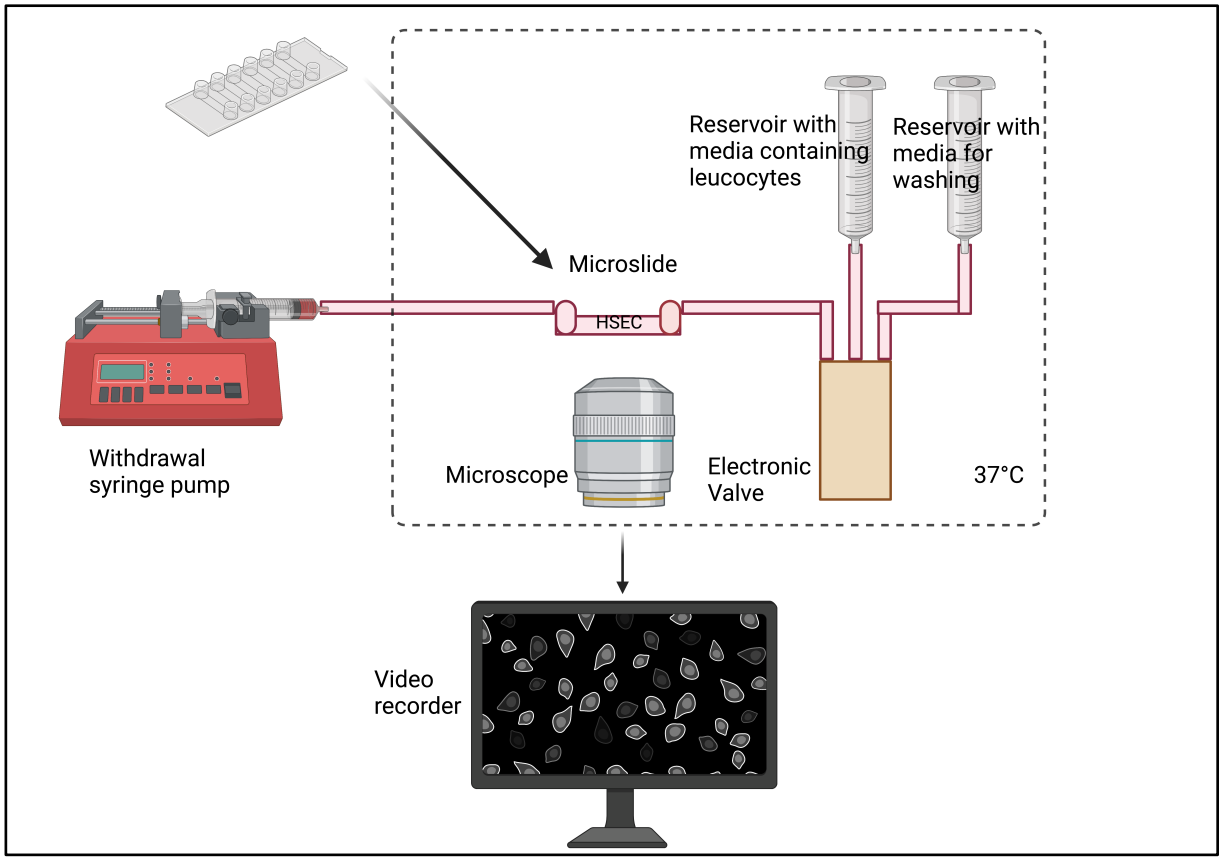


Figure 12. Neutrophil flow assay set-up.

HSEC were cultured in IBIDI microslides and media containing neutrophils flowed over the HSEC using silicone tubing. Following washing, images were captured using a phase contrast microscope and video recorder. The experiment was done in an enclosed chamber kept at 37°C.

2.18 Monoclonal antibody generation

The work was carried out under home office license number PB119DB6B. Two Wistar rats were first immunised with antigen MMRN2 495-674-Fc (50µg) and Freund's complete adjuvant subcutaneously (SC). Subsequently, the rats were injected SC every two weeks with 50µg of antigen and Freund's incomplete adjuvant. Bleeds from saphenous veins were taken thirteen days after each immunisation to check for antibody production by ELISA; the rats had two final boosts of 10µg of antigen in PBS intraperitoneally before being culled three days after the final boost. The spleen was harvested to isolate splenocytes to fuse with NS0 mouse myeloma cells. The spleen was mechanically disrupted in RPMI, and cells were passed through a 40µm filter to generate a single-cell suspension. The cells were washed three times in RPMI. NS0 mouse myeloma cells were precultured and harvested from plates, and washed. NS0s and rat spleen cells were then mixed at a ratio of 1:5. 1ml polyethylene glycol (PEG) (Stemcell)50% v/v was added slowly to the cell pellet over one minute while stirring cells slowly. 20ml of RPMI was added over 20 minutes while gently stirring the cells. Cells were then left for 5 minutes. After adding another 30ml of RPMI, cells were pelleted by centrifugation, and the supernatant was removed. The pellet was resuspended in 50ml of RPMI 20% (v/v) FCS. Cells were counted and seeded on 96 well plates in RPMI 15% (v/v) FCS at 150µl per well. The next day 150µl of RPMI 15% (v/v) FCS and 2 x HAT (100 µM hypoxanthine, 400 nM aminopterin and 16 µM

Thymidine) was added to the wells. After 10 days, the plates were screened for colonies. The wells containing colonies were sampled by collecting media and screened by ELISA.

2.18.1 Screening Rat test bleeds for antibody production.

300µl blood and 600µl of sterile PBS were mixed and then centrifuged at 5000g for 1 minute. ELISA plates were coated overnight with 1ng/µl of MMRN2 495-674-His. Plates were then washed x5 in PBST and blocked in 1% (w/v) BSA for 3 hours, followed by washing. Serum was added at serial dilutions and incubated for 1 hour. Following further plate washing anti-Rat HRP was added for 30 minutes and following washing substrate solution, Tetramethylbenzidine, TMB, was added and incubated for 15 min at room temperature. Finally, 3 M HCl was added, and absorbance at 450 nm was read with a plate reader. The same method was used for screening the media from hybridomas.

2.18.2 Haemagglutination assay for supernatants of clones

In this haemagglutination assay, sheep red blood cells were used. This assay enabled the quantification of the concentration of antibody in clone supernatants. 3ml of Sheep red blood cells in Alsever's solution (TCS Biosciences) were added to 17ml of sterile saline. This was centrifuged at 2,500 rpm for 10 minutes. The supernatant was aspirated and discarded, and 20 ml of sterile saline was added, centrifuged, and saline aspirated. This was repeated for a third time. 300µg of sheep anti-rat was added to the sheep red blood cells and flicked to mix. A solution of 10mg of Chromium chloride hexahydrate ($CrCl_3 6H_2O$) (Sigma) in 10ml saline is

adjusted to pH 5 with 2M NaOH and filter sterilised 2 weeks in advance. 500µl of 1/10 dilution of the prepared $CrCl_3$ stock solution is added to the sheep red blood cells and flicked to mix. This is left overnight at 4°C. The cells are then washed x3 in HEPES buffered RPMI. Cells are then resuspended in 4ml HEPES/RPMI and stored at 4 °C. For assay 2ml of sheep red blood cell suspension is added to 10ml HEPES/RPMI. Media from clones and a negative control media were added to 96 well plates, serial dilutions using HEPES/RPMI were performed, and then 1 drop of red blood cells was added to each well (Ling et al., 1977). Before a button was seen resembling the negative control, the number well from the serial dilutions was used as a marker of antibody concentration relative to other supernatants.

2.18.3 Isotype determination

A Rat Ig Isotyping ELISA Kit (Invitrogen) was used to determine the monoclonal antibody isotype.

2.19 CLEC14A ELISA

The CLEC14A ELISA used for the quantification of CLEC14A in serum samples was optimised by the Nagy Group (Lab ES2, SOP 072 v5). I consented and collected serum samples from patients at the Queen Elizabeth Hospital Birmingham and Mr Bempong (technician from the Nagy Group) kindly quantified CLEC14A levels using the labs ELISA. In summary a sandwich ELISA was performed using serum samples diluted 1/10. A 96 well plate was coated with 100 µl of Sheep IgG anti-CLEC14A 0.4 µg/ml (R&D) overnight. Wells were then washed x 3 and blocked for 1 hour with 1% (w/v) BSA for 1 hour. 50µl of sample was added in triplicates for 1

hour. Wells were then washed x3 and 100µl of CRT3 11.6 µg/ml was added for detection. After 1 hour the plate was washed x 3 and 100 µl of Goat anti-Mouse HRP (1/1000) (R&D) added and incubated for 1 hour. Following washing x3 100µl of TMB (R&D) was added for 20 minutes followed by 100µl of 2N to stop the reaction. The plate was then read at 450nm and 540nm. Standard curves were generated using recombinant human CLEC14A (R&D).

2.20 Digital spatial profiling

See Chapter 8 for specific methodology and statistical approach.

2.21 Statistical analysis

Statistics were performed using the software package Graphpad Prism 9. A value of $P<0.05$ was considered statistically significant. The statistical test used is described with each result. In summary the distributions of continuous variables were assessed prior to analysis. Normally distributed factors were reported as mean and standard deviation (SD). Statistically significant differences between the means of two groups were tested using a *t* test. Medians and interquartile ranges (IQRs) were reported for non-normal data, the Mann-Whitney test was conducted when comparing continuous variables between two independent groups and analysis of variance through Kruskal- Wallis test for multiple-groups. Categorical variables were stated as absolute values with percentages and comparisons made using Fishers exact test. Kaplan Meier curves were used when survival analysis was required.

2.22 Illustrations

Illustrations in this thesis were created either in powerpoint or using Biorender illustration software.

3

3 The expression of CLEC14A and MMRN2 in human hepatic tissue

3.1 Introduction

CLEC14A has been described to be upregulated in pathological angiogenesis, particularly associated with tumour angiogenesis. A recent study on CLEC14A in hepatocellular carcinoma described how it is upregulated in tumour tissue compared to adjacent tissue (Yan et al., 2022). It was important to determine if high CLEC14A expression had an impact on outcomes in hepatocellular carcinoma and whether expression of its ligand MMRN2 had an influence. The other ligands of MMRN2: CD93 and CD248 were also explored using TCGA data. Whether CLEC14A can be detected in normal liver and chronic liver disease or the distribution of CLEC14A expression in hepatocellular carcinoma has not been described. For example, whether CLEC14A is found in sinusoidal endothelium only or if it can also be found in larger vessels is unknown. It is also unknown whether CLEC14A is uniformly distributed in tumours. No studies have reported the expression of CLEC14A within the diseased human liver, which will be addressed. This is important to define when evaluating whether CLEC14A has a future as a potential therapeutic target in hepatocellular carcinoma.

The expression studies aim to

1) Look at TCGA data to explore the effect of CLEC14A, MMRN2, CD93 and CD248 expression in hepatocellular carcinoma, on outcomes.
2) Identify the presence or absence of CLEC14A expression within the normal liver in vivo.
3) Identify if CLEC14A is present in diseased (non-cancer) hepatic tissue.
4) Look at the expression of CLEC14A in hepatocellular carcinoma and correlate it with clinical characteristics and outcomes.

3.1.1 Cancer genome atlas interrogation for CLEC14A, CD93, MMRN2 expression in hepatocellular carcinoma and association with clinical outcomes

Transcriptomic data from 371 patients diagnosed with HCC were obtained from the TCGA (https://cancergenome.nih.gov/). Kaplan Meier plots were created (https://kmplot.com) with the overall survival data available for 364 patients (Menyhart et al., 2018), shown in **Figure 13**. We can see that high CLEC14A and MMRN2 expressions are associated with better overall survival, and the difference is very significant in both cases. However, the trend for CD93 and CD248 was the opposite in that high expression was associated with poorer overall survival, this did not reach statistical significance, and therefore no firm conclusion can be drawn from this.

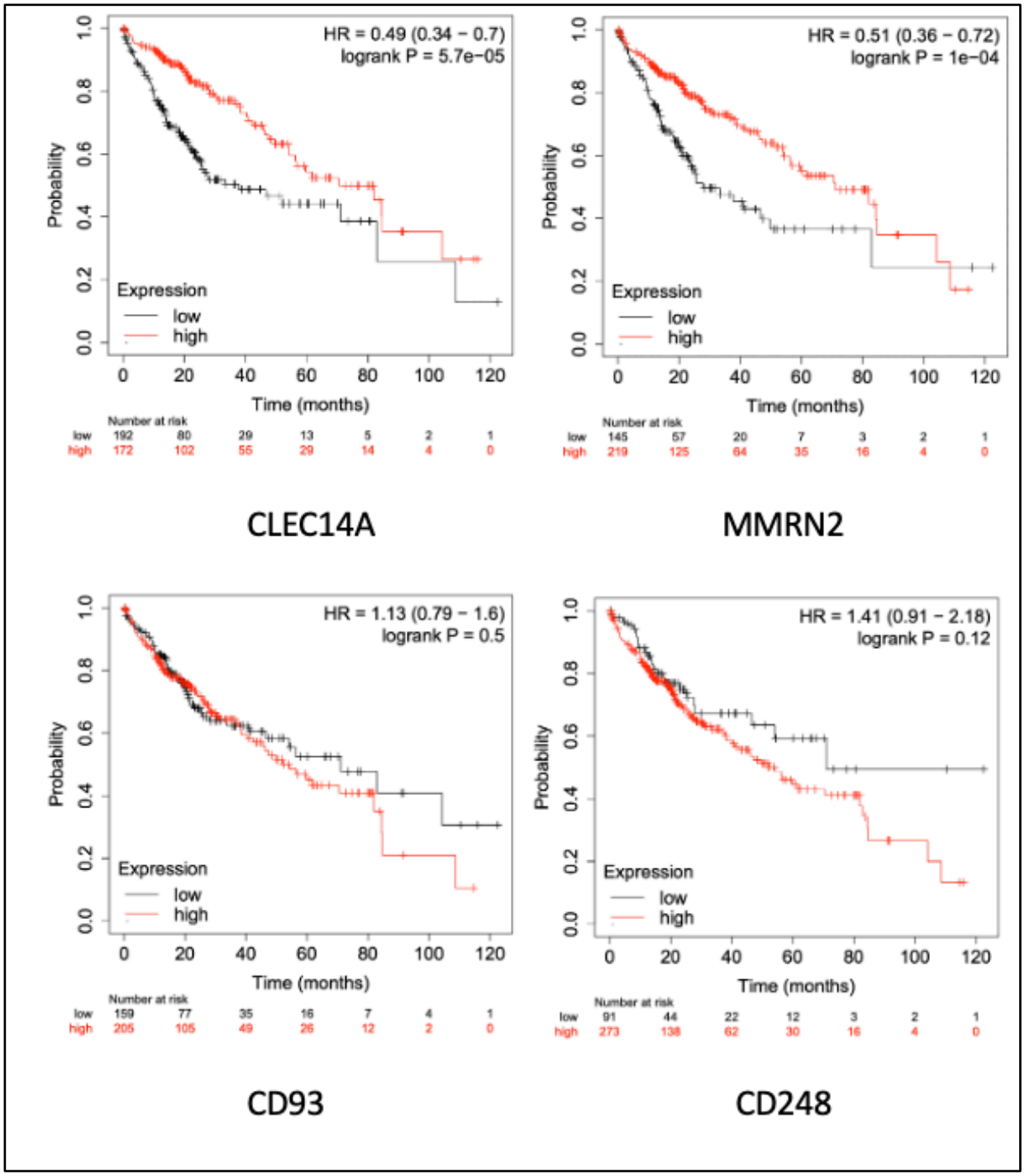


Figure 13. TCGA data for CLEC14A, MMRN2, CD93 and CD248 expression and relationship to overall survival. Kaplan Meier plots displaying overall survival in 364 patients with HCC with either high or low expression of CLEC14A, MMRN2, CD93 or CD248. (https://kmplot.com)

3.2 The expression of CLEC14A, in normal and diseased liver tissue by immunohistochemistry

The following section includes immunohistochemistry images from human liver tissue stained for CLEC14A. Where identifiable, the distribution of CLEC14A positivity is described. **Figure 14** shows a labelled example of specific liver structures evaluated in the sections.

Immunohistochemistry images for CLEC14A reveal a paucity of CLEC14A staining in normal liver tissue. No sinusoidal staining was seen, and in a couple of cases, very weak large vessel staining was noted **Figure 14** and **Figure 15**. Many chronic liver disease cases evaluated did not have CLEC14A expression. Still, where it was detected, it was localised to the fibrotic septa. Looking at the portal triad and central vein, CLEC14A was found in areas of bridging fibrosis arising from and connecting the portal tracts. In cases of autoimmune hepatitis, there was some large vessel staining, but there was also some weak sinusoidal staining **Figure 16.** In cases of alcoholic and non-alcoholic disease with fibrosis, there was positive staining in some large vessels within the portal triad and vessels within fibrous septa but no diffuse sinusoidal positivity **Figure 17**. In the representative cases of Primary biliary cholangitis (PBC), CLEC14A is expressed in the fibrous septa and arises from the portal tracts; the sinusoids around the portal tract also express CLEC14A. Still, there was no diffuse sinusoidal expression **in Figure 18** and **Figure 19**.

In hepatocellular carcinoma sections, it was striking that diffuse CLEC14A sinusoidal staining was seen in some cases that was not present in adjacent non-

tumour tissue **Figure 21** and **Figure 22**. However, that was not seen in all HCC cases **Figure 20**.

3.2.1 CLEC14A in normal liver

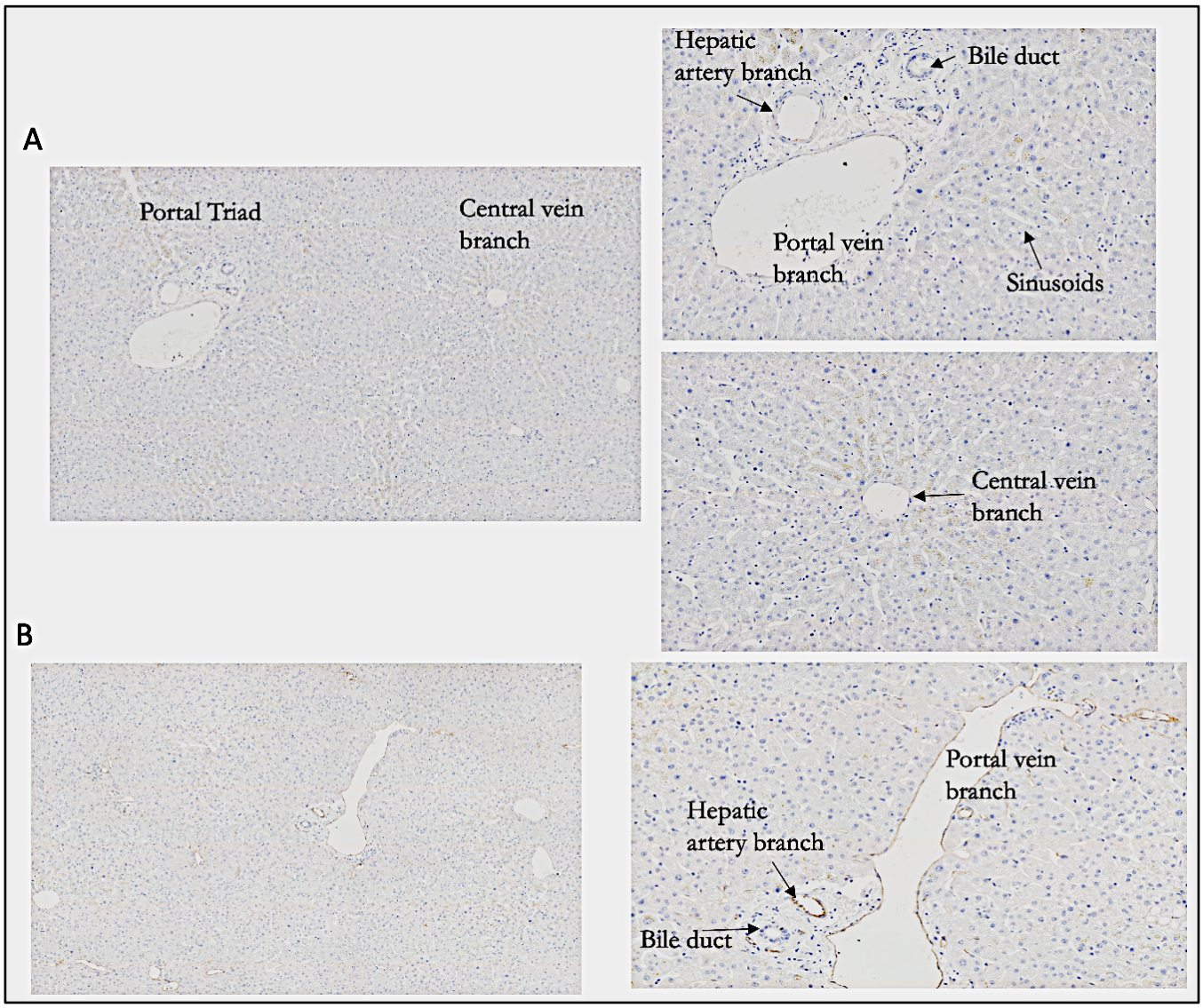


Figure 14. Structures found in a normal liver.

A)Normal liver showing portal triad and central vein with surrounding sinusoids. Fields captured by 20x objective. On the right a close up of image on left **B**) Example of portal triad showing very weakly positive CLEC14A staining on portal vein and artery but not the bile duct or sinusoids

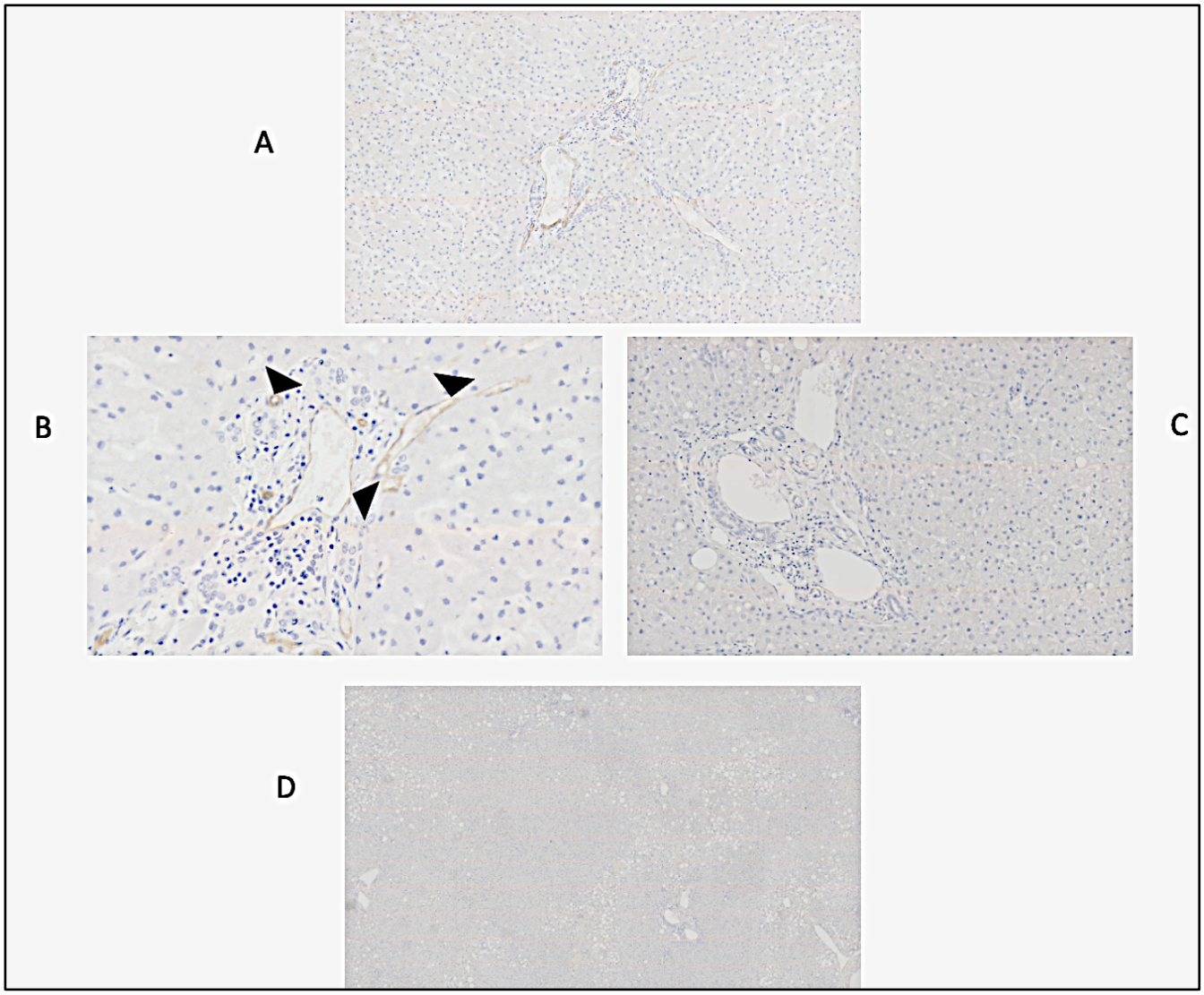


Figure 15. Second example: Expression of CLEC14A in normal human liver.

Representative images from normal liver samples stained for CLEC14A expression. Fields captured by 20x objective. **A)** Liver section stained for CLEC14A. **B**) A close-up of A) showing weak CLEC14A staining on large vessels but no sinusoidal positivity. **C**) Close-up of another normal section with no CLEC14A expression. **D**) Isotype-matched control antibody.

3.2.2 CLEC14A in chronic liver disease

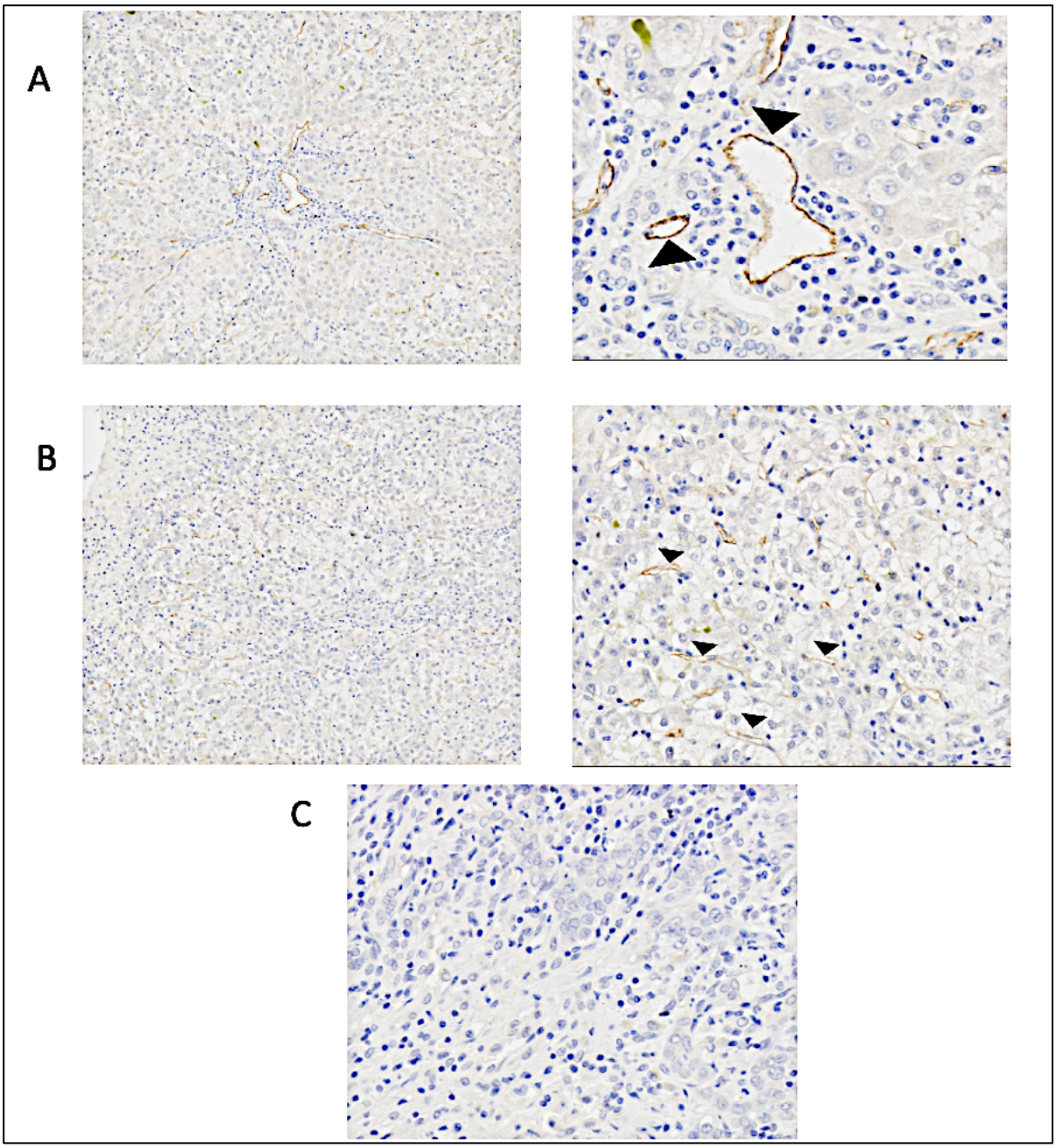


Figure 16. Expression of CLEC14A in autoimmune hepatitis

Representative images from autoimmune hepatitis cases (AIH) stained for CLEC14A expression. Fields captured by 20x objective. **A**) Liver section stained for CLEC14A showing large vessel staining. **B**) Liver section showing weak CLEC14A sinusoidal positive staining **C**) Isotype-matched control antibody.

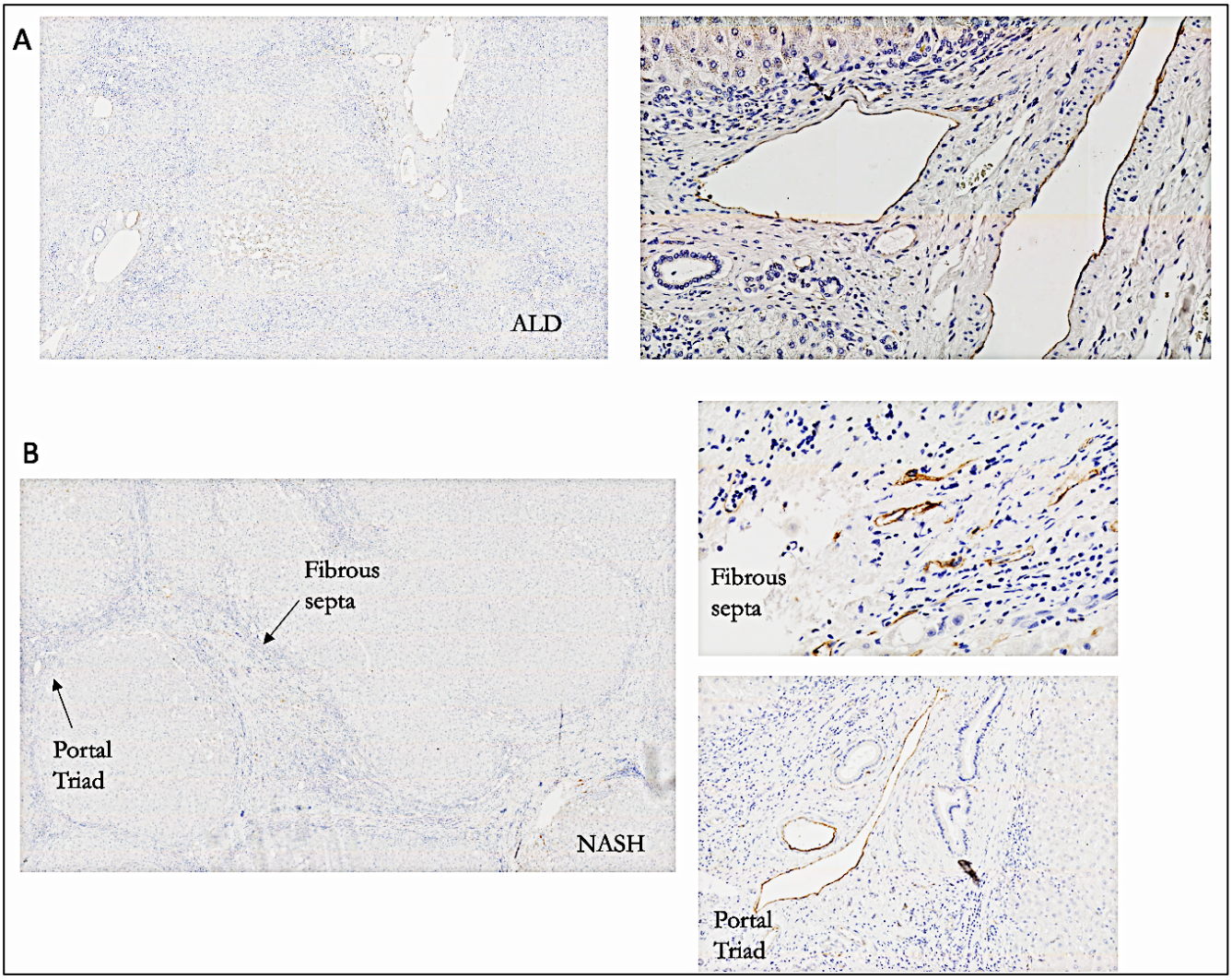


Figure 17. Expression of CLEC14A in A) Alcoholic liver disease, B) Non-alcoholic fatty liver disease

Representative images from ALD and NASH cases stained for CLEC14A expression. Fields captured by 20x objective. **A**) ALD liver section stained for CLEC14A showing portal vein and artery moderate staining. **B**) NASH liver section showing moderate CLEC14A positive staining in vessels in the fibrous septa, portal vein and hepatic artery branch in the portal triad.

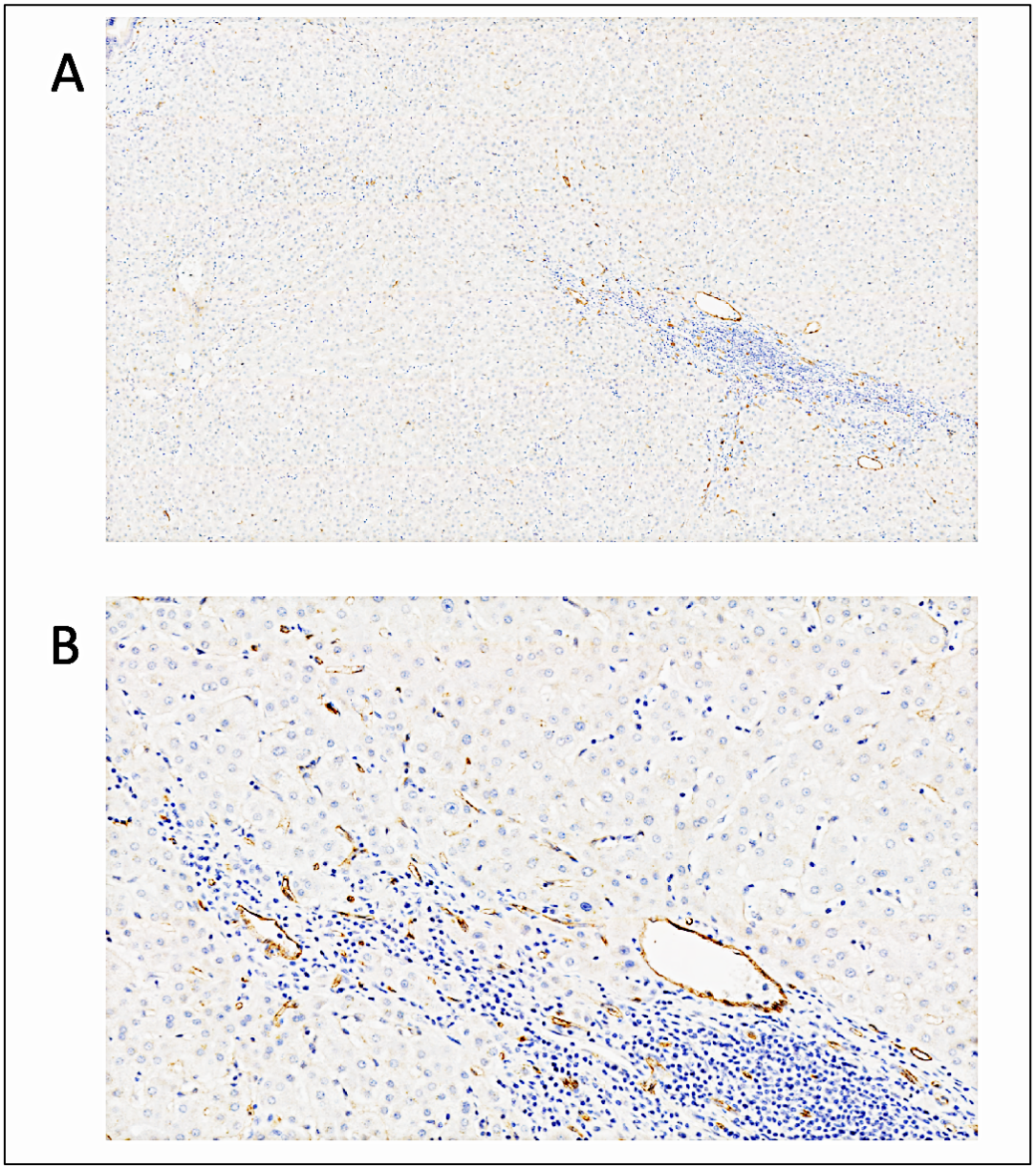


Figure 18. Expression of CLEC14A in Primary biliary cholangitis.

Representative images from a PBC case stained for CLEC14A expression. Fields captured by 20x objective. **A**) PBC liver section stained for CLEC14A **B**) Close up of large vessel with moderate staining and CLEC14A positivity of adjacent sinusoids only and associated inflammatory infiltrate.

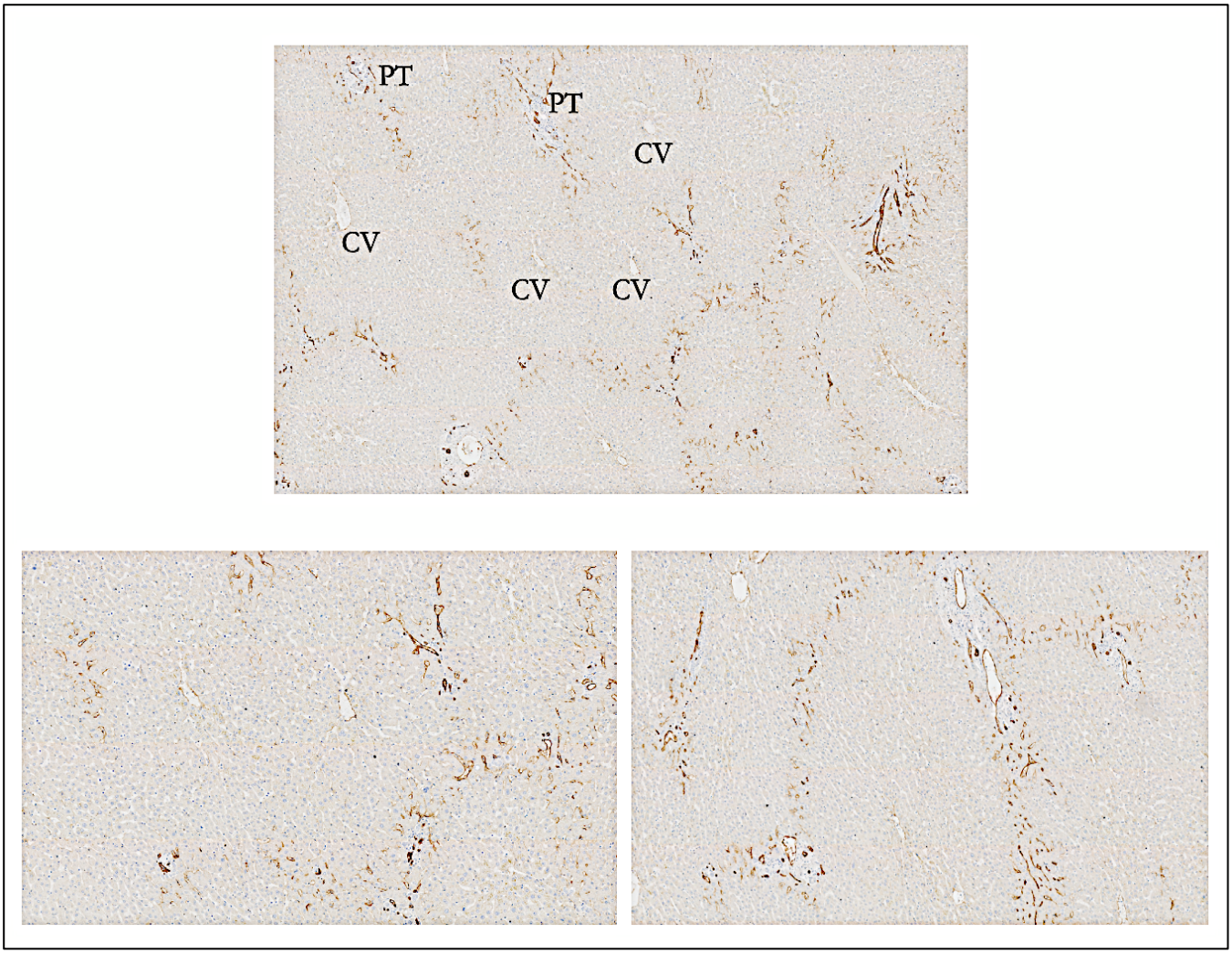


Figure 19. Expression of CLEC14A in Primary biliary cholangitis.

Representative images from a PBC case stained for CLEC14A expression. Fields captured by 20x objective. There is positive staining for CLEC14A in the fibrotic areas, and the top image shows the relationship between the portal triads and central veins. The bottom images are enlargements of the top image.

3.2.3 CLEC14A in hepatocellular carcinoma

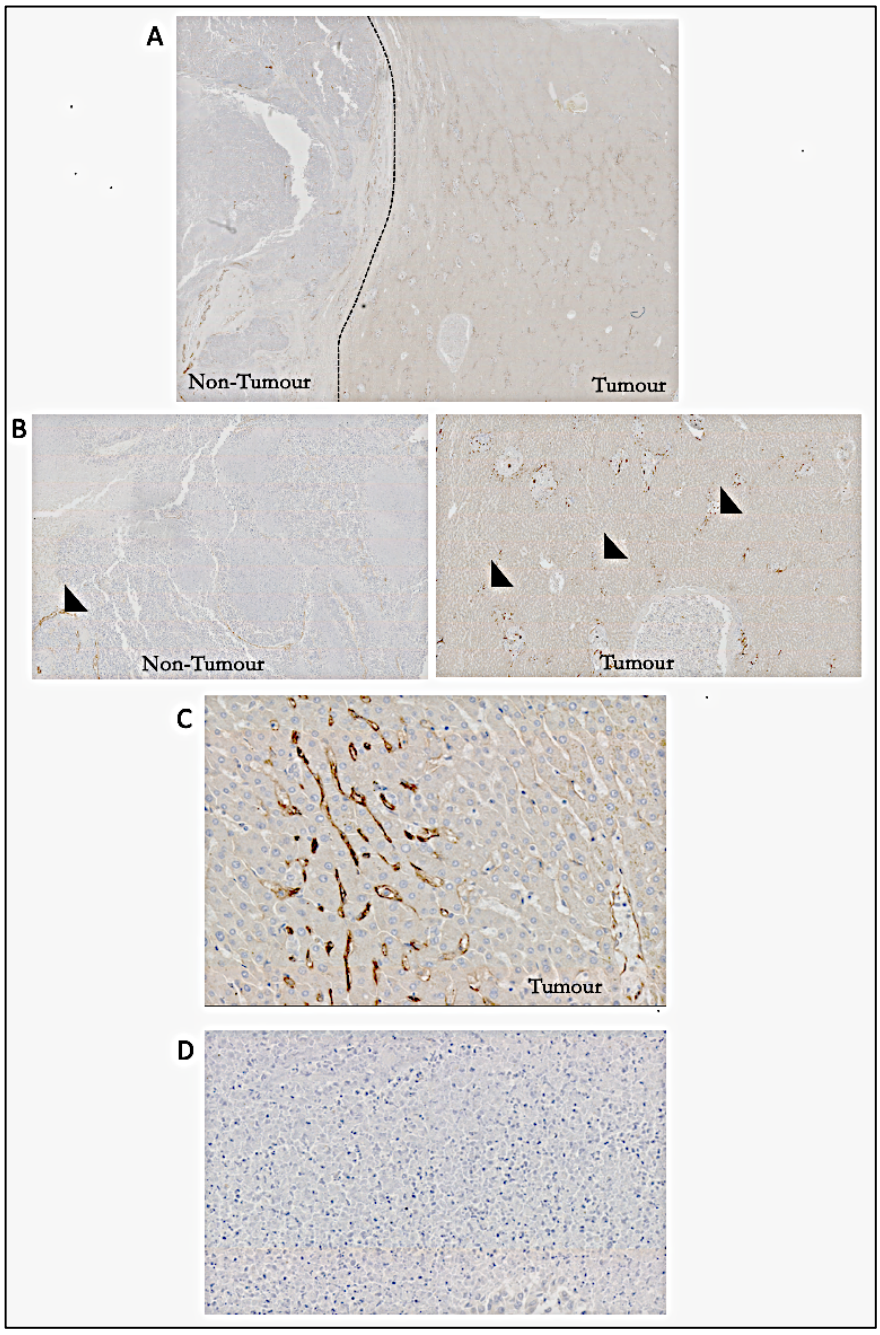


Figure 20. Expression of CLEC14A in a case of HCC with patchy CLEC14A sinusoidal positivity.

Fields captured by 20x objective. **A**) Liver section stained for CLEC14A with HCC tissue and adjacent non-tumour tissue. **B**) Enlargement of non-tumour and tumour areas. Only few large vessels positive for CLEC14A in non-tumour tissue. In HCC tissue patchy sinusoidal CLEC14A expression. Note some cytoplasmic positivity in tumour hepatocytes. **C**)Example of patchy CLEC14A expression. **D**) Isotype-matched control antibody.

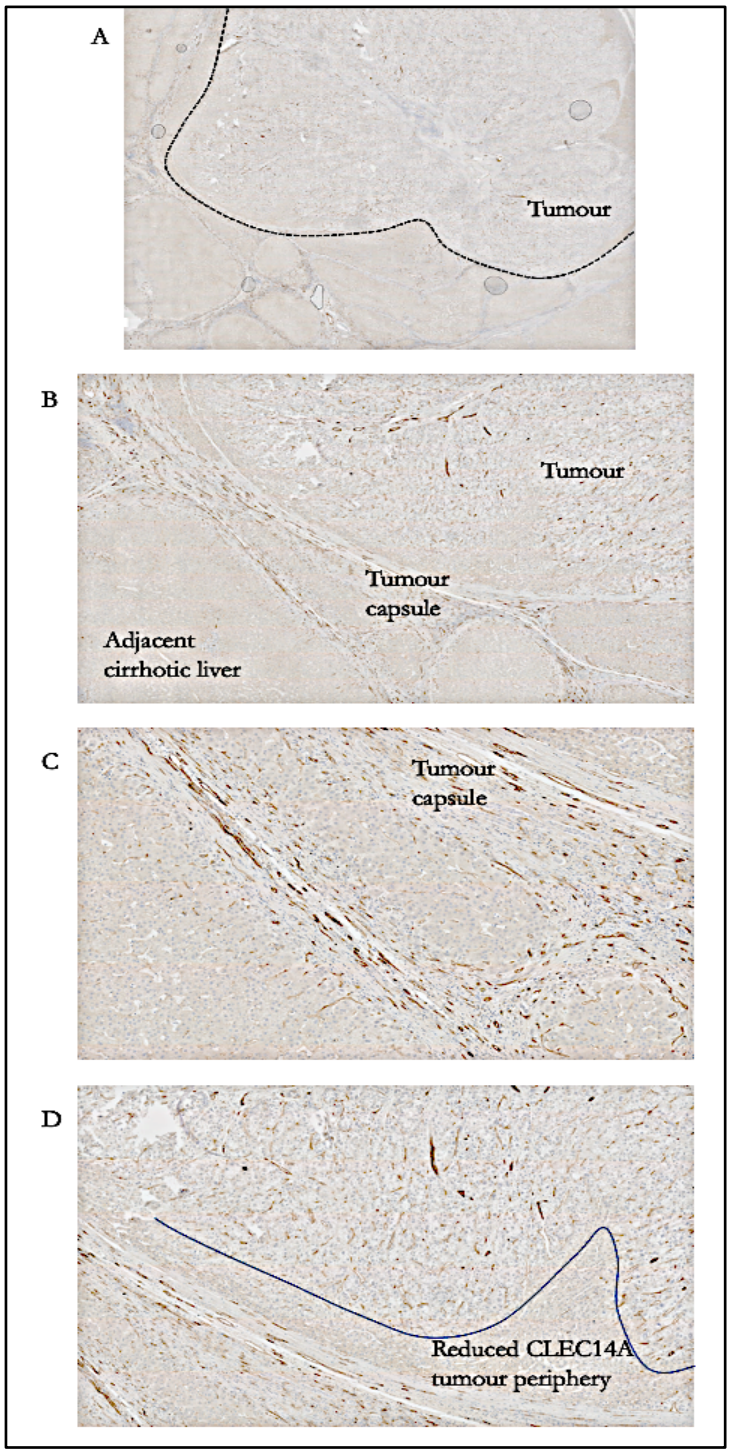


Figure 21. Expression of CLEC14A in a case of HCC with diffuse sinusoidal staining.

Fields captured by 20x objective. A) Liver section stained for CLEC14A with HCC tissue and adjacent non-tumour tissue on the same section. B) Enlargement of tumour/non-tumour border. C) High CLEC14A seen in tumour capsule D) Diffuse positive staining in tumour sinusoids but sparing of tumour periphery.

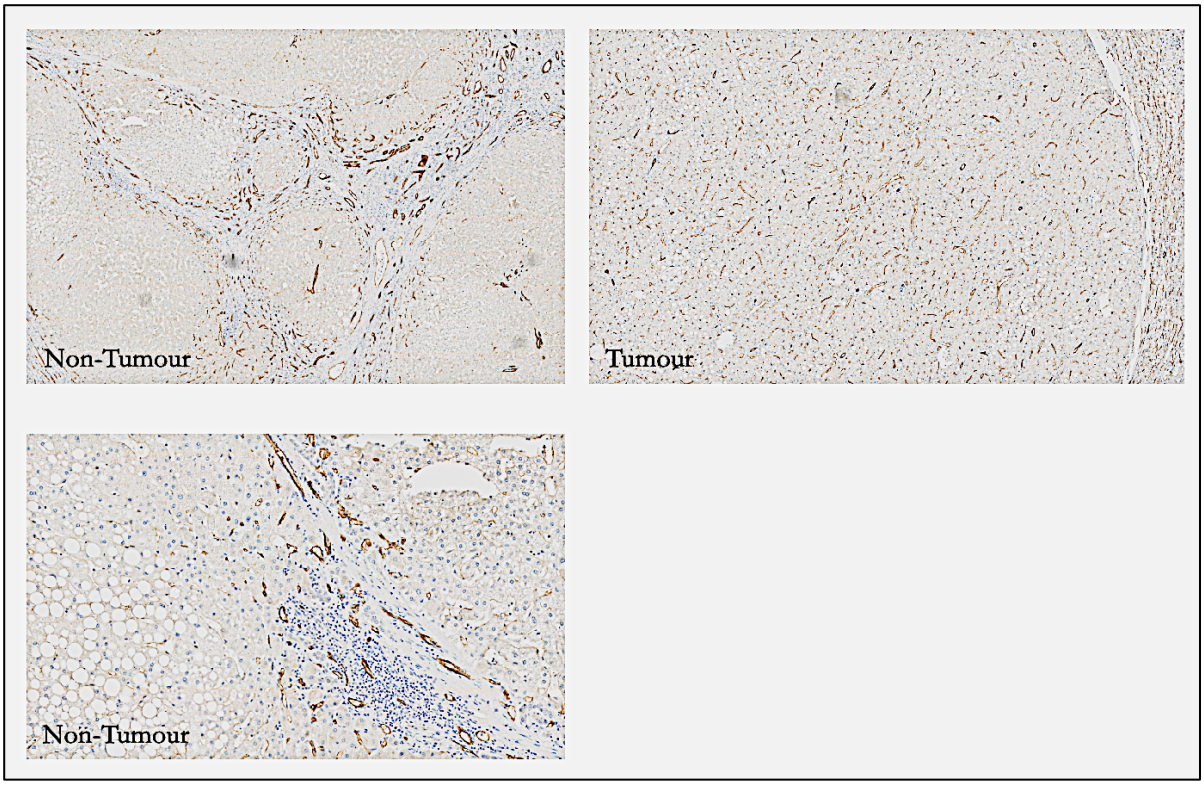


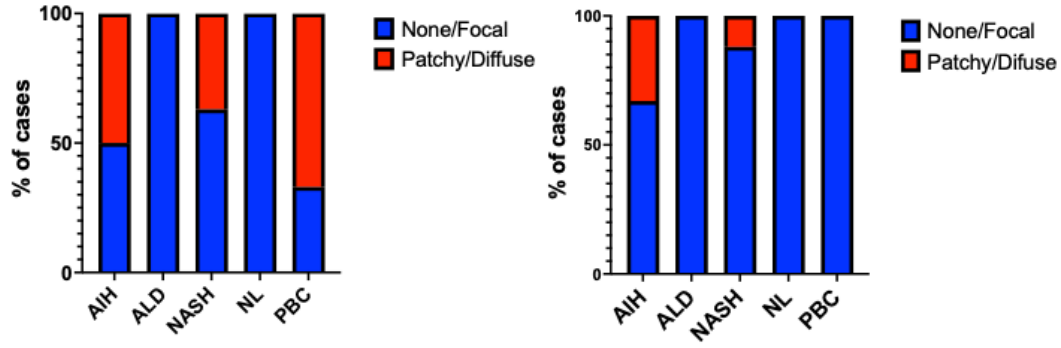


Figure 22. Expression of CLEC14A in hepatocellular carcinoma and adjacent non-tumour cirrhotic tissue.

Fields captured by 20x objective. 2 further HCC cases: diffuse sinusoidal staining can be seen in tumour tissue and note in adjacent non-tumour steatotic cirrhotic tissue CLEC14A can found in the fibrotic scar.

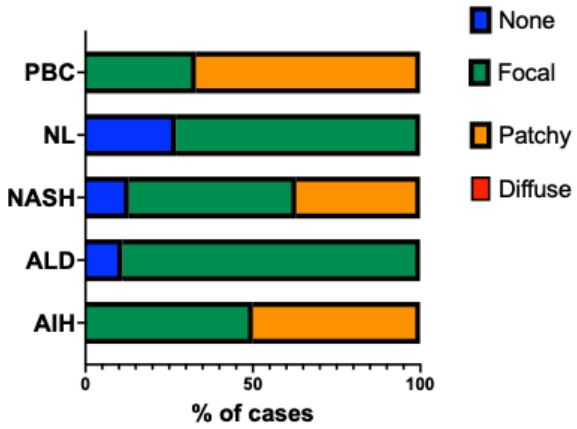
The following charts summarise the distribution of CLEC14A staining across all the tissue sections, and they include sections from 6 AIH, 9 ALD, 8 NASH, 3 PBC and 11 normal livers **Figure 23**. In addition, 87 HCC cases (**Figure 24**) and the adjacent normal liver were evaluated for CLEC14A expression, and the background liver was normal in 14 cases, early fibrosis in 17 cases and cirrhotic in 56 cases. The background aetiologies included ALD 19, HCV 25, HBV 5, HFE 3, PBC 5, secondary siderosis 1, NASH 12, AIH 2, NCPH 1, PSC 1 and unknown/none in 13 cases.

In tumours, 97% of cases had some large vessel positive CLEC14A expression, diffuse in over 30% of cases. Sinusoidal staining was detected in 82% of tumour cases, and this was diffuse in 40 % of cases. Looking at the adjacent non-tumour tissue, 95% of cases had at least some large vessel staining detectable. Only 48% of cases had some positive sinusoidal staining detectable, and in all cases, it was very weak staining and focal in nature. It is most commonly found in the fibrotic septa and immediately adjacent to the fibrotic septa.

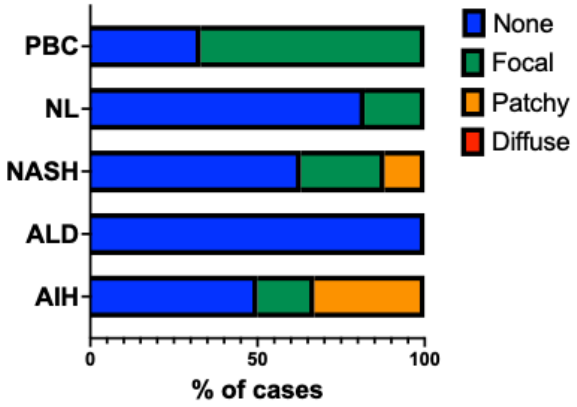


A) Large vessel positivity for CLEC14A

B) Sinusoidal positivity for CLEC14A



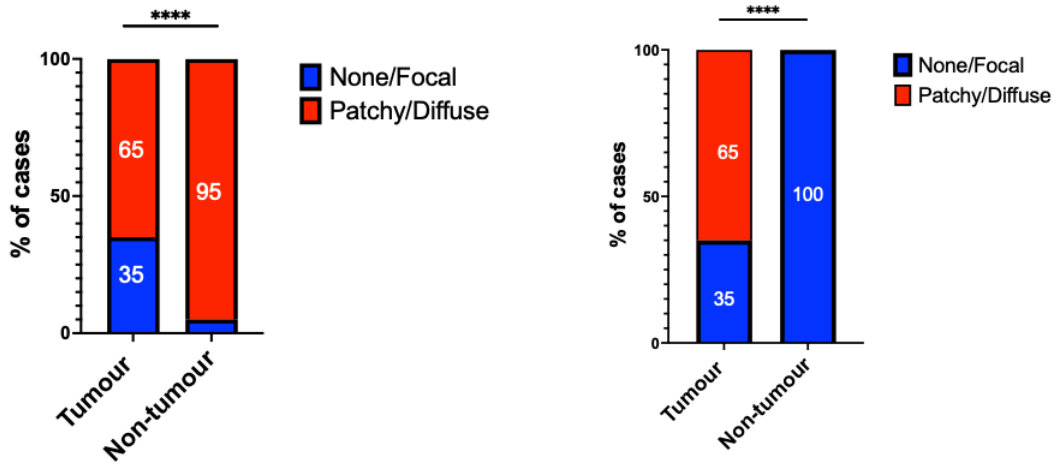
A) Large vessel positivity for CLEC14A - further breakdown none, focal, patchy, diffuse



B) Sinusoidal positivity for CLEC14A - further breakdown none, focal, patchy, diffuse

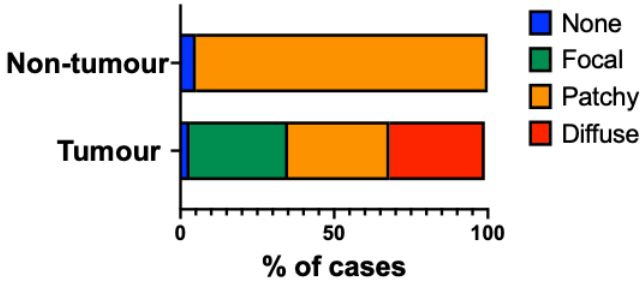
Figure 23. Chronic liver disease tissue cases and CLEC14A expression.

Chronic liver disease tissue cases and CLEC14A expression. **Top Panels:** Sections stained for CLEC14A. A) % of cases with large vessel CLEC14A B) % of cases with sinusoidal CLEC14A. **Bottom Panels:** Same cases staining classified as none, focal, patchy or diffuse for each case. The number of cases looked at AIH 6, ALD 9, NASH 8, NL 11 and PBC 3.

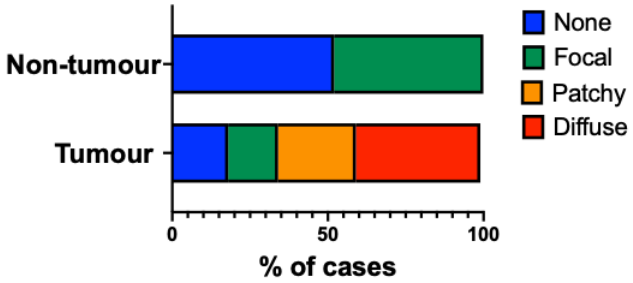


A) Large vessel positivity for CLEC14A

B) Sinusoidal positivity for CLEC14A



C) Large vessel positivity for CLEC14A- further breakdown none, focal, patchy, diffuse



D) Sinusoidal positivity for CLEC14A - further breakdown none, focal, patchy, diffuse

Figure 24. HCC tumour tissue and adjacent non-tumour CLEC14A expression.

Sections stained for CLEC14A. A) % of cases with large vessel CLEC14A expression B) % of cases with sinusoidal CLEC14A expression. C) and D) further breakdown of A) and B) detailing level of expression. 87 cases reviewed 36 liver resection cases and 51 liver explants.

Demographic data and tumour characteristics for the cases are shown in **Table 16** and **Table 17**. There was no significant difference in patient demographics based on whether there was high or low CLEC14A expression in tumours. When looking at tumour characteristics, high CLEC14A expression was associated with poorer differentiation **Figure 25**. There was no significant difference in overall survival or risk of tumour recurrence based on CLEC14A expression at the protein level **Figure 26** . However, after three years, there was a trend that higher CLEC14A expression was associated with longer survival, but this was not significant.

	N	Tumour CLEC14A non/focal (N=30)	Tumour CLEC14A patchy/diffuse (N=57)	P-value
Demographics				
Age (years)	87	58.7 ± 9	63.6 ± 9.6	0.0230
Male	87	22 (73%)	44 (77%)	0.7933
Ethnicity	85			>0.9999
Caucasian		25/73 (34%)	4/12 (33%)	
Non-Caucasian		48/73 (66%)	8/12 (67%)	
Laboratory tests				
ALT (U/L)	87	45 (25-63)	36 (26-61)	0.2804
Bilirubin (µmol/L)	87	16 (11-21)	11 (7-24)	0.0479
Albumin (g/L)	87	38 ± 7.4	40 ± 7.0	0.2208
Sodium (mmol/L)	87	139± 3.4	138 ± 17.0	0.7074
Creatinine (µmol/L)	87	78 (66-100)	79 (65-90)	0.6779
Haemoglobin (g/L)	87	132 ± 15.6	135 ± 16.6	0.3198
Platelets (10^9/L)	87	128 (78-169)	138 (88-229)	0.2887
INR	86	1.2 (1.1-1.3)	1.1 (1-1.2)	0.0468
WCC (10^9/L)	87	6 ± 2.1	6 ± 2.1	0.9437
Neutrophils (10^9/L)	87	3.3 (2.7-4.5)	3 (2.5-4.5)	0.8329
Lymphocytes (10^9/L)	87	1.5 (1.2-2)	1.6 (1.1-2.3)	0.7338
NLR	87	2.6 (1.5-3.2)	2.1 (1.6-3.1)	0.5622
AFP (ng/mL)	78	10.5 (4-67)	11 (3-103)	0.8176

Table 16. Summary of patient demographics, laboratory tests and tumour markers.

The two groups are low CLEC14A and high CLEC14A sinusoidal staining. Data presented as Number (%), mean ±SD or median (IQR), with p-values from Fishers exact test, t-test or Mann-Whitney test.

	N	Tumour CLEC14A non/focal	Tumour CLEC14A patchy/diffuse	P-value
Tumour Characteristics				
Size of largest tumour (mm)	86	29.5 (19.5-42.8)	34.5 (21.3-57.5)	0.1951
Tumour number	87	1 (1-2)	1 (1-3)	0.0557
Cirrhosis				0.1633
Yes		22/30 (73%)	32/57 (56%)	
No		8/30 (27%)	25/57 (44%)	
Type of surgery				0.6507
Resection		12/30 (40%)	27/57 (47%)	
Transplant		18/30 (60%)	30/57 (53%)	
Differentiation				0.0175
Well		10 (33%)	6 (11%)	
Moderate/poor		20 (67%)	51(89%)	
Vascular invasion				0.8166
Yes		20 (67%)	36 (63%)	
No		10 (33%)	21 (37%)	
Invasion type				0.3478
Microvascular		18/39 (46%)	4/14 (29%)	
Macrovascular		21/39 (54%)	10/14 (71%)	
PT Stage				0.6048
1		6 (21%)	14 (25%)	
>1		23 (79%)	41 (75%)	

Table 17. Summary of Clinicopathological Characteristics.

The two groups are low CLEC14A and high CLEC14A sinusoidal staining. Data presented as Number (%), mean ±SD or median (IQR), with p-values from Fishers exact test, t-test or Mann-Whitney test.

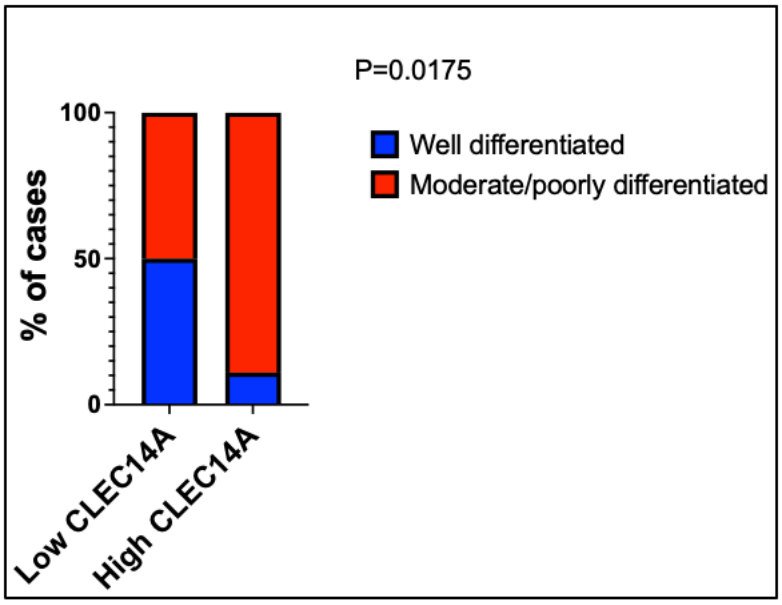


Figure 25. Tumour CLEC14A expression and tumour characteristics.

89% of cases with high CLEC14A expression were moderately or poorly differentiated compared to 50% of tumours with low CLEC14A expression. Fisher's exact test for difference between the groups p=0.0175.

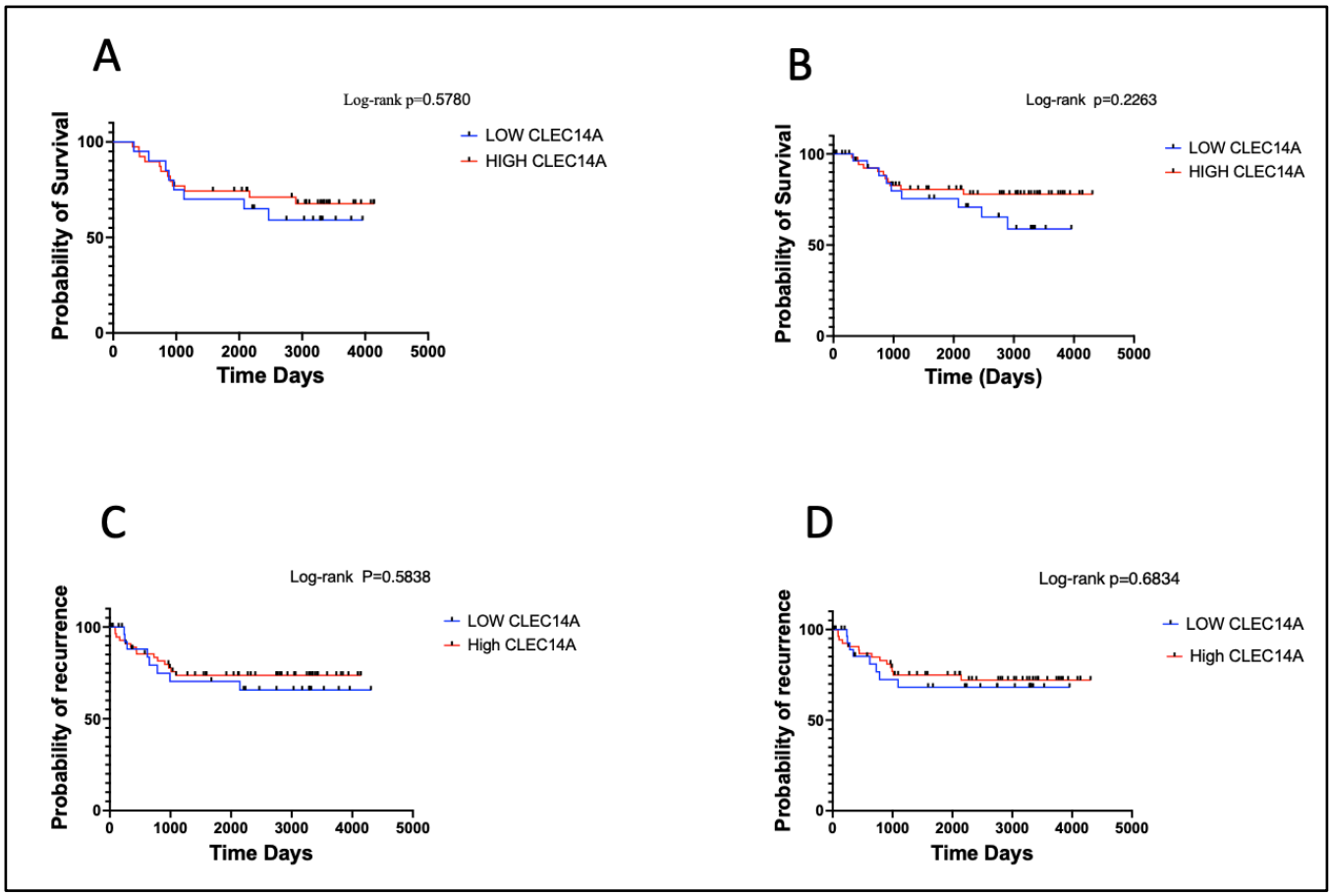


Figure 26. Probability of survival/recurrence based on tissue CLEC14A protein expression.

Probability of survival/recurrence based on tissue CLEC14A protein expression. A) and B) Kaplan Meier curves for survival probability based on tumour CLEC14A protein expression A) based on sinusoidal staining B) based on large vessel staining. C) and D) Kaplan Meier curves for risk of recurrence based on tumour CLEC14A protein expression C) based on sinusoidal staining D) based on large vessel staining. No significance difference was found between the CLEC14A high and CLEC14A low groups.

3.3 CLEC14A expression in HSEC

3.3.1 Dual staining of CLEC14A with endothelial cell markers

The previous immunohistochemistry studies highlighted that in liver tissue CLEC14A when present is associated with the vasculature. It was however not clear if this was on the endothelium or associated with neighbouring cells, for example Kupffer cells. HSEC were isolated from human liver and stained for CLEC14A expression and the endothelial marker CD31. This showed that CLEC14A localised with the cell membrane of HSEC and co-localised with CD31 **Figure 27**.

Interestingly it was observed that endothelial cells isolated from HCC and normal tissue are microscopically different in appearance **Figure 28**. With tumour ECs appearing elongated. After several weeks of observation, it was clear they also behaved very differently. I found that endothelial cells isolated from HCC tissue failed to proliferate, suggesting epigenetic changes have occurred and that they are in a state of senescence. Unfortunately, there were insufficient cells from tumour samples for experiments.

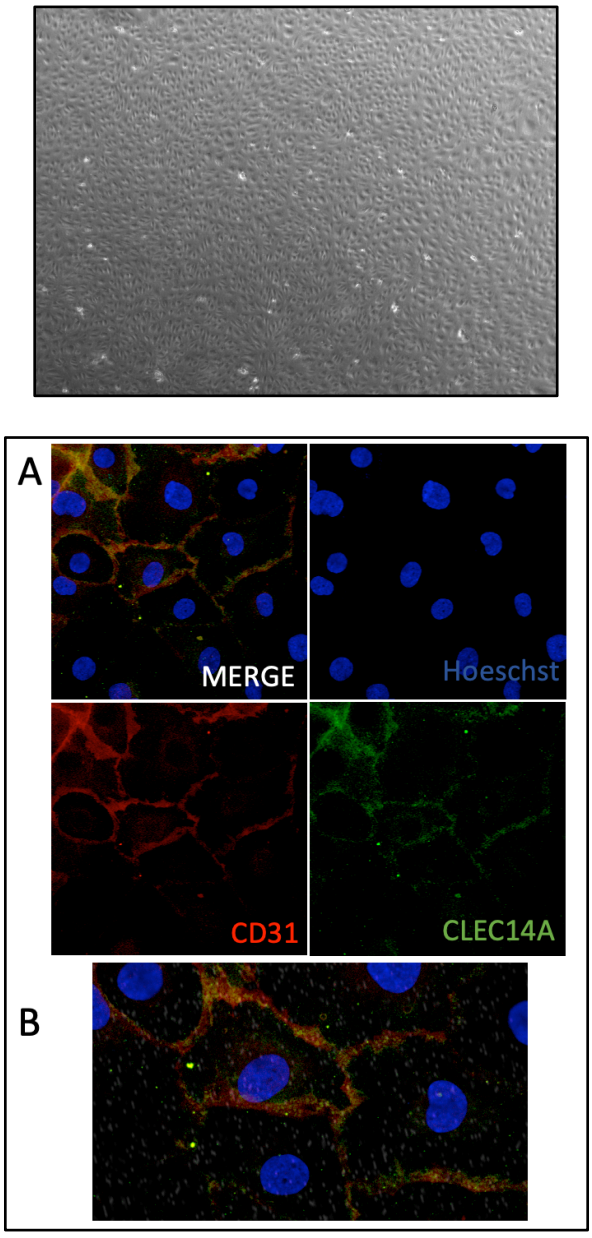


Figure 27. CLEC14A expression on cultured HSEC.

CLEC14A expression on cultured HSEC. Top image showing cultured HSEC isolated from a human liver. Bottom image showing CLEC14A expression on HSEC and colocalization with CD31

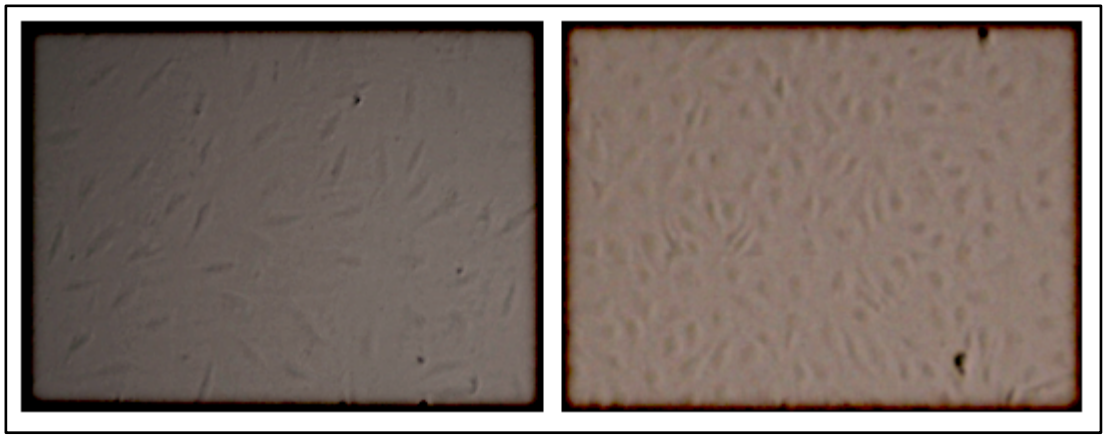


Figure 28. HSEC isolated from HCC tissue and non-tumour tissue.

On the left tumour, endothelial cells isolated from a HCC tumour and on the right endothelial cells from distal non-tumour tissue. Note the elongated appearance of the tumour endothelial cells on the left, which also failed to proliferate in standard HSEC culture media.

3.3.2 Protein quantification of CLEC14A in HSEC

To confirm and quantify the presence of CLEC14A in HSEC isolated from different livers , lysate from cultured HSEC were run on a gel under reducing conditions and western blotted for CLEC14A. This confirmed one distinct band at just under 100kDa, **Figure 29**. A western blot of HSEC lysates isolated from 5 cirrhotic livers and 2 isolates from normal liver tissue was performed under non-reducing conditions, **Figure 30**. Densiometry was performed to quantify CLEC14A expression normalised to loading control beta-actin. The HSEC were lysed at passage two and there was CLEC14A expression in all HSEC, but we see that some of the cells isolated from cirrhotic livers had higher levels of CLEC14A. I hypothesised that the second band seen at 250kDa was CLEC14A bound to

MMRN2 and that the interaction was maintained under non-reducing conditions. Therefore, I re-probed the blot for MMRN2, which was indeed identified as MMRN2 **Figure 31**. This provides insight into the relative strength of this interaction, and, interestingly, not all CLEC14A was bound to MMRN2.

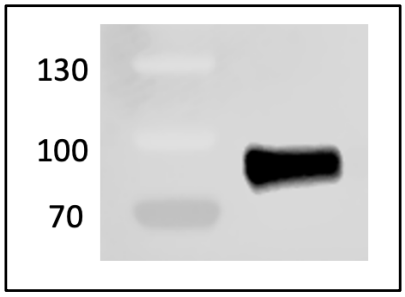


Figure 29. Western blot of HSEC lysate probed for CLEC14A.

HSEC lysate ran under reducing conditions, probed with anti-CLEC14A, and showed one distinct band just below 100kDa.

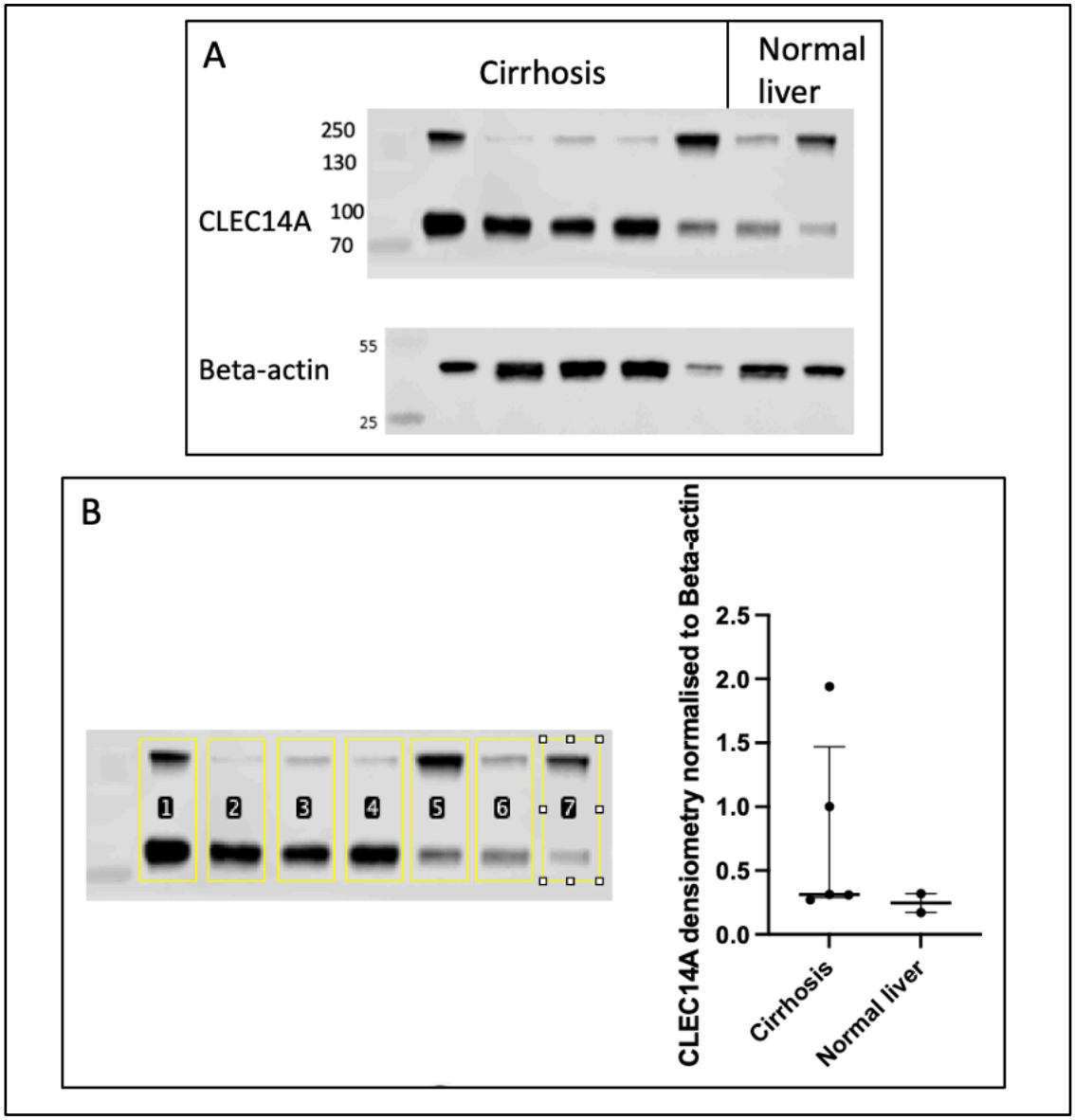


Figure 30. Western blot of HSEC lysates probed for CLEC14A.

A) HSEC from 5 cirrhotic and 2 normal livers isolated and cultured until passage two before lysates were western blotted under non-reducing conditions and probed for CLEC14A and beta-actin. We see 2 bands for CLEC14 under non-reducing conditions. B) Densiometry was performed to quantify CLEC14A after normalisation to the loading control beta actin.

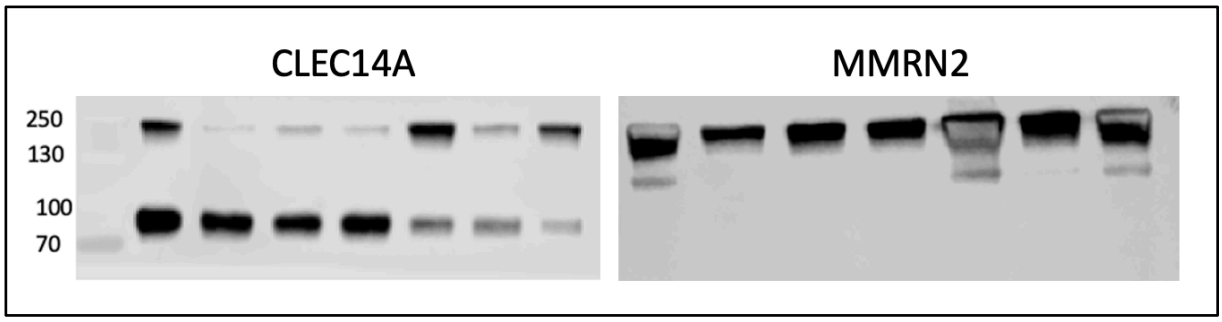


Figure 31. Western blot demonstrating CLEC14A binds MMRN2 in HSEC.

A western blot of HSEC lysates run under non-reducing conditions was probed for CLEC14A and then re-probed for MMRN2, demonstrating that some of the CLEC14A in the HSEC lysate was bound to MMRN2.

3.4 Multimerin 2 and CD248 expression

Multimerin 2 is expressed in HCC at the protein level and in liver fibrosis. In liver fibrosis, it localises to the fibrous septa, in the same distribution we see with CLEC14A **Figure 32**. Similarly, CD248 can be seen localising to the fibrotic septa **Figure 33**. Finally, **Figure 34** shows that CLEC14A, MMRN2 and CD248 colocalise in tumours, the tumours looked at included primary HCC, colorectal liver metastases and neuroendocrine liver metastases.

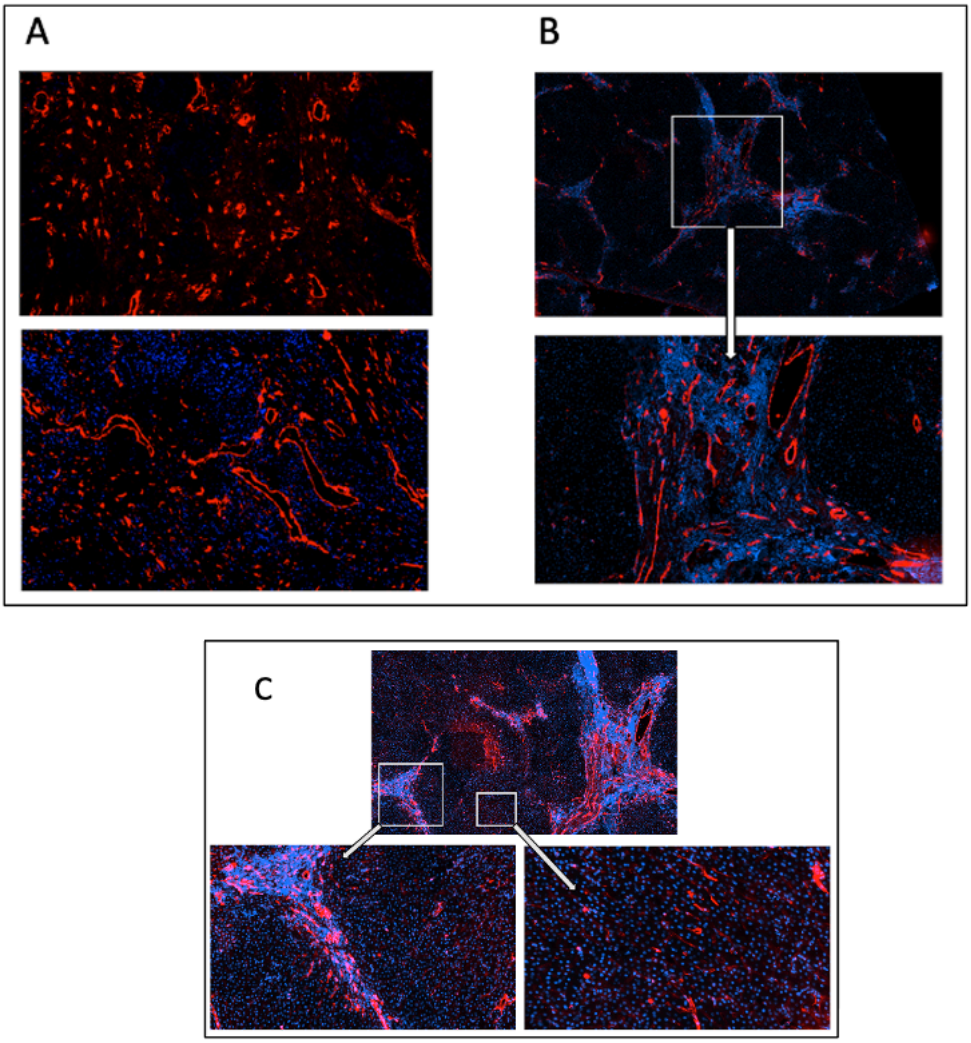


Figure 32. Multimerin 2 tissue expression in HCC and chronic liver disease.

A)Frozen HCC sections. Multimerin 2 (red) is found on vessels in HCC. **B)**Frozen PBC tissue section with Multimerin 2 (red) expression localising to vascular structures in the fibrous septa. **C)**PBC section with MMRN2 expression seen on fibrous septa and expression on liver sinusoids. Fields captured by 20x objective.

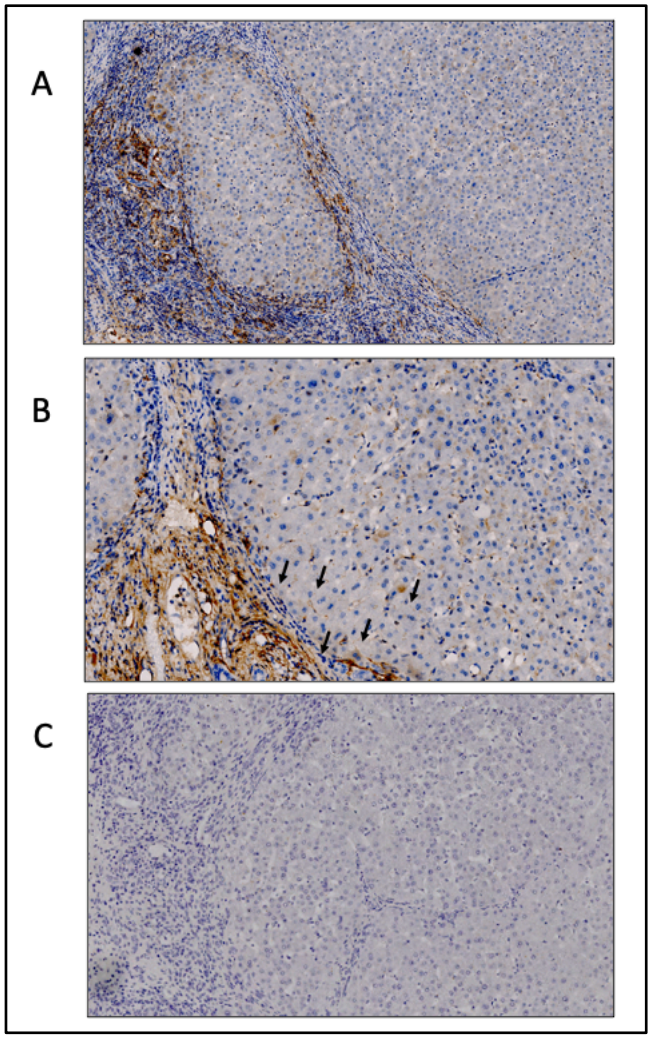


Figure 33. CD248 expression in a fibrotic human liver.

A)CD248 expression predominantly associated with the fibrous septa. **B)**Enlargement of A) can see diffuse CD248 in the fibrous septa and also weak sinusoidal staining in adjacent sinusoids. **C)**Isotype control. Fields captured by 20x objective.

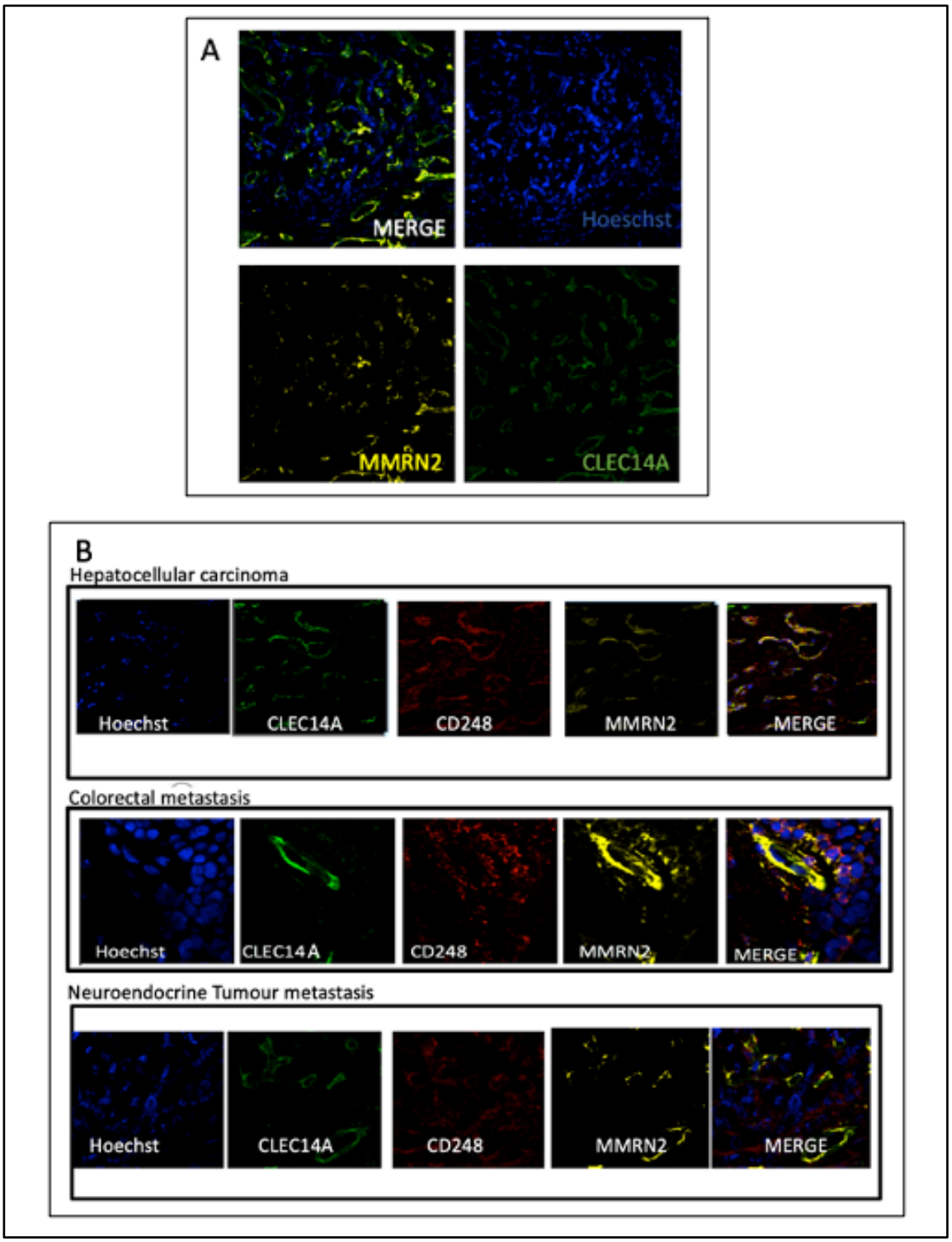


Figure 34. Co-localisation of CLEC14A, MMRN2 and CD248 in tumours.

A)CLEC14A and MMRN2 expression co-localise in HCC. **B)**CLEC14A, MMRN2 and CD248 co-localisation in tissue from HCC, colorectal liver metastases and neuroendocrine liver metastases.

3.5 CD248 binding to MMRN2

To confirm that CD248 binds to MMRN2 as described by Khan et al (Khan et al., 2017) and to determine the binding site of CD248 to MMRN2, new fragments of MMRN2 were produced via restriction enzyme cloning using the existing laboratory plasmid containing MMRN2-FL-His. When planning the cloning of new Multimerin-2 constructs, regions were narrowed down, considering highly conserved regions across different species, which were likely to have functional significance using PRALINE sequence alignment software. Fragments MMRN2 134-350 (size 638bp) and MMRN2 351-487 (size 408bp) were generated, fused to a His tag. I also expressed and purified CD248-Fc in HEK293T cells from a plasmid donated by the Protein expression facility at Birmingham University.

Far Western blotting was performed to look for protein-protein interactions. The MMRN2 constructs were expressed in HEK293T cells, and cell lysates run on a gel and transferred to a PVDF membrane, then probed for using my purified CD248-Fc. Using anti-Fc HRP to detect the interaction, I showed that the smallest MMRN2 fragment CD248 binds is MMRN2 351-487 **Figure 35**. This is a significant finding because it was previously unclear if VEGF and CD248 bound MMRN2 at the same site and I have shown that these are at two distinct sites (Colladel et al., 2016, Khan et al., 2017).

Next Page:

Figure 35. Western blot demonstrating that recombinant CD248 binds MMRN2.

Confirmation of the interaction of MMRN2 and CD248 and narrowing down the region of MMRN2 that interacts with CD248. **A)**His tagged fragments of MMRN2 were cloned and transfected into HEK293T cells. **B)**Gel showing Coomassie Blue staining of purified CD248-Fc. Recombinant CD248-Fc was generated using a secretory plasmid transfected into HEK293T cells, and the media collected and protein purified. **C)** Schematic showing how the MMRN2-CD248 interaction was tested for using far-western blotting. **D)** Far western blotting: Plasmids containing MMRN2 constructs were transfected into HEK293T cells, and the lysates ran on a gel. A far western blot was then performed by incubating the blot with CD248-Fc and then probing the blot with Fc-HRP for detection of CD248 binding MMRN2. The anti-His blot on the left is to show that each of the His tagged MMRN2 fragments were expressing. **E)** The fragment MMRN2 351-487 binds CD248-Fc and we can see that it is at a distinct region from where VEGF interacts with MMRN2, previously, it was unclear if they bound at the same site (see introduction **Figure 11**).

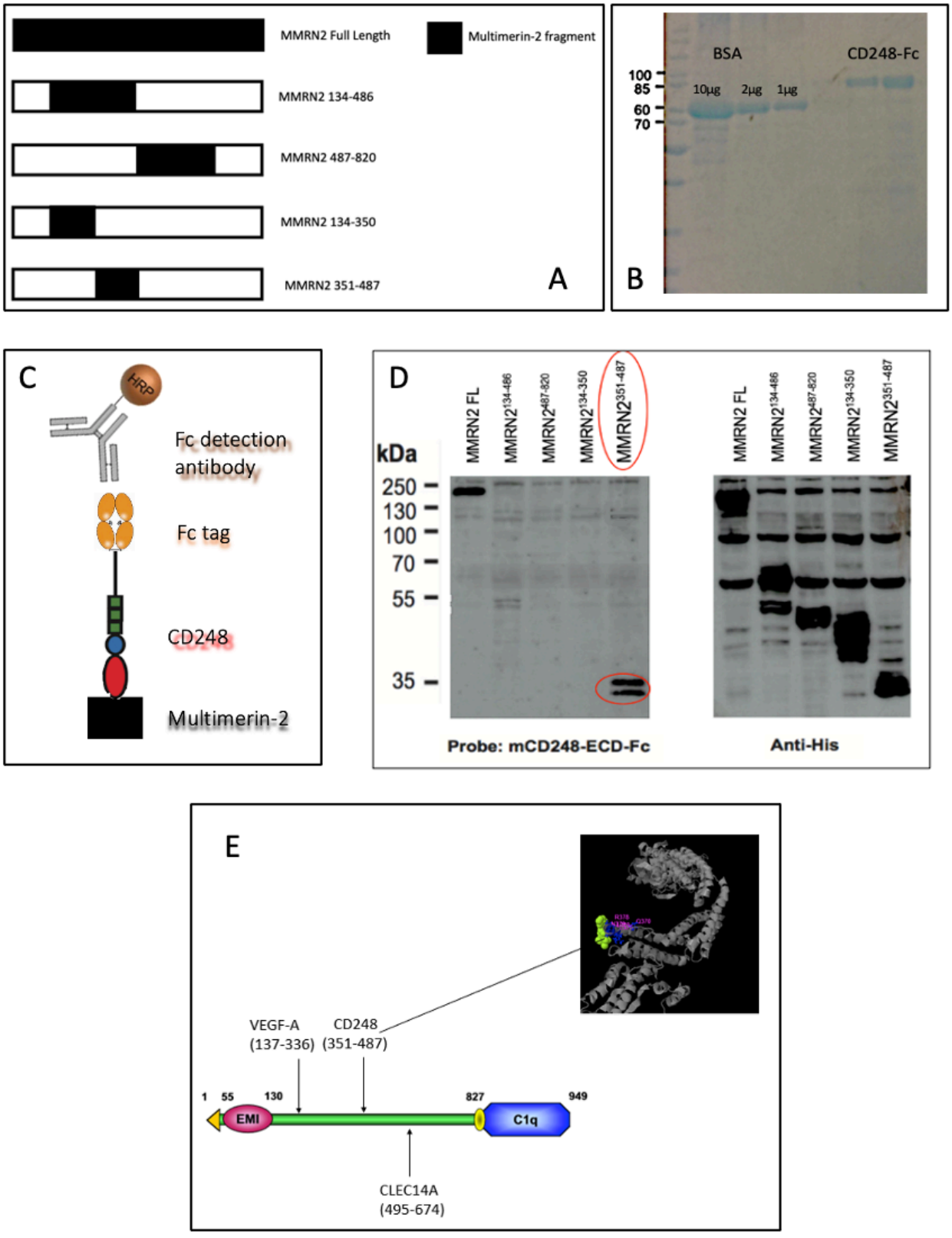


Figure 35. See previous page for caption.

3.6 Summary of expression studies

The focus of this chapter was predominantly to look at the expression of CLEC14A in human hepatic tissue. With a recent study describing how CLEC14A is upregulated in HCC (Yan et al., 2022) it was important to have a look at whether in HCC CLEC14A and its ligand MMRN2 affect survival outcomes. Two other ligands of MMRN2: CD93 and CD248 were also explored in this context using TCGA data. It was interesting to see that high CLEC14A expression was significantly associated with better outcomes in HCC, and this was also the case with MMRN2. CD93 and CD248 expression did not have any significant effect on survival in the TCGA data, and therefore CLEC14A remained the focus of my studies.

CLEC14A expression had not been looked at previously in normal and diseased liver tissues and it is notable that CLEC14A is upregulated in chronic liver disease and in HCC. CLEC14A was restricted to the endothelium and in chronic liver disease expression could be seen on portal vein and hepatic artery branches and there was also some sinusoidal expression, but this was predominantly associated with fibrotic septa and the sinusoids around the portal triads in ALD, NAFLD and PBC cases. It was noteworthy that expression of CLEC14A in chronic liver disease was not only associated with the portal triad but in areas of bridging fibrosis extending between the portal triads, with reduced expression in the central vein branches and surrounding sinusoids. One hypothesis would be that these are known to be areas of active angiogenesis. Fibrotic septa are associated with hypoxaemia (Cai et al., 2021) which we know upregulates angiogenesis. If we think

about the liver in terms of zones, the zones where CLEC14A was high are zones normally considered to be oxygen rich in a healthy liver and perhaps these areas are therefore more sensitive to the hypoxaemia in diseased liver states. It will therefore be useful to look at hypoxia as a regulator of CLEC14A.

In a hepatocellular carcinoma it could clearly be seen that CLEC14A is upregulated in tumour compared to non-tumour adjacent tissue. However, between the cases sinusoidal positivity varied between patchy to diffuse and in some cases, it was notable that although CLEC14A expression was high in the tumour and the tumour capsule, there was sparing of the tumour periphery. The reason for this is not clear.

We also see that both CLEC14A and MMRN2 co-localise in the liver and indeed both are expressed by HSEC in culture; even HSEC isolated from normal livers, in culture expressed CLEC14A, although this was less than in cells isolated from cirrhotic livers. This is the first time CLEC14A has been shown to be expressed by HSEC and previous published data has focused on cells from the macrovasculature. The CLEC14A-MMRN2 interaction also persisted on western blotting in non-reducing conditions and illustrates the strength of this interaction. It was notable that not all the CLEC14A was bound to MMRN2, and this interaction may therefore have a functional role.

I have been able to confirm that CD248 does interact with MMRN2 and show that this is at a distinct site from where VEGF binds MMRN2. This makes it likely that

MMRN2 isn't simply a molecular glue for endothelial cells and pericytes but that it may also have a regulatory role in angiogenesis.

The most significant finding when looking at tumour characteristics was that high CLEC14A expression was associated with poorer tumour differentiation. This is a curious finding because in the TCGA data high CLEC14A expression was associated with improved survival which we would not expect with poorly differentiated tumours. However, when performing survival analysis using CLEC14A protein expression in my samples, although the result wasn't significant, after 3 years the survival curves separated and high CLEC14A expression seem to be having a positive impact on overall survival and risk of recurrence. It is not clear why this should be the case, but it is a noteworthy finding. Previous publications looking at CLEC14A in tumours have shown CLEC14A in primary solid organ tumours (Mura et al., 2012) but I have been able to show that CLEC14A, along with CD248 and MMRN2, are also present in liver metastases and therefore it is not unique to primary tumours.

4

4 Evaluation of CLEC14A as a potential serum biomarker

4.1 Introduction and aims.

The ideal surveillance maker for HCC needs to be highly sensitive, have a high specificity, be easy to use and not operator dependent. Biomarkers can also be used to assess response to treatment and predict prognosis. In the case of AFP, it is known to be associated with tumour VEGF pathway activation and therefore ramucirumab is only recommended in cases where the AFP is >400 (Zhu et al., 2019). Therefore, a biomarker has the potential to predict who may or may not respond to a particular treatment. Another example is PDL1 expression in tumours which is associated with poorly differentiated tumours, high levels of AFP and a poor prognosis (Li et al., 2020). However, measuring PDL1 expression requires histology, and the ideal biomarker would be measurable in a non-invasive manner.

Hepatocellular carcinoma frequently occurs on the background of cirrhosis. In many countries, including the UK, once cirrhosis is identified, we use a

combination of ultrasound scans and AFP to survey patients with cirrhosis to identify the development of HCC at an early stage. Despite this, a cohort of patients are still identified with advanced HCC, and many patients with HCC will not be producers of AFP. Therefore, there is a requirement to identify new diagnostic biomarkers that can identify HCC at a very early stage. Biomarkers also play a role in predicting response to cancer treatments. They can help identify patients with an excellent response to a particular treatment and, conversely, those with a poor outcome. It is essential that a non-invasive biomarker needs to be highly sensitive and specific to be used as a screening tool.

CLEC14A can be detected in the serum, and therefore evaluating CLEC14A as a potential biomarker in a cohort of HCC patients was conducted to see if there was any utility for CLEC14A as a biomarker for the early detection of HCC or as a prognostic marker. It was also hoped that this might also increase our understanding of the role of CLEC14A in cancer by looking to see if there is any relationship with the corresponding clinical data.

Serum CLEC14A has been explored in a small cohort of colorectal cancer patients (Pietrzyk and Torres, 2022). The study found that CLEC14A could be detected in the serum in both healthy controls and in colorectal cancer patients but at a significantly higher level in colorectal cancer and that the level correlated with the TNM stage. There was not, however, a significant fall in serum CLEC14A at three months post-surgery.

Aims

This study aimed to assess whether CLEC14A could be a useful biomarker in patients with HCC.

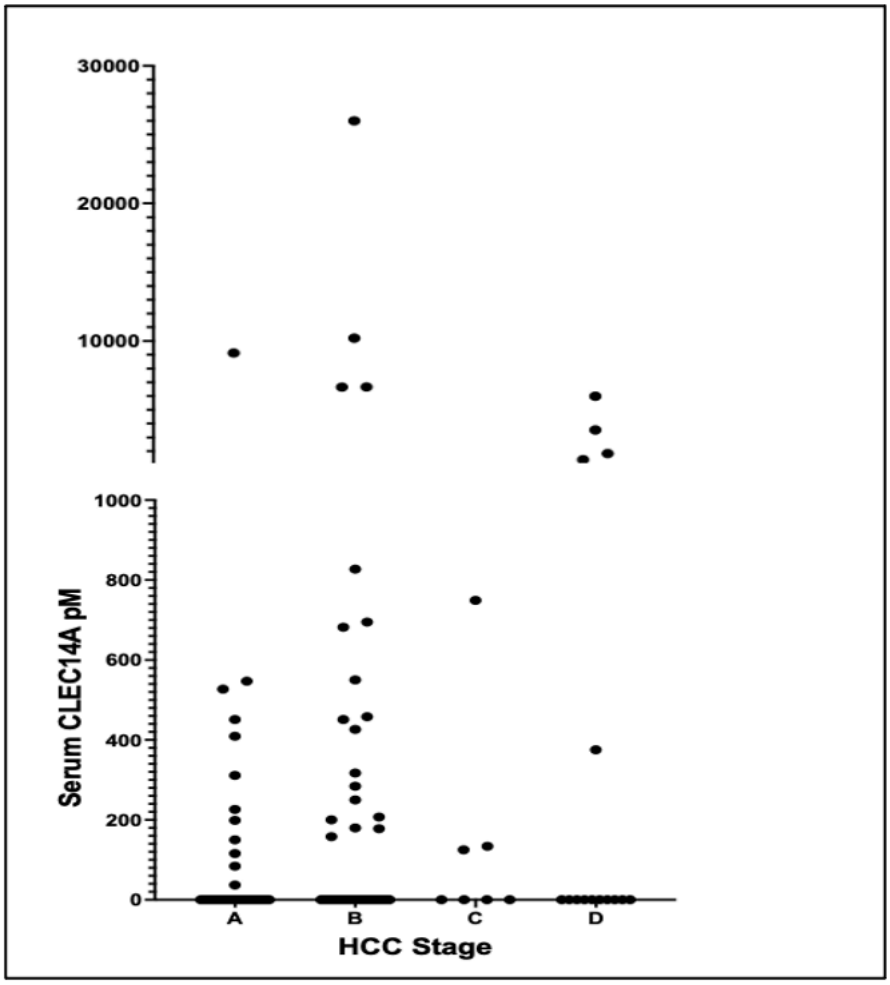
The aims of this study include:

a) Evaluate the detection of CLEC14A in the serum of a cohort of HCC patients and compare this with our traditional biomarker AFP.
b) Determine if CLEC14A is detectable in liver patients without HCC, including patients with liver fibrosis and cirrhosis.
c) Assess if CLEC14A levels predict outcomes to treatment in HCC in terms of recurrence-free survival and transplant-free survival.

4.2 Results

4.2.1 Serum CLEC14A and AFP for each HCC Barcelona Stage

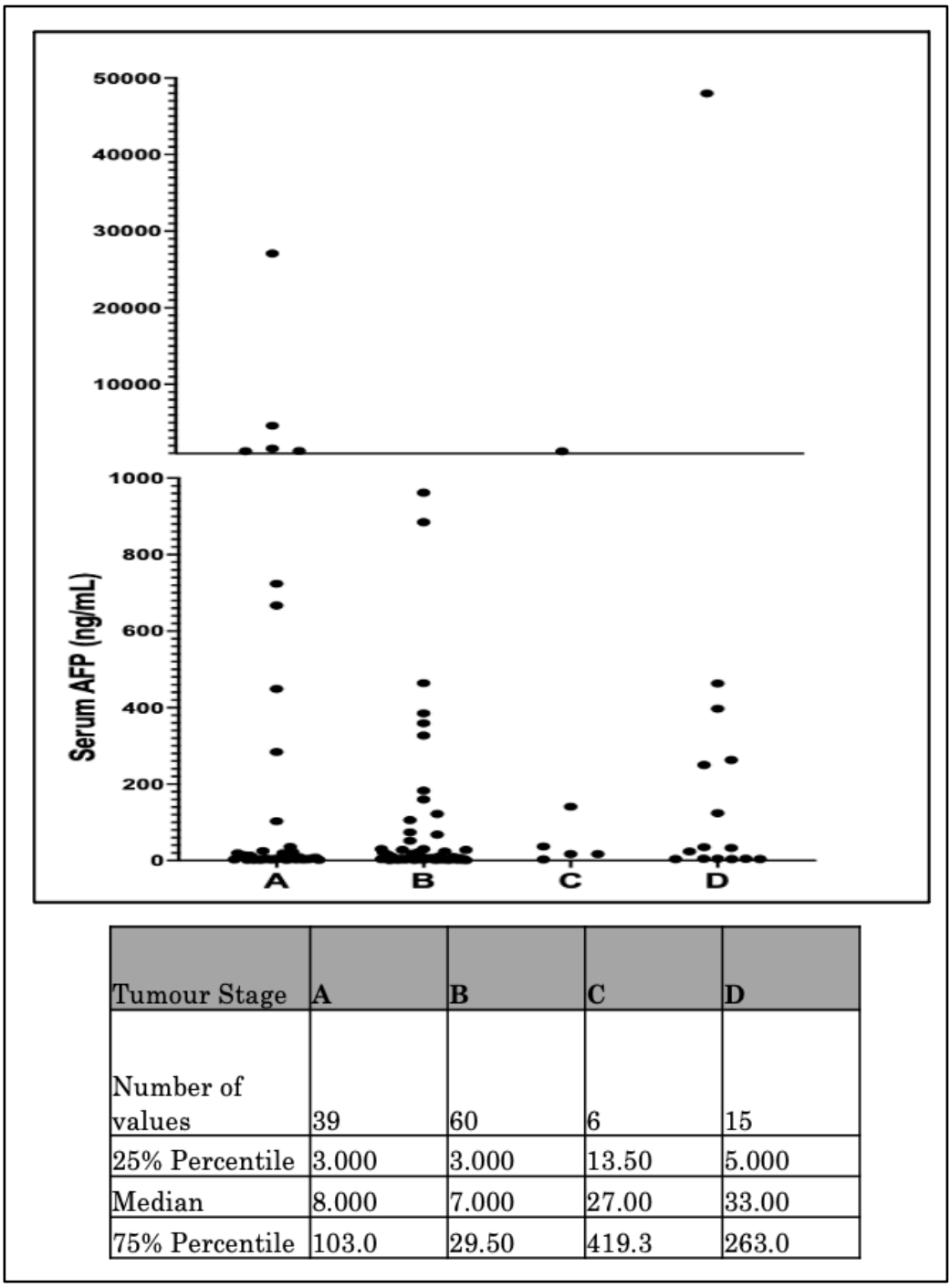
The CLEC14A serum value was evaluated in 142 treatment-naive patients with HCC. The patients were classified according to Barcelona criteria for HCC. We found that in many patients, CLEC14A was not detectable in the serum: Stage A 27/60 (45%), Stage B 41/60 (68%), Stage C 4/7 (57%), Stage D 10/15 (67%) had undetectable levels of CLEC14A. The CLEC14A values for each patient are shown in **Figure 36**. The Kruskal-Wallis test found no significant difference in values across the groups P=0.8864. The median values for AFP were higher for more advanced Barcelona stages but did not reach statistical significance. Kruskal-Wallis test P=0.1500, **Figure 37**.



HCC Stage	A	B	C	D
Number of cases	39	60	7	15
25% Percentile	0.000	0.000	0.000	0.000
Median	0.000	0.000	0.000	0.000
75% Percentile	116.0	205.3	134.0	1383

Figure 36. CLEC14A serum values according to Barcelona tumour staging.

CLEC14A serum values according to Barcelona tumour staging. Early HCC n= 39, Intermediate n= 60, Advanced n=7, Terminal n= 15. The Kruskal-Wallis test showed no significant difference in values across the groups P=0.8864.



Tumour Stage	A	B	C	D
Number of values	39	60	6	15
25% Percentile	3.000	3.000	13.50	5.000
Median	8.000	7.000	27.00	33.00
75% Percentile	103.0	29.50	419.3	263.0

Figure 37. AFP serum values with tumour stage.

Median and IQR across four HCC stages. Early HCC n= 39 , Intermediate n= 60, Advanced n=7, Terminal n= 15. Kruskal-Wallis test was performed and showed no significant difference across the groups P=0.1500

4.2.2 Serum CLEC14A and AFP in fibrosis, cirrhosis and HCC

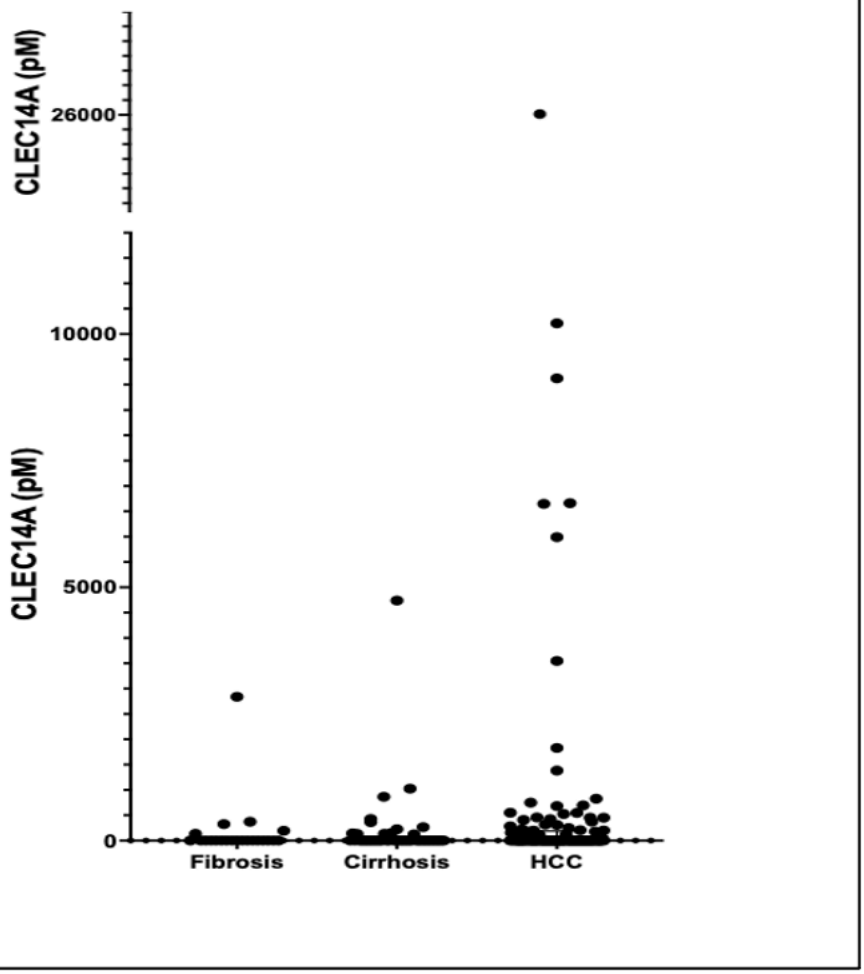
Clinical data from 192 patients and serum CLEC14A and AFP values were examined. 22 patients had liver fibrosis, 49 cirrhosis and 121 HCC. Baseline characteristics were compared for the 3 groups. A significant age difference was found between the three groups, P<0.0001, patients with cirrhosis were older than those with fibrosis and patients with HCC older than those with cirrhosis alone. The mean ±SD age was 50.3 ±13 for the fibrosis group, 59.3±11.3 for cirrhosis and 64.9±9.2 in the HCC cohort. There were more males in all three cohorts compared to females. There was a significant difference in the percentage of males in the HCC cohort compared to the cirrhosis cohort, 79% vs 53% p=0.0026. There were more Caucasian patients in the cirrhosis and HCC cohort compared to the fibrosis group p=0.005. When looking at standard laboratory variables, a significant difference between the 3 groups was found for 6 variables, ALT p=0.0086, bilirubin 0.0031, albumin p=<0.0001, sodium p=0.0004, platelets <0.0001, INR p=0.0004. This is unsurprising as these variables are associated with liver function or inflammation. Looking at AFP and CLEC14A, only AFP was statistically different between the groups p<0.0001. Post-hoc analysis of AFP found that statistical difference was present between Fibrosis vs HCC groups p= 0.0328, and Cirrhosis vs HCC p= <0.0001. The median values were all zero for CLEC14A, the 75% percentile was highest in the HCC group, followed by the cirrhosis group, but differences did not reach a statistical significance p=0.3524. A summary of the patient characteristics for the 3 groups in shown in **Table 18**, and a dot plot for individual CLEC14A values is shown in **Figure 38**.

	N	Fibrosis (N=22)	Cirrhosis (N=49)	HCC (N=121)	P-value
Demographics					
Age (years)	191	50.3 ±13	59.3±11.3	64.9±9.2	<0.0001
Male	191	16 (73%)	26 (53%)	96 (79%)	0.0026
Ethnicity	169				0.0050
Caucasian		16/22 (73%)	45/48 (94%)	93/99 (94%)	
Non-Caucasian		6/22 (27%)	3/48 (6%)	6/99 (6%)	
Laboratory tests					
ALT (U/L)	189	36 (26-61)	24 (18-36)	32 (23-46)	0.0086
Bilirubin (µmol/L)	189	10 (6-14)	15 (10-22)	16 (10-25)	0.0031
Albumin (g/L)	177	48±4.3	44±5.1	42±5.5	<0.0001
Sodium (mmol/L)	189	141±2	142±3	139±3	0.0004
Creatinine (µmol/L)	189	77 (61-95)	75 (62-88)	74 (64-91)	0.8383
Haemoglobin (g/L)	189	147±19	137±21	138±18	0.1224

Platelets (10^9/L)	189	234(189-289)	109(68-171)	118(82-172)	<0.0001
INR	185	1(1-1.1)	1.2(1.1-1.3)	1.2(1.1-1.2)	0.0004
Tumour markers					
AFP (ng/mL)	177	3 (1.3-16.8)	4 (2.5-5)	8.5(4-64)	<0.0001
CLEC14A (pM)	192	0 (0-33.5)	0 (0-62.5)	0 (0-189.5)	0.3524

Table 18. Summary of patient demographics, laboratory tests and tumour markers.

The three groups are fibrosis, cirrhosis and HCC. Data presented as Number (%), mean ±SD, or median (IQR); with p-values from Chi-square test, one-way ANOVA or Kruskal-Wallis test. Dunn's multiple comparison test for AFP & CLEC14A: AFP: Fibrosis vs cirrhosis (p= >0.9999), Fibrosis vs HCC (p= 0.0328), Cirrhosis vs HCC (p= <0.0001). CLEC14A: Fibrosis vs cirrhosis (p= >0.9999), Fibrosis vs HCC (p= 0.9444), Cirrhosis vs HCC (p= 0.6612)



	Fibrosis	Cirrhosis	HCC
Number of values	22	49	121
25% Percentile	0.000	0.000	0.000
Median	0.000	0.000	0.000
75% Percentile	33.50	62.50	189.5

Figure 38. A dot plot of individual CLEC14A values in the fibrosis, cirrhosis and HCC cohorts.

A dot plot of individual CLEC14A values in the fibrosis, cirrhosis and HCC cohorts. P-value 0.3524 from Kruskal-Wallis test.

4.2.3 Tumour characteristics and serum CLEC14A and AFP.

A higher AFP was significantly associated with the presence of more than one tumour p=0.0489 but there was no significant difference in serum AFP and the size of the largest tumour, vascular invasion or tumour differentiation. Although the number of samples available with histological data was smaller because it could only be obtained for surgical treatments. For CLEC14A serum values, there was no significant difference between the presence or absence of vascular invasion P= 0.3450. Still, a significant difference in CLEC14A values between micro and macrovascular invasion was found, p= 0.0468, and the median value for microvascular invasion was 117 vs 0 for the presence of macrovascular invasion **Table 19**.

		CLEC14A		AFP	
	N	**Serum CLEC14A value (pM)**	**P value**	**Serum AFP value (ng/mL)**	**P value**
Number of lesions			0.1623		0.0489
1	89	0 (0-216.5)		6 (3-35)	
>1	32	0 (0-0)		18 (5-137)	
Size of largest lesion			0.8379		0.4449
<5cm	101	0 (0-189)		8 (4-37)	
≥ 5cm	20	0 (0-194)		11 (3-962)	
Vascular invasion			0.3450		0.7226
No	11	0 (0-200)		5 (3-22)	
Yes	24	0 (0-283)		6 (3-667)	
Vascular invasion			0.0468		0.6136
Micro	14	117 (0-340)		6 (3-47)	
Macro	10	0 (0-0)		64 (3-7313)	
HCC Differentiation			0.1342		0.2050
Well	6	0 (0-369.5)		6 (4-9)	
Moderately	26	0 (0-199.3)		6 (3-52)	
Poorly	8	0 (0-0)		250 (4-1293)	

Table 19. CLEC14A and AFP values based on tumour characteristics.

Serum CLEC14A and AFP values based on tumour characteristics. Data on vascular invasion and differentiation only available from transplanted or surgical resections for HCC and therefore smaller numbers. Data presented as median (IQR), and p-values from Mann-Whitney tests.

4.2.4 Correlation of laboratory values to CLEC14A for all cohorts of patients

No significant correlation was found for AFP, ALT, Albumin, Bilirubin, Sodium, Creatinine, Haemoglobin, Platelets, INR or Child-Pugh score. There was, however, a significant negative correlation with the white cell count, neutrophils and lymphocytes in peripheral blood P= 0.0205, P=0.0201, P=0.0096 respectively, **Table 20.**

	CLEC14A	
	Rho	**P-value**
AFP	0.06606	0.3824
ALT	0.1389	0.0567
Albumin	-0.1393	0.0645
Bilirubin	0.09342	0.2010
Sodium	0.004684	0.9490
Creatinine	-0.03974	0.5871
Haemoglobin	-0.1000	0.1709
Platelets	-0.09265	0.2048
INR	0.05367	0.4681
Child Pugh Score	0.01748	0.8103
WCC	-0.1684	0.0205
Neutrophils	-0.1690	0.0201
Lymphocytes	-0.1879	0.0096
NLR	0.03064	0.6755

Table 20. Correlation between laboratory values and CLEC14A for the whole patient cohort.

Correlation between laboratory values and CLEC14A for the whole patient cohort. NLR: Neutrophil Lymphocyte Ratio.

4.2.5 Detectable serum CLEC14A HCC and effect on recurrence and transplant-free survival

All pre-treatment CLEC14A serum samples were divided into CLEC14A not detectable vs CLEC14A detectable in the serum. Analysis was then performed using Kaplan-Meier curves to evaluate the impact of detectable CLEC14A on time to recurrence post-treatment and overall survival. We found no statistically significant difference in time to recurrence post-treatment between the two groups P- value from log-rank test 0.7786. However, from 11 months to 3 years, the curves appear to separate with possible survival advantage from low pre-treatment CLEC14A serum levels after the first 11 months. Similarly for transplant free survival in the HCC cohort there is no significant difference between the groups log rank 0.7461, however, the curves do separate after the first couple of years with a survival advantage if CLEC14A is not detectable in the serum.

Looking at all patients from all cohorts again, there appeared to be a survival advantage if CLEC14A wasn't detectable in the serum, but this did not achieve significance Log-rank 0.1444. The median survival was 2014 days if CLEC14A negative and 1392 days if CLEC14A was detectable. In the cirrhosis cohort the trend was the same but again not statistically significant log rank p=0.0952.

We then looked at the same cohort of HCC patients and evaluated the effect of AFP, existing biomarker used in clinical practice and there was a significant difference in survival depending on whether AFP was less than or greater than 100. With a higher AFP associated with reduced overall survival. log-rank 0.0031 Median survival 1092 days vs 535 days **Figure 39.**

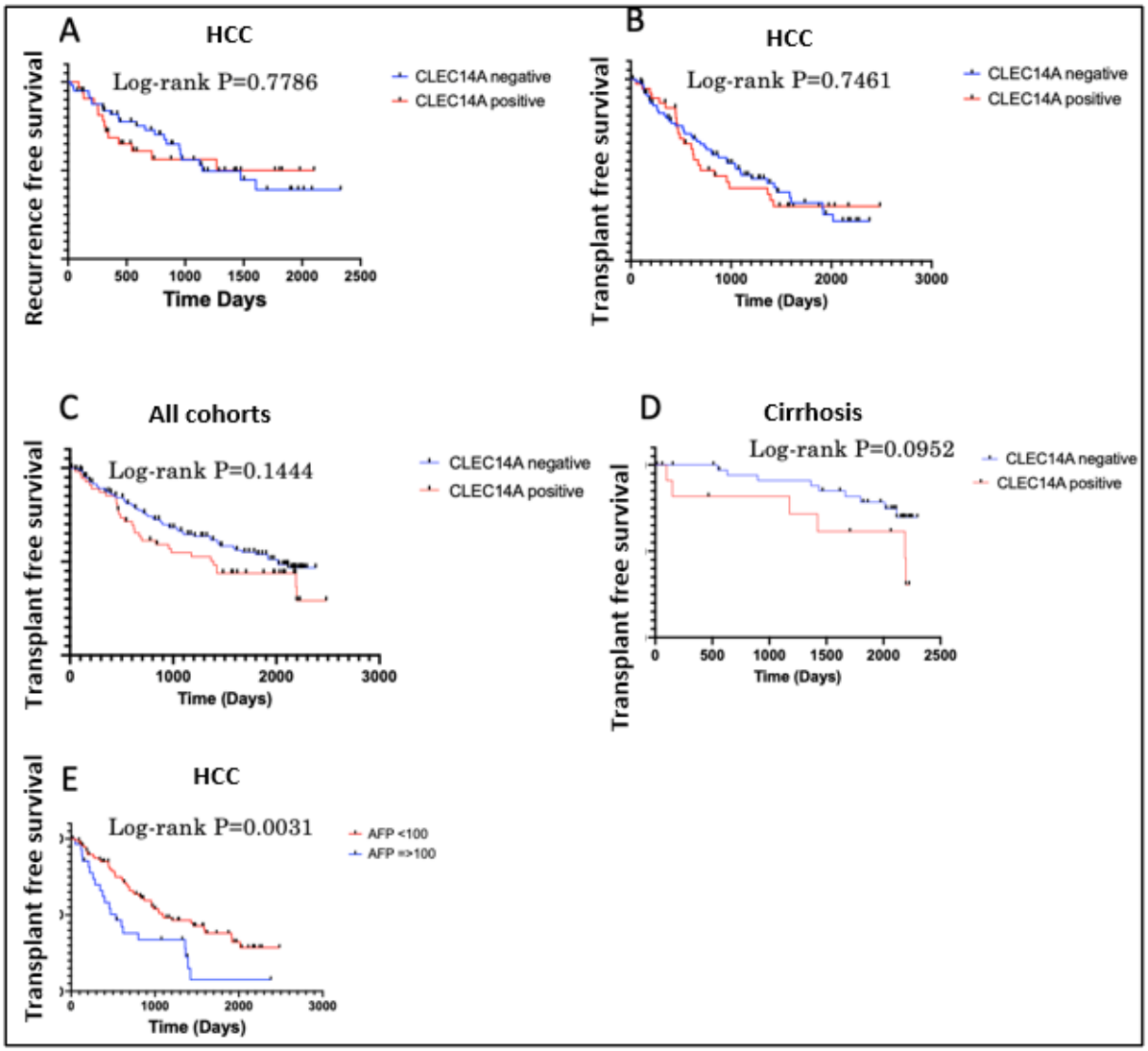


Figure 39. Kaplan Meier curves for recurrence and transplant free survival by serum AFP or serum CLEC14A level.

A)Recurrence probability post HCC treatment by whether CLEC14A is detectable in the serum pre-treatment or not, P-value from log-rank test 0.7786 . **B)** Transplant free survival by whether CLEC14A is detectable in the serum pre-treatment. Median survival 1092 days if CLEC14A undetectable vs 694 days if serum CLEC14A detectable. P-value from log-rank test 0.7461. **C)** Transplant-free survival for all patients. The Kaplan-Meier curve for transplant-free survival for all patients (fibrosis, cirrhosis or HCC) from the time of CLEC14A serum sample. Median survival 2014 days if CLEC14A is undetectable vs 1392 days if serum CLEC14A is detectable. P-value from log-rank test 0.1444. **D)** Transplant-free survival for the cirrhosis cohort. The Kaplan-Meier curve for transplant-free survival for patients with cirrhosis from the time of CLEC14A serum sample. P-

value from log-rank test 0.0952. **E)** Transplant-free survival for HCC cohort by AFP. The Kaplan-Meier curve for transplant-free survival for patients with HCC from the time of pre-treatment AFP by whether AFP was less than or greater than 100. Median survival 1092 days if AFP was less than 100 vs 535 days if AFP was greater than 100. There was a statistically significant difference P-value from log-rank test 0.0031. (22 patients had liver fibrosis, 49 cirrhosis and 121 HCC)

4.2.6 CLEC14A serum values and expression in HCC tissue

Finally, in 7 cases HCC tissue was available to match the serum sample and this was evaluated for CLEC14A expression. 75% of cases with no detectable serum CLEC14A also had no CLEC14A present in the tumours on chromogenic staining. In the 3 cases with high serum CLEC14A levels, CLEC14A was found to be diffusely positive in the tumour tissue. **Figure 40.**

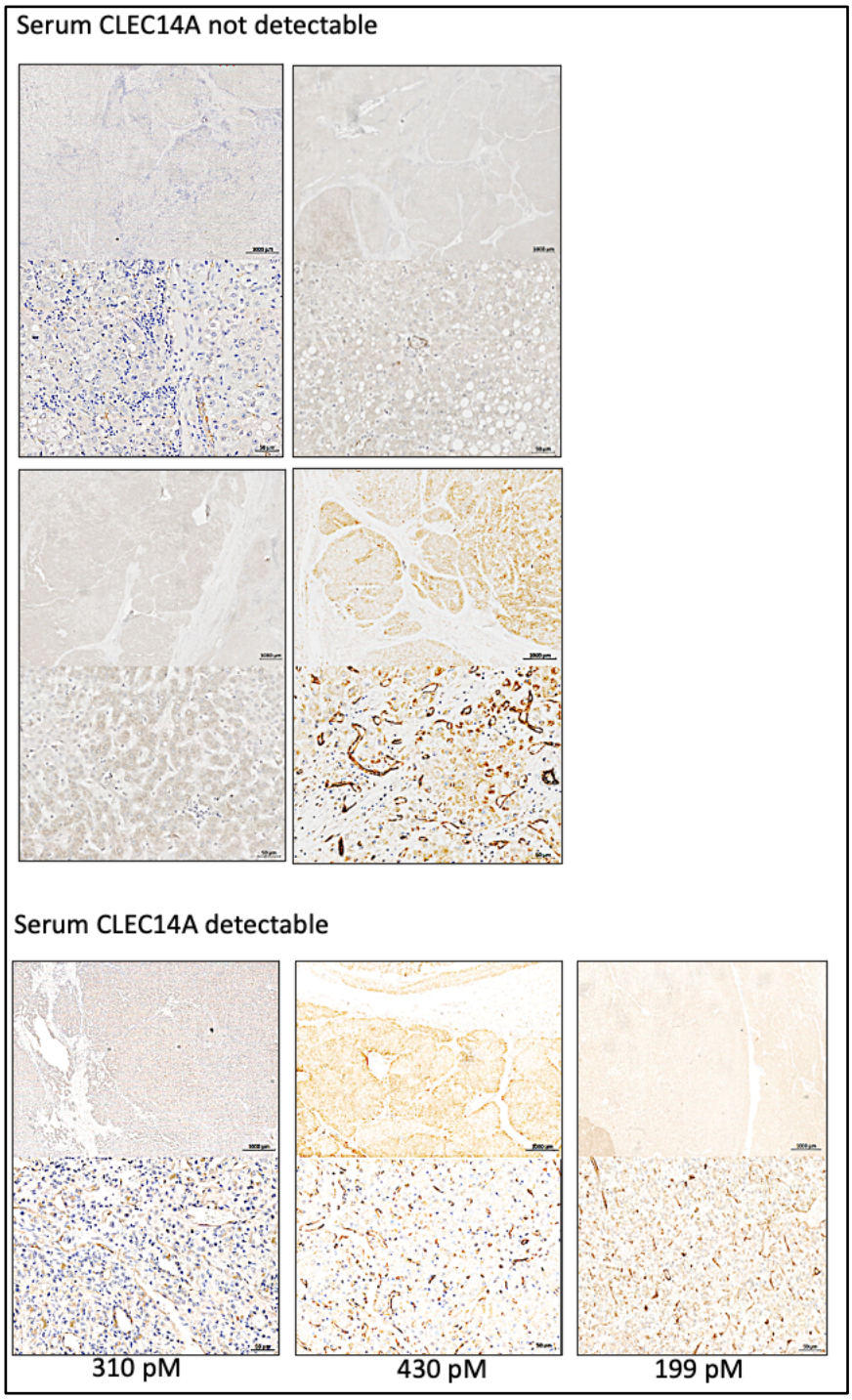


Figure 40. HCC cases with matched CLEC14A serum values and tissue CLEC14A immunohistochemistry.

75% (3/4) of cases with no serum CLEC14A detectable also had no CLEC14A protein staining in the tumour tissue. 100% (3/3) of cases with detectable CLEC14A had detectable CLEC14A protein staining in the tumour tissue. Each case shown with enlarged image below. Detectable CLEC14A serum values shown below the images.

4.3 CLEC14A RNA expression in different tumour types

The only published paper looking at CLEC14A serum levels was in colorectal cancer (Pietrzyk and Torres, 2022), and the paper found that high serum CLEC14A was associated with worse outcomes. In chapter 3 I looked at TCGA data for CLEC14A in HCC and survival outcomes, and CLEC14A tissue RNA in liver cancer is associated with better overall survival. I therefore used this approach to look at tissue expression and outcomes in other cancers including colorectal cancer **Figure 41**. I found that at the tissue level CLEC14A expression in tissue is not always associated with better survival outcomes (using the TCGA dataset). It did however show that high tissue CLEC14A expression in colorectal cancer is associated with worse outcomes which corresponds to the findings for high serum CLEC14A values by Pietrzyk at al.

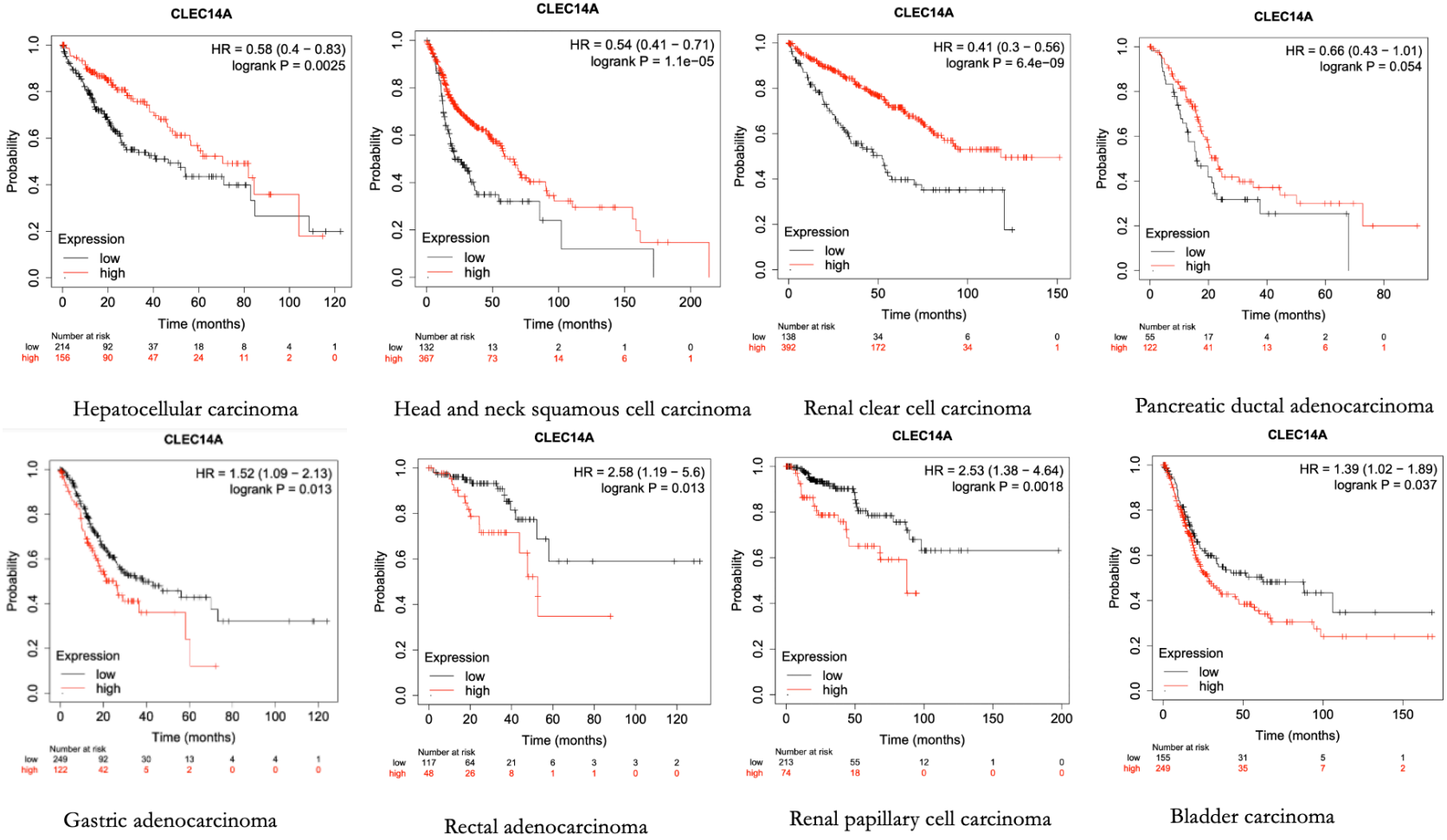


Figure 41. CLEC14A RNA expression in different tumour types.

RNA-seq data and survival analysis from publicly available databases GEO, EGA and TCGA. Nagy A, Munkacsy G, Gyorffy B: Pancancer survival analysis of cancer hallmark genes, **Sci Rep.**, 2021 Mar 15;11(1):6047, Plots created using https://kmplot.com/analysis/. Top row displays cancers with better overall survival when CLEC14A in the tumour is high. Bottom row cancers with better overall survival when CLEC14A expression is low. Log-rank values are displayed on each image and are all statistically significant.

4.4 Discussion

There has only been one previously published study looking at serum CLEC14A and exploring it as a biomarker in cancer. The study looked at colorectal cancer and found CLEC14A detectable in healthy controls and patients with colorectal cancer. There was a significant increase in serum CLEC14A in patients with colorectal cancer, which was associated with the stage of cancer, with a high level associated with a higher TNM stage (Pietrzyk and Torres, 2022). The ELISA used in their study was a commercially available ELISA, and our serum samples were run using an in-house ELISA using different detection antibodies. Still, the ELISA has been extensively validated by the Nagy group using CLEC14A spike protein, commercial serum from healthy controls and different cancer cohorts. Publicly available gene expression data from patients with hepatocellular carcinoma indicate that a high tumour CLEC14A RNA level is associated with better overall survival. This study therefore aimed to evaluate if CLEC14A would be a valuable serum biomarker in patients with hepatocellular carcinoma.

One of the data analysis challenges was that serum CLEC14A was not detectable in 58% of HCC patient samples. When looking at CLEC14A values by Barcelona tumour staging, there was no significant difference between the groups; however, AFP was also not statistically different between the Barcelona staging groups. The median values for AFP were however higher for stages C and D, representing a more advanced stage of hepatocellular carcinoma. Hepatocellular carcinoma predominantly occurs on the background of cirrhosis and based on previous

immunohistochemistry studies showing that CLEC14A can be present in cirrhosis, we wanted to see if CLEC14A was detectable in patients with cirrhosis but no cancer. This is key to determining if this will be a useful biomarker. The clinical data was as expected regarding demographics, in that older patients develop HCC. The mean age was higher in cirrhosis than in fibrosis, and HCC compared to cirrhosis; in keeping with the order of liver disease progression. HCC was also more common in males. There was a significant difference between the groups for various laboratory values, including a higher bilirubin in more advanced liver disease and a lower albumin and platelet count in cirrhosis than fibrosis. When looking at tumour markers, the AFP value was higher in the cohort of HCC patients compared to cirrhosis and fibrosis, which is what we expected as this is a validated biomarker in HCC. However, we could not find a significant difference between fibrosis or cirrhosis and HCC for serum CLEC14A; although the upper quartile value was higher in patients with cirrhosis compared to fibrosis and higher in patients with HCC compared to cirrhosis, this did not reach statistical significance. The lack of difference between the groups for serum CLEC14A indicates that CLEC14A cannot be used as an early detection biomarker for HCC. The dot plot of individual serum CLEC14A values demonstrates that we do see some very high levels of CLEC14A in the HCC cohort; however, we can see detectable levels (some high) in cirrhosis.

Disappointingly, it was evident that CLEC14A would not be a helpful screening tool for HCC, so we went onto look at tumour characteristics and laboratory values

to see if any insight could be gained regarding the role of CLEC14A in chronic liver disease and HCC. When looking at tumour characteristics, serum CLEC14A significantly differs between microvascular and macrovascular invasion in tumours. The levels were higher with microvascular invasion, which may fit with CLEC14A's role in pathological angiogenesis. Correlating CLEC14A serum values with laboratory markers, there was a statistically significant inverse correlation with leucocytes overall and neutrophils and lymphocytes, which is an interesting observation. The data cannot reveal the significance of this. It could be that peripheral CLEC14A affects the bone marrow or because CLEC14A is increased in cirrhosis which can be associated with pancytopenia. Against this theory, there was no correlation with platelet count.

Evaluating HCC recurrence and transplant-free survival, there was no significant relationship with serum CLEC14A. However, there was interestingly a trend that CLEC14A being undetectable was associated with improved survival, which was evident at 11 months in the case of recurrence. Detectable CLEC14A also trended towards a survival advantage in HCC from 18 months, but this was not statistically significant.

Looking at CLEC14A across all patient groups and cirrhosis in isolation, the same trend was observed that undetectable CLEC14A trended to a survival advantage. Disappointingly this did not reach significance, and the closest it came was a log-rank p-value of 0.0952 in the cirrhosis without HCC cohort. CLEC14A at the

tumour RNA level in publicly available databases suggests it is associated with increased survival in HCC, which implies that CLEC14A in tumours is a good thing. One hypothesis could be that CLEC14A is cleaved during microvascular invasion and released into the serum, which might explain the opposing serum trends with survival. When you look at public databases for other cancers and tumour CLEC14A RNA expression, it varies between cancers whether CLEC14A is associated with better survival. The complicating factor in HCC is the presence of cirrhosis. Given that most HCC occurs on the background of cirrhosis, this may explain why we haven't seen a clear-cut relationship like the published study on colorectal cancer and serum CLEC14A.

5

5 CHAPTER 5: The regulation of CLEC14A and MMRN2 in liver sinusoidal endothelial cells

This chapter focuses on the regulatory factors that influence CLEC14A and MMRN2 expression in hepatic sinusoid endothelial cells in vitro. There is currently no published data relating to the regulation of CLEC14A and MMRN2 in HSEC. In view of findings in the previous chapters where CLEC14A was found to be expressed in the fibrotic septa in chronic liver disease and diffusely in HCC, inflammatory stimuli and hypoxia were looked at to see if they impacted CLEC14A expression. In addition, although in tissue from normal livers there was no sinusoidal expression of CLEC14A I did find that cultured HSEC from normal livers did express CLEC14A and therefore the effect of flow on HSEC was evaluated because this has not been looked at previously in these specialised endothelial cells.

The aims of this chapter were to

1) Assess the effect of cytokine and growth factor stimulation on CLEC14A and MMRN2 expression in HSEC.

2) Investigate if hypoxia influences CLEC14A and MMRN2 expression in HSEC.

3) Ascertain if CLEC14A expression in HSEC is affected by flow.

5.1 Response to cytokine stimulation

To measure the basal level of CLEC14A expression in HSEC and the response to cytokine and growth factor stimulation in HSEC qPCR was performed to measure mRNA levels. Cells were exposed to 24 hours of stimulation before being lysed. HSEC from 3 or 4 different donors were used for the analysis. Overall, there was no significant effect seen but it could be observed that CLEC14A expression in HSEC isolated from different livers responded differently to the same cytokine or growth factor. In the case of inflammatory stimuli 3 HSEC isolated from NASH, ALD and PBC livers all had a twofold increase in CLEC14A in response to interferon, but a reduction was seen in response to LPS and interferon. The HSEC isolated from a liver with AIH responded in the opposite way. The ALD and PBC HSEC had a twofold increase in HSEC in response to BMP9 but this was not replicated with the HSEC isolated from the NASH liver. The data is shown in **Figures 42, 43 and 44.**

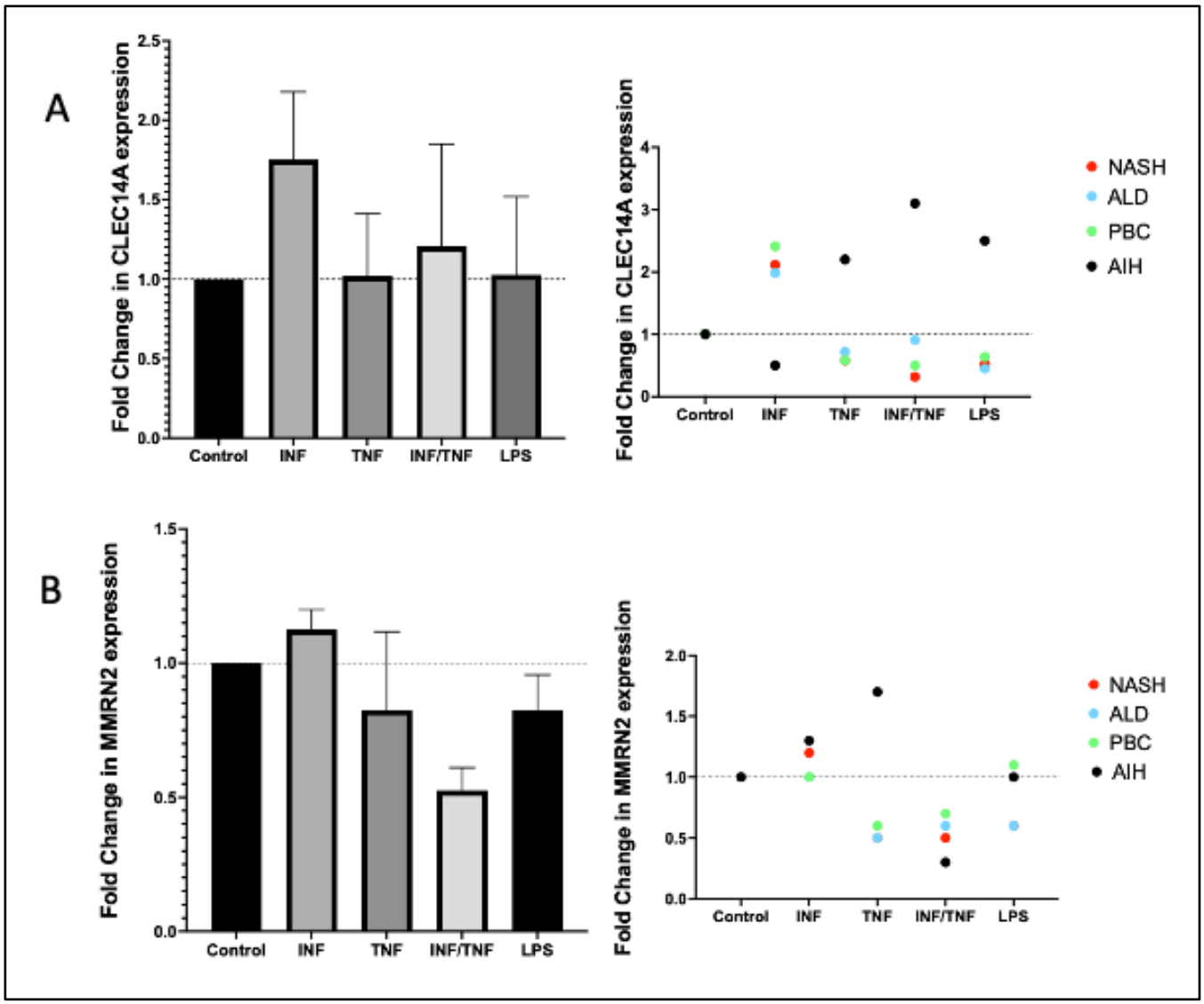


Figure 42. CLEC14A mRNA expression in HSEC in response to inflammatory stimuli.

qPCR analysis of CLEC14A mRNA in stimulated HSEC, normalised to housekeeping gene GAPDH. Graphs on left are the mean and SEM of 3-4 independent experiments (with 3 replicates for each condition) and dot plots on the right breaking down the individual cases and aetiology of liver disease the HSEC were isolated from. **A)** CLEC14A response to inflammatory stimuli, **B)** MMRN2 response to inflammatory stimuli.
Overall there was no significant change for each condition compared to control.

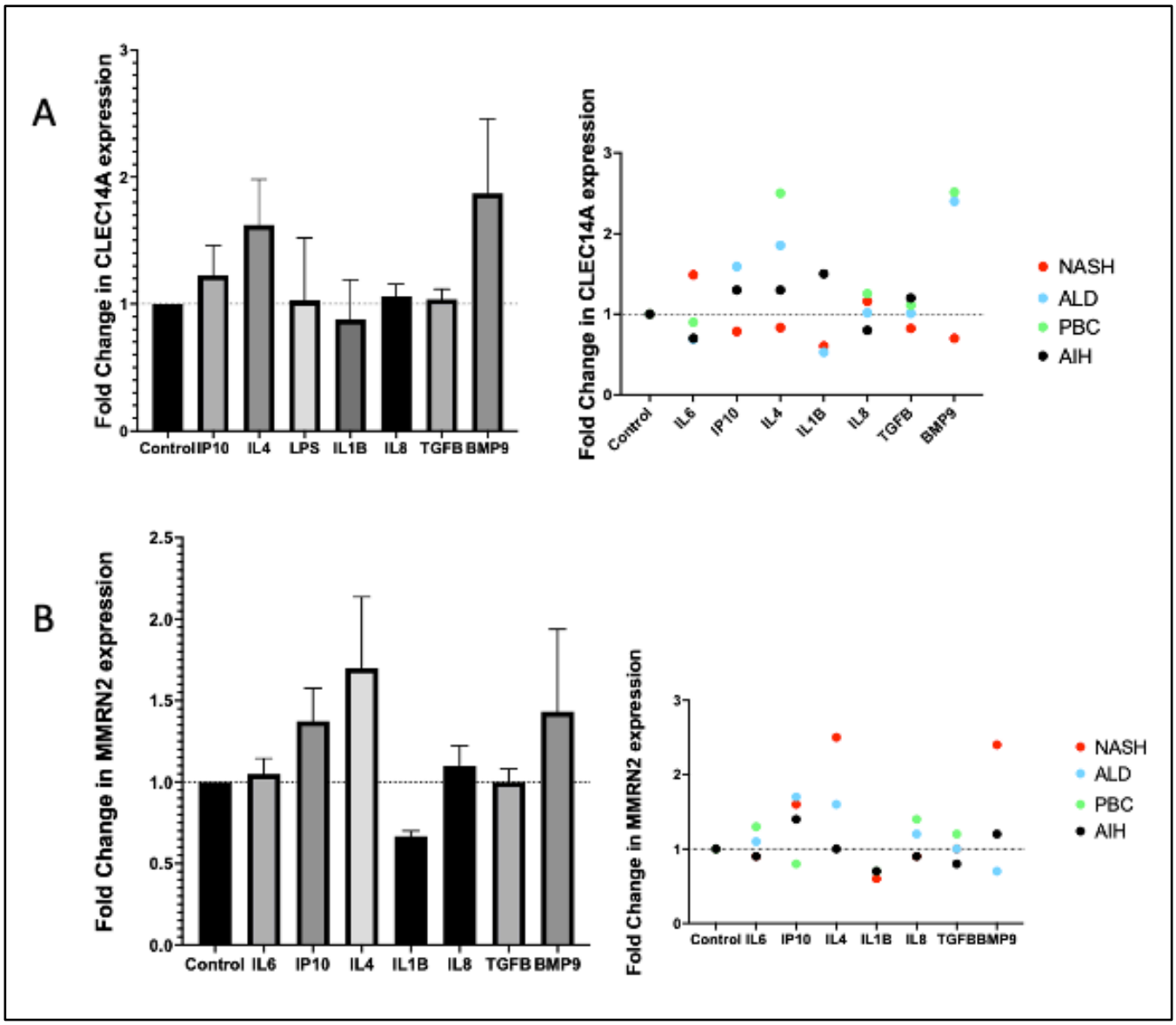


Figure 43. CLEC14A mRNA expression in HSEC in response to cytokine stimulation.

qPCR analysis of CLEC14A mRNA in stimulated HSEC, normalised to housekeeping gene GAPDH. Graphs on left are the mean and SEM of 3-4 independent experiments (with 3 replicates for each condition) and dot plots on the right breaking down the individual cases and aetiology of liver disease the HSEC were isolated from **A)** CLEC14A response to cytokine stimulation, **B)** MMRN2 response to cytokine stimulation.
Overall there was no significant change for each condition compared to control.

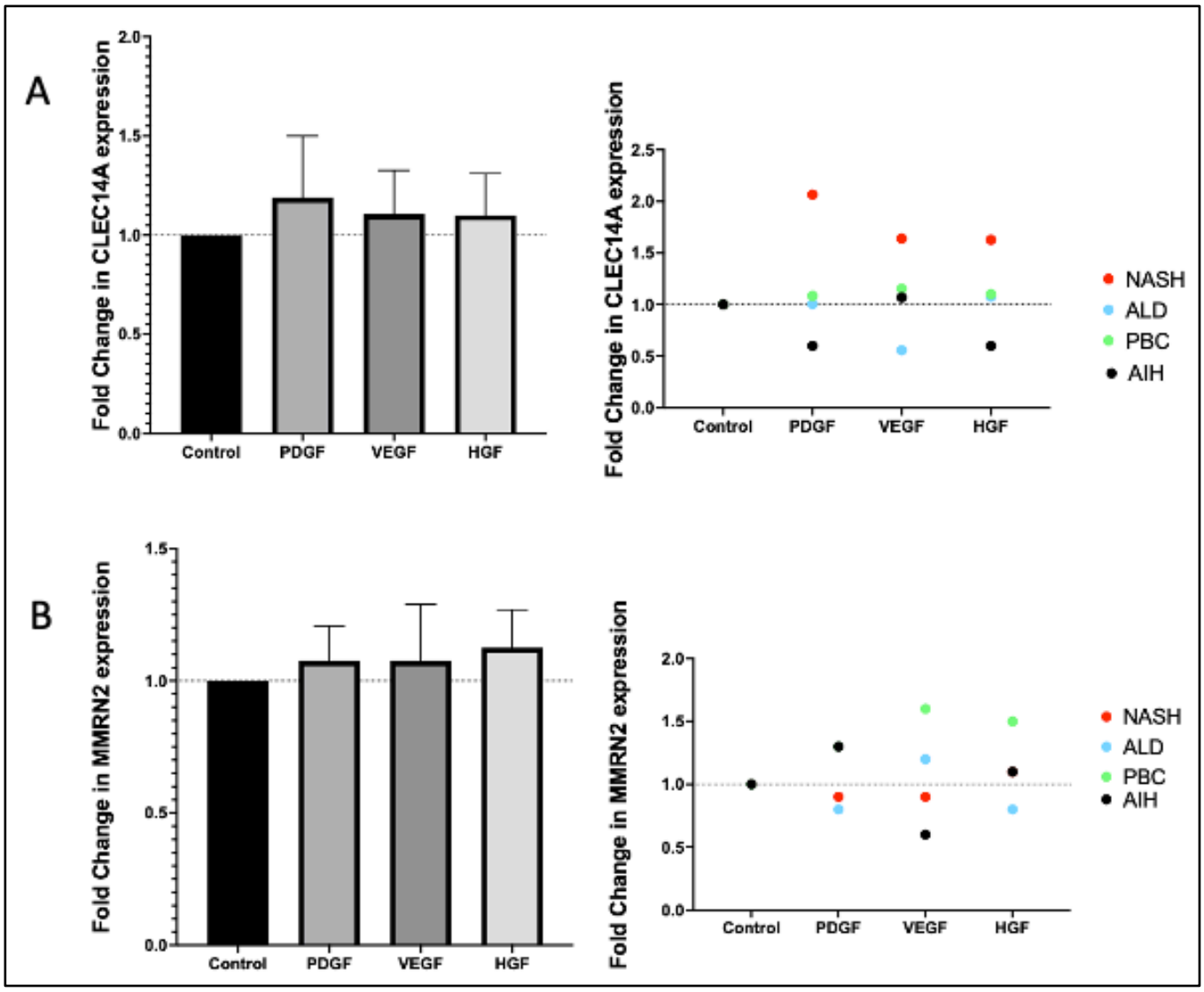


Figure 44. CLEC14A mRNA expression in HSEC in response to growth factors.

qPCR analysis of CLEC14A mRNA in stimulated HSEC, normalised to housekeeping gene GAPDH. Graphs on left are the mean and SEM of 3-4 independent experiments (with 3 replicates for each condition) and dot plots on the right breaking down the individual cases and aetiology of liver disease the HSEC were isolated from **A)** CLEC14A response to growth factors, **B)** MMRN2 response to growth factors.
Overall there was no significant change for each condition compared to control.

5.2 Response to hypoxia

Hypoxia is a key feature of the tumour microenvironment and promotes the progression of liver fibrosis in chronic liver disease. Therefore, HSEC were exposed to hypoxia and compared to HSEC maintained in standard laboratory culture conditions to see if the level of CLEC14A expression was affected. I also looked at the ligand for CLEC14A, MMRN2; and CD93 which binds MMRN2 in the same region as CLEC14A. I saw on immunohistochemistry in some chronic liver disease cases, particularly obvious in PBC, that CLEC14A was found in areas of bridging fibrosis which are associated with hypoxia.

The results of the hypoxia experiment demonstrated that CLEC14A expression increases when HSEC are exposed to reduced oxygen levels, although this didn't quite reach a level of significance p=0.0889. Hypoxia had the opposite effect on CD93 and MMRN2 and this was significant with p values of 0.0068 and 0.0042 respectively. Data shown in **Figure 45.**

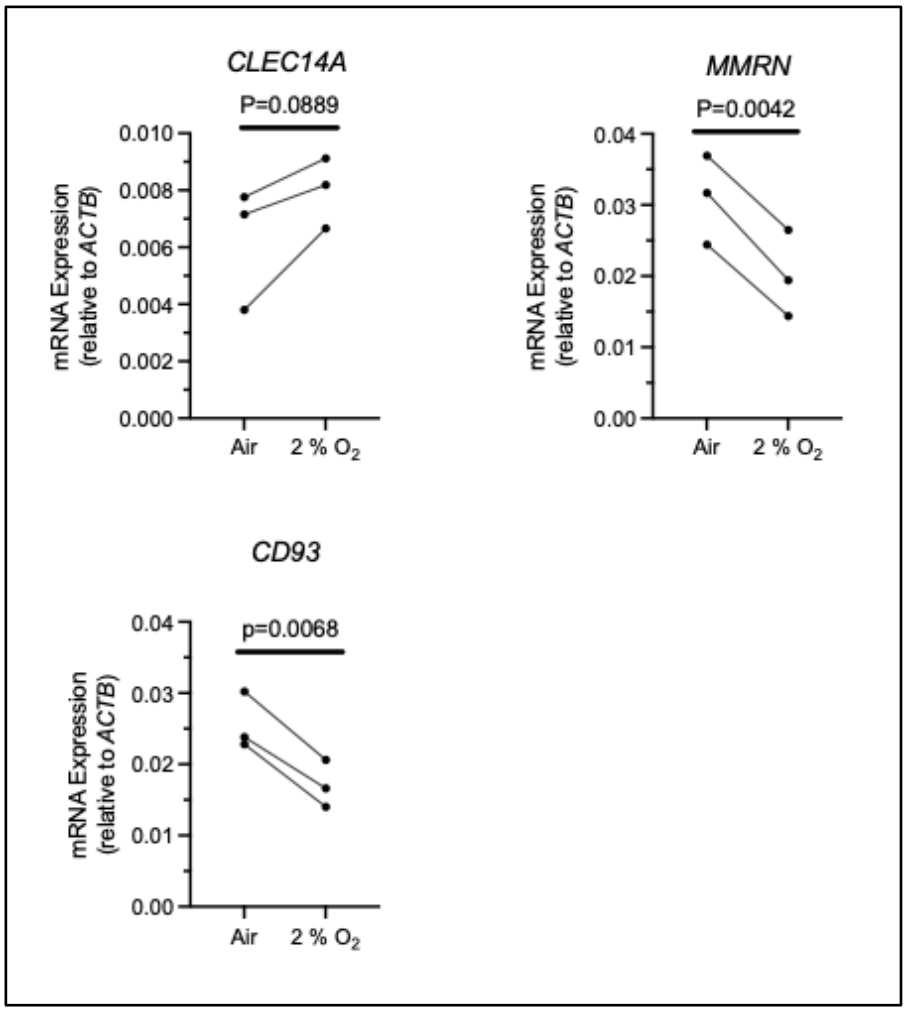


Figure 45. CLEC14A, MMRN2 and CD93 expression in response to hypoxia.

Relative expression of CLEC14A mRNA in HSEC. HSEC cultured in standard conditions were compared to HSEC cultured for 24 hours in a hypoxic chamber. A paired t-test showed there was a significant difference for MMRN2 and CD93, $p<0.005$ and $p<0.05$ respectively. CLEC14A did not quite reach significance $p=0.0889$.

5.3 Response to shear stress

We know that as liver disease progresses to cirrhosis, one of the hall marks is remodelling of not only the liver parenchyma but also loss of endothelial cell fenestrations (Szafranska et al., 2021) and increased angiogenesis. We have known for a long time that resistance within the liver increases and we see clinically that flow is reduced within the portal vein which can eventually lead to portal vein thrombosis (Moreno et al., 1967) .

To evaluate if CLEC14A in HSEC is regulated by flow, HSEC were cultured under standard conditions i.e. no flow and loss of shear stress and also cultured under flow i.e. comparably high shear stress for 72 hours. Although not a replicate model of blood flow in the liver it was a preliminary investigation to see if this changed CLEC14A expression in this specialised group of endothelial cells, which in the setting of cirrhosis can be exposed to reduced blood flow and also in the setting of tumours the vasculature is frequently disorganised, distorted and torturous reducing laminar flow.

It was observed that after exposure to flowing media the morphology of the HSEC changed and the cells appeared to elongate and line up in the direction of flow. HSEC isolated from 3 different livers all expressed CLEC14A at a higher level when cultured in static media compared to flow, overall, this didn't quite reach significance at a p value of 0.0881. Like for the effect of hypoxia the opposite affect was seen on MMRN2, and MMRN2 increased with high shear stress p=0.0502. In this experiment flow had no consistent effect on CD93 p=0.5410 **Figure 46**.

Finally, it had been previously noted by the Bicknell group that a delay in tissue fixation affects the expression of CLEC14A in tissue, but this had not been looked at in liver tissue. In our laboratory tissue is collected from theatres and immediately fixed in Formaldehyde for pathological examination. To investigate the effect of delay in fixation in CLEC14A expression in liver tissue over time I collected fresh liver tissue from a normal liver (non-fibrotic liver distal to tumour), and I divided it into three and fixed it at three time points 0hr, 24hr and 48 hour. The samples for fixation at 24 and 48 hours were kept in media with no supplements at +4 °C. The results revealed no positive CLEC14A staining at 24 hours but at 24 hours there was positive CLEC14A expression around the portal triads and by 48 hours there was more extensive CLEC14A staining, and it was most intense distal to the central vein **Figure 47**.

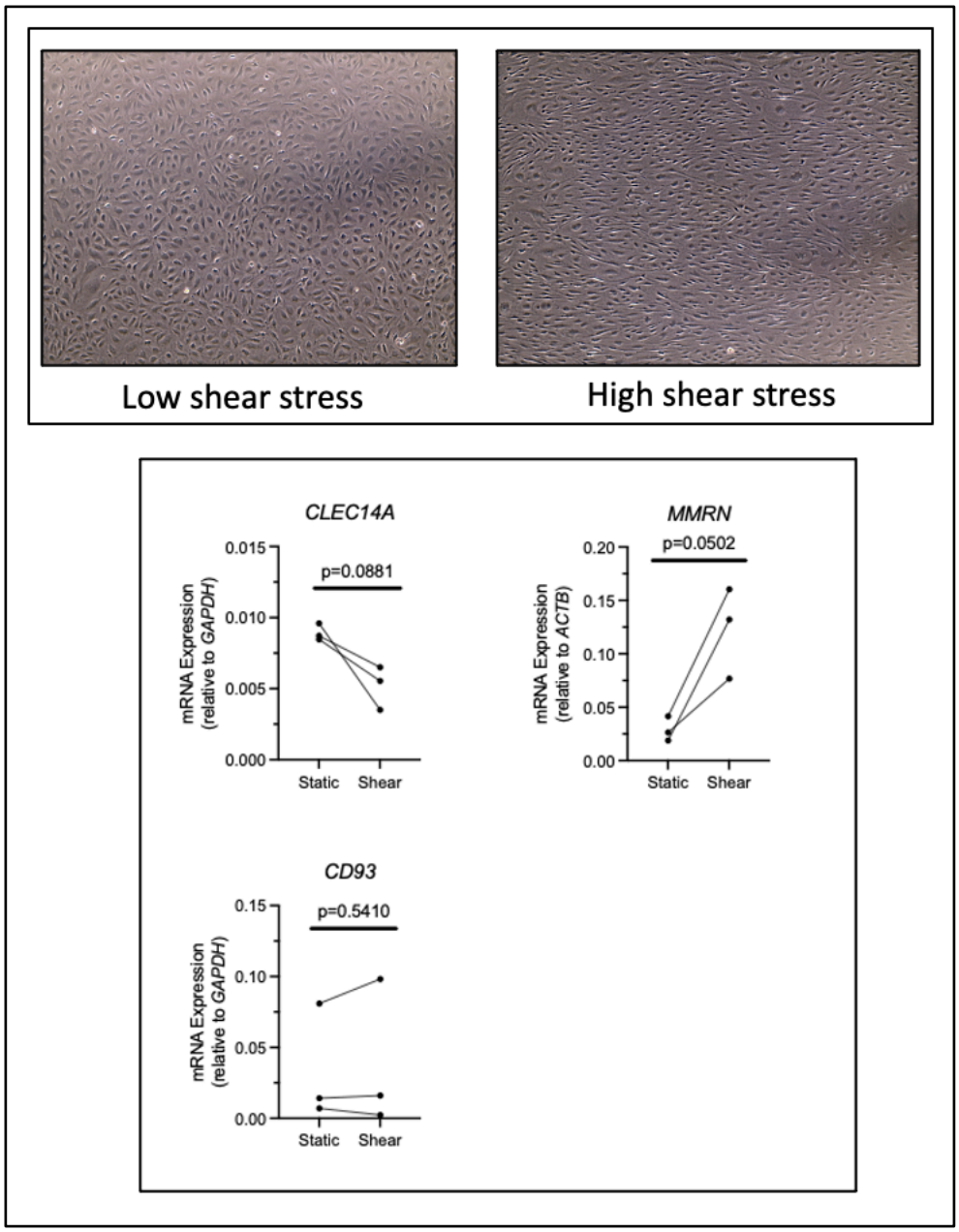


Figure 46. CLEC14A, MMRN2 and CD93 expression in response to shear stress.

Top images show the appearance of HSEC after being exposed to static media or flowing media for 72 hours. Under flow conditions the HSEC aligned with the direction of flow. Relative expression of CLEC14A mRNA in HSEC. HSEC cultured in static media were compared to HSEC cultured for 72 hours under flow. A paired t-test showed there was no significant difference for CLEC14A, MMRN2 or CD93. However the trend was consistent and significance was nearly achieved for CLEC14A and MMRN2, p=0.0881 and p=0.0502 respectively.

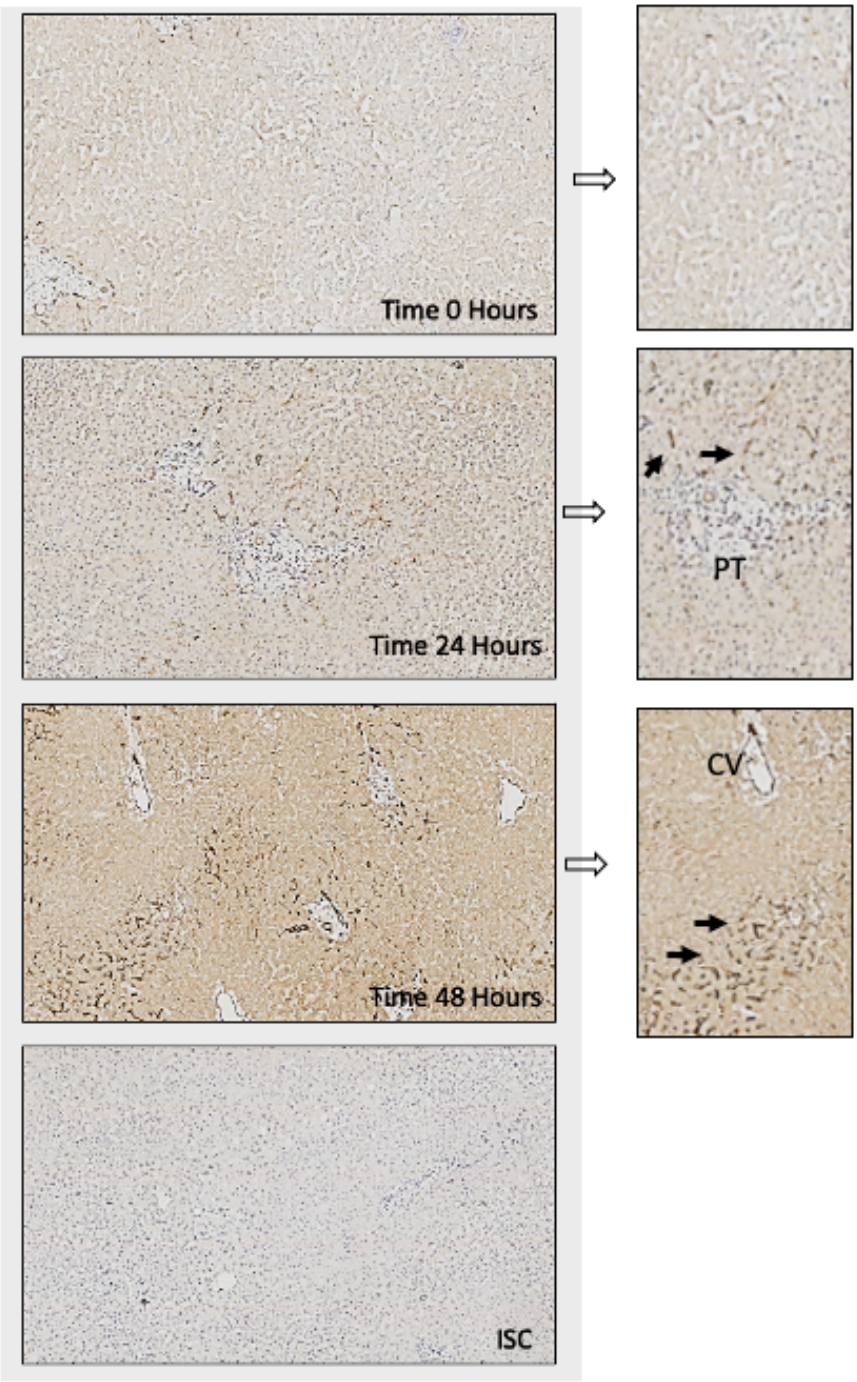


Figure 47. The effect of delayed tissue fixation on CLEC14A expression in liver tissue.

Normal liver was fixed at three different time points and then sectioned, and immunohistochemistry performed for CLEC14A expression. We can see positive large vessel and sinusoidal staining emerging after 24 hours. At 24 hours the sinusoidal staining was limited to around the portal tracts but by 48 hours it was strongest distal to the central veins and the sinusoids were still not diffusely positive throughout the section. **PT** Portal Triad. **CV** Central vein.

5.4 Discussion

The cytokine experiments did not produce consistent results from different donor HSEC although in 3 out of 4 donors INF lead to a 2 fold increase in CLEC14A expression and BMP9 in 2 out of 3 donors lead to a 2 fold increase in CLEC14A expression. A study by Bocci et al also found that CLEC14A was upregulated in response to BMP 9 in murine endothelial MS1 cells (Bocci et al., 2019). The results indicate that although all the cells are isolated in the same manner and were at the same passage, they did not behave the same suggesting that epigenetic changes have taken place and they are maintained in culture.

We know that hypoxia is a major stimulus for angiogenesis and the result from three replicates from three donors indicated that CLEC14A is upregulated in hypoxia but curiously the opposite effect is seen with MMRN2 and CD93 expression. We know that liver fibrosis is associated with hypoxia and increased angiogenesis in chronic liver disease and this may be why there was increased expression of CLEC14A seen in the fibrous septa in my immunohistochemistry studies, particularly in areas of bridging fibrosis. It was most pronounced in cases of PBC I looked at and therefore it would be interesting in the future to expose HSEC to bile and see if this regulates CLEC14A expression.

It had been previously published that CLEC14A is upregulated by low shear stress in HUVEC but this is now confirmed to be the case in HSEC also. It has not been previously demonstrated that MMRN2 is also affected by shear stress and in HSEC it is down regulated by low shear stress, i.e. shear stress has the opposite effect on CLEC14A compared to its ligand MMRN2.

There are of course limitations to performing in vitro experiments and we are not replicating the physiological environment of a normal liver, diseased liver, or a liver tumour. However, it does give insight into the regulation of CLEC14A and helps us to understand why CLEC14A is upregulated in some tumours and diseased livers. In the delayed tissue fixation experiment it was interesting to see where CLEC14A appeared over the time course. After 24 hours it was most noticeable on large vessels and around the portal triad and after 48 hours there was very prominent staining of sinusoids distal to the central veins and not all the sinusoids were positive for CLEC14A. The area distal to the central vein corresponds to zone 1 of a liver lobule which is considered in vivo to be oxygen rich, and I hypothesise therefore that this area was most sensitive to hypoxia, and this may be why CLEC14A expression was strongest in this region. The sinusoids closest to the central vein maybe more resistant to the effects of hypoxia. It was noticeable that there was more non-specific background staining of the tissue with the CLEC14A antibody when there was a delay in fixation and the tissue was stored in media, however the sinusoidal staining was clearly distinctly different from background staining. It is clearly not possible to precisely determine if the emergence of CLEC14A expression by delayed fixation is a result of no shear stress in the vessels or because of hypoxia or a combination of both factors.

6

6 Investigating the functional role of CLEC14A in HSEC

To investigate the functional role of CLEC14A in HSEC two areas were chosen to explore. The first was to confirm if HSEC behaved the same as macrovascular endothelial cells in angiogenesis assays in response to a change in CLEC14A expression and secondly to explore if CLEC14A influences immune cell recruitment. It has been published that CD93, which binds MMRN2 at the same site as CLEC14A influences immune cell infiltration in a mouse model of peritonitis (Greenlee-Wacker et al., 2011). To explore if CLEC14A was associated with any immune signatures, TNM plot, a web based tool for comparing gene expression in normal and tumour tissues was utilised (Bartha and Gyorffy, 2021), https://tnmplot.com/analysis/. Using RNA-seq data an analysis of genes which correlated positively with CLEC14A in liver tissue was performed and the top 1000 significant genes and their p-values were entered into https://biit.cs.uk.ee/gprogiler/gost which performs functional profiling and the Reactome pathways were looked at for any clues which suggest CLEC14A is involved in modulating the immune landscape. 21 pathways were identified. The

top 2 pathways were Neutrophil degranulation and Immune system **Figure 48**. Neutrophils were therefore looked at first in assays involving HSEC and neutrophils. Interestingly when just tumour tissue was looked at NCAM1 interactions were also significant P adj = 0.0031.

	Term name	**Padj**
REAC	Neutrophil degranulation	2.59E-08
REAC	Immune System	1.16E-07
REAC	Extracellular matrix organization	5.06E-07
REAC	Platelet activation, signaling and aggregation	7.2721E-06
REAC	Hemostasis	7.6398E-06
REAC	Signal Transduction	3.8212E-05
REAC	Immunoregulatory interactions between a Lymphoid and a non-Lymphoid cell	5.5639E-05
REAC	Integrin cell surface interactions	5.6201E-05
REAC	Innate Immune System	7.4976E-05
REAC	Scavenging by Class A Receptors	0.0020974
REAC	Glycosaminoglycan metabolism	0.00232024
REAC	Neurophilin interactions with VEGF and VEGFR	0.00491279
REAC	Degradation of the extracellular matrix	0.00555377
REAC	Hyaluronan uptake and degradation	0.01065789
REAC	MHC class II antigen presentation	0.02770427
REAC	ECM proteoglycans	0.03233613
REAC	Platelet degranulation	0.03470302

Figure 48. Reactome pathways associated with the top 1000 genes that correlate positively with CLEC14A in liver tissue.

Correlation data accessed from https://tnmplot.com/analysis/ and pathway analysis performed using https://biit.cs.ut.ee/gprofiler/gost.

6.1 si RNA knockdown of CLEC14A

Two duplexes were evaluated for their ability to knockdown CLEC14A. Duplex 2 was used in assays based on its ability to provide a more robust knock down and western blocking was used each time a knock down was performed to confirm this was successful. **Figure 49** shows the effect of both duplexes, together with blots for the loading control.

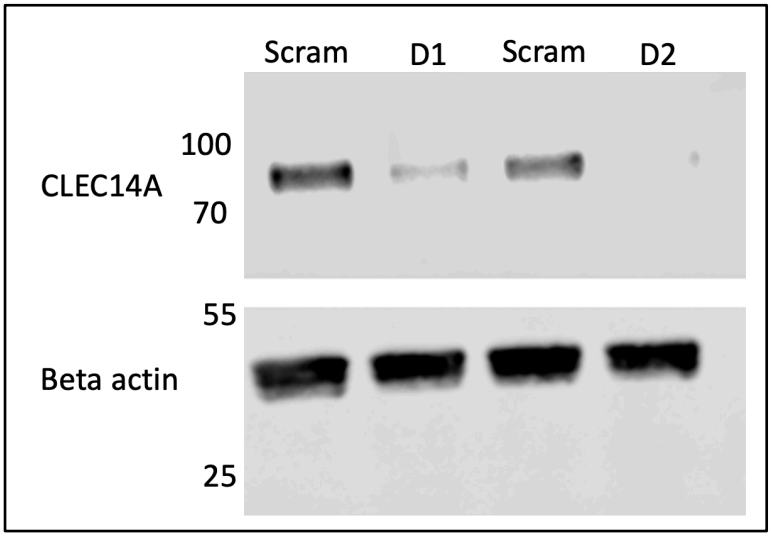


Figure 49. CLEC14A knockdown in HSEC.

Western blot showing the knockdown of CLEC14A using 2 duplexes. Duplex 2 provided a more robust knockdown and so was used for experiments. Lower image is a blot for the loading control beta actin.

6.2 Angiogenesis assays

6.2.1 Endothelial cell migration

A scratch wound assay on HSEC was performed using either scram knockdown or CLEC14A knockdown **Figure 50** and the percentage wound area remaining at 6

hours, 12 hours, 18 hours, and 24 hours was assessed. The results of three independent experiments with three HSEC donors are shown in **Figure 51**. I found that the wound was slower to close following CLEC14A knockdown suggesting that CLEC14A is important for the migration of HSEC.

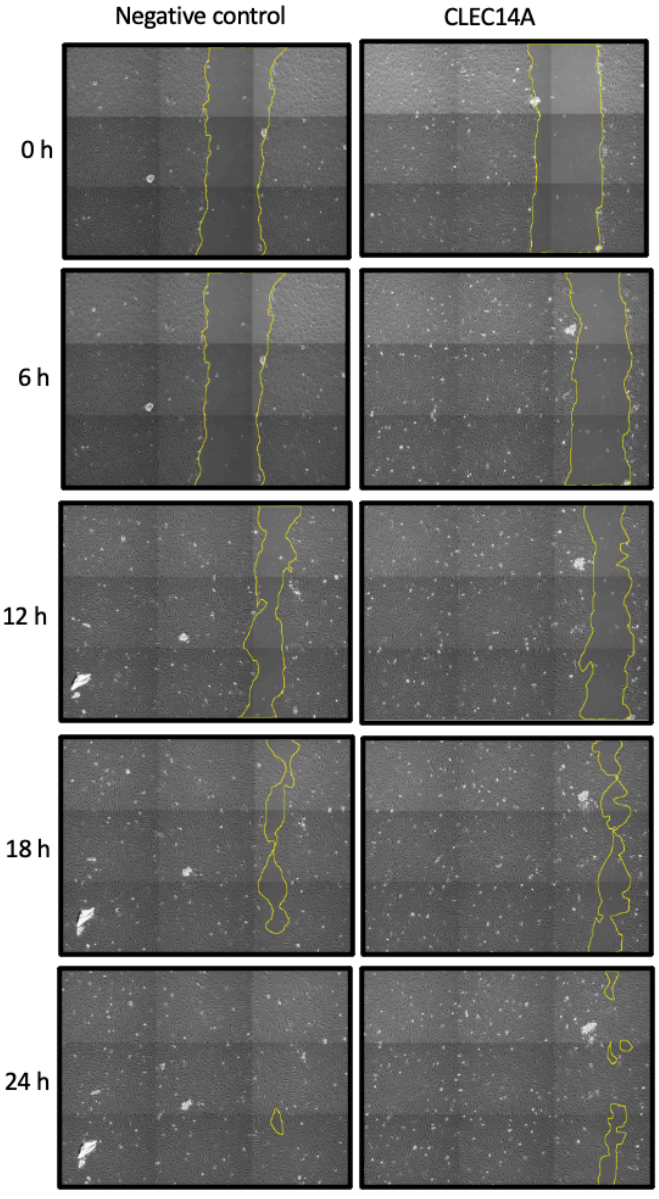


Figure 50. Representative images for the wound scratch assay.

HSEC from 3 different livers were cultured and then either a scram knockdown or CLEC14A knockdown was performed followed by a wound scratch. Images were then taken every 6 hours for 24 hours and the percentage closure measured. Figure shows example images from each time point.

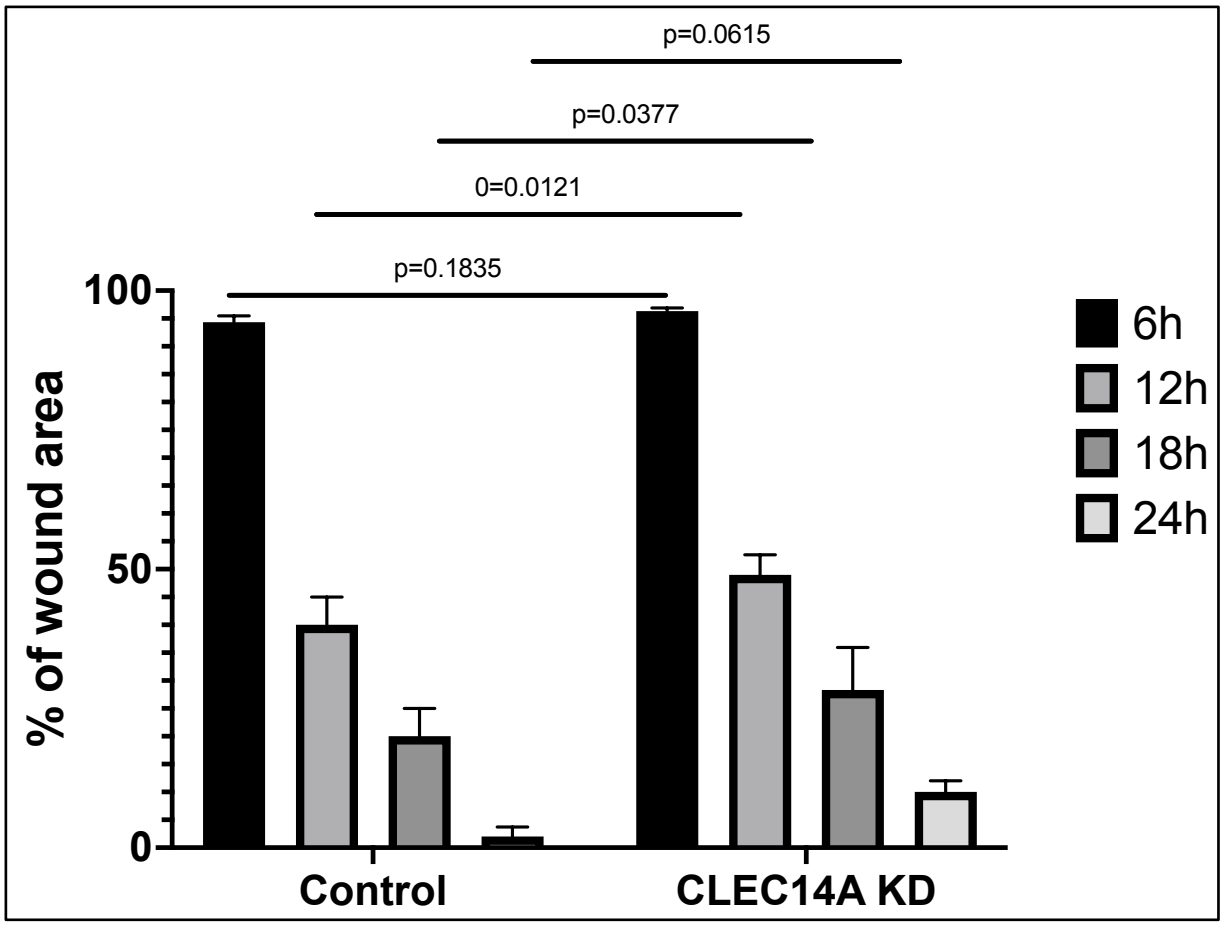


Figure 51. Wound scratch assay % closure following CLEC14A knockdown.

A paired t-test was performed for each time point. Three independent experiments were performed using HSEC isolated from three different livers. Significant differences are noted at 12 hours and 18 hours in the two experimental conditions.

6.2.2 HSEC tubule formation in Matrigel

HSEC were plated on matrigel and then mesh formation observed for 24 hours. The following demonstrates how rapidly the HSEC rearrange to form tubules and after 3 hours you can already see the outline of mesh like structures **Figure 52**.

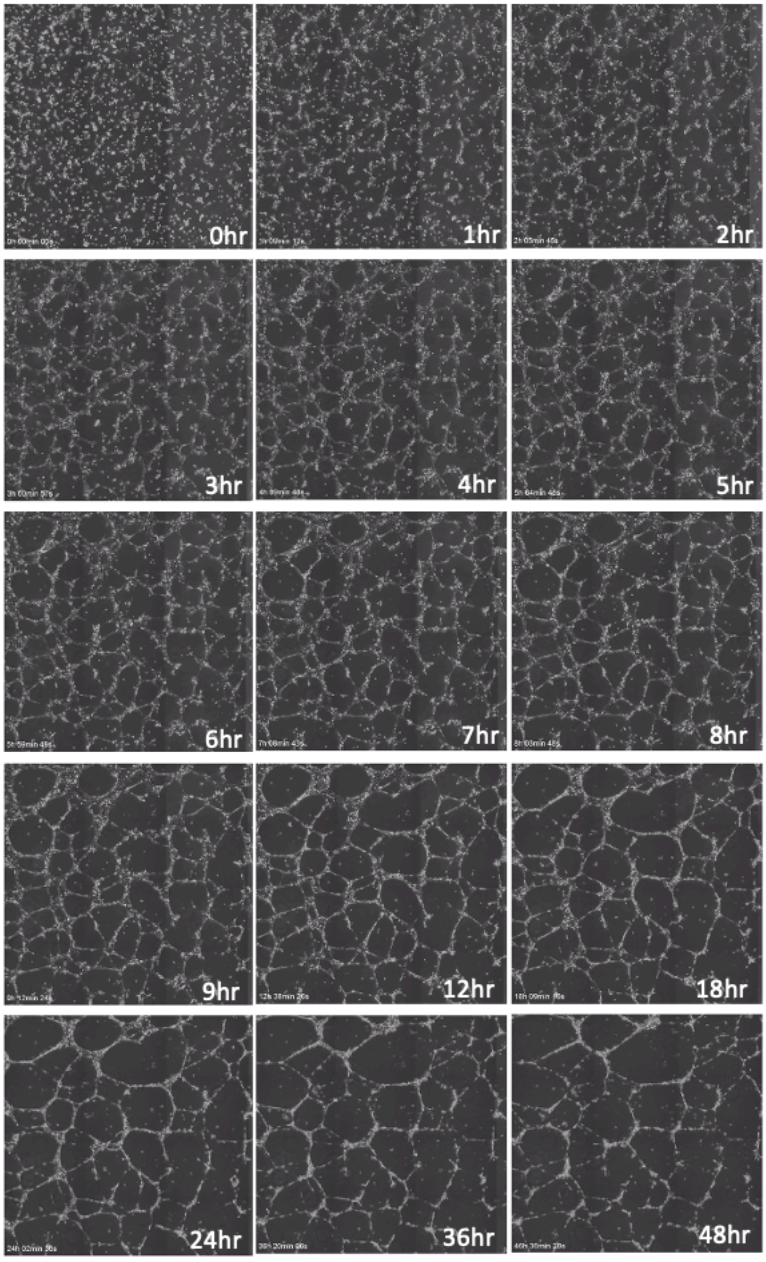


Figure 52. Example of HSEC matrigel tubule formation assay.

HSEC were plated on matrigel and images captured every hour for 48 hours. To investigate the effect of CLEC14A in the matrigel tubule assay. CLEC14A was knocked down in HSEC and after 48 hours plated on matrigel. Images were captured after 6, 12, 18 and 24 hours and tubule formation analysed using the imagej angiogenesis plugin. A paired t test was performed for each time point and at 6 hours there was a significant reduction in the number of tubules formed in the CLEC14A KD compared to the scram KD p= 0.0198. At 12, 18 and 24 hours there was also a reduction in tubule formation in the CLEC14A KD but this did not reach significance with p values of 0.0934, 0.0799 and 0.0914 respectively **Figures 53 and 54**.

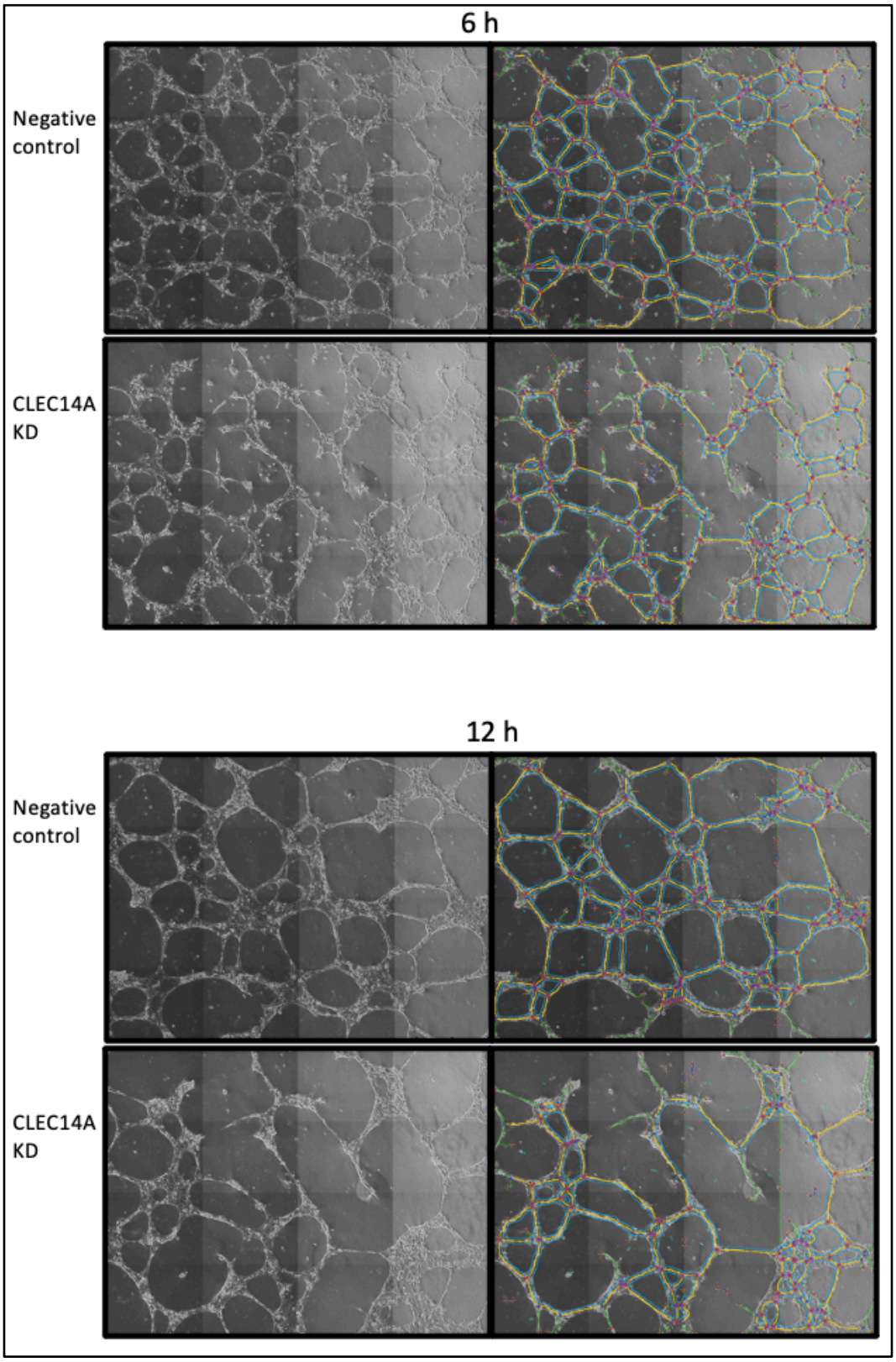


Figure 53. Matrigel tubule formation assay CLEC14A KD vs control representative images.

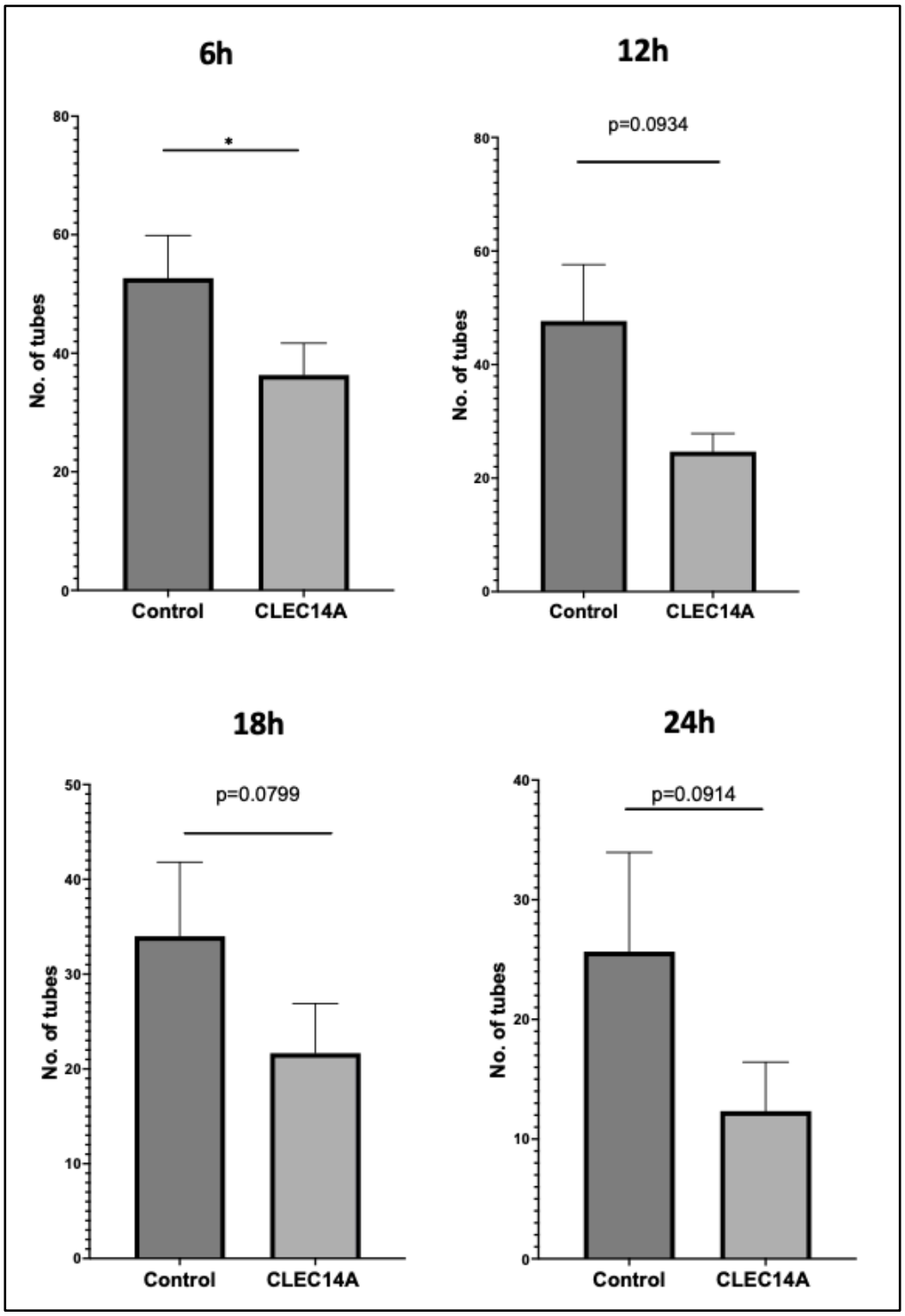


Figure 54. Matrigel tubule formation assay, number of tubules at 6, 12, 18 and 24 hours.

The results from three experiments. Data was analysed using a paired t test at each time interval. *$p<0.05$.

6.3 Leucocyte adhesion assays

It was decided to look at neutrophils in adhesion assays on the basis of the Reactome pathway data. Assays included looking at the adhesion of neutrophils to HSEC in static conditions and flow assays. In static assays cells were either preconditioned with flow for 72 hours because I had shown previously that this reduces CLEC14A expression or CLEC14A was knocked down using siRNA. In flow adhesion assays CLEC14A was knocked down or CLEC14A monoclonal antibodies were added to HSEC prior to flowing neutrophils over the cells.

The aims of this section

1) To ascertain if preconditioning HSEC with flow effects the adhesion of neutrophils
2) To determine if knockdown of CLEC14A influences the adhesion of neutrophils
3) To determine if monoclonal antibodies to CLEC14A effect the recruitment of neutrophils.

6.4 Neutrophil adhesion in the static condition following preconditioning with flow

Previous experiments have shown that CLEC14A expression is higher in low flow (static) conditions compared to high shear stress. HSEC were therefore either cultured in a standard manner for 72 hours or in an orbital shaker generating flow of media over the cells for 72 hours. Again, under the condition of flowing media the HSEC aligned. Neutrophils were added to each set of HSEC and left for 5 minutes in a standard incubator before gently washing the cells with media. When taking fields of view for analysis the outer edges and centre of the wells were avoided because flow will be more disturbed in these areas. The results are shown in **Figure 55** and we can see that the cells preconditioned to relative high shear stress had significantly less neutrophil adhesion p=0.0068 and the percentage of neutrophils that transmigrated was also less p=0288. This clearly does not tell us however that the effect is due to CLEC14A and there will be many other genes that are regulated by shear stress.

The experiment was therefore repeated using HSEC which had CLEC14A KD performed. In the CLEC14A KD there was less adhesion of neutrophils $P<0.05$ **Figure 56**.

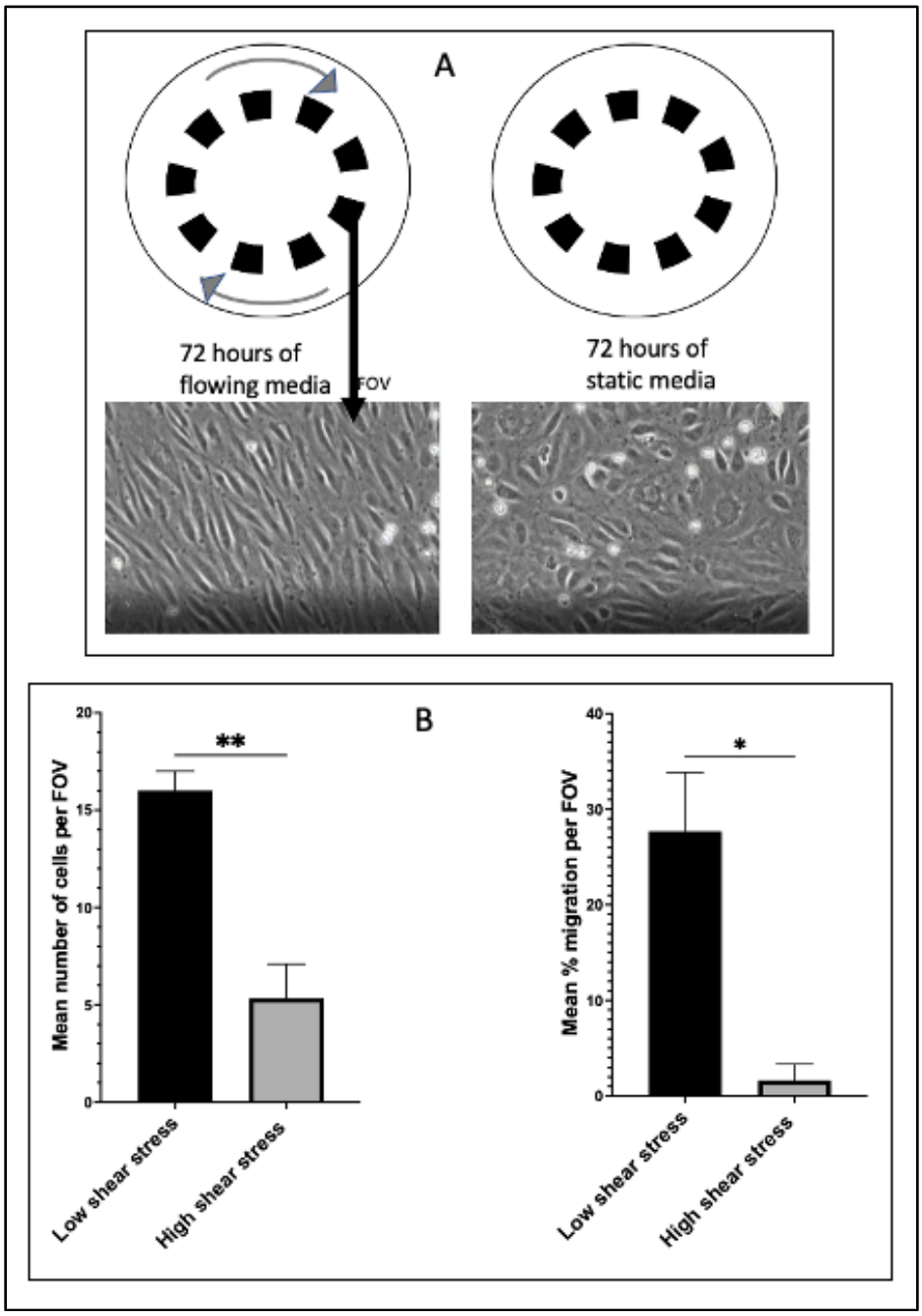


Figure 55. Adhesion and transmigration of neutrophils under static conditions following preconditioning of HSEC with either low or high shear stress.

A) HSEC were cultured under standard static conditions or exposed to shear stress for 72 hours and then neutrophils added for 5 minutes followed by removal of unadhered neutrophils, FOV were selected avoiding the outer edges and centre of the plates as shown in **A).** The number of adhered neutrophils were counted the percentage transmigration was calculated for each field of view (Liu et al.) and the mean calculated. This was repeated with HSEC from three different donors. **B)** The results are shown as mean and SEM and significance from a paired t test is displayed *p<0.05 and ** P<0.005

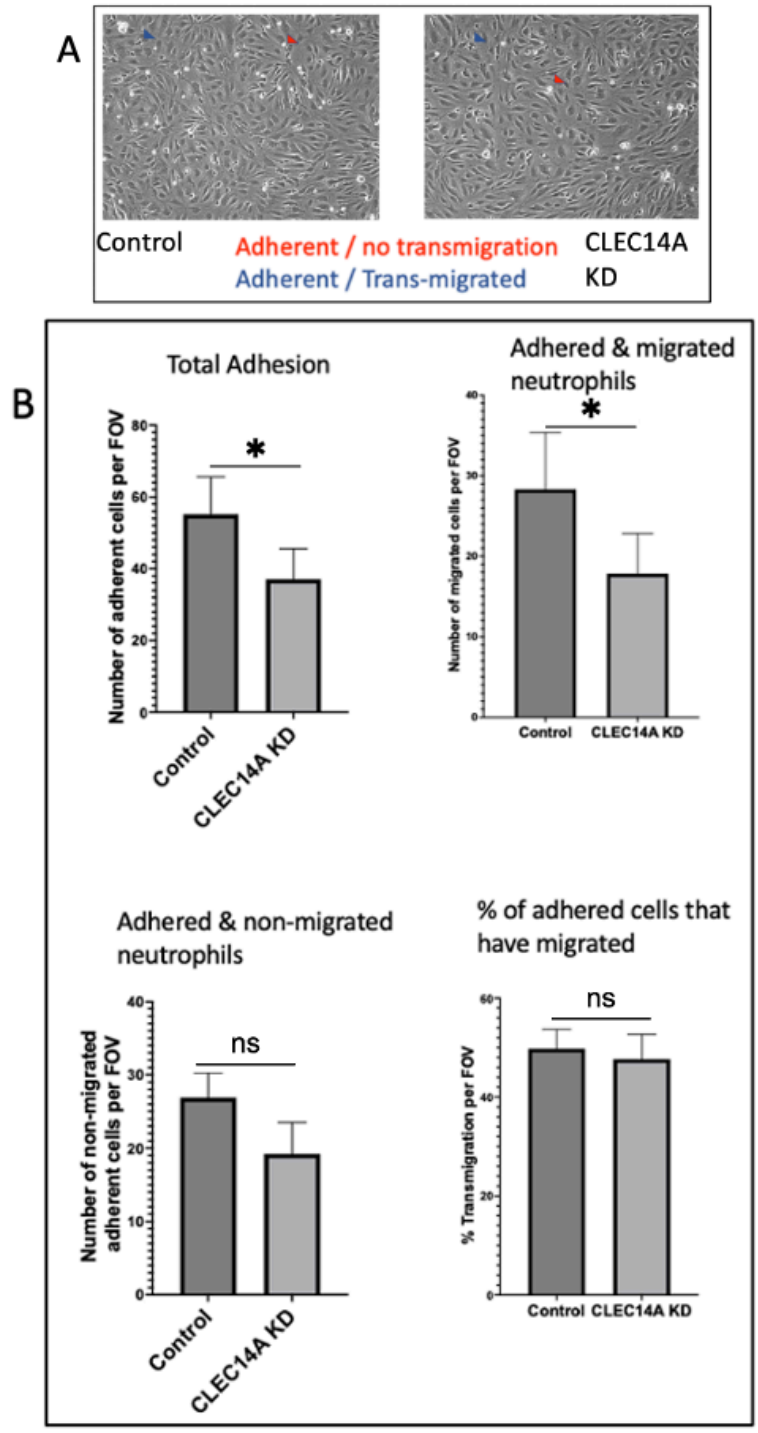


Figure 56. siRNA knockdown of CLEC14A and neutrophil adhesion under static conditions.

A)Representative images of neutrophils adhering to HSEC which have undergone either mock/scram KD or CLEC14A KD. **B)** Mean and SEM of three independent experiments using HSEC isolated from different donor livers. Data for total adhesion, migrated, non-migrated and % migration is displayed. Statistical significance from a paired t test is displayed. *P<0.05.

HSEC with CLEC14A KD were also exposed to neutrophils under flow and once again a significant reduction in neutrophil adhesion was observed $P<0.05$ **Figure 57.** However no significant effect on neutrophil adhesion was seen from incubating HSEC with CLEC14A monoclonal antibodies compared to Isotype control. **Figure 58** shows the results from flowing neutrophils over HSEC incubated with CLEC14A monoclonal antibodies CRT 1, CRT 2 and CRT3. **Figure 59** shows the results using CLEC14A antibodies CRT 4 and CRT5.

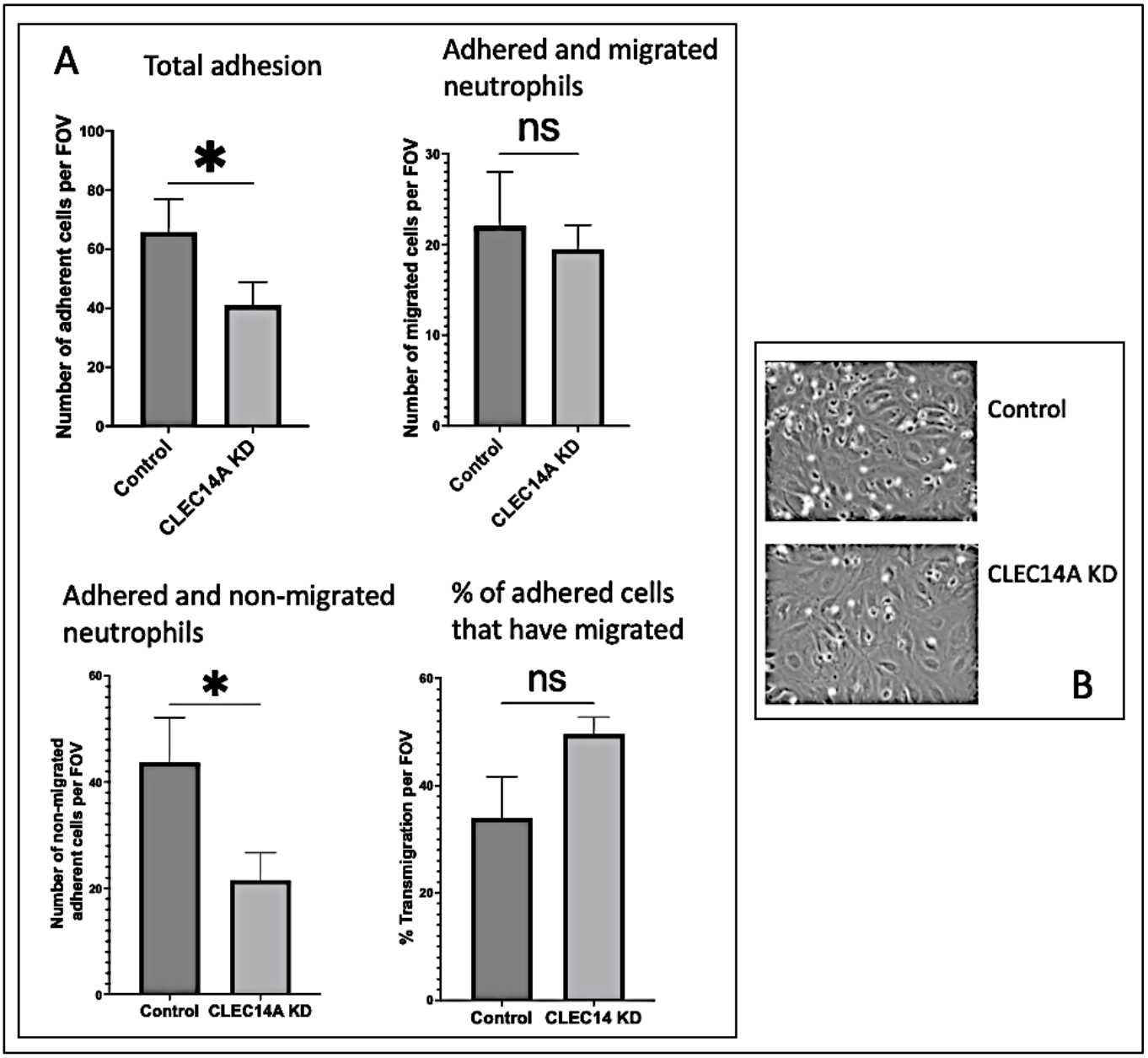


Figure 57. siRNA knockdown of CLEC14A and neutrophil adhesion under flow.

A)Neutrophils adhering under flow to HSEC which have undergone either scram KD or CLEC14A KD. Mean and SEM of three independent experiments using HSEC isolated from different donor livers. Data for total adhesion, migrated, non-migrated and % migration is displayed. Statistical significance from a paired t test is displayed. *P<0.05 **B)** Representative images of neutrophil adhesion to HSEC, scram KD vs CLEC14A KD.

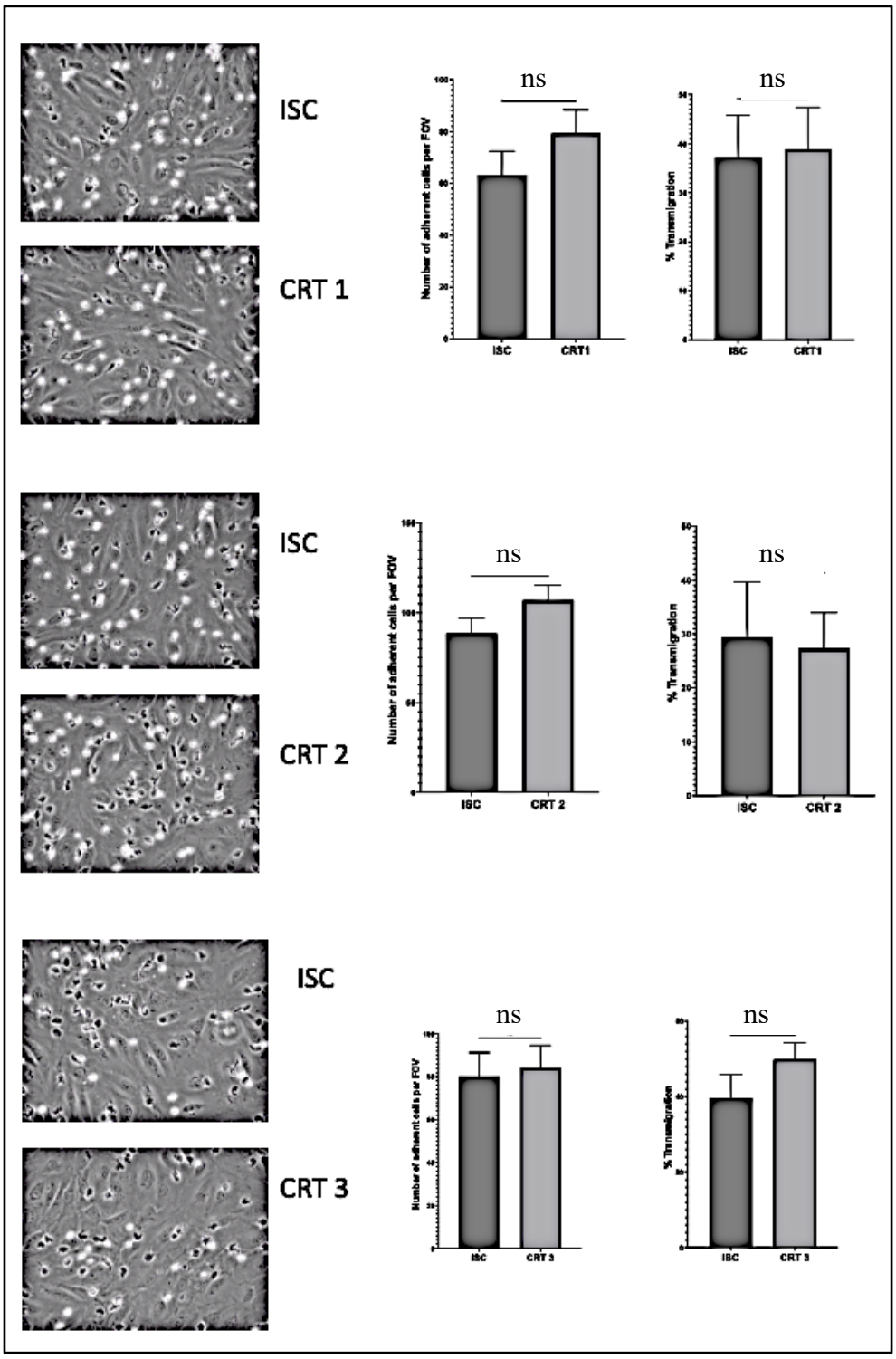


Figure 58. Neutrophil flow assays with HSEC in the presence of CLEC14A monoclonal antibodies CRT1, CRT2, CRT3.

Representative images shown and mean and SEM displayed for the number of adhered and transmigrated neutrophils. A paired t test was performed and no statistical difference between the CLEC14A antibodies and Isotype control (ISC) was found.

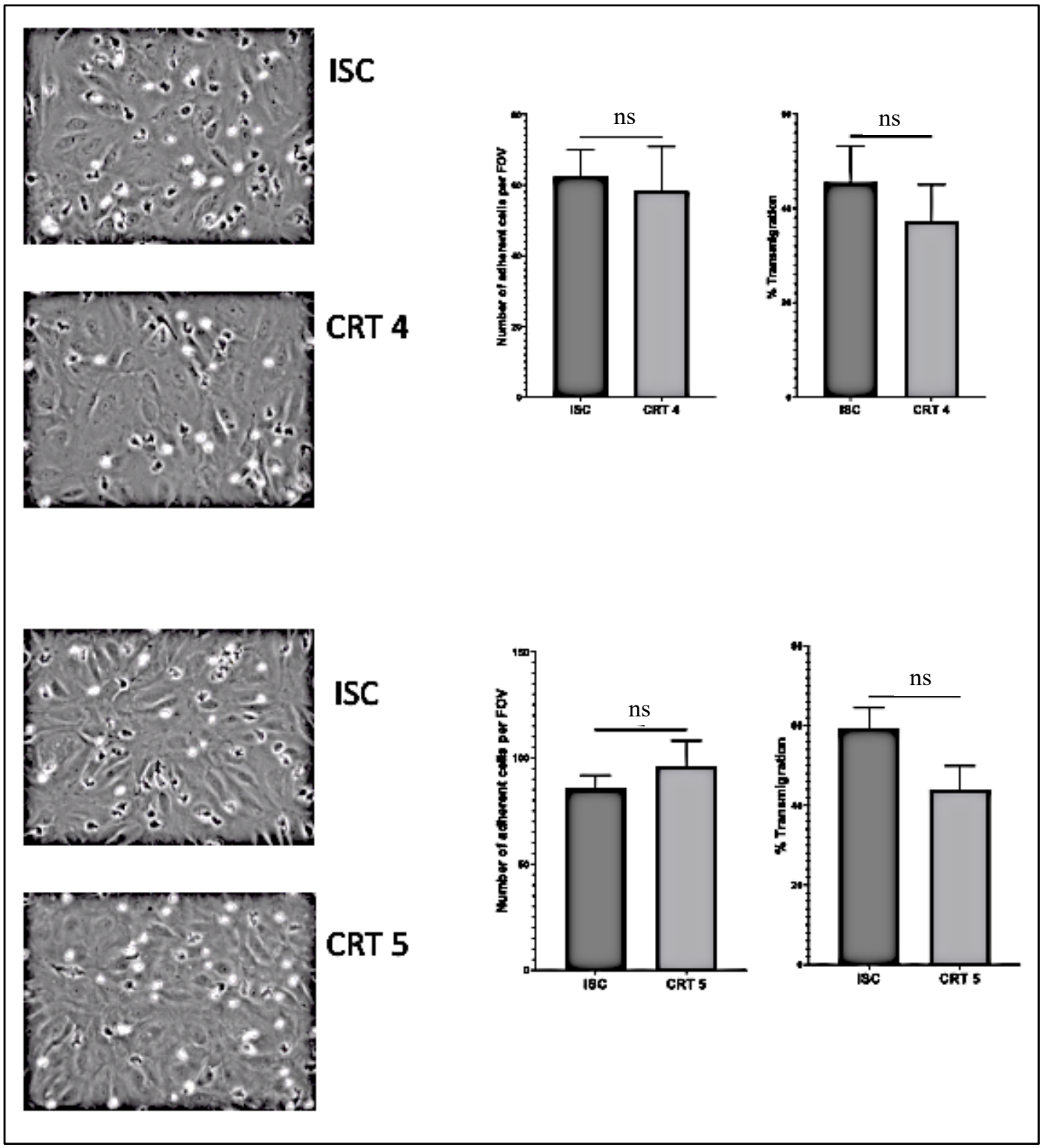


Figure 59. Neutrophil flow assays with HSEC in the presence of CLEC14A monoclonal antibodies CRT4 and CRT5.

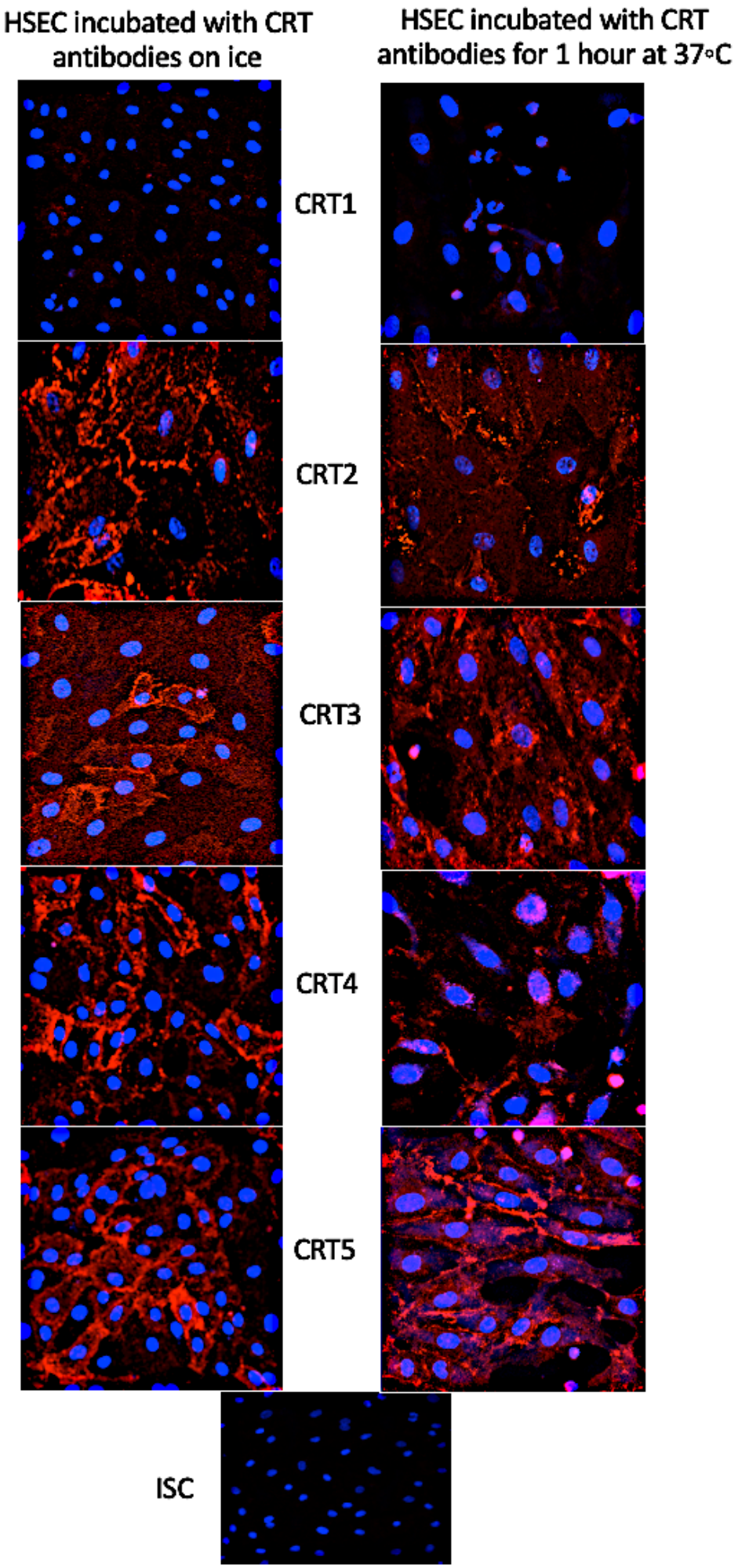
Representative images shown and mean and SEM displayed for the number of adhered and transmigrated neutrophils. A paired t test was performed and no statistical difference between the CLEC14A antibodies and Isotype control (ISC) was found.

To assess where CLEC14A was on HSEC following incubation with the monoclonal antibodies, following the neutrophil flow assays HSEC cells were fixed and fluorescently labelled with secondary antibodies. These antibodies had been incubated with the HSEC for one hour at 37 ◦C prior to flow assays. Following flow assays and fixation fluorophore conjugated secondary antibody was added and cells visualized. Additionally, HSEC were incubated with CRT antibodies on ice before being fixed. Later fluorophore conjugated secondary antibody was added and cells visualized (note that previously I found when HSEC were fixed, and CRT antibodies added to fixed cells they do not interact with CLEC14A). **Figure 60** shows that CLEC14A CRT monoclonal antibodies 2-4 internalise CLEC14A. There was no clear staining of CRT1, and CRT5 remained on the surface of the HSEC after the one hour incubation at 37◦C suggesting this antibody does not internalize CLEC14A.

Next Page:

Figure 60. HSEC incubation with monoclonal antibodies CRT1-5.

CLEC14A monoclonal antibodies incubated with HSEC either on ICE then fixed or at 37◦C and fixed following neutrophil flow assays. CLEC14A internalization seen with CRT2-4 antibodies.


HSEC incubated with CRT antibodies on ice
HSEC incubated with CRT antibodies for 1 hour at 37◦C
CRT1
CRT2
CRT3
CRT4
CRT5
ISC

6.4.1 Recombinant CLEC14A binding to neutrophils

To determine if CLEC14A is capable of interacting directly with neutrophils recombinant CLEC14A-Fc and human Fc were fluorescently labelled and incubated with neutrophils or lymphocytes. CLEC14A-Fc was found to interact with neutrophils using flow cytometry but a mutant form with residue 161 (heparin binding site (Sandoval et al., 2020)) substituted did not bind neutrophils when assessed by flow cytometry. This was repeated using recombinant MADCAM-1-Fc as a control and again CLEC14A interacted with the neutrophils **Figure 61**.

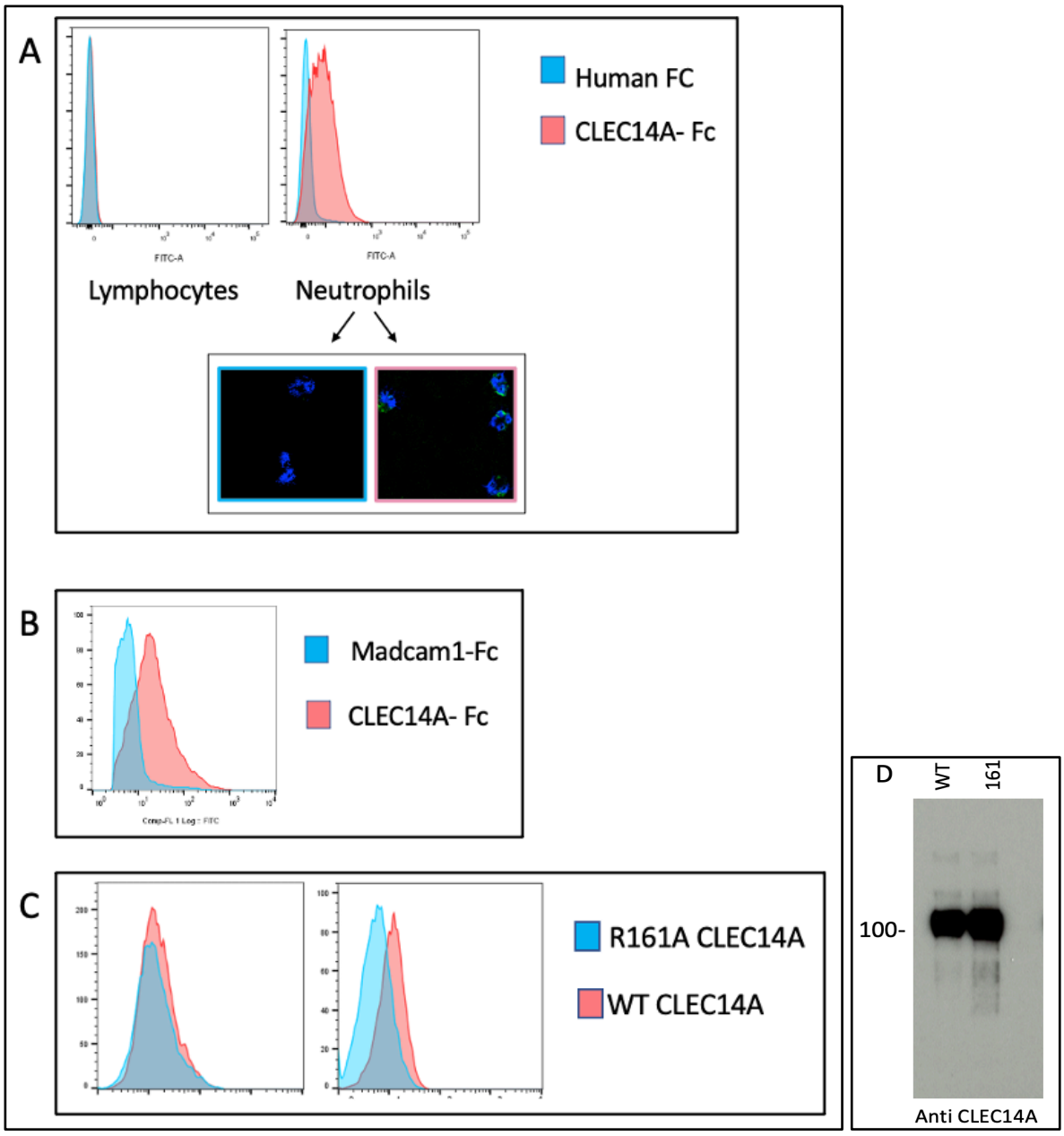


Figure 61. Recombinant CLEC14A interacting with neutrophils.

A)Neutrophils incubated with fluorescently labelled human Fc or recombinant CLEC14A-Fc and the CLEC14A bound neutrophils. Underneath, cells imaged using fluorescent microscopy and fluorescently labelled CLEC14A Fc seen to be attached to the neutrophils. **B)**Madcam1 is not known to interact with neutrophils in humans therefore recombinant Madcam1-Fc and CLEC14A-Fc, both fluorescently labelled, were incubated with neutrophils and the CLEC14A-Fc adhered to the neutrophils but Madcam1-Fc did not. **C)** WT CLEC14A (no Fc) bound to neutrophils but CLEC14A with residue 161 (heparin binding site) substituted (no Fc) lost neutrophil binding capacity, CLEC14A was detected using CLEC14A primary and anti-sheep FITC secondary. D) Western blot to show both forms of CLEC14A expressed.

To see if CLEC14A in tissue strongly associates with the presence of neutrophils in HCC. Cases of HCC were stained for CLEC14A and Neutrophil elastase. There was no obvious relationship with the presence of CLEC14A and a strong neutrophil infiltrate. Examples are shown in **Figures 62, 63 and 64**. This is perhaps not unsurprising because it would be quite simplistic to assume that a single protein would modify the recruitment of an immune cell in isolation especially in an immune microenvironment as complex as the liver. In **Figure 62** it was however striking that in one area where CLEC14A was very high there was a large presence of neutrophils also localised to that region.

Dual staining of CLEC14A and neutrophil elastase using immunofluorescent was performed in 2 cases of AIH, 1 PBC, 1 paracetamol overdose and 2 HCC cases (one HCC case with high CLEC14A and one with low CLEC14A expression) **Figure 65**. Neutrophils could be identified in all cases, but even when CLEC14A was not present and therefore we can conclude that CLEC14A is not essential for neutrophil recruitment, but it is possible that it still contributes to neutrophil recruitment under yet unidentified circumstances.

To see if neutrophils expressed MMRN2 a western blot was performed using lysates from PBMCs and neutrophils. There was a clear band at 130kDa in the PBMC lane indicating PBMCs express MMRN2 but no band in the neutrophil lane **Figure 66.** However, neutrophils contain proteolytic enzymes, so it is possible that MMRN2 was degraded at lysis, or neutrophils don't express MMRN2.

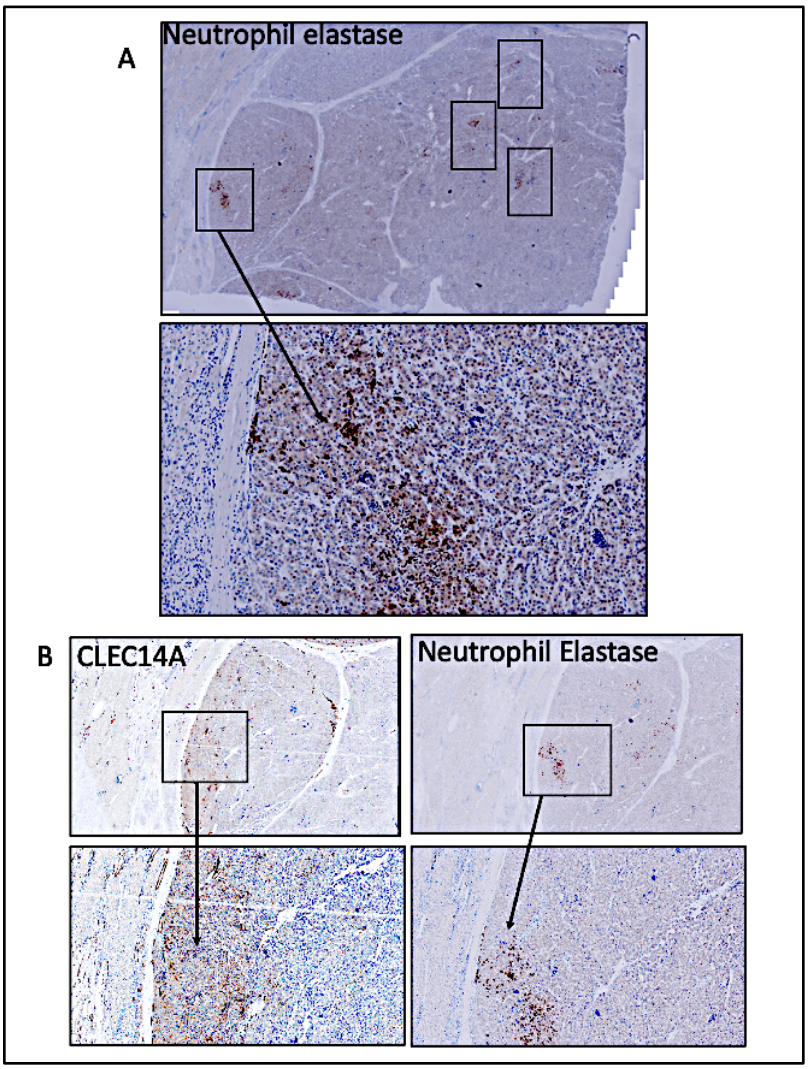


Figure 62. HCC case with high neutrophil infiltration.

A)Multiple areas with neutrophil infiltrate **B)** Area of high neutrophil infiltration and also strongly positive CLEC14A staining.

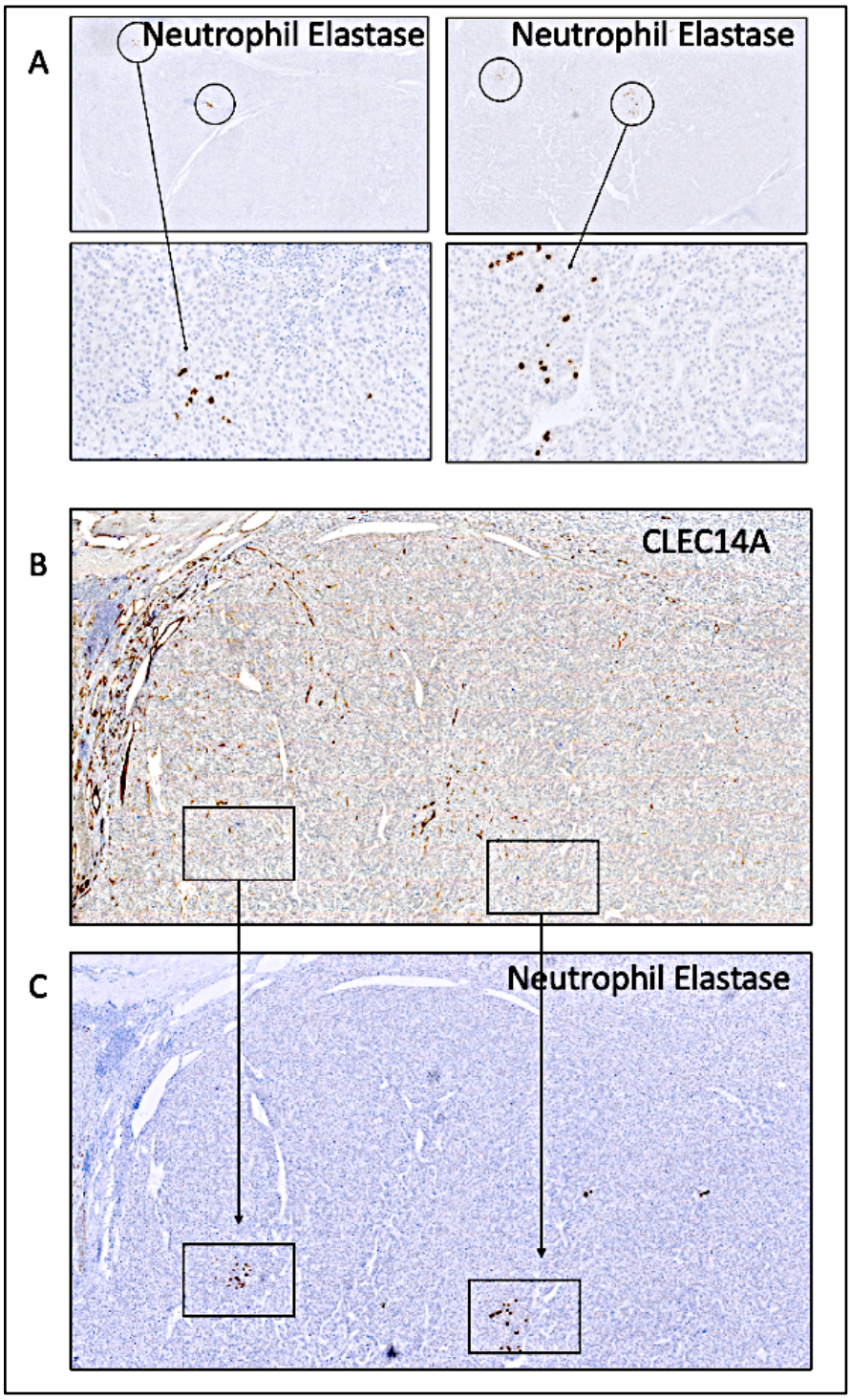


Figure 63. HCC case example with just a couple of areas of neutrophil infiltration.

A)HCC section with neutrophil infiltration in a couple of areas highlighted. **B)** 2 regions with high neutrophil infiltrate but no strong CLEC14A expression in those areas although there is patchy CLEC14A expression elsewhere in the tumour. **C)** Showing the corresponding areas with neutrophil elastase positive staining.

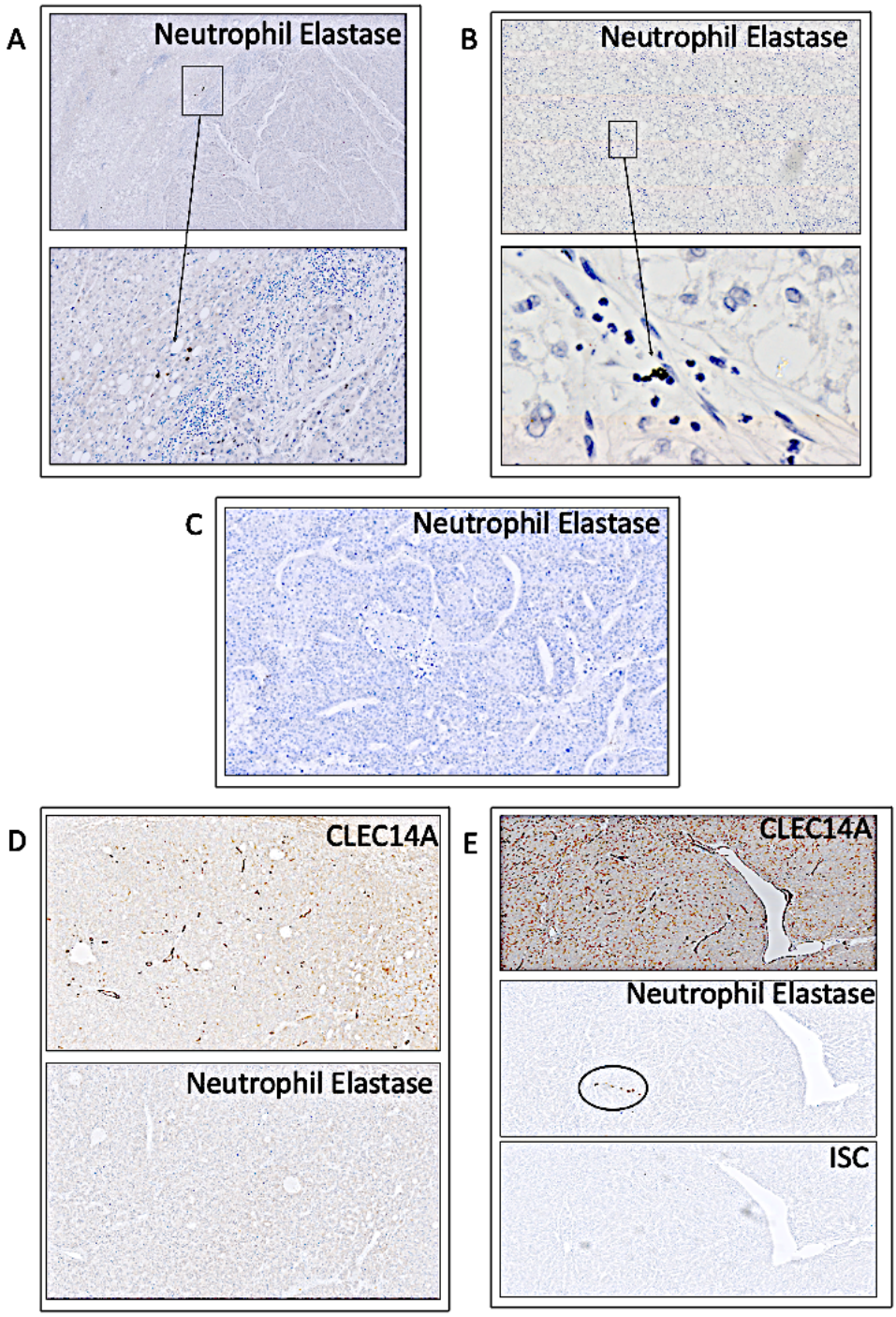


Figure 64. 4 HCC cases with minimal neutrophil infiltrate.

A)&B) only a few neutrophils seen in entire HCC section. **C)**HCC case with no neutrophils present. **D)** HCC case with patchy CLEC14A vessel positivity but no neutrophils seen. **E)** HCC case with strong and diffuse CLEC14A expression but only one small area where neutrophils were found.

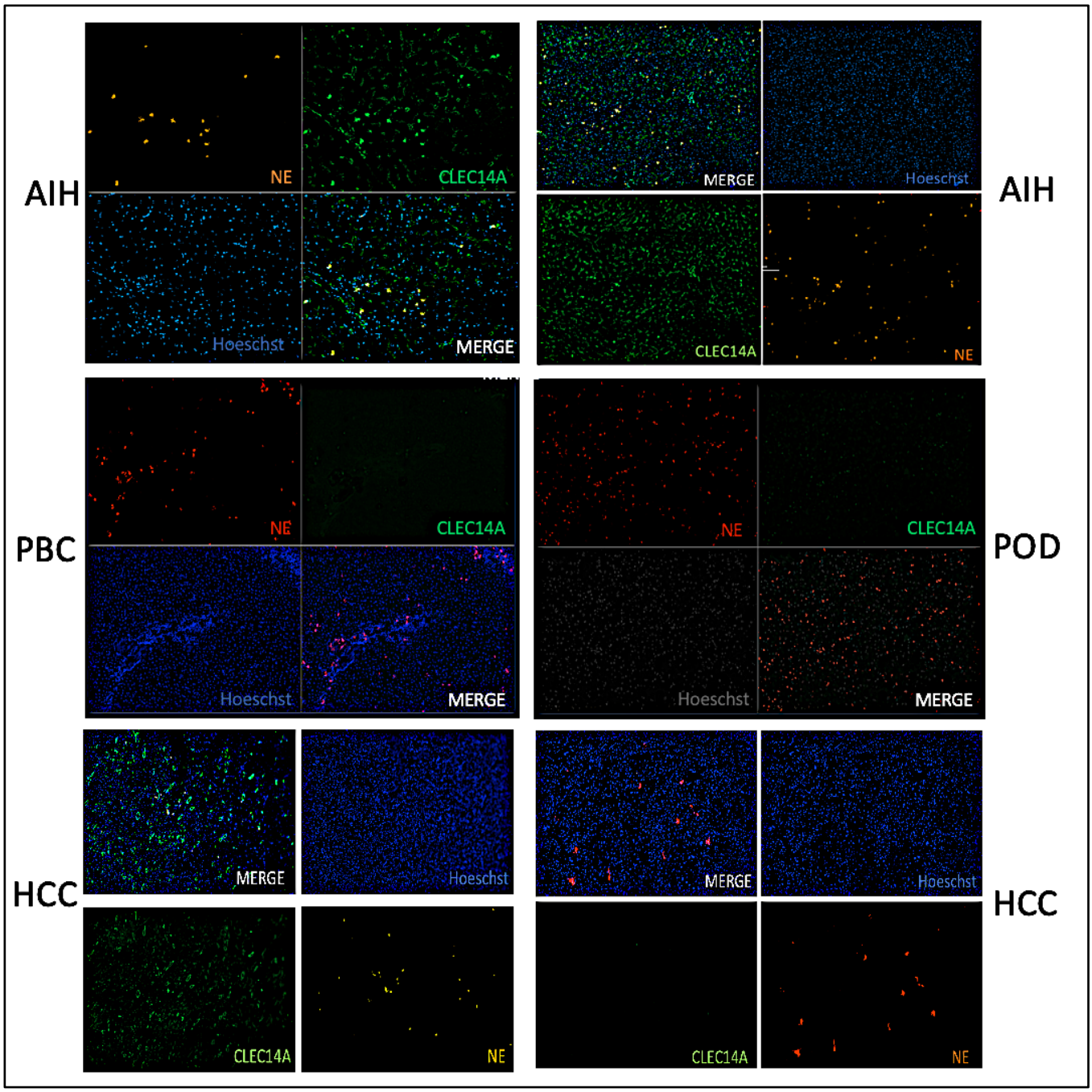


Figure 65. Immunofluorescence images of CLEC14A and neutrophil elastase.

2 AIH, 1 PBC, 1 paracetamol overdose (POD) and 2 HCC cases (one high and one low in CLEC14A) where stained for CLEC14A and neutrophil elastase.

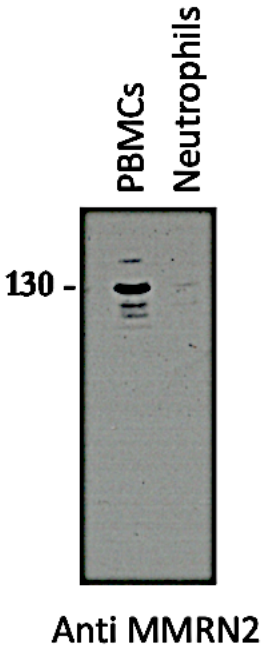


Figure 66. PBMCs express MMRN2.

A western blot of PBMC and Neutrophil lysates run under reducing conditions and probed with MMRN2 antibody. There is a clear band at ~130kDa in the PBMC lane corresponding to MMRN2. No band was seen in the neutrophil lane.

6.4.2 The effect of CD93 and MMRN2 knock down on CLEC14A expression in HSEC.

To see if knock down of CD93 or MMRN2 expression had an effect on CLEC14A at the mRNA level, HSEC were transfected with control, CLEC14A, MMRN2 or CD93 knockdown and lysed at 48 hours. The mRNA was extracted, and qPCR performed. The expression levels were normalised to GAPDH and expressed as fold change compared to control. The analysis revealed that CD93 and MMRN2 KD led to increased CLEC14A expression **Figure 67**. This was n=1 but it would be interesting to repeat this using other HSEC donors. The reason for this is that in

the adhesion assays it has not been possible to determine that it is CLEC14A directly having an effect and the effect maybe mediated by other proteins that are influenced by changes in CLEC14A expression. A previous study suggested that CD93 has anti-inflammatory effects (Greenlee-Wacker et al., 2011) and it is possible that they have opposing effects on immune cell recruitment. In Chapter 5 I also demonstrated that hypoxia also has opposing effects on CD93, MMRN2 and CLEC14A expression and flow has opposing effects on CLEC14A and MMRN2.

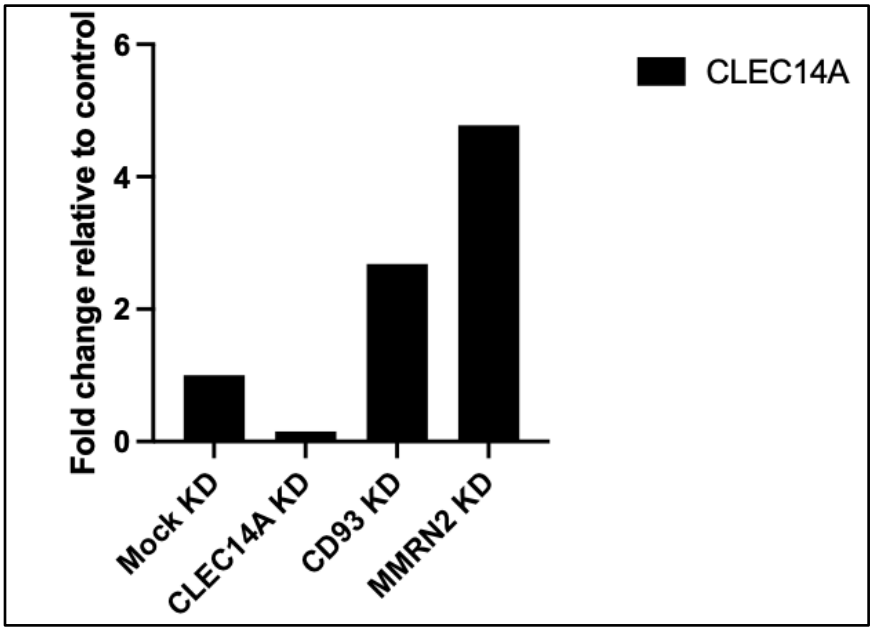


Figure 67. The effect of knock down of CD93 and MMRN2 on CLEC14A expression.

HSEC were transfected with SiRNA for CLEC14A, MMRN2 and CD93. After 48 hours cells were lysed, and qPCR performed. n=1.

6.4.3 Summary of functional studies

It is important to consider the effect of altered flow on EC function and leucocyte recruitment. Changes in blood flow causes changes in adhesion proteins. Studies previously have looked at binding of leucocytes and found that it is affected by

shear stress (Nagel et al., 1994, Morigi et al., 1995). It was previously thought this was due to primarily upregulation of ICAM-1 (Steeber et al., 1998). It has been published that endothelial cells can modify expression of genes depending on flow and shear stress, However, this has not been looked at in specialised endothelial cells, like HSEC, and the impact it may have on their function. It has been previously shown with HUVEC that exposure of endothelial cells to high shear stress, followed by activation with TNF, abated the capture of neutrophils and the authors concluded that the flow environments may contribute to how endothelium responds to inflammatory stimuli (Sheikh et al., 2003). It is therefore very plausible that the upregulation of CLEC14A in low shear stress modulates immune cell recruitment and my data has shown it may impact the recruitment of neutrophils.

Preliminary investigation looking at RNAseq data and taking the top 1000 genes which correlated positively with CLEC14A followed by functional profiling suggested that CLEC14A is involved in modulating the immune landscape and the top pathways were neutrophil degranulation and the immune system. Previously published studies (Mura et al., 2012) have also confirmed CLEC14A is involved in angiogenesis but none of these studies looked at sinusoid endothelial cells. I first looked to see if HSEC behaved the same in angiogenesis assays following CLEC14A knockdown and confirmed that CLEC14A increases HSEC migration and tubule formation in Matrigel supporting that these cells behave the same as macrovascular cells like HUVEC.

Experiments looking at neutrophil adhesion to HSEC in static conditions and flow were performed in two settings, preconditioning cells with flow versus standard static culture conditions or following siRNA knockdown of CLEC14A. We know from the previous chapter that CLEC14A is reduced when cells are preconditioned with flow. Following preconditioning with flow and using siRNA KD both reduced neutrophil adhesion to HSEC, in both static and flow adhesion assays. The limitations of these assays are that they do not confirm that the effect is mediated by CLEC14A, and other proteins will be affected by flow and also we do not know what impact CLEC14A knockdown is having on other proteins which may be mediating the neutrophil adhesion effect. To overcome this neutrophil flow assays were performed with CLEC14A monoclonal antibodies CRTs 1-5 but unfortunately no significant difference was seen in neutrophil adhesion. To try to understand the effect monoclonal antibodies had on CLEC14A, antibodies were incubated with HSEC on ice and for one hour at 37°C. Following fixation immunofluorescence was performed to see where CLEC14A was distributed in the presence of the monoclonal antibodies. This revealed that CRTs 2-4 internalised CLEC14A, CRT1 could not be visualised by immunofluorescence and CRT5 remained bound to CLEC14A at the HSEC cell membrane. The internalisation of CLEC14A did not have an impact on neutrophil recruitment which suggests that it is not CLEC14A directly that is mediating this process. However, a simple experiment using recombinant human CLEC14A suggested that CLEC14A does interact directly with neutrophils but not with lymphocytes and the heparin binding site (Sandoval et al., 2020) on CLEC14A may be relevant for this. This was looked at by flow

cytometry so the functional significance of this is unclear. Whatever the mechanism, in vitro when there is less CLEC14A neutrophil adhesion is clearly affected. Therefore, immunohistochemistry on liver tissue sections was performed to see if CLEC14A was associated with a high neutrophil infiltrate and in one case of HCC we could see very clearly that CLEC14A distribution correlated with the presence of high neutrophil infiltration. However, in other cases with high CLEC14A expression there was paucity of neutrophil infiltration and conversely neutrophil infiltration is not always associated with the presence of CLEC14A. This is not particularly surprising as it would be too simplistic a model to assume that neutrophil recruitment is influenced by only CLEC14A in isolation.

It was interesting to see that PBMC's express MMRN2, and this is the first time this has been described, but I was unable to confirm if neutrophils do also. The method of using western blotting for this has limitations because of the proteases contained within neutrophils which may lead to a false negative result, therefore whether neutrophils express MMRN2 is still unclear. It may be too simplistic to suggest that it is the MMRN2-CLEC14A interaction contributing to the recruitment of neutrophils and by flow cytometry CLEC14A was not found to bind to lymphocytes. But it is unknown if it may adhere to other PBMC's, and this is something to explore.

A knockdown experiment, albeit n=1, does show that KD of CD93 or MMRN2 increases CLEC14A expression and if this is reproducible in different donor HSEC it adds support that MMRN2 and its ligands CD93 and CLEC14A together, as a

unit, have regulatory functions. Indeed, in my shear stress studies opposing effects on CLEC14A and MMRN2 expression were seen, and hypoxia also has opposing effects on CD93 and MMRN2 expression compared to CLEC14A.

The functional studies presented in this chapter have not been able to elucidate a mechanism as to why CLEC14A knockdown reduces neutrophil adhesion but does raise multiple theories for further consideration. Despite this the evidence does seem to be mounting that CLEC14A presence is associated with increased neutrophil recruitment in vitro.

7

7 CHAPTER 7: Generation of monoclonal antibodies to human MMRN2 495-674

7.1 Introduction

To investigate the significance and functional role of the CLEC14A- MMRN2 interaction I generated monoclonal antibodies targeting the region of MMRN2 that binds CLEC14A. The workflow consisted of immunising rats with the human MMRN2 fragment which binds CLEC14A (495-674) identified by my predecessor. I first needed to generate a Fc tagged version of the antigen for immunisation and then a His tagged version of the same fragment was used for screening purposes. 2 Wistar rats were immunised with the antigen **Figure 68** and test bleeds performed to check for antibody response. Once an antibody response could be detected in the rat serum this was monitored to ensure sustained response and an ELISA was used for this purpose.

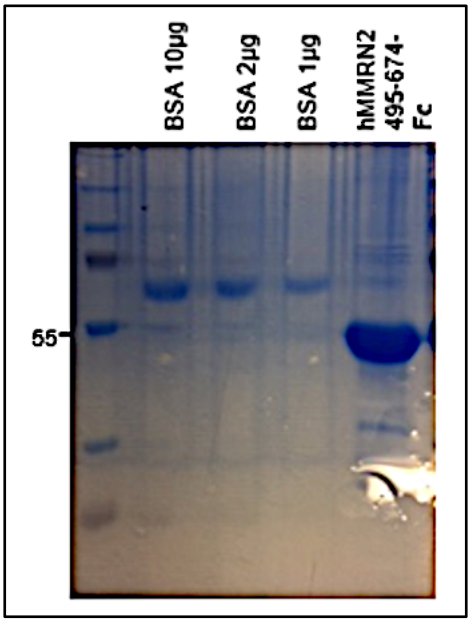
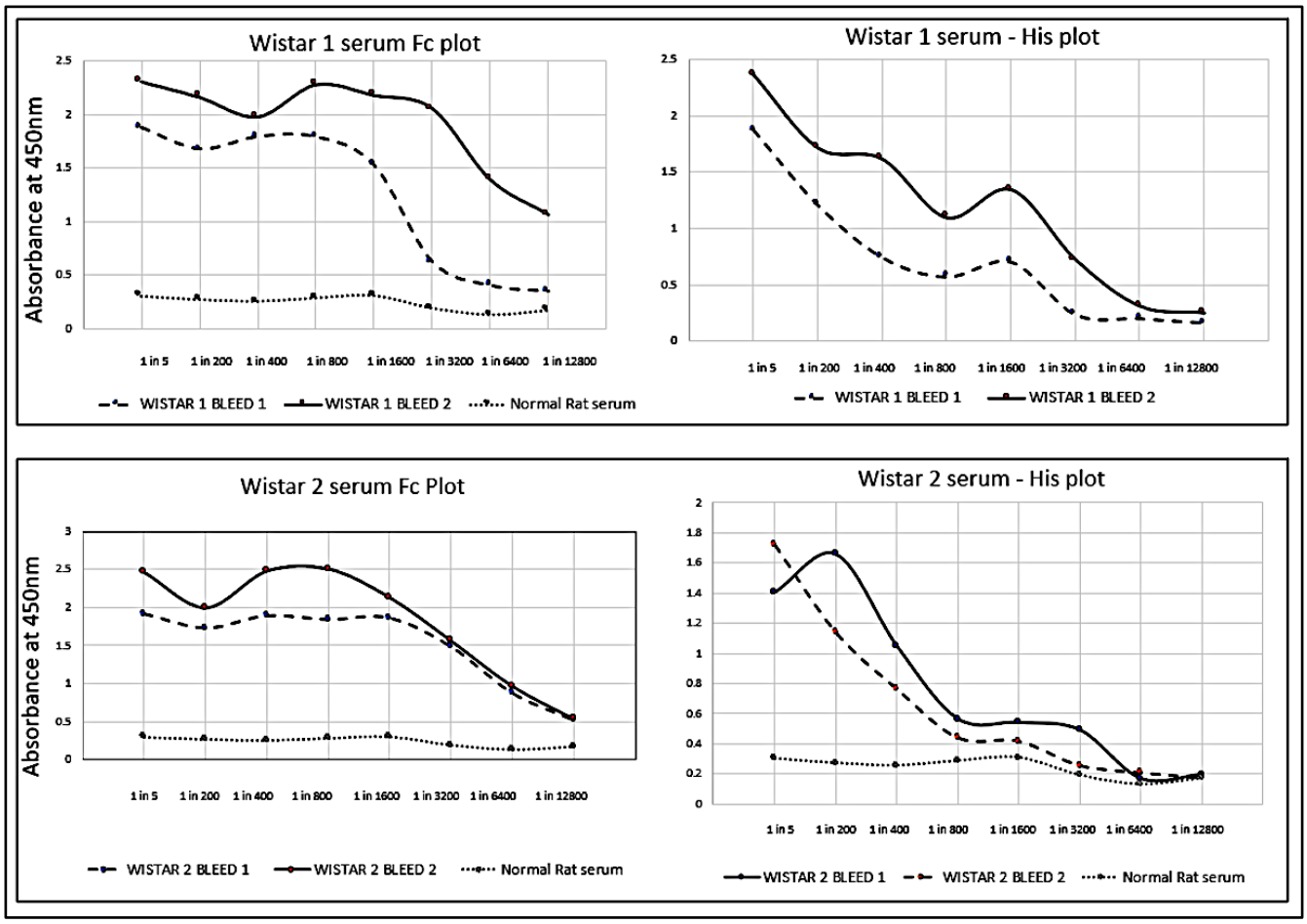


Figure 68. MMRN2 495-674-Fc antigen used for immunisation.

Expression and purification of MMRN2 495-674 Fc, antigen to be used for rat immunisations, following generation of plasmid by Gibson assembly. Gel showing successful expression and purification of MMRN2 495-674 Fc The predicted molecular weight of MMRN2 495-674 is 19.5kDA and together with the Fc tag the combined molecular weight would be just under 50kDa.

7.1.1 Screening of immune response in rat serum by ELISA

ELISA plates were coated in hMMRN2 495-674-Fc or hMMRN2 495-674-His and were incubated with serum from the test bleeds, followed by anti-Rat HRP for detection. A better response was seen on the plate coated with the Fc tagged fragment suggesting antibody response to both the MMRN2 fragment and the Fc tag but there was also a good response to MMRN2 495-674 alone on the plate coated with MMRN2 495-674-His **Figure 69**. Normal rat serum was used as a negative control.



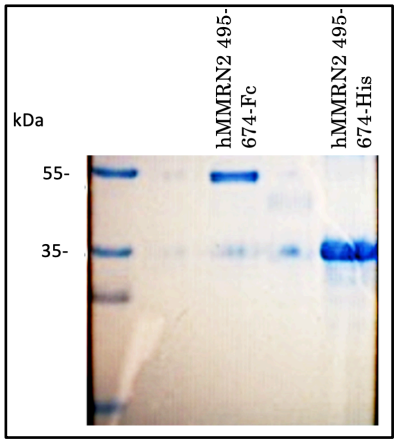
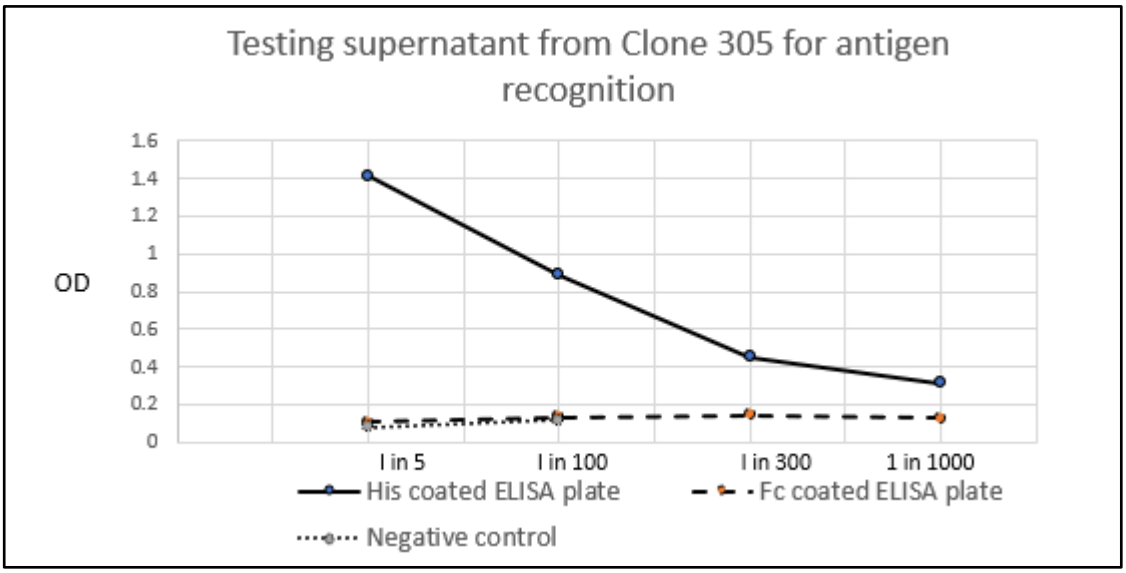


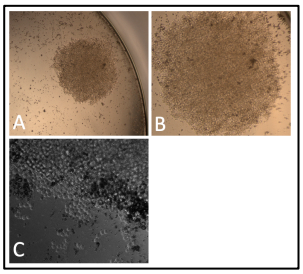
Figure 69. Test bleeds from immunised rats immunised with hMMRN2 495-674-Fc.

ELISA plates coated in MMRN2 495-674-Fc or MMRN2 495-674-His were incubated with rat serum from animals immunised with MMRN2 495-674-Fc. Following washing anti-rat HRP was used for detection. Normal rat serum was used as a negative control. Lower image showing purified MMRN2 495-674 heavier band with the Fc tagged version and lighter band His tagged version.

7.1.2 Screening of hMMRN2 positive hybridoma clones by ELISA

Once the rats were culled the spleen cells were fused to NS0 myeloma cells and cultured. Supernatants from clones were then screened for antibody of interest ie recognising hMMRN2 495-674 epitopes. The first positive clone was clone number 305. Media from clone 305 produced a very obvious response to the MMRN2 495-674 His coated ELISA plate but not to human Fc coated plate **Figure 70.**





Clone 305

Figure 70. Elisa to test supernatant from clone 305 for antibody response to antigen coated plates.

Two plates coated with dilutions of either MMRN2 495-674-His or human Fc alone were used for screening purposes and antibody-antigen recognition detected using anti- rat HRP.

7.2 ELISA to evaluate ability to block CLEC14A -MMRN2 interaction.

The ability of the antibodies produced to block the MMRN2-CLEC14A interaction were tested using an ELISA. MMRN2 496-674 -His was coated onto an ELISA plate and clone supernatant added followed by CLEC14A Fc and then Anti FC HRP used to detect if the CLEC14A bound the MMRN2 fragment. CRT4 was used as a positive control because we know this CLEC14A monoclonal antibody blocks the interaction **Figure 71**. Unfortunately, none of the supernatants containing MMRN2 antibodies blocked the interaction, even with high titres being confirmed by haemagglutination assays. This maybe because MMRN2 is a highly conserved protein **Figure 72** and the region of MMRN2 that interacts with CLEC14A maybe a very conserved epitope that the rats did not raise a response to.

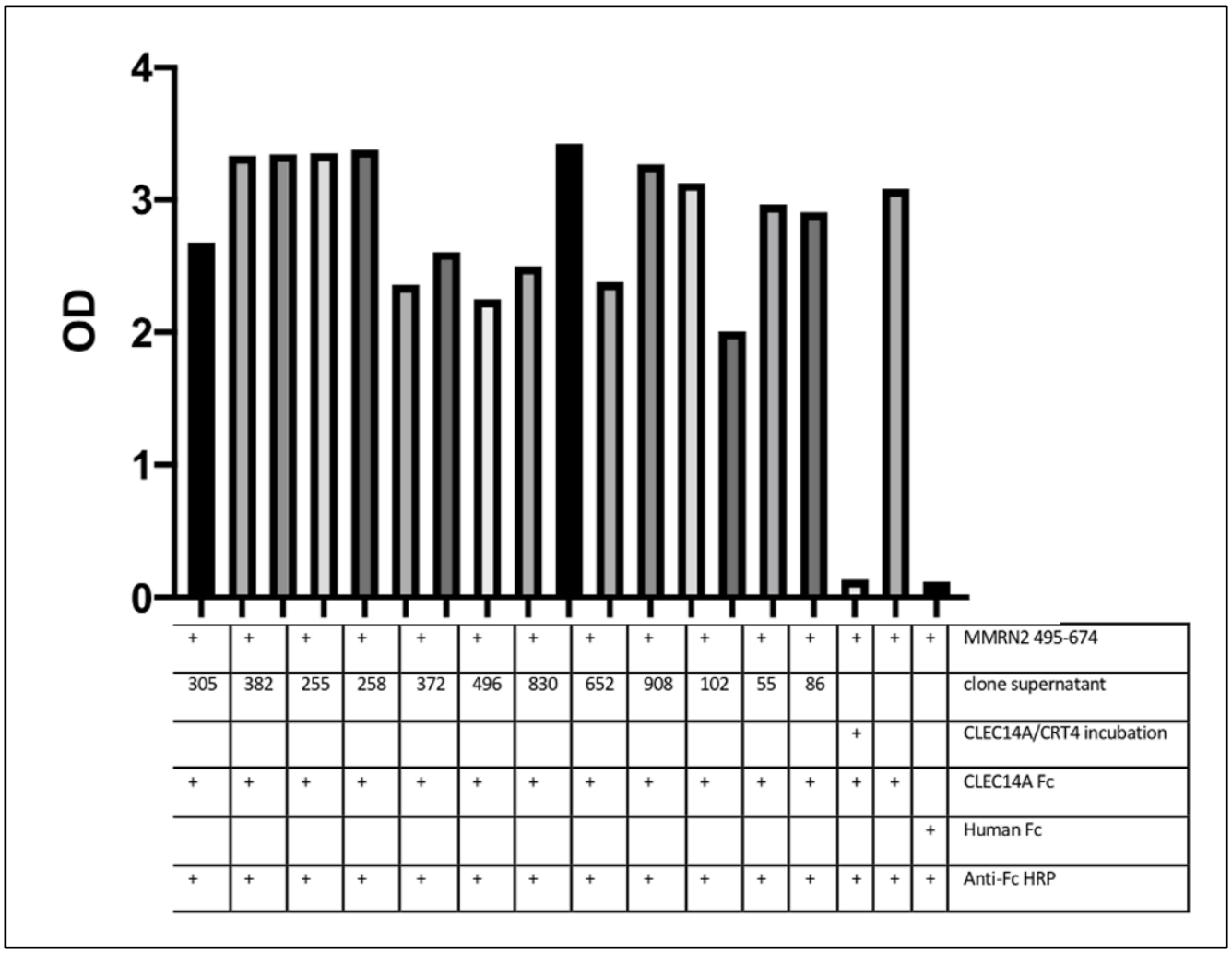


Figure 71. Testing monoclonal antibodies for the ability to block the CLEC14A -MMRN2 interaction.

ELISA plate coated with MMRN2-His, the supernatant from clones was added followed by CLEC14A-Fc and then Anti-Fc HRP for detection. The supernatants from the clones did not block the MMRN2 interaction but the CLEC14A monoclonal antibody CRT4 did.

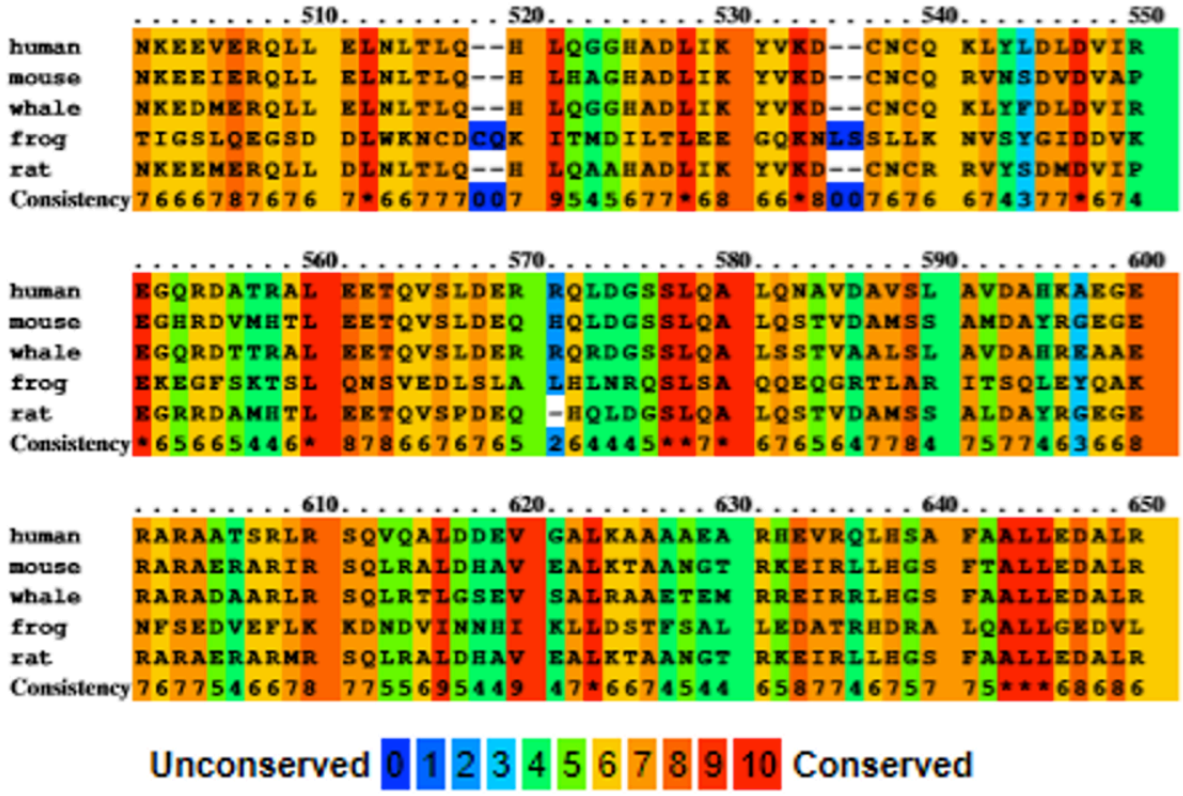


Figure 72. The region of MMRN2 that binds CLEC14A (530-624) contains many highly conserved regions.

7.3 Summary of monoclonal antibody production

Early on we saw a good response in the serum of the immunised rats to the antigen and following harvesting of the splenocytes and development of clones 12 clones were producing antibodies to the antigen. Haemagglutination assays were regularly performed on the clone supernatants to confirm high levels of antibody production during culture, this is because some clones can stop producing. Only supernatants with high antibody content in the media were used in the ELISA to test to see if they could block the CLEC14A- MMRN2 interaction. The antibodies generated did not block the CLEC14A -MMRN2, one reason for this maybe that the epitope required for this was not recognised by the rat's immune system due to the presence of cross species conserved regions of MMRN2.

The results were disappointing that the antibodies generated did not block the CLEC14A- MMRN2 interaction. Due to time constraints, it was not possible to fully evaluate the monoclonal antibodies and there may be uses for the monoclonal antibodies and using them in functional assays already performed in previous chapters is something that can be considered in the future.

8

8 CHAPTER 8: Transcriptomic digital Spatial profiling of high and low CLEC14A expressing hepatocellular carcinoma tissue

8.1 Introduction

When it comes to protein or gene quantification, to date, the work presented in this thesis has focussed on an individual protein or gene selected to be quantified in isolation. Techniques have included immunohistochemistry (IHC), western blot and qPCR. This is useful when you have a particular question about a specific protein or gene. One of the downsides is that it consumes valuable samples in the case of human tissue. In addition, we lose helpful information on the heterogeneity of the tissue. Using IHC, data can be obtained about the distribution of the expression of a particular protein, for example, in a tumour. Still, we lose valuable information about what is associated with that protein. There is the option to do immunofluorescence and overlay detection antibodies, but the technique is limited by the number of proteins that can be studied simultaneously.

In recent years there has been an increase in the availability of spatial molecular profiling where not only can we analyse samples looking for thousands of genes, which of course is possible by standard sequencing, but will also provide spatial information to look at where genes are highly expressed within a tumour

enhancing our understanding of the tumour microenvironment. In this chapter, I outline the methodology used, show that we can correlate genes with CLEC14A high and CLEC14A low expressing regions, and compare how the expression of genes changes from the non-tumour, the tumour capsule, pericapsular and the centre of a tumour to evaluate the heterogeneity. This is achieved by geometric profiling and looking at the expression of different markers across the sample in preselected tissue regions. I then went on to do a form of segment profiling comparing regions of tumour and non-tumour. Given that the tissue is preserved during this process, it is possible to return to the original tissue if required.

Literature to date has described a role for CLEC14A in angiogenesis and tumour growth. However, there have yet to be studies looking at CLEC14A, its relationship to other angiogenic signatures, and immune cell infiltration. Based on the data presented in the previous chapter, it is interesting to see if there is a relationship with a neutrophil signature. Data has yet to be published looking at how CLEC14A expression changes from the tumour periphery to the central tumour and expression in peri-tumoural areas.

The aims of the tissue digital spatial profiling studies were to

1) Compare differential gene expression between the tumour, peri-tumour and non-tumour regions.
2) Look at concordance with CD 31 and CD34 expression.
3) To see if there is a relationship between angiogenic and neutrophil signatures.

4) Explore how CLEC14A expression changes from the periphery of a tumour to the centre of the tumour.
5) Look at the differential gene expression between high and low CLEC14A-expressing tumours and perform a pathway enrichment analysis.

8.2 Tissue preparation overview

The workflow consists of seven stages; cases were selected based on high and low CLEC14A expression from previous chromogenic immunohistochemistry studies. A 5 µm section of tissue was freshly cut under molecular biology conditions (thank you to the Queen Elizabeth Hospital for facilitating this). Fluorescent markers were added to identify morphology facilitating the selection of regions of interest downstream, and profiling reagents were added. This included specific RNA detection reagents, each barcoded with unique photocleavable oligonucleotides. Regions of interest (Devaud et al.) were selected, and areas of non-tumour and tumour were confirmed with the assistance of a consultant liver histopathologist. Using the GeoMx platform based in the Birmingham Tissue Analytics department, selected ROIs were then exposed to UV light which led to the decoupling of the oligonucleotides from the profiling reagents. The released oligonucleotides are aspirated into a microtiter plate well, each well representing an ROI.

A summary of the main steps is described below and shown in **Figure 73** (see manufacturers NanoString GeoMx DSP User Manual for details of the full protocol).

Tissue sections were prepared from FFPE blocks. The tissue sections were cut at 5µm thick, under molecular biology conditions, and placed on the slide in the scan area highlighted in pink **Figure 73**. Slides are baked in a 60°C drying oven and then deparaffinised and rehydrated. Antigen retrieval is performed using 1X Tris-EDTA (pH 9.0), followed by washing in PBS. RNA targets are exposed by incubating in Proteinase K solution at 37°C followed by washing in PBS. This is followed by washes in 10% NBF, NBF stop buffer and lastly, PBS. A hybridisation solution is added to each slide which consists of the RNA panel in Buffer R (found in GeoMx RNA Slide prep kit) and DEPC-treated H_2O. After this step, protecting the samples from light is essential to preserve the photocleavable barcodes. A Grace Bio-labs HybriSlip is applied, avoiding air bubbles. This is then incubated overnight at 37 °C. Slides are then washed in SSC and formamide. The slides are blocked with Buffer W (GeoMx RNA Slide Prep Kit) for 30 minutes in a humidity chamber protected from light.

Fluorescent morphology markers, Alexa532-CD3, Alexa594-CD34, and Alexa647-PanCK were used to visualise the tissue, combined with SYTO13 nuclear stain in Buffer W and added to the tissue incubating for 1 hour in the humidity chamber. Slides are then washed in SCC followed by loading onto the GeoMx DSP. Regions of interest were selected using the GeoMx DSP analysis suite **Figure 74** and labelled as tumour, non-tumour or peri-capsular. Each region of interest is exposed to UV light in turn, and this decouples the oligonucleotide tags from the profiling reagents. The decoupled tags from each ROI are aspirated by a microcapillary tube

and placed in an individual well indexed to an ROI. The oligonucleotide tags are then sequenced facilitating quantification during data processing.

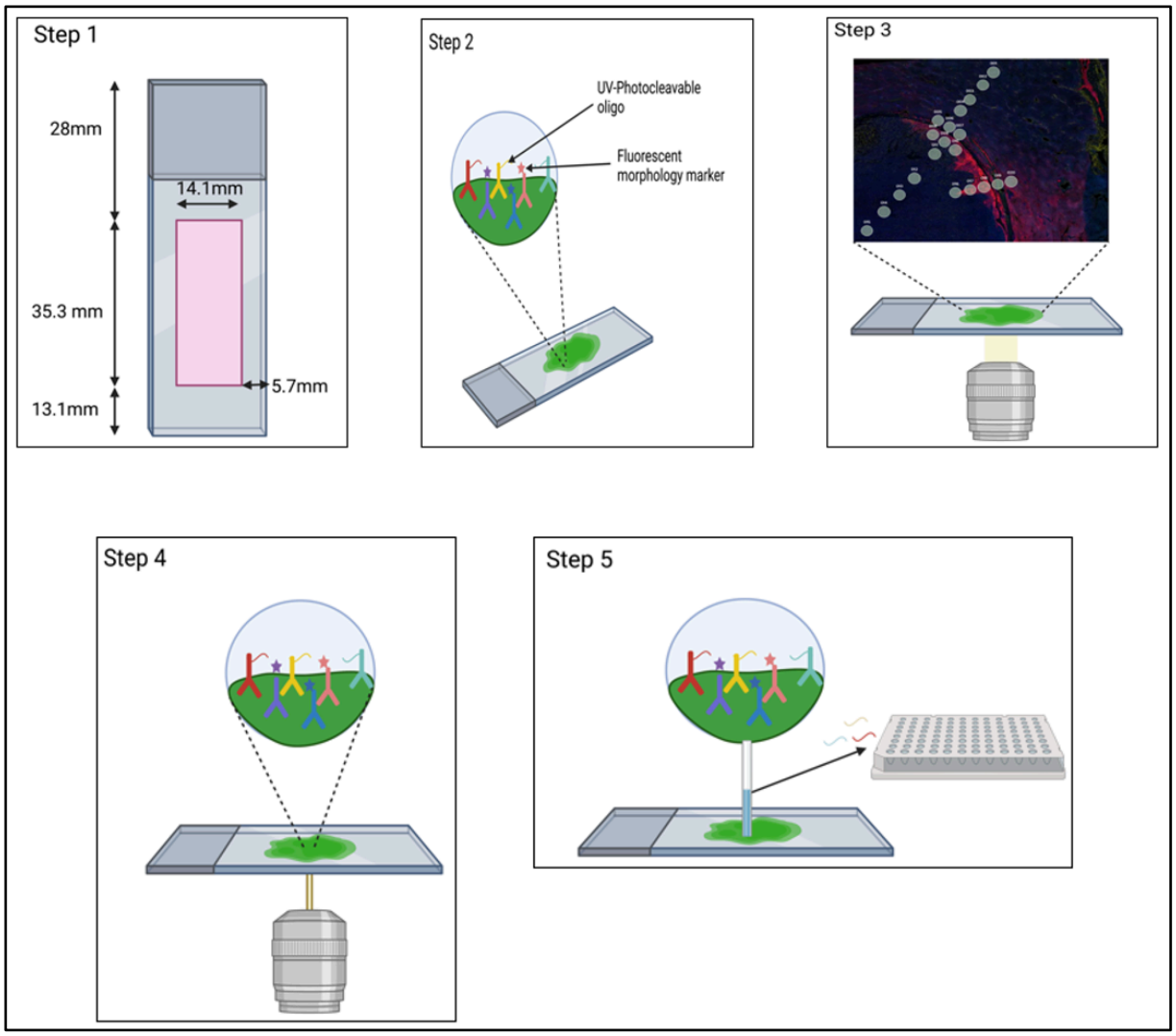


Figure 73. Summary of the main processes for the DSP experiment.

Step 1: preparation of tissue samples, Step 2: RNA slide preparation, Step 3: select regions of interest, Step 4: decoupling of oligonucleotide tags, Step 5: aspiration of oligonucleotide tags for library preparation and sequencing

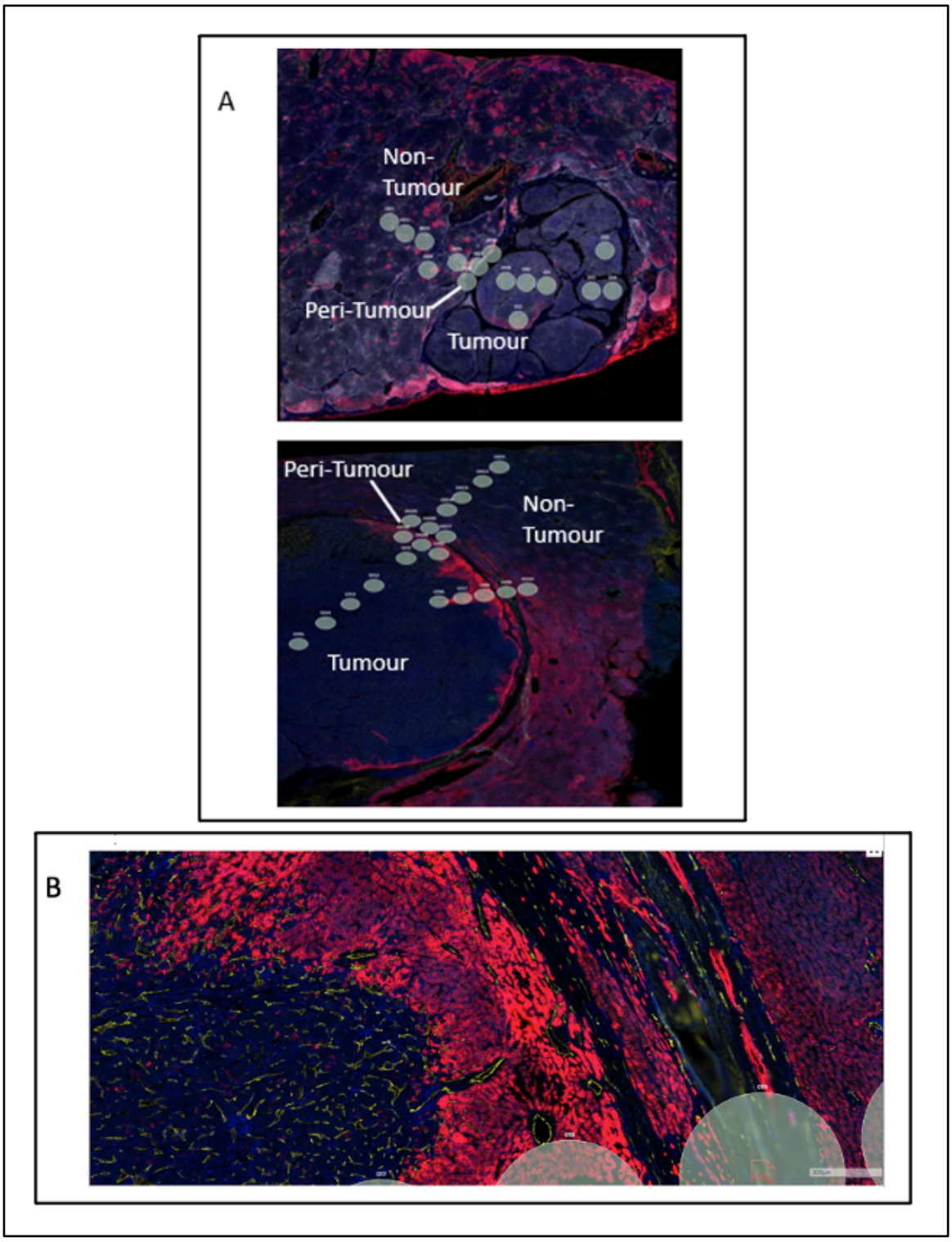
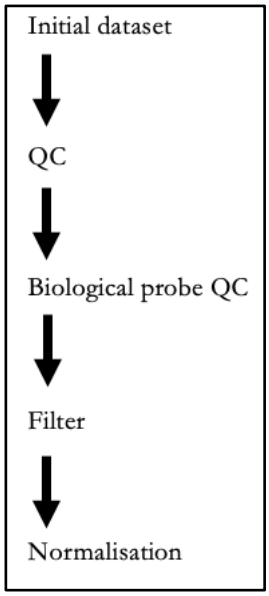


Figure 74. Examples of selection of regions of interest for DSP.

Visualisation of FFPE tissue using antibodies to CD3 (red), CD34 (yellow) and PanCK (Grey) was used to select regions of interest (Devaud et al.). A) Overview of 2 cases and can see the tumour, tumour capsule and non-tumour tissue on each slide. B) Close up of morphology markers.

8.3 Data Processing

Following library preparation and sequencing, FASTQ files were converted to compatible DCC files via an automated data processing pipeline for GeoMx analysis. DCC files containing the counts for the experiment were uploaded, and a study was created with a file containing annotations relevant to the regions of interest, for example, denoting whether a particular ROI is tumour or non-tumour. There is then a sequence of steps completed before analysis is commenced.



In total, 12 tumours and adjacent non-tumour tissues were processed for the experiment. The genes were from the Cancer Transcriptomic Atlas panel and contained 1800 genes. There were five different probes per gene in the RNA panel applied to the tissue at hybridisation. The first QC step was to generate line plots to show the sequencing metrics shown in **Figure 75**.

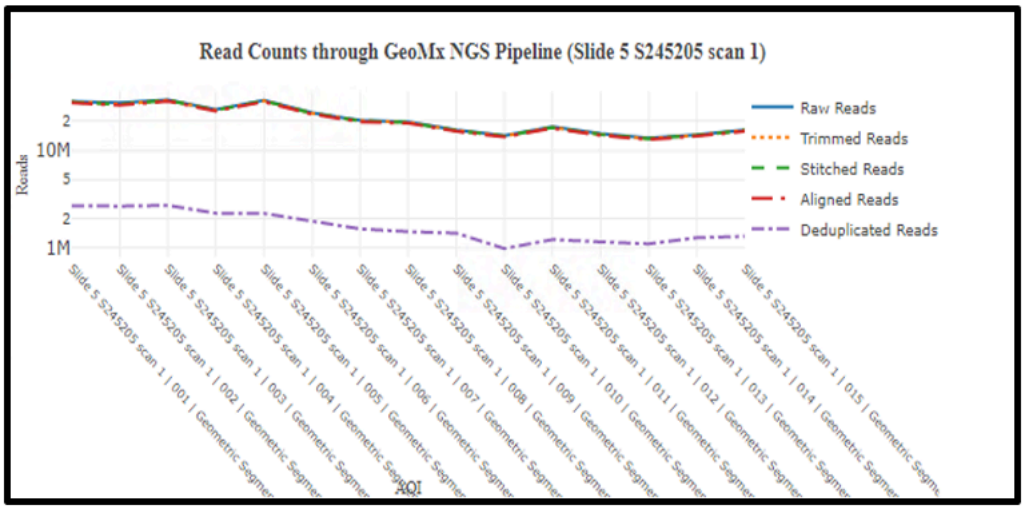


Figure 75. Line plot showing sequencing metrics.

The Raw Reads is the total number of full-length barcodes counted by the sequencer in each segment. A computational algorithm trims the reads, removes the I5 and I7 index, and then combines the forward and reverse reads. Aligning matches the sequenced barcodes with the genomics library linking the barcode to the gene panel. De-duplication is performed to remove duplicates which would have been created during PCR amplification when the library was being prepped. This accounts for why this line is lower than the aligned reads.

After looking at the line plots, parameters are set for the rest of the QC. The raw read is set to flag segments which contain less than a thousand reads because sequencing likely failed for that segment and was therefore excluded; 2 ROIs were excluded at this stage, see **Figure 76**. The percentage of the aligned barcode reads should be high, matching the GeoMx library of barcodes; this was set to flag if it was less than 80%. Looking at sequencing depth, i.e. sequencing saturation, if this was low, then low expressing targets may not have been captured. Each tag has a unique molecular identifier (UMI) specific to that tag, and the number of tags will

have been amplified during the PCR step and de-duplication removes duplicates using:

UMI sequencing saturation = 1- duplicated reads / aligned reads (default value set at 50%).

The RNA panels contained negative probes that do not bind any biological sequences; however, it was expected that they would be counted at a low level, and this is due to non-specific binding to the tissue. Detection of these tells us the floor of detection for a panel, which is flagged if the geometric mean is less than 10. The first well on each plate sequenced had a no template control therefore, no aspirate from the tissue was placed in it. If there are counts detected, cross-contamination has taken place at PCR, this was flagged if the no template control count was greater than 1000. Segments with low cell numbers were set to be flagged if less than 200, because we wanted ideally greater than 100 nuclei per ROI.

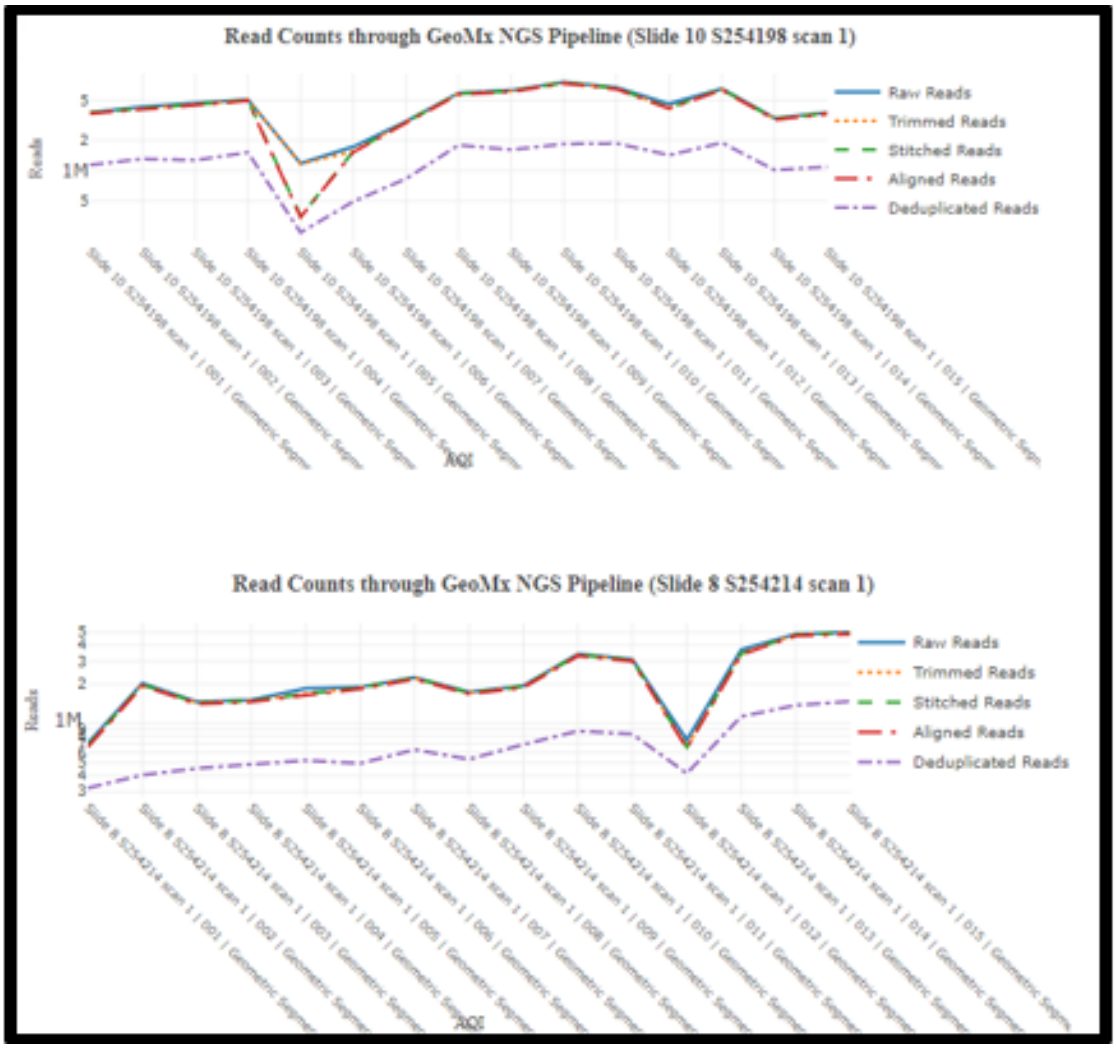


Figure 76. Line plots showing 2 ROIs where sequencing likely failed.

An ROI from slide 10 and an ROI from slide 8 were excluded based on line plots which showed significantly lower read counts for these 2 areas.

Next, a biological probe QC was performed to remove low-performing probes. If the geometric mean of one probe across all segments was less than 10% of the geometric mean of all probes within the target, this was considered a low signal probe, deemed not performing adequately, and was considered for exclusion. The Fais-Grubbs test was used to identify probes that were consistently higher or lower than other probes used for the same target. It was removed if a probe was an outlier in over 20% of segments. The final step was to set the Limit of Quantification (LOQ) per segment. This is the threshold above which the target is detected with high confidence. This was set at 2SD above the geometric mean of the negative probes.

Filtering was performed to remove segments with low signal and insufficient gene detection, followed by normalisation; for this experiment, Q3 normalisation was used. Q3 normalisation is a per-segment calculation; in a given segment, the 75th percentile gene count is determined, and all genes are divided by that Q3 value, which is done for each segment. The gene counts from all segments are multiplied by a constant which is the geometric mean of all Q3 counts in the complete set of data. (Count/Q3 count) x (Geometric mean of all Q3 counts). Box plots pre and post-normalisation are shown in **Figure 77**. Following this I removed 2 cases where the probe counts were low across the tissue and only kept 822 gene targets detected in greater than 5 percent of ROIs.

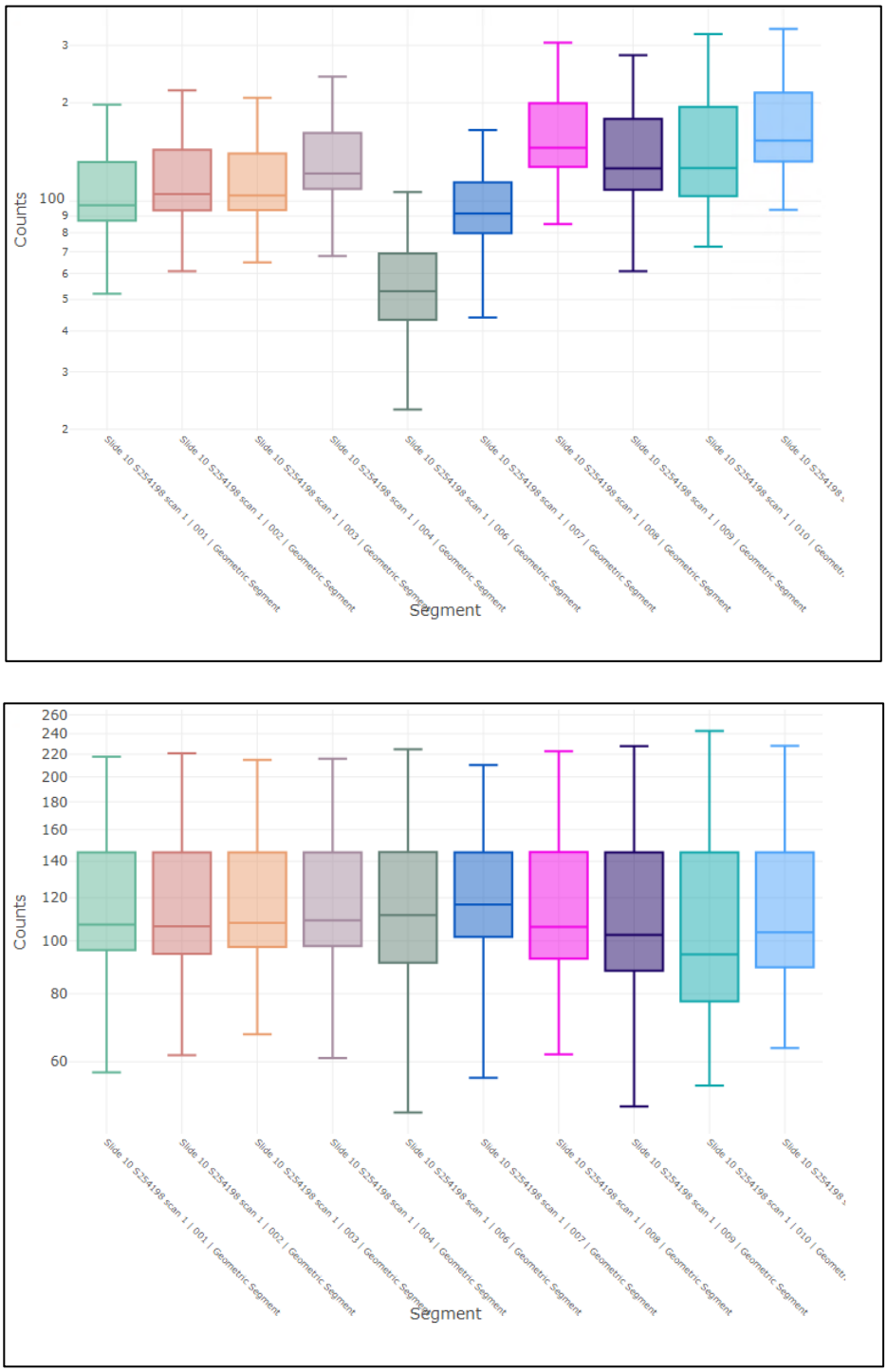


Figure 77. Example box plots for a gene count pre and post-normalisation.

Box plots for case 10 showing gens count pre and post Q3 normalisation.

8.4 Statistical analysis

For statistical analysis, a linear mixed model test was applied to the data to look at differential gene expression; this was because repeated measurements from each piece of tissue were used and, therefore, not genuinely independent. When looking for a relationship between CLEC14A and other genes in the same ROI, Spearman's correlation was used. When comparing gene expression in an ROI to clinical data, variables are reported as medians and IQRs and comparisons made using Mann-Whitney U tests or Kruskal-Wallis test if there were more than two groups.

8.5 Results

8.5.1 Exploration of the data

Following data normalisation, an initial exploration of the dataset was performed. This included generating PCA plots to look at the tumour, non-tumour and peri-tumour ROIs across the cohort individually for each case. These are shown in **Figures 78 and 79**. We can see a degree of clustering for the tumour, non-tumour and peri-tumoral regions.

Differential gene expression was then performed between tumour and non-tumour tissue, tumour and peri-tumour tissue and tumour and non-tumour across the whole cohort. The significance was determined by applying a linear mixed model test. There were 304 genes differentially expressed in tumour and 236 in non-tumour (Adjusted p-value <0.05). There were 314 genes differentially expressed in the tumour and 267 in peri-tumour regions

(Adjusted p-value <0.05). There were 179 genes differentially expressed in peri-tumour regions and 143 in the non-tumour areas (Adjusted p-value <0.05). This is illustrated in the volcano plots shown in **Figure 80**.

Exploring the data looking at immune markers beginning with CD45, CD4 and CD8, we could see that they were all significantly lower in the tumour compared to non-tumour and peri-tumour areas. In the case of CD45, it was significantly higher in the peri-tumour capsule than in the non-tumour and tumour. CD4 was also higher in the peri-tumour region than in the tumour and non-tumour. CD8 was higher in non-tumour and peri-tumour compared to the tumour. Looking at immune checkpoint-associated markers, PDCD1 was significantly lower in the tumour compared to the Peri-tumour and non-tumour regions and VSIR was significantly lower in the tumour compared to the peri-tumour and tumour. Looking at markers associated with Treg differentiation which were in our panel, STAT3 was significantly increased in the tumour compared to the non-tumour and peri tumour, TGFB1 was significantly higher in the peri-tumour compared to non-tumour and tumour, and this also was true for TGFBR2 and IL10RA **Figure 81**.

Considering the relatively immune hot nature of the peri-tumour microenvironment, I then looked at the same cell populations to see if there was any relationship with those markers in the peri-tumoral environment and whether there was vascular invasion present. SMAD 2, SMAD 3 and CD40 in the peri-tumoural area was associated with vascular invasion. High

TGFB1 in the peri-tumoural space with associated with less vascular invasion **Figure 82**.

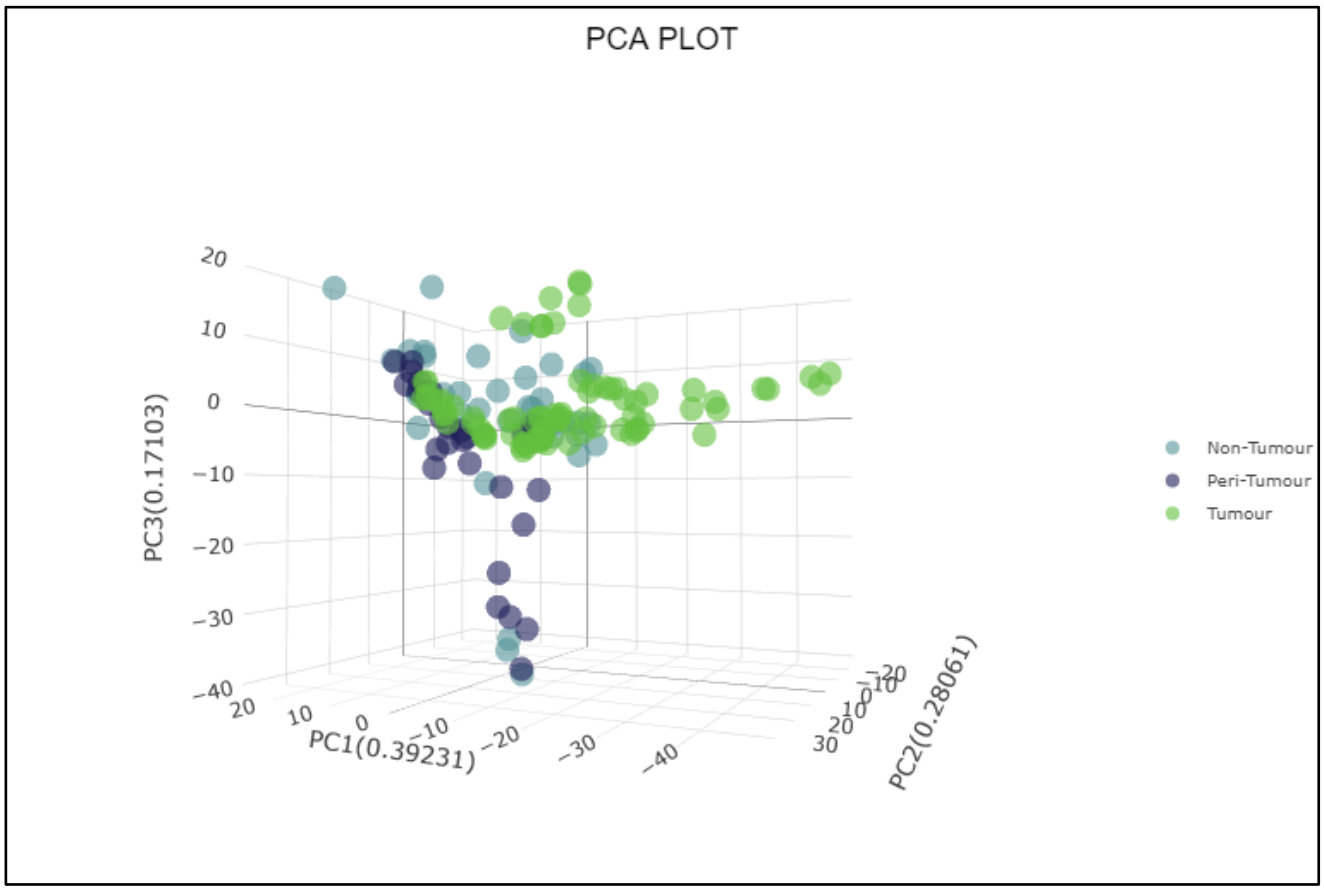


Figure 78. PCA plot for the whole cohort.

PCA plot for all tissue sections, tumour in green, peri-tumour in purple and non-tumour in blue

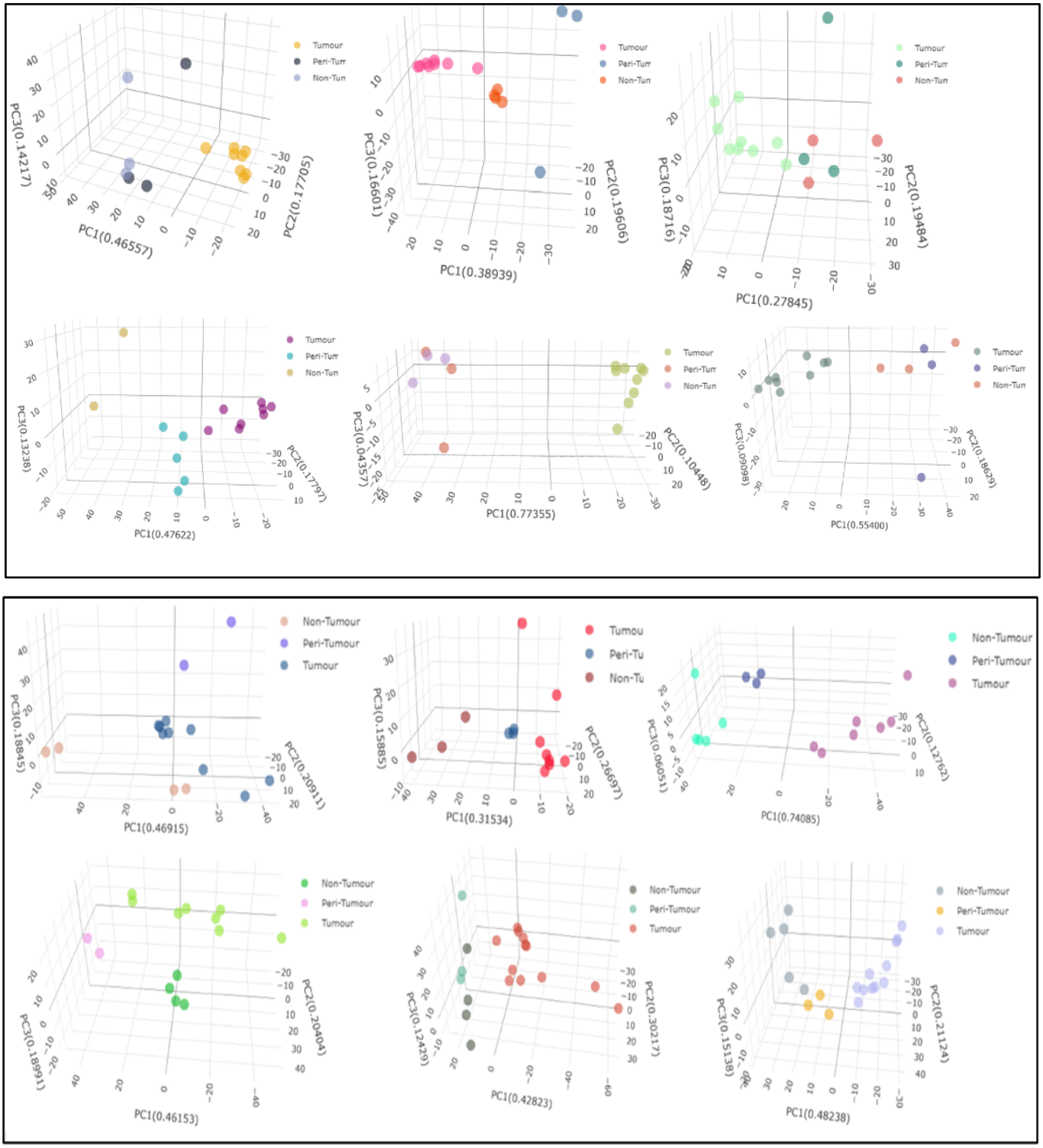


Figure 79. PCA plots for individual cases.

PCA plots for each tissue section with groupings for tumour, non-tumour and peri-tumour regions for each patient case.

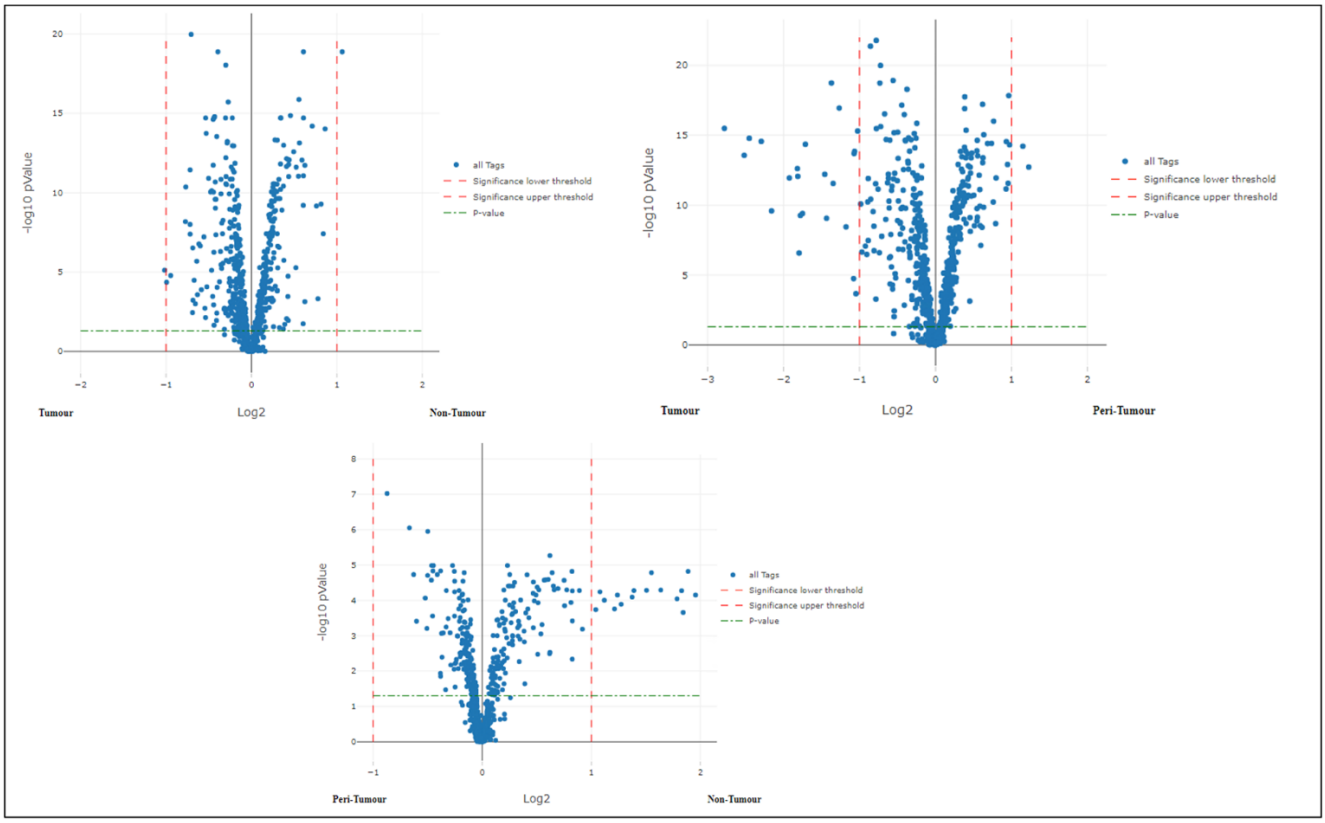


Figure 80. Volcano plots showing differential gene expression between tumour, non-tumour and peri-tumour regions.

Volcano plot to visualise the differential gene expression between tumour and non-tumour regions, tumour and peri-tumour and peri-tumour and non-tumour. There were 304 genes differentially expressed in tumour and 236 in non-tumour (Adjusted p-value <0.05). There were 314 genes differentially expressed in tumour and 267 in peri-tumour regions (Adjusted p-value <0.05). There were 179 genes differentially expressed in peri-tumour regions and 143 in the non-tumour areas (Adjusted p value <0.05). See Appendix 1.

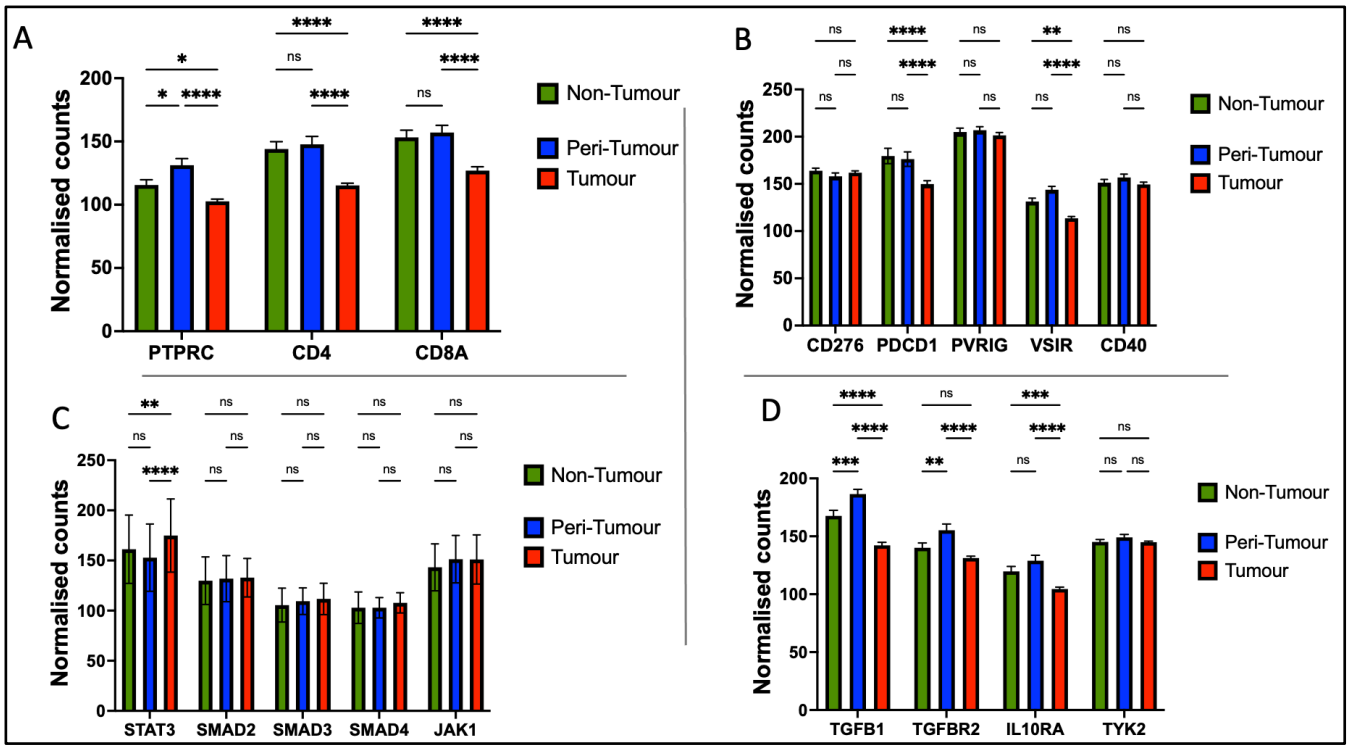


Figure 81. Exploration of DSP data looking at immune markers.

Looking across the whole cohort, **A**) Immune cell markers PTPRC, CD4, CD8 **B**)Immune checkpoint associated markers **C**) & **D**) Treg differentiation-associated markers. Adjusted p-values are shown *P<0.05, **P<0.005, ***P<0.0005, ****P<0.0001.

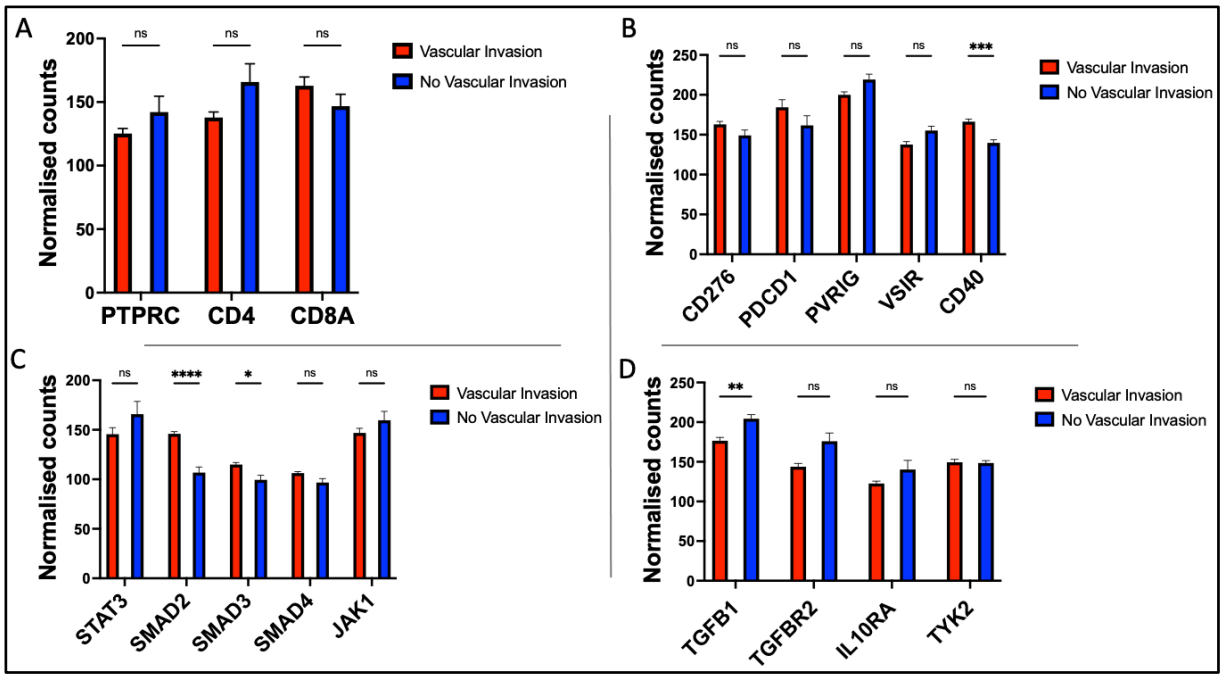


Figure 82. Exploration of the data looking at immune markers and vascular invasion.

Peri-tumoural areas and the presence or absence of vascular invasion. **A**) Immune cell markers PTPRC, CD4, CD8 **B**)Immune checkpoint associated markers **C**) & **D**) Treg differentiation-associated markers. Adjusted p-values are shown *P<0.05, **P<0.005, ***P<0.0005, ****P<0.0001.

This thesis focuses on CLEC14A, and earlier chromogenic immunohistochemistry studies were used to select the cases for DSP; at the protein level, 6 cases of high CLEC14A expression and 6 cases of low CLEC14A expression were chosen for this experiment. The CLEC14A cases with high expression were 1,4,7,8,11, and 12; the patients with low expression were 2,3,5,6,9 and 10. To validate if the cases high or low in CLEC14A at the protein level could be identified from the normalised CLEC14A gene counts in the experiment, box plots were generated with median and interquartile ranges displayed and whiskers showing the maximum and minimum normalised counts for CLEC14A; these are shown in **Figure 83**. In the tumour, non-tumour and peri-tumour regions, a significant difference was seen between the patients selected for CLEC14A high or low at the protein level. The difference was most pronounced for the tumour regions $p<0.005$ compared to $p<0.05$ in the peri-tumour and non-tumour regions **Figure 83**.

Finally, I looked at CLEC14A expression across the cohort for the first part of the analysis. I found that there was no significant difference detectable between the tumour and non-tumour regions. Still, there was a difference between the tumour and peri-tumour and peri-tumour and non-tumour, $p<0.05$ in the latter two instances. However, when looking at just the CLEC14A high expressing tumours, there was a significant difference in CLEC14A expression between the tumour and non-tumour $p<0.05$ and the non-tumour peri-tumour regions, **Figure 84**.

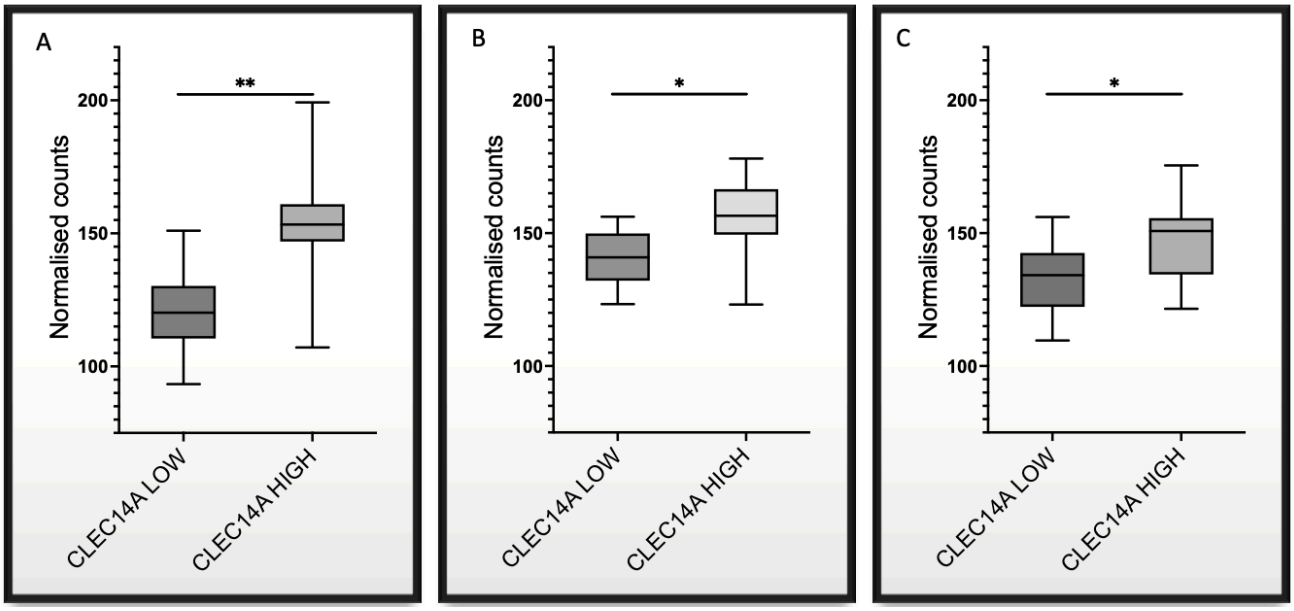


Figure 83. Box plots showing CLEC14A gene expression in 2 cohorts: CLEC14A low expressing tumours and CLEC14A high expressing tumours based on protein staining by immunohistochemistry.

Box plots with median and interquartile ranges are shown and whiskers are for the maximum and minimum CLEC14A normalised counts **A)Tumour ROIs B)Peri-tumour ROIs C)Non-tumour ROIs**
The first box plot on each graph is from tumours with low CLEC14A expression at the protein level with IHC, and the box plot on the right from tumours with high CLEC14A expression. A detectable difference was also seen at the gene level. The difference was more significant for tumour regions than peri-tumour and non-tumour regions. *P<0.05 **P<0.005.

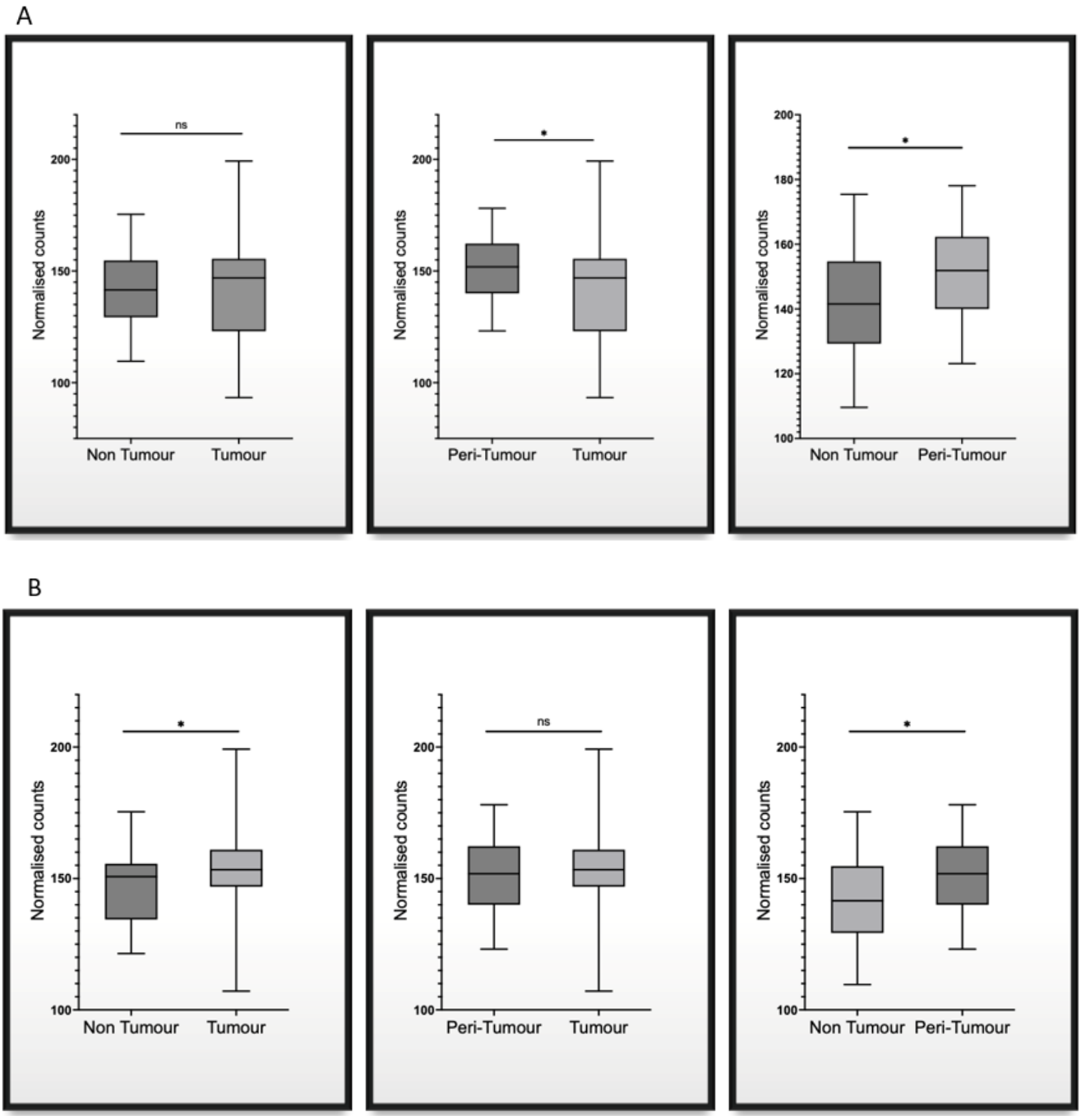


Figure 84. CLEC14A expression A) across whole cohort, B) CLEC14A high only cases.

A)Expression of CLEC14A in non-tumour, tumour and peri-tumour tissues across the whole cohort of patients and the lower figure **B**)Comparing CLEC14A in CLEC14A high expressing tumours only with non-tumour and peri-tumour counterparts. Significance difference denoted by * $P<0.05$, ns non-significant.

8.5.2 Differences in CLEC14A expression by region of the tumour

Taking just the tumour area in each case, I wanted to test the hypothesis that central regions of HCC tumours may differ in their expression of CLEC14A and that CLEC14A expression would be higher in the centre of a tumour compared to the periphery of the tumour due to differences in blood flow dynamics. In previous experiments, I found that CLEC14A expression was upregulated by hypoxia in an in vitro experimental setting.

Normalised counts for CLEC14A expression in the centre of a tumour compared to the periphery were looked at in three cohorts: in all cases, CLEC14A high expressing tumours and CLEC14A low expressing tumours. There was a significant increase in CLEC14A expression in the centre of the tumours in all groupings, which was most pronounced in the group with high CLEC14A expressing tumours $P<0.005$, shown in **Figure 85**. **Figure 86** shows individual cases of CLEC14A levels at each tumour's most central and peripheral points. For one of the larger tumours, where there were multiple regions of interest in a line across the tumour, a bubble diagram has been created, where the bubble size represents the CLEC14A count in that region and alongside a graph with the values plotted. It demonstrated on an individual tumour level that CLEC14A can be expressed in a gradient fashion and does not appear uniform across a tumour. The bubble plot also shows how CLEC14A expression increases in the tumour capsule and is also detectable in the cirrhotic nodule, although at reduced levels. This is shown in **Figure 87**.

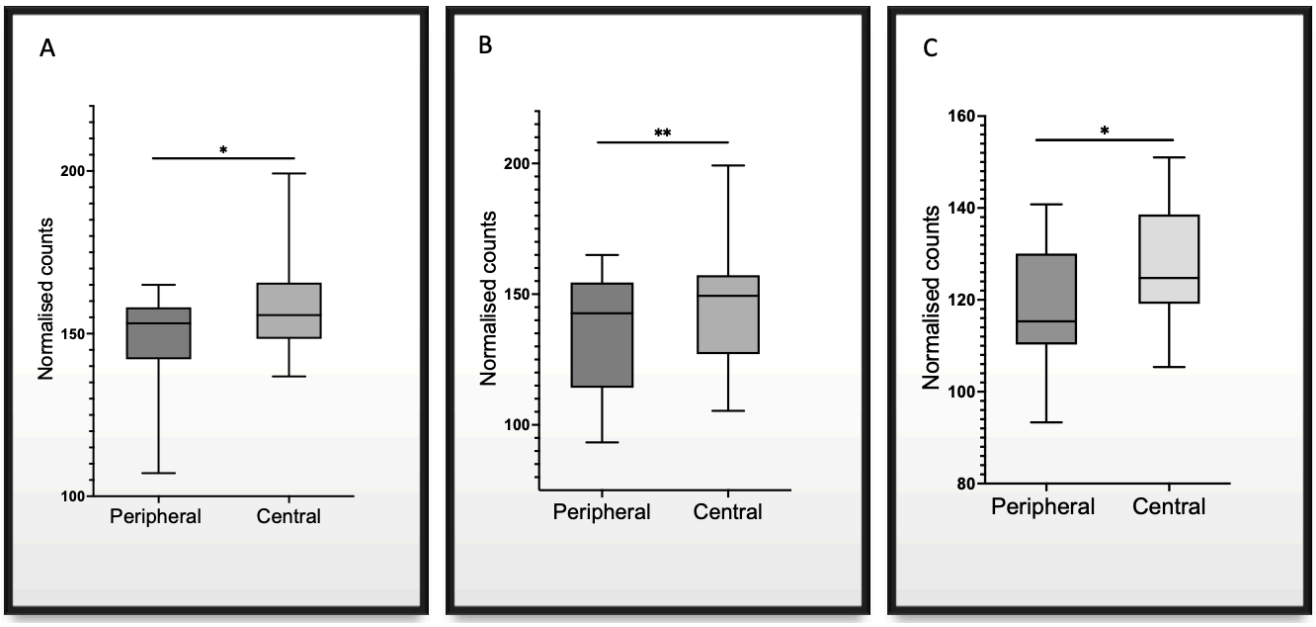


Figure 85. CLEC14A expression in peripheral and central regions of tumours.

CLEC14A expression in peripheral and central regions of tumours for **A)** all tumours in the cohort, **B)** CLEC14A high tumours and **C)** CLEC14A low expressing tumours. There was a significant increase in CLEC14A expression in the centre of the tumours in all groupings * P<0.05, **P<0.005.

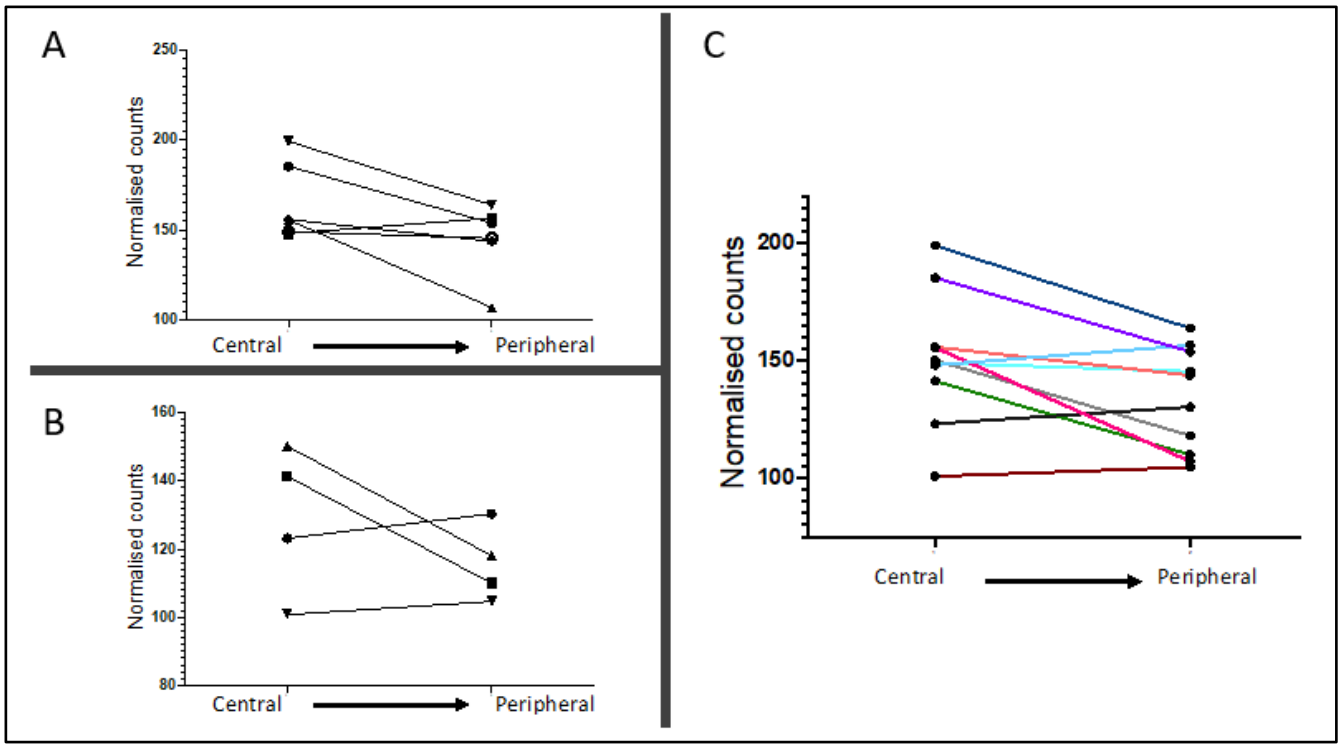


Figure 86. The most central and peripheral CLEC14A counts for each tumour.

The most central and peripheral CLEC14A counts for each tumour. **A**) CLEC14A high expressing tumours, **B**) CLEC14A low expressing tumours on the right, **C**) a graph combining the two cohorts.

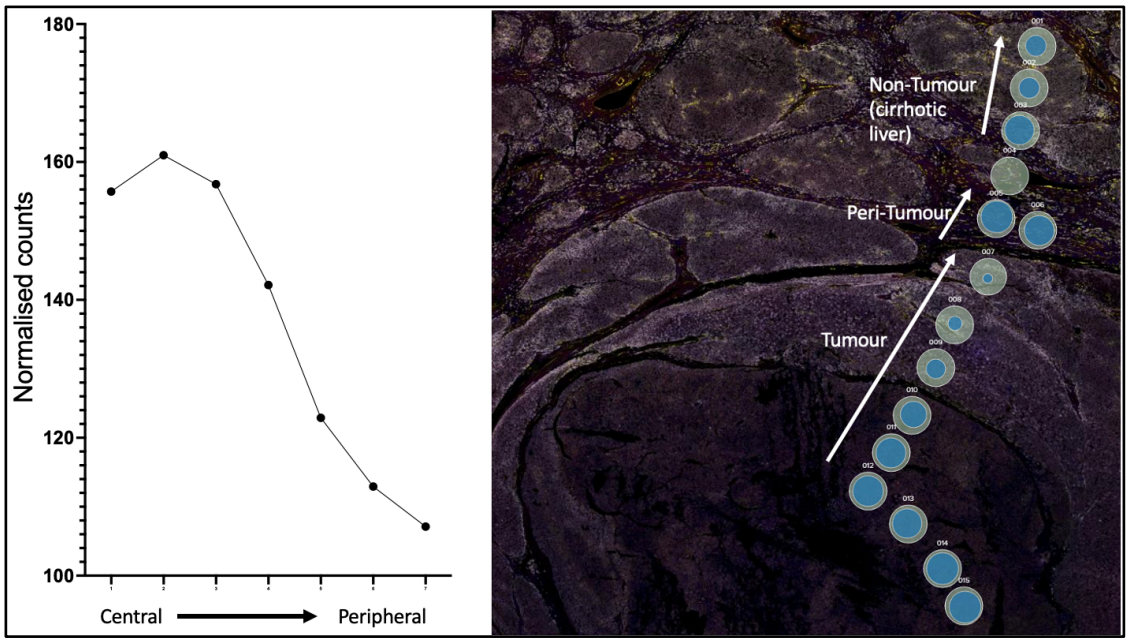


Figure 87. Profiling CLEC14A expression across a tumour.

Profiling CLEC14A expression across a tumour. Line graph and bubble plot showing CLEC14A normalised counts from the centre of a tumour to the periphery of a tumour.

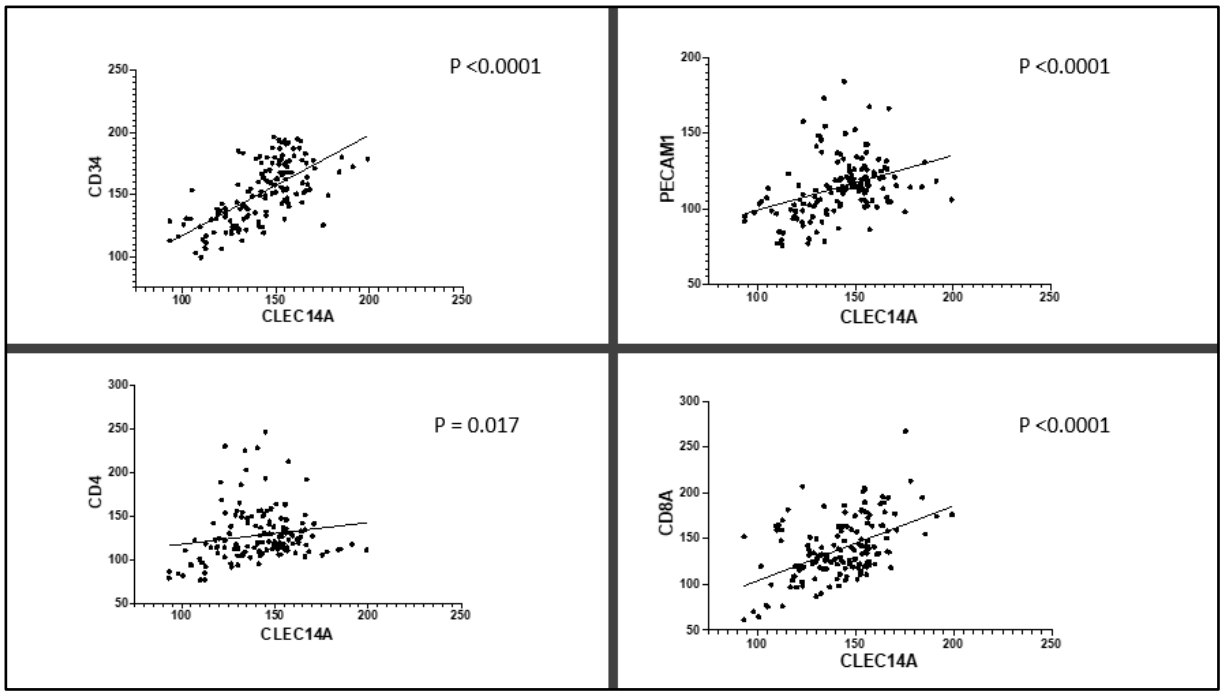
8.5.3 Correlation studies

Two main areas were looked at in the next stage of the analysis. Correlating CLEC14A with other vascular markers and looking for a correlation with genes that create an angiogenesis signature. From what we already know about CLEC14A, it was anticipated that this would be strong. The second part of the correlation studies looked at a neutrophil signature to see if there was any correlation based on the results of the in vitro studies described in the previous chapter.

Before performing correlations with genes associated with an angiogenic and neutrophil signature, CLEC14A, as an endothelial marker, was correlated with CD31 and CD34 in each ROI and analysed using Spearman's correlation to look for the association. In addition, CD4+ and CD8+ were looked at to see if there was any relationship with T cells. The results are shown in **Figure 88**. There was a positive correlation with CD34, CD31, CD4+ and CD8+. There was a significant correlation with CD34, CD31 and CD8+ $p<0.0001$ and at a lower significance level with CD4+ $P=0.017$. The correlation coefficient was highest for CD34 at 0.67.

Genes were selected that have been grouped previously to form an angiogenesis panel and are included in the Cancer Transcriptome panel by Nanostring. These genes, along with CLEC14A, which interestingly wasn't included in the angiogenesis panel, are shown in a correlation matrix for tumour and separately non-tumour tissues in **Figure 89** and **Figure 90**, followed by tables with the correlation coefficient and significance values for CLEC14A correlations **Table 21** and **Table 22**. In the tumour cohort, 30 genes significantly correlated with

CLEC14A; 6 negatively correlated with CLEC14A, which is explored further in the discussion section. In the non-tumour cohort, there were 23 genes identified as significant, although the significance level was less compared to the values from tumour tissue. 5 of the genes had a negative correlation with CLEC14A, which is discussed further in the discussion section. Finally, and interestingly the third table, **Table 23**, shows data from the peri-tumour region, and in this area, only 8 genes correlated with CLEC14A expression and 2 of these had an inverse correlation.



	Spearman r	95% confidence interval	P value	P value summary
CD34	0.67	0.57 to 0.76	<0.0001	****
PECAM1	0.44	0.30 to 0.56	<0.0001	****
CD4	0.20	0.03 to 0.35	0.017	*
CD8A	0.46	0.31 to 0.58	<0.0001	****

Figure 88. Correlation graphs for CLEC14A vs CD34, PECAM1, CD4 and CD8.

Spearman r is reported along with P value to determine the significance of the correlation. CLEC14A positively correlated with CD34, CD31, CD4 and CD8. The correlation was strongest for CD34+ but was found to be very significant for CD34, CD31 and CD8+.

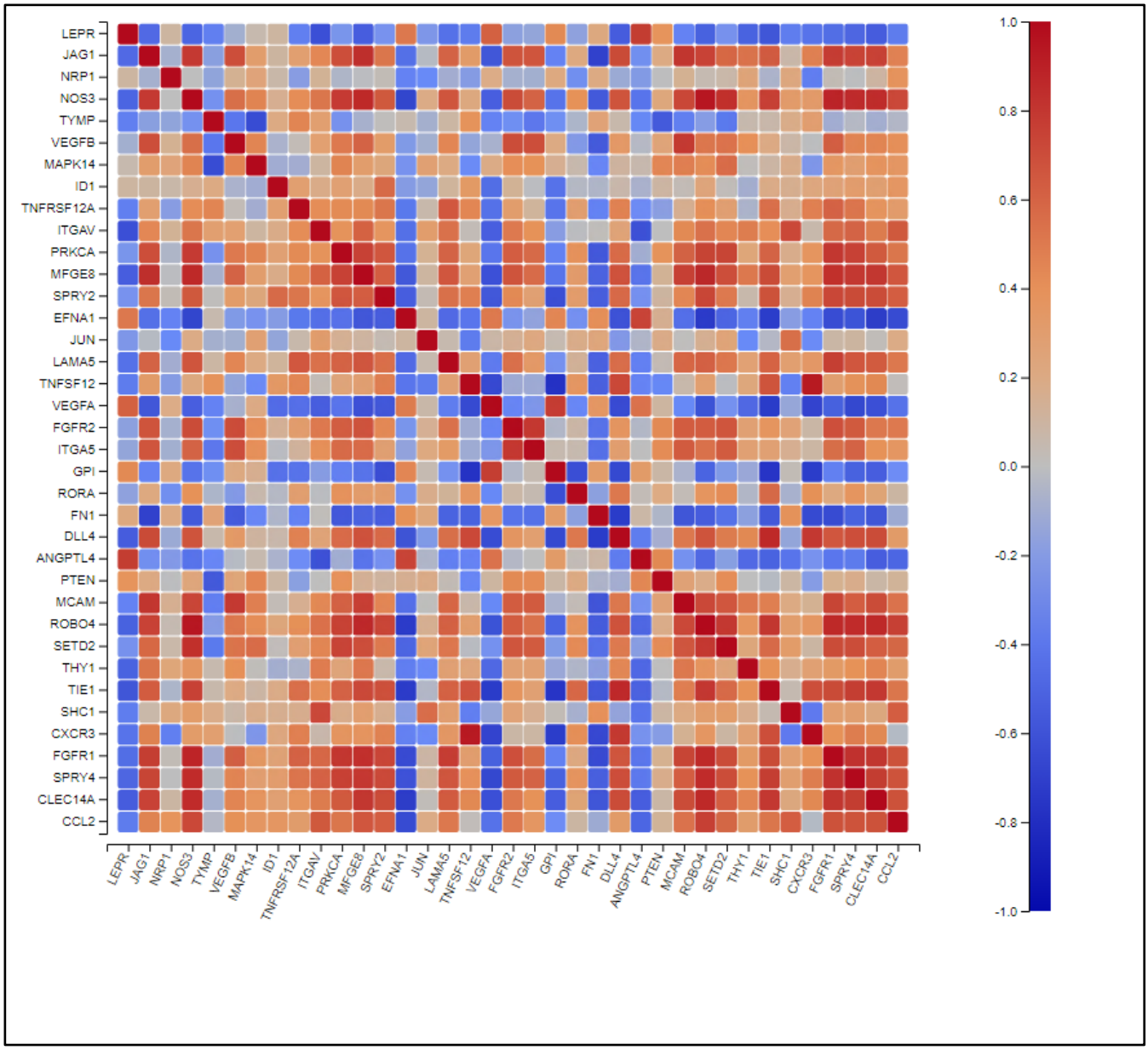


Figure 89. Correlation matrix for genes associated with angiogenesis in tumour areas.

CLEC14A is second from the bottom. The bar on the right shows the correlation coefficient for each coloured square. The table of values follows.

CLEC14A	Spearman	95% CI	P value	P value
LEPR	-0.42	-0.58 to -0.21	<0.0001	****
JAG1	0.78	0.68 to 0.86	<0.0001	****
NRP1	0.13	-0.10 to 0.34	0.2469	ns
NOS3	0.82	0.73 to 0.88	<0.0001	****
TYMP	-0.19	-0.40 to 0.03	0.0813	ns
VEGFB	0.53	0.35 to 0.67	<0.0001	****
MAPK14	0.35	0.14 to 0.53	0.0011	**
ID1	0.26	0.04 to 0.45	0.0172	*
TNFRSF12A	0.28	0.06 to 0.47	0.0103	*
ITGAV	0.37	0.16 to 0.54	0.0006	***
PRKCA	0.62	0.46 to 0.74	<0.0001	****
MFGE8	0.80	0.70 to 0.87	<0.0001	****
SPRY2	0.73	0.61 to 0.82	<0.0001	****
EFNA1	-0.74	-0.83 to -0.62	<0.0001	****
JUN	-0.02	-0.24 to 0.20	0.8229	ns
LAMA5	0.64	0.49 to 0.76	<0.0001	****
TNFSF12	0.43	0.23 to 0.60	<0.0001	****
VEGFA	-0.55	-0.69 to -0.38	<0.0001	****
FGFR2	0.49	0.31 to 0.65	<0.0001	****
ITGA5	0.45	0.25 to 0.61	<0.0001	****
GPI	-0.43	-0.59 to -0.23	<0.0001	****
RORA	0.02	-0.20 to 0.24	0.8439	ns
FN1	-0.55	-0.69 to -0.38	<0.0001	****
DLL4	0.67	0.53 to 0.77	<0.0001	****
ANGPTL4	-0.40	-0.57 to -0.20	0.0001	***
PTEN	0.02	-0.20 to 0.24	0.8585	ns
MCAM	0.77	0.66 to 0.85	<0.0001	****
ROBO4	0.85	0.78 to 0.90	<0.0001	****
SETD2	0.59	0.43 to 0.72	<0.0001	****
THY1	0.53	0.35 to 0.67	<0.0001	****
TIE1	0.83	0.75 to 0.89	<0.0001	****
SHC1	0.19	-0.03 to 0.40	0.0808	ns
CXCR3	0.40	0.19 to 0.57	0.0002	***
FGFR1	0.85	0.78 to 0.90	<0.0001	****
SPRY4	0.80	0.71 to 0.87	<0.0001	****
CCL2	0.69	0.55 to 0.79	<0.0001	****

Table 21. Correlation values for genes associated with angiogenesis in tumour areas.

Genes associated with an angiogenic signature and correlation with CLEC14A. Table shows gene ID, correlation coefficient and significance value for correlation in tumour only tissue. Significant positive correlation is highlighted in pink and a significant negative correlation highlighted in blue.

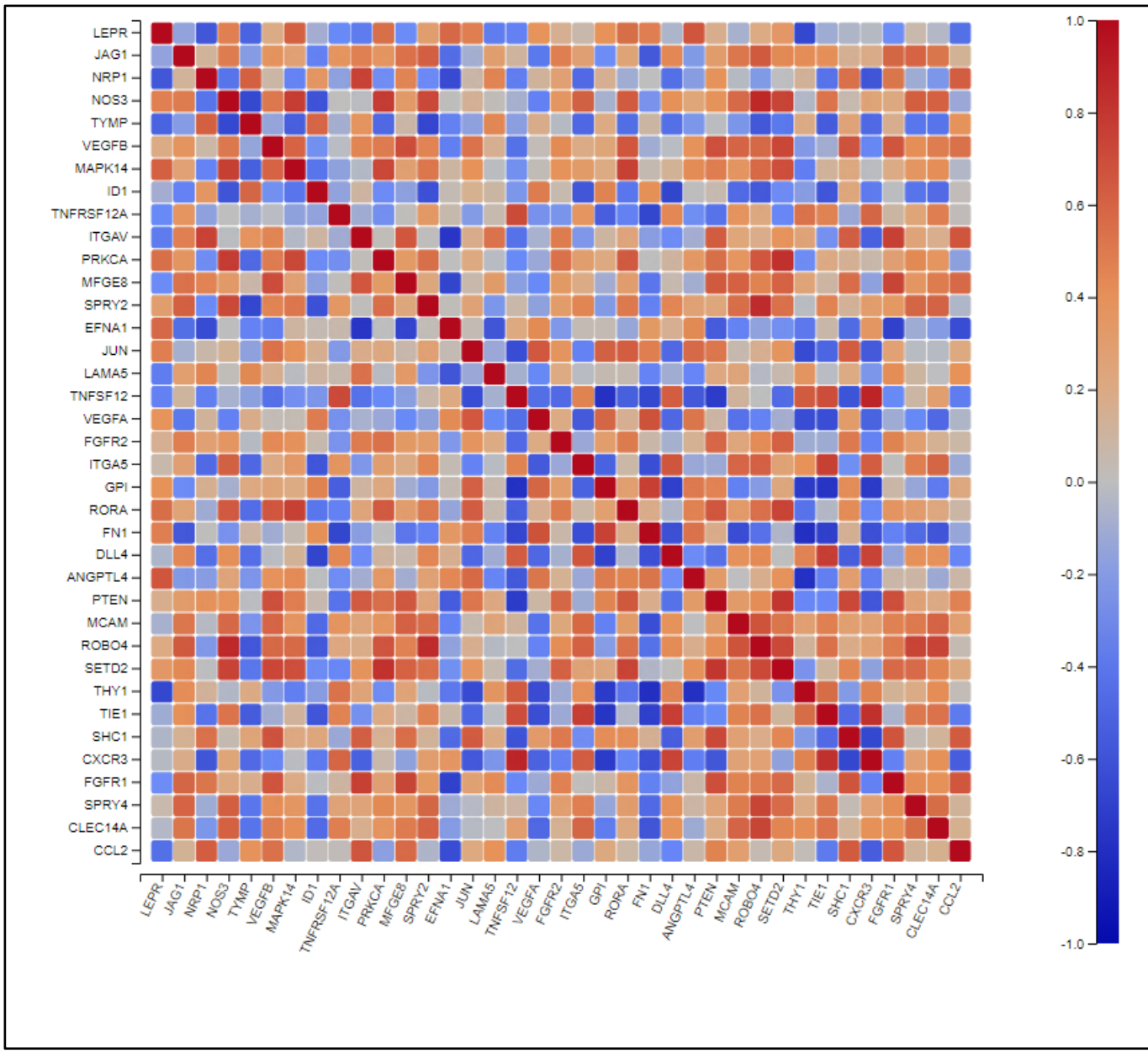


Figure 90. Correlation matrix for genes associated with angiogenesis in non-tumour areas.

CLEC14A is second from the bottom. The bar on the right shows the correlation coefficient for each coloured square. The table of values follows.

CLEC14A	Spearman	95% CI	P value	P value
LEPR	-0.14	-0.46 to 0.21	0.4162	ns
JAG1	0.52	0.22 to 0.73	0.0013	**
NRP1	-0.18	-0.48 to 0.17	0.3051	ns
NOS3	0.63	0.37 to 0.80	<0.0001	****
TYMP	-0.40	-0.65 to -0.07	0.0161	*
VEGFB	0.50	0.19 to 0.71	0.0021	**
MAPK14	0.41	0.083 to 0.66	0.0133	*
ID1	-0.44	-0.68 to -0.12	0.0071	**
TNFRSF12A	0.39	0.057 to 0.64	0.0196	*
ITGAV	0.18	-0.17 to 0.49	0.2944	ns
PRKCA	0.51	0.21 to 0.72	0.0014	**
MFGE8	0.52	0.23 to 0.73	0.001	**
SPRY2	0.65	0.39 to 0.81	<0.0001	****
EFNA1	-0.29	-0.57 to 0.055	0.0882	ns
JUN	-0.01	-0.34 to 0.33	0.9703	ns
LAMA5	0.09	-0.25 to 0.42	0.5951	ns
TNFSF12	0.25	-0.09 to 0.54	0.139	ns
VEGFA	-0.47	-0.70 to -0.16	0.0039	**
FGFR2	0.30	-0.05 to 0.58	0.0799	ns
ITGA5	0.52	0.22 to 0.73	0.0011	**
GPI	-0.38	-0.63 to -0.046	0.0232	*
RORA	0.22	-0.13 to 0.52	0.2026	ns
FN1	-0.61	-0.78 to -0.34	<0.0001	****
DLL4	0.43	0.10 to 0.67	0.0094	**
ANGPTL4	-0.13	-0.45 to 0.22	0.4572	ns
PTEN	0.23	-0.12 to 0.53	0.178	ns
MCAM	0.69	0.45 to 0.83	<0.0001	****
ROBO4	0.73	0.53 to 0.86	<0.0001	****
SETD2	0.57	0.28 to 0.76	0.0003	***
THY1	0.43	0.11 to 0.67	0.0082	**
TIE1	0.54	0.25 to 0.74	0.0007	***
SHC1	0.22	-0.13 to 0.52	0.2015	ns
CXCR3	0.36	0.02 to 0.62	0.0314	*
FGFR1	0.43	0.10 to 0.67	0.0087	**
SPRY4	0.66	0.41 to 0.81	<0.0001	****
CCL2	0.19	-0.15 to 0.50	0.2599	ns

Table 22. Correlation values for genes associated with angiogenesis in non-tumour areas.

Genes associated with an angiogenic signature and correlation with CLEC14A. Table shows Gene ID, correlation coefficient and significance value for correlation in non-tumour only tissue. Significant positive correlation is highlighted in pink and a significant negative correlation highlighted in blue.

CLEC14A	Spearman	95% CI	P value	P value
LEPR	-0.07	-0.44 to 0.33	0.7419	ns
JAG1	0.12	-0.28 to 0.48	0.5528	ns
NRP1	-0.27	-0.59 to 0.12	0.1579	ns
NOS3	0.29	-0.10 to 0.61	0.1305	ns
TYMP	-0.29	-0.61 to 0.10	0.1327	ns
VEGFB	-0.06	-0.43 to 0.33	0.7651	ns
MAPK14	0.02	-0.37 to 0.40	0.9339	ns
ID1	-0.12	-0.48to 0.28	0.5472	ns
TNFRSF12A	0.26	-0.13 to 0.59	0.174	ns
ITGAV	-0.26	-0.58 to 0.14	0.1853	ns
PRKCA	0.36	-0.02 to 0.66	0.0565	ns
MFGE8	-0.14	-0.50 to 0.25	0.4666	ns
SPRY2	0.03	-0.36 to 0.40	0.8966	ns
EFNA1	0.15	-0.25 to 0.50	0.4496	ns
JUN	-0.34	-0.64 to 0.05	0.0733	ns
LAMA5	0.11	-0.29 to 0.47	0.5773	ns
TNFSF12	0.28	-0.12 to 0.60	0.1486	ns
VEGFA	-0.27	-0.59 to 0.13	0.1649	ns
FGFR2	0.35	-0.041 to 0.64	0.0699	ns
ITGA5	0.38	0.00 to 0.67	0.0432	*
GPI	-0.46	-0.72 to -0.09	0.0144	*
RORA	0.01	-0.37 to 0.39	0.9493	ns
FN1	-0.59	-0.80 to -0.27	0.0009	***
DLL4	0.44	0.065 to 0.70	0.02	*
ANGPTL4	0.19	-0.21 to 0.53	0.333	ns
PTEN	-0.14	-0.50 to 0.25	0.4683	ns
MCAM	0.48	0.12 to 0.73	0.01	*
ROBO4	0.43	0.058 to 0.70	0.0217	*
SETD2	0.24	-0.15 to 0.57	0.2138	ns
THY1	-0.11	-0.48 to 0.28	0.5603	ns
TIE1	0.49	0.14 to 0.74	0.0074	**
SHC1	-0.28	-0.60 to 0.12	0.1545	ns
CXCR3	0.41	0.03 to 0.68	0.0312	*
FGFR1	-0.10	-0.47 to 0.29	0.6101	ns
SPRY4	0.32	-0.08 to 0.62	0.1003	ns
CCL2	-0.21	-0.55 to 0.18	0.2754	ns

Table 23. Correlation values for genes associated with angiogenesis in peri-tumour areas.

Genes associated with an angiogenic signature and correlation with CLEC14A. Table shows Gene ID, correlation coefficient and significance value for correlation in peri-tumour only tissue. Significant positive correlation is highlighted in pink and a significant negative correlation highlighted in blue.

Previous in vitro results suggested a potential role for CLEC14A and neutrophil recruitment by HSEC; therefore, a correlation was performed for CLEC14A expression and genes from a neutrophil degranulation signature panel. The panel is not specifically for neutrophil markers but is part of a signature associated with neutrophil degranulation in the microenvironment. 67 genes had a significant correlation with CLEC14A, and most of these were at a level of $p<0.0001$. However, for 24 of these, the correlation was negative with CLEC14A **Table 24**.

CLEC14A	Spearman	95%CI	P value	P value summary
ADGRE5	0.6759	0.54 to 0.78	<0.0001	****
ALDOA	-0.1349	-0.35 to 0.09	0.2212	ns
ALDOC	0.6519	0.50 to 0.76	<0.0001	****
ARG1	-0.7675	-0.85 to -0.66	<0.0001	****
ATG7	0.7061	0.58 to 0.80	<0.0001	****
B2M	-0.6833	-0.79 to -0.54	<0.0001	****
BST2	-0.4166	-0.58 to -0.22	<0.0001	****
C3	-0.8954	-0.93 to -0.84	<0.0001	****
CCL2	0.6865	0.55 to 0.79	<0.0001	****
CCL5	0.6985	0.57 to 0.80	<0.0001	****
CD14	-0.4771	-0.63 to -0.29	<0.0001	****
CD300A	0.8547	0.78 to 0.90	<0.0001	****
CD36	0.437	0.24 to 0.60	<0.0001	****
CD44	0.5982	0.44 to 0.72	<0.0001	****
CD47	0.6414	0.49 to 0.76	<0.0001	****
CD53	0.8475	0.77 to 0.90	<0.0001	****
CD59	0.4436	0.25 to 0.60	<0.0001	****
CD63	-0.619	-0.74 to -0.46	<0.0001	****
CD68	0.2351	0.02 to 0.43	0.0314	*
CFD	0.8067	0.71 to 0.87	<0.0001	****
CHIT1	0.7446	0.63 to 0.83	<0.0001	****
CMTM6	-0.02015	-0.24 to 0.20	0.8557	ns
CSF3R	0.4857	0.30 to 0.64	<0.0001	****
CTSH	-0.06435	-0.28 to 0.16	0.5609	ns
CXCL1	0.2206	00 to0.42	0.0438	*
DSP	-0.2542	-0.45 to -0.04	0.0196	*
ELANE	0.7304	0.61 to 0.82	<0.0001	****
FCER1G	0.6131	0.45 to 0.73	<0.0001	****
FGCR2A/B	0.4855	0.30 to 0.64	<0.0001	****
GPI	-0.4263	-0.59 to -0.23	<0.0001	****
GUSB	-0.3844	-0.56 to -0.18	0.0003	***
HLA-A	-0.2674	-0.46 to -0.05	0.0139	*
HLA-B	-0.3227	-0.51 to -0.11	0.0028	**
HLA-C	-0.6538	-0.76 to -0.51	<0.0001	****
HSPA1A	-0.2059	-0.41 to 0.02	0.0602	ns
HSPA6	0.8347	0.75 to 0.89	<0.0001	****
IDH1	-0.439	-0.60 to -0.24	<0.0001	****
IGF2R	-0.2185	-0.42 to 0.00	0.0459	*
ITGAV	0.368	0.16 to 0.54	0.0006	***
ITGAX	0.8721	0.81 to 0.92	<0.0001	****
ITGB2	0.7914	0.69 to 0.86	<0.0001	****
JUP	-0.07863	-0.29 to 0.14	0.4771	ns
LAMP1	-0.7195	-0.81to -0.59	<0.0001	****
LCN2	0.5022	0.32 to 0.65	<0.0001	****
LGALS3	0.2254	0.01 to 0.42	0.0392	*
LILRB2	0.6899	0.55 to 0.79	<0.0001	****

LYZ	0.06038	-0.16 to 0.28	0.5853	ns
MAPK14	0.3501	0.14 to 0.53	0.0011	**
MIF	-0.2875	-0.48 to -0.07	0.008	**
MME	0.5636	0.39 to 0.70	<0.0001	****
MPO	0.7702	0.66 to 0.85	<0.0001	****
NFAM1	0.8934	0.84 to 0.93	<0.0001	****
NFKB1	0.6588	0.51 to 0.77	<0.0001	****
PECAM1	0.5897	0.42 to 0.72	<0.0001	****
PKM	0.6648	0.52 to 0.77	<0.0001	****
PRKCD	0.7283	0.60 to 0.82	<0.0001	****
PSEN1	0.3677	0.16to 0.54	0.0006	***
PSMB7	-0.2281	-0.43 to -0.01	0.0369	*
PSMD7	0.04726	-0.18 to 0.27	0.6694	ns
PTPRC	0.7279	0.60 to 0.82	<0.0001	****
RAB7A	-0.5663	-0.70 to -0.40	<0.0001	****
RAC1	-0.2495	-0.45 to -0.03	0.0221	*
RHOA	-0.4876	-0.64 to -0.30	<0.0001	****
S100A9	0.7296	0.61 to 0.82	<0.0001	****
SERPINA1	-0.7816	-0.85 to -0.68	<0.0001	****
SIRPA	0.5063	0.32 to 0.65	<0.0001	****
SLC11A1	0.8056	0.71 to 0.87	<0.0001	****
STING1	0.729	0.61 to 0.82	<0.0001	****
STK11IP	0.7117	0.58 to 0.81	<0.0001	****
TNF	0.5133	0.33 to 0.66	<0.0001	****
TNFRSF1B	0.8003	0.70 to 0.87	<0.0001	****
TOLLIP	0.07697	-0.15 to 0.29	0.4865	ns
TTR	-0.5248	-0.67 to -0.34	<0.0001	****
TUBB	-0.4114	-0.58 to -0.21	0.0001	***

Table 24. Genes associated with a neutrophil degranulation signature and correlation with CLEC14A expression in tumour regions.

Table shows Gene ID, correlation coefficient and significance value for correlation in peri-tumour only tissue. Significant positive correlation is highlighted in pink and a significant negative correlation highlighted in blue.

In view of the limitations of using signatures to look for an association, an R script (Danaher et al., 2022) was run, which is designed to interpret gene signatures to create an abundance score for the cell populations that reside in a particular region. The abundance scores were looked at in CLEC14A high tumours, and predicted cell types correlated to CLEC14A normalised counts in different regions **Table 25**; this was repeated in the corresponding non-tumour regions **Table 26**. Strikingly there was a negative correlation with endothelial cells, which was surprising. This was repeated by comparing the abundance scores to CD31 **Table 27** and CD34 **Table 28** across regions. This time, there was a positive correlation with the abundance scores for endothelial cells, and both were statistically significant. Abundance scores correlated with high CLEC14A also revealed a significant correlation with Natural killer cells and this was in both tumour and non-tumour tissues.

CLEC14A vs.	Spearman r	95% CI	P value	P value
Macrophages	-0.63	-0.78 to -0.43	<0.0001	****
Mast cells	0.33	0.05 to 0.56	0.0186	*
Plasma cells	0.62	0.41 to 0.77	<0.0001	****
T.CD4.memory	-0.14	-0.41 to 0.15	0.3316	ns
T.CD8.naive	0.68	0.48 to 0.80	<0.0001	****
T.CD8.memory	-0.44	-0.64 to -0.17	0.0014	**
NK cells	0.56	0.33 to 0.73	<0.0001	****
pDCs	-0.05	-0.33 to 0.24	0.7267	ns
Monocytes.Classical	-0.23	-0.48 to 0.057	0.1044	ns
Monocytes. Non	-0.21	-0.46 to 0.08	0.1446	ns
Neutrophils	-0.12	-0.39 to 0.17	0.3963	ns
Treg	-0.45	-0.65 to -0.19	0.0011	**
Endothelial.cells	-0.54	-0.71 to -0.30	<0.0001	****
Fibroblasts	-0.66	-0.80 to -0.47	<0.0001	****

Table 25. Cell abundance scores correlated with CLEC14A normalised counts in tumour tissue.

Significant positive correlation is highlighted in pink and a significant negative correlation highlighted in blue.
**** P<0.00005, ** P<0.005, ns non-significant.

CLEC14A vs.	Spearman r	95% CI	P value	P value
Macrophages	-0.63	-0.80 to -0.38	<0.0001	****
Mast cells	-0.19	-0.49 to 0.15	0.2519	ns
B.naive	-0.13	-0.45 to 0.21	0.4287	ns
B.memory	0.20	-0.14 to 0.50	0.2284	ns
Plasma cells	0.05	-0.29 to 0.38	0.7751	ns
T.CD4.memory	-0.18	-0.48 to 0.17	0.2968	ns
T.CD8.naive	0.24	-0.10 to 0.53	0.1532	ns
T.CD8.memory	-0.47	-0.69 to -0.16	0.0035	**
NK cells	0.63	0.37 to 0.79	<0.0001	****
pDCs	-0.59	-0.77 to -0.32	0.0001	***
Monocytes.Classical	-0.31	-0.58 to 0.03	0.0659	ns
Monocytes.Non	-0.06	-0.39 to 0.28	0.7118	ns
Neutrophils	-0.24	-0.53 to 0.10	0.1511	ns
Treg	-0.16	-0.47 to 0.19	0.352	ns
Endothelial Cells	-0.64	-0.80 to -0.39	<0.0001	****
Fibroblasts	-0.64	-0.80 to -0.39	<0.0001	****

Table 26. Cell abundance scores correlated with CLEC14A normalised counts in non-tumour tissue.

Cell abundance scores correlated with CLEC14A normalised counts in non-tumour tissue. Significant positive correlation is highlighted in pink and a significant negative correlation highlighted in blue. **** P<0.00005, *** P<0.0005, ** P<0.005, ns non-significant.

CD31	Spearman	95% CI	P value	P value
Macrophages	-0.04	-0.25 to 0.19	0.742	ns
Mast cells	0.02	-0.20 to 0.24	0.8776	ns
Plasma cells	0.00	-0.22 to 0.22	0.9732	ns
T.CD4.memory	0.17	-0.05 to 0.38	0.1126	ns
T.CD8.naive	0.17	-0.06 to 0.37	0.1306	ns
T.CD8.memory	0.25	0.03 to 0.45	0.0208	*
NK cells	-0.10	-0.31 to 0.12	0.3706	ns
pDCs	0.20	-0.02 to 0.40	0.0672	ns
Monocytes.Classical	0.30	0.09 to 0.49	0.0051	**
Monocytes.Non	-0.08	-0.30 to 0.14	0.4692	ns
Neutrophils	0.14	-0.08 to 0.35	0.2059	ns
Treg	-0.21	-0.41 to 0.01	0.0512	ns
Endothelial.Cells	0.40	0.19 to 0.57	0.0002	***
Fibroblasts	-0.02	-0.24 to 0.20	0.8548	ns

Table 27. Cell abundance scores correlated with CD31 normalised counts in tumour tissue.

Cell abundance scores correlated with CD31 normalised counts in tumour tissue. Significant positive correlation is highlighted in pink and a significant negative correlation highlighted in blue.*** P<0.0005, ** P<0.005, * P<0.05, ns non-significant.

CD34	Spearman	95% CI	P value	P value
Macrophages	0.11	-0.11 to 0.33	0.3064	ns
Mast	-0.09	-0.31 to 0.13	0.3969	ns
Plasma cells	-0.22	-0.42 to -0.00	0.0434	*
T.CD4.memory	0.26	0.04 to 0.46	0.016	*
T.CD8.naive	0.08	-0.14 to 0.30	0.4622	ns
T.CD8.memory	0.02	-0.20 to 0.24	0.8376	ns
NK cells	-0.02	-0.24 to 0.20	0.8806	ns
pDCs	0.36	0.15 to 0.53	0.0009	***
Monocytes.Classical	0.29	0.08 to 0.48	0.0071	**
Monocytes.Non	-0.13	-0.34 to 0.10	0.2465	ns
neutrophils	0.38	0.17 to 0.55	0.0004	***
Treg	-0.16	-0.36 to	0.1539	ns
Endothelial.Cells	0.33	0.12 to 0.51	0.002	**
fibroblasts	0.09	-0.13 to 0.30	0.4165	ns

Table 28. Cell abundance scores correlated with CD34 normalised counts in tumour tissue.

Cell abundance scores correlated with CD34 normalised counts in tumour tissue. Significant positive correlation is highlighted in pink and a significant negative correlation highlighted in blue.**** P<0.00005, ** P<0.005, ns non-significant.

8.5.4 Clinical data

For the last part of this chapter, the corresponding clinical data was looked at to see if there were any relationship with CLEC14A gene expression. **Table 29** summarises the patient demographics and laboratory results for the CLEC14A high and CLEC14A low cohorts, followed by **Table 30** displaying the results of a correlation analysis between laboratory values, and CLEC14A normalised counts. Bilirubin and Child-Pugh scores had a significant inverse correlation with CLEC14A expression; unsurprisingly, both had the same trend, given that bilirubin feeds into the Child-Pugh scoring system. The next thing to be analysed was the tumour characteristics and the number of tumours inversely correlated with CLEC14A expression **Table 31**, however, poor tumour differentiation was found to be positively associated with higher CLEC14A expression $p<0.0857$ **Figure 91**, although it did not quite reach significance likely due to sample size. Tumours with vascular invasion were also associated with higher CLEC14A expression median153 (138-171) vs 128 (119-141) but didn't reach significance $p<0.1143$, because one tumour was an outlier otherwise this would have been a significant result **Figure 92**.

Demographics	N	Tumour CLEC14A High cases (N=6)	Tumour CLEC14A Low cases (N=4)	p-Value
Age (Years)	10	65 ± 11.4	58.3 ± 13.6	0.4193
Male	6	4 (67%)	2 (50%)	>0.9999
Ethnicity	10			>0.9999
Caucasian		5 (83%)	3 (75%)	
Non-Caucasian		1 (17%)	1 (25%)	
Laboratory tests				
Haemoglobin (g/L)	9	138.4 ± 13.59	128.5 ± 8.737	0.2498
Platelets (10^9/L)	9	169 (133.5-236)	169 (55.3-279.5)	0.9048
INR	9	1.1 (1-1.2)	1.1 (1-1.3)	>0.9999
Albumin (g/L)	9	43.6 ± 4.722	41.3 ± 6.7	0.5553
Bilirubin (µmol/L)	9	11 (8.5-19.5)	16.5 (11.8-24.3)	0.3175
ALT (U/L)	9	39 (26-189)	35 (23.8-58.3)	0.6111
Sodium (mmol/L)	9	140 ± 4.062	139 ± 2.2	0.6725
Creatinine (µmol/L)	9	72 (67.5-178.5)	85 (60.8-86.8)	0.7302
AFP (ng/mL	9	5 (1.5-1224)	6.5 (3.5-106.3)	0.7778
Aetiology of liver disease				
Alcohol	1	1 (17%)	0 (0%)	
NASH	3	1 (17%)	2 (50%)	
Secondary haemosiderosis	1	0 (0%)	1 (25%)	
HCV	2	1 (17%)	1 (25%)	
HBV	1	1 (17%)	0	
Normal liver	2	2 (33.3%)	0	
Surgery type				0.5714
Transplant	6	3 (50%)	3 (50%)	
Resection	4	3 (75%)	1 (25%)	

Table 29. Summary of patient demographics, laboratory results and tumour characteristics for CLEC14A high expression and CLEC14A low expression.

Data is expressed as Number (%), mean+-SD, median and IQR with p-values from Fisher's exact tests, unpaired t-test or from Mann-Whitney tests. N=10

	Spearman r	95% confidence interval	P value	P value summary
Bilirubin	-0.34	-0.483to -0.18	<0.0001	****
INR	-0.15	-0.31 to 0.025	0.0846	ns
Albumin	0.09	-0.079 to 0.26	0.2726	ns
Platelets	0.20	0.032 to 0.36	0.0168	*
AFP	-0.11	-0.27 to 0.067	0.2155	ns
Lymphocytes	0.03	-0.15 to 0.20	0.752	ns
Neutrophils	0.06	-0.11 to 0.23	0.4696	ns
Neutrophil: lymphocyte ratio	-0.04	-0.21 to 0.13	0.6581	ns
WCC	-0.04	-0.21 to 0.13	0.6462	ns
ALT	0.03	-0.14 to 0.20	0.7226	ns
Child Pugh Score	-0.32	-0.46 to -0.15	0.0001	***

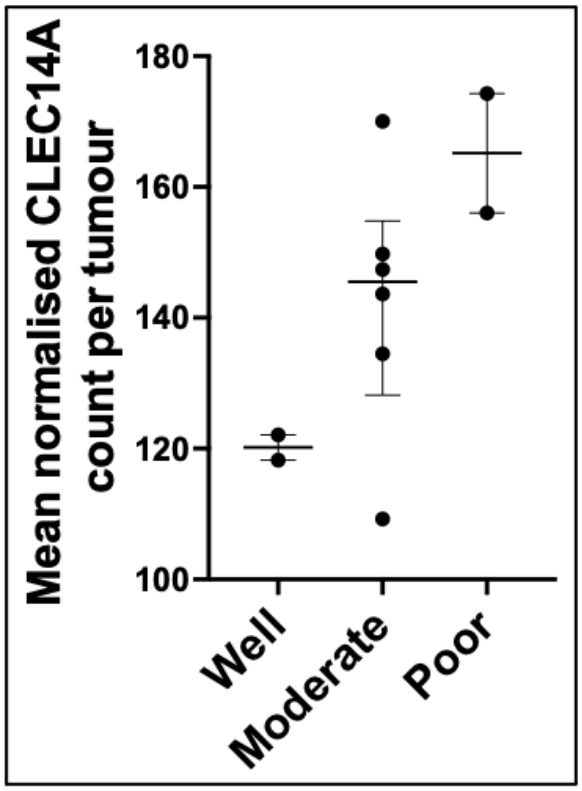
Table 30. Correlations between laboratory values and CLEC14A normalised counts.

Correlations between laboratory values and CLEC14A normalised counts. Spearman's r correlation coefficients, confidence intervals, and P values are detailed.

	Spearman r	95% confidence interval	P value	P value summary
Size of largest tumour	0.01	-0.16 to 0.17	0.9071	ns
Number of tumours	-0.47	-0.59 to -0.33	<0.0001	****

Table 31. Size and number of HCC tumours and correlation with CLEC14A expression.

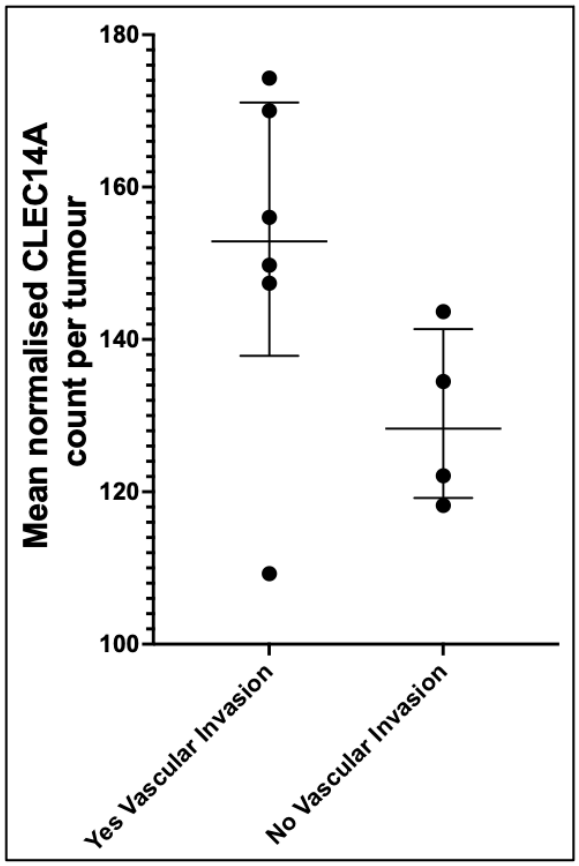
Size and number of HCC tumours and correlation with CLEC14A expression. Spearman r correlation coefficient, confidence intervals and P value are reported. N=10



HCC differentiation	P=0.0857
	CLEC14A normalised counts Median and IQR
Well	120 (118-122)
Moderate	146(128-155)
Poorly	165 (156-174)

Figure 91. CLEC14A expression in tumours vs tumour differentiation.

CLEC14A expression in tumours vs tumour differentiation. Median and IQR values shown and the p-value is from Kruskal Wallis test for comparison across the 3 groupings. N=10



Vascular invasion	P<0.1143
	CLEC14A normalised counts Median and IQR
Yes	153 (138-171)
No	128 (119-141)

Figure 92. CLEC14A expression in tumours vs vascular invasion.

CLEC14A expression in tumours vs vascular invasion. Median and IQR values shown and p-value is from Mann-Whitney tests for comparison across two groups.N=10.

8.5.5 Pathway analysis

The last DSP analysis to learn more about the role of CLEC14A in HCC involved pathway analysis of differential gene expression associated with high CLEC14A expression. First, the genes differentially expressed in CLEC14A high tumours were identified, **Figure 93**, followed by functional gene enrichment analysis using g:Profiler (https://biit.cs.ut.ee/gprofiler/gost) and significantly associated pathways from the KEGG Reactome are displayed in **Table 32**. Along with their adjusted P value.

Finally, using https://reactome.org associated biological pathways were examined, and the outputs are shown in **Figure 94** and **Figure 95**. Interestingly immune system processes were overrepresented in CLEC14A high tumours.

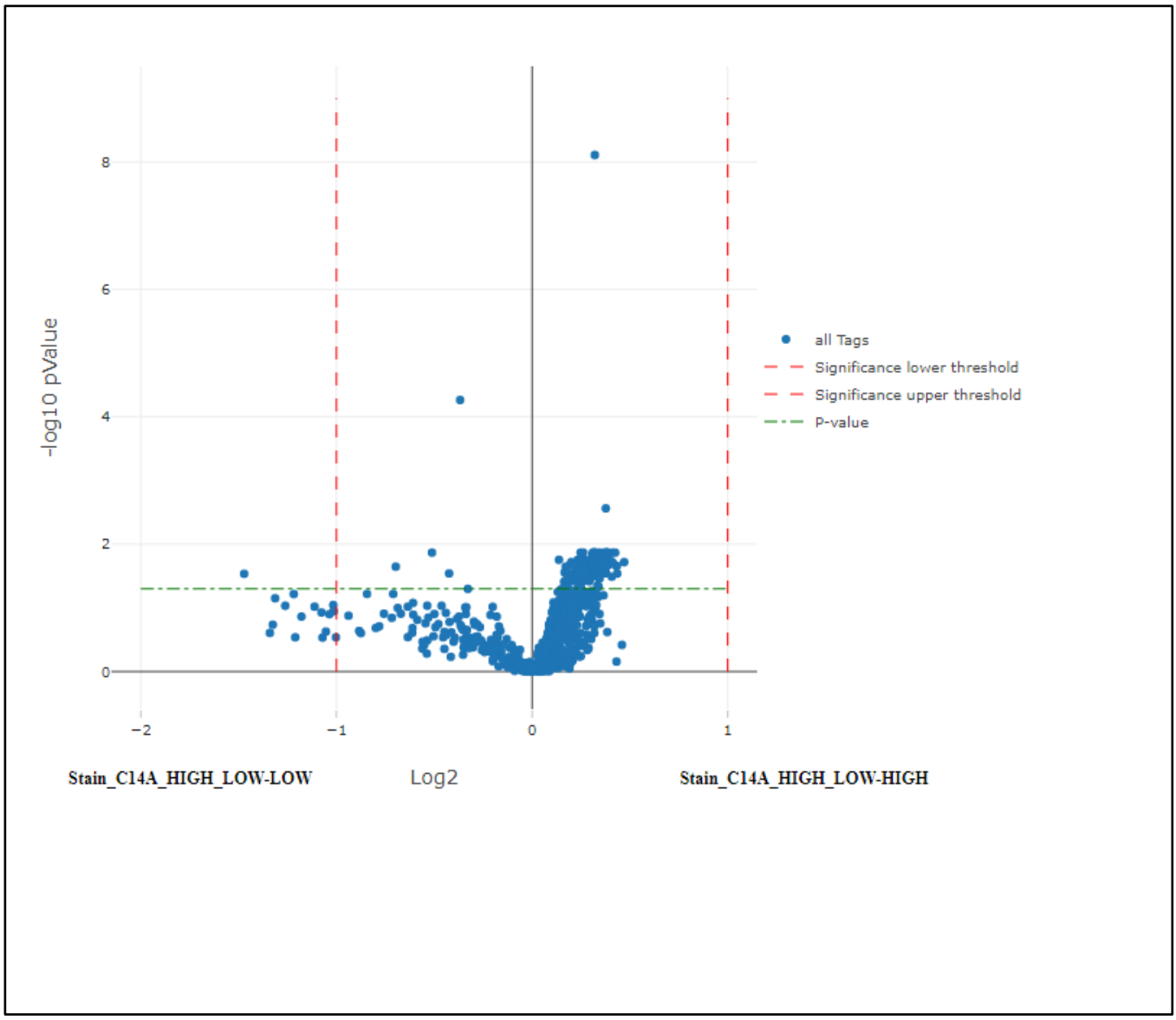


Figure 93. Volcano plot showing differential gene expression for CLEC14A high vs CLEC14A low expressing cases.

Volcano plot showing differential gene expression for CLEC14A high vs CLEC14A low expressing cases. Significance threshold adjusted P value<0.05. The genes upregulated in CLEC14A high cases are listed in appendix 2, along with adjusted P values. See Appendix 2.

Name	term_id	adjusted_p	-log10 (Padj
Pathways in cancer	KEGG:0520	1.43E-11	1.08E+01
Acute myeloid leukemia	KEGG:0522	1.87E-07	6.73E+00
MAPK signaling pathway	KEGG:0401	4.28E-07	6.37E+00
Epstein-Barr virus infection	KEGG:0516	1.57E-06	5.80E+00
Th17 cell differentiation	KEGG:0465	2.37E-06	5.63E+00
Colorectal cancer	KEGG:0521	2.84E-06	5.55E+00
Hippo signaling pathway	KEGG:0439	3.82E-06	5.42E+00
Hepatocellular carcinoma	KEGG:0522	7.75E-06	5.11E+00
Basal cell carcinoma	KEGG:0521	2.06E-05	4.69E+00
Human immunodeficiency virus 1 infection	KEGG:0517	2.34E-05	4.63E+00
Human T-cell leukemia virus 1 infection	KEGG:0516	4.02E-05	4.40E+00
Transcriptional misregulation in cancer	KEGG:0520	4.72E-05	4.33E+00
Measles	KEGG:0516	5.39E-05	4.27E+00
Alcoholic liver disease	KEGG:0493	6.79E-05	4.17E+00
Wnt signaling pathway	KEGG:0431	7.22E-05	4.14E+00
Signaling pathways regulating pluripotency of s	KEGG:0455	7.32E-05	4.14E+00
Gastric cancer	KEGG:0522	0.000106	3.98E+00
Toll-like receptor signaling pathway	KEGG:0462	0.000155	3.81E+00
Lipid and atherosclerosis	KEGG:0541	0.000174	3.76E+00
Hepatitis B	KEGG:0516	0.000276	3.56E+00
Toxoplasmosis	KEGG:0514	0.000285	3.54E+00
Yersinia infection	KEGG:0513	0.000311	3.51E+00
Kaposi sarcoma-associated herpesvirus infectio	KEGG:0516	0.00032	3.49E+00
TNF signaling pathway	KEGG:0466	0.000365	3.44E+00
PD-L1 expression and PD-1 checkpoint pathw	KEGG:0523	0.000406	3.39E+00
IL-17 signaling pathway	KEGG:0465	0.000535	3.27E+00
TGF-beta signaling pathway	KEGG:0435	0.000586	3.23E+00
Breast cancer	KEGG:0522	0.000663	3.18E+00
Leishmaniasis	KEGG:0514	0.000698	3.16E+00
Prostate cancer	KEGG:0521	0.00083	3.08E+00
Osteoclast differentiation	KEGG:0438	0.00098	3.01E+00
Salmonella infection	KEGG:0513	0.00102	2.99E+00
Pancreatic cancer	KEGG:0521	0.001049	2.98E+00

AGE-RAGE signaling pathway in diabetic com	KEGG:0493	0.001066	2.97E+00
Chagas disease	KEGG:0514	0.001156	2.94E+00
NF-kappa B signaling pathway	KEGG:0406	0.001253	2.90E+00
C-type lectin receptor signaling pathway	KEGG:0462	0.001468	2.83E+00
Human papillomavirus infection	KEGG:0516	0.001558	2.81E+00
VEGF signaling pathway	KEGG:0437	0.00172	2.76E+00
Apoptosis	KEGG:0421	0.00206	2.69E+00
Influenza A	KEGG:0516	0.002354	2.63E+00
Proteoglycans in cancer	KEGG:0520	0.003045	2.52E+00
Th1 and Th2 cell differentiation	KEGG:0465	0.003369	2.47E+00
Tuberculosis	KEGG:0515	0.00344	2.46E+00
NOD-like receptor signaling pathway	KEGG:0462	0.00469	2.33E+00
Hematopoietic cell lineage	KEGG:0464	0.005402	2.27E+00
Adherens junction	KEGG:0452	0.005823	2.23E+00
mTOR signaling pathway	KEGG:0415	0.006337	2.20E+00
Melanogenesis	KEGG:0491	0.008366	2.08E+00
Chronic myeloid leukemia	KEGG:0522	0.009027	2.04E+00
T cell receptor signaling pathway	KEGG:0466	0.009613	2.02E+00
B cell receptor signaling pathway	KEGG:0466	0.011555	1.94E+00
HIF-1 signaling pathway	KEGG:0406	0.014309	1.84E+00
Endometrial cancer	KEGG:0521	0.015203	1.82E+00
Shigellosis	KEGG:0513	0.017582	1.75E+00
Inflammatory bowel disease	KEGG:0532	0.022047	1.66E+00
Cushing syndrome	KEGG:0493	0.029733	1.53E+00
Human cytomegalovirus infection	KEGG:0516	0.029927	1.52E+00
Small cell lung cancer	KEGG:0522	0.029992	1.52E+00
Alzheimer disease	KEGG:0501	0.031771	1.50E+00
Fc epsilon RI signaling pathway	KEGG:0466	0.03378	1.47E+00
Hepatitis C	KEGG:0516	0.035993	1.44E+00
Fc gamma R-mediated phagocytosis	KEGG:0466	0.038941	1.41E+00
RIG-I-like receptor signaling pathway	KEGG:0462	0.042871	1.37E+00
Type II diabetes mellitus	KEGG:0493	0.043274	1.36E+00
Choline metabolism in cancer	KEGG:0523	0.044153	1.36E+00

Table 32. Gene enrichment analysis using g:profiler.

Gene enrichment analysis was performed using g:profiler (https://biit.cs.ut.ee/gprofiler/gost) and significantly associated pathways from the KEGG Reactome are displayed along with their KEGG ID and adjusted p value. The green bar in the final column denotes the -log10 (p-adjusted value) i.e. the longer the bar the more significant the result.

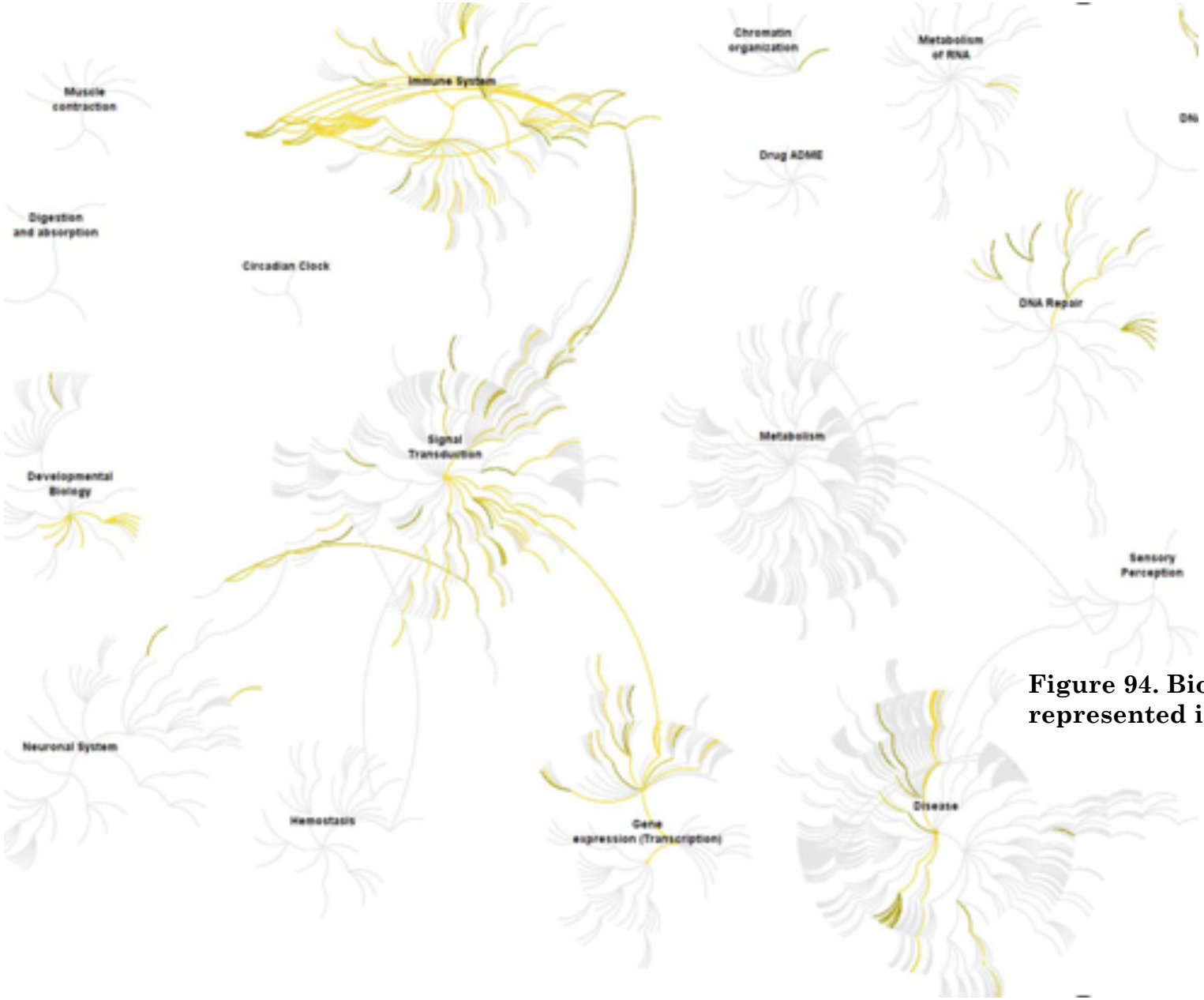


Figure 94. Biological systems over-represented in CLEC14A high tumours.

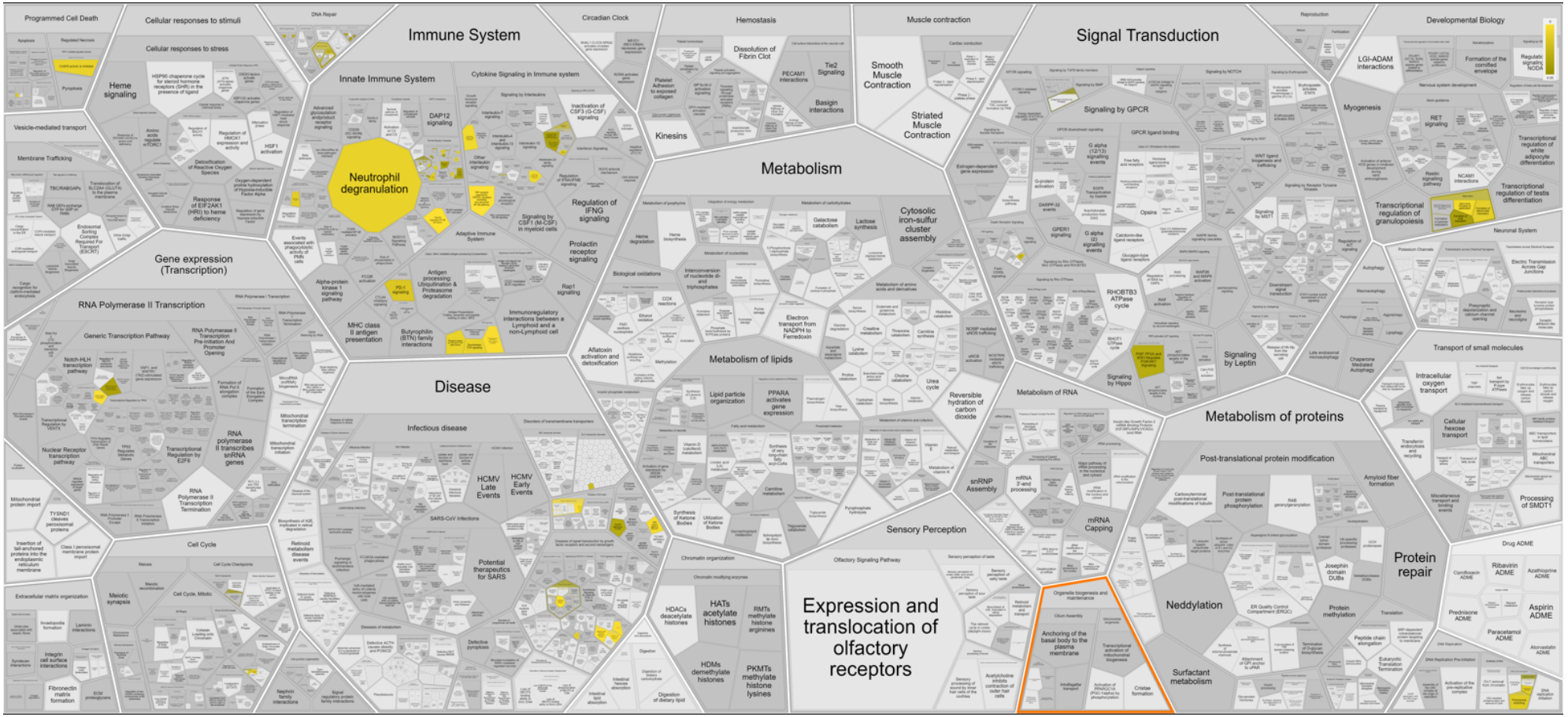


Figure 95. Voronoi pathway visualisation.

Reactome for the genes associated with high CLEC14A expression. The yellow denotes the over-expression of that pathway in the dataset. Light grey – that pathway is not significantly overrepresented.

8.6 Discussion

8.6.1 General overview

The DSP study aimed to examine differences between gene expression in CLEC14A high and CLEC14A low tumours to support existing knowledge and identify new avenues to explore. The analysis started with a general exploration of the data. As expected, the PCA plots demonstrated that the tumour and non-tumour have different clusters, and interestingly, the tumour capsule also separates as a cluster on its own. This is also demonstrated by the differential gene expression, which differs between the three regions, as shown in our volcano plots and Appendix 1. This discussion focuses on the significantly upregulated genes with a fold change greater than 2. Comparing the tumour and non-tumour, the highest upregulated gene was secreted phosphoprotein 1 (SPP1). This is an up-regulated signature gene in HCC tissues (Wang et al., 2019). In the non-tumour, the FOS gene was the most differentially increased compared to the tumour. In several studies, FOS has been revealed to be an essential hub gene in NASH (Meng et al., 2022) and given that most of our samples had a background of steatohepatitis, even if not the primary aetiology, it is probably not that unsurprising that it was significant. However, it is also reported to be highly expressed in HCC, and it was surprising in this series to be higher in the non-tumour. This may be because the non-tumour is in such proximity to the tumour – i.e., on the same section and in other RNA studies, the non-tumour tissue sampled may be more distal. It has been demonstrated that c-Fos is essential for hepatocyte

transformation and HCC development, so maybe this represents a field change in the tumour's proximity (Bakiri et al., 2017).

Surprisingly, the highest number of genes differentially expressed at a higher fold change >2 were found between the tumour and peri-tumoural regions. For example, in the peri-tumour, CD74 had a fold change greater than 2 compared to the tumour. Xiao et al. have recently also shown that CD74 expression is increased in peri-tumoural areas and is expressed predominantly by macrophages (Xiao et al., 2022).

8.6.2 Using DSP to learn more about CLEC14A

The primary purpose of this analysis was to discover more about CLEC14A associations. It was pleasing to see that the high or low protein expression of CLEC14A in the tumours, which we used to select cases, was replicated in the gene counts. Interestingly this not only holds for the tumour, which was selected based on high CLEC14A expression, but you also find that in cases where the tumour is high in CLEC14A expression, it was also high in the peri-tumour and non-tumour regions, suggesting that in the individual cases, there is global up-regulation of CLEC14A.

When we looked at all the tumours compared to non-tumour, we didn't see a significant difference in CLEC14A expression. However, when we looked at just the high CLEC14A cases, there was a significant difference compared to the non-tumour, and in the high cases, the peri-tumour region didn't differ significantly from the tumour. However, the peri-tumour was higher than the non-tumour

across the entire cohort. It has previously been described that CLEC14A is higher in tumours compared to non-tumour tissue in various cancers (Mura et al., 2012). We have found that this also applies to peri-tumoural areas at the RNA level. It is suggested that the tumour capsule is one vital aspect to consider when considering microvascular invasion (Wang et al., 2021b).

We have shown that the central regions of a tumour have higher CLEC14A expression than the periphery of the tumour. This was seen across the whole cohort, including when we looked at high or low cases of tumour CLEC14A expression. In one of the larger tumours, it was even possible to demonstrate that a gradient could be seen where CLEC14A levels were highest towards the centre of the tumour and reduced at the periphery of the tumour but then increased again in the peri-tumour capsule and could still be detected in the cirrhotic non-tumour liver. It is unclear why this should be the case, and studies do not suggest a predictable distribution of hypoxia and hypoxia and angiogenesis do not appear to always correlate (Picchio et al., 2008). A study, however, looking at tumour blood perfusion found reduced perfusion in the centre of tumours. There may be more blood stasis in the centre of a tumour (Benjaminsen et al., 2004).

We have shown that CD34 correlates significantly with CLEC14A expression, with a higher correlation coefficient than CD31. We know that normal sinusoidal cells do not stain for CD34, whereas the abnormal capillaries of HCCs are diffusely CD34 positive. Whereas in the case of CD31, there is expression by the normal liver sinusoids as well as malignant liver lesions being positive for CD31.

The number of genes associated with angiogenesis correlating positively with CLEC14A was higher in tumour areas than in non-tumour areas, although there was overlap in the correlation pattern. Many publications describe shear stress's influence on gene expression and angiogenesis. Some of the genes that correlated positively with CLEC14A expression, which is upregulated by low shear stress, are also upregulated by low shear stress: ROBO4, DLL4, SPRY2, TIE1, FGFR1, CCL2, ITGAV ((Zhuang et al., 2011, Driessen et al., 2018, Mandrycky et al., 2020, Woo et al., 2011, Chen et al., 2015, Lee et al., 2017a, Chu and Peters, 2008). It was interesting that VEGF, which we expect to promote angiogenesis, had a significant inverse correlation with CLEC14A. Interestingly the ligand for CLEC14A Multimerin-2 has been shown to sequester VEGF (Colladel et al., 2016, Lorenzon et al., 2012). VEGF expression is typically increased in many cancers and is important for new vessel formation, so this finding is curious. In my previous data, shear stress appeared to have the opposite effect on CLEC14A and Multimerin-2 and so did hypoxaemia. It has been published that CLEC14A deficiency increases VEGF-A–dependent EC sprouting and vessel density and loss of CLEC14A enhances VEGFR-2 expression so an inverse relationship maybe plausible (Lee et al., 2017b).

In peri-tumour areas MCAM, ROBO4 and TIE 1 had the highest positive correlation with CLEC14A. This correlation was also seen in non-tumour areas and VEGF again had a negative correlation. It has been shown in an invitro model that VEGF is upregulated by shear stress applied to HUVEC which maybe an

explanation (dela Paz et al., 2012). However, the tumour environment is complex, and many cells including tumour cells can produce VEGF.

Several genes associated with neutrophil degranulation correlated with CLEC14A expression, increasing evidence that CLEC14A may be involved in the recruitment of neutrophils. However, there was no positive correlation from the cell abundance scores this may be due to the lack of specific neutrophil markers in the panel. Comparing the cell abundance scores with CD31 and CD34 expression, they correlated positively with endothelial cell abundance, but CLEC14A was inversely correlated. This may be because CLEC14A is upregulated on endothelial cells when there is a reduction in vessel density. This would also correspond to areas with increased hypoxia and reduced blood flow. Natural killer cells correlate significantly with CLEC14A in both tumour and non-tumour regions. This complements the data from an earlier chapter where Reactome analysis revealed that CLEC14A was associated with NCAM1 (CD56) interactions. The significance of this needs to be looked at by immunohistochemistry, but the result is promising that CLEC14A may influence the recruitment of Natural Killer cells.

The clinical correlation of data was interesting, albeit a small number of patients, it gave a signal that CLEC14A expression is inversely associated with advanced liver disease indicated by a negative correlation with Child-Pugh Score. This is not the first time the Child-Pugh score has been associated with angiogenesis markers, and Ang-2 has been associated with a higher Child-Pugh score, more advanced HCC, and reduced overall survival. (Pestana et al., 2018). CLEC14A is associated

with more poorly differentiated tumours and microvascular invasion which highlights its potential utility as a prognostic marker.

One of the final things looked at was the differential expression of genes in just tumour areas with high versus low CLEC14A expression. Pathway analysis revealed that the top pathway upregulated in CLEC14A high tumours was Pathways in cancer; hepatocellular carcinoma and alcoholic liver disease were also in the top 15. The HIF-1 signalling pathway was also significant. Overall, the main biological systems overrepresented in CLEC14A high tumours were the immune system and developmental biology. The association with developmental biology has been well documented, but to date, there has been no literature looking at the influence CLEC14A has on the immune profile of the microenvironment. Veronoi pathway visualisation also highlights the potential for CLEC14A to influence the immune microenvironment, including neutrophil degranulation supporting some of my earlier work.

9

9 CHAPTER 9: Discussion and future work

9.1 Overview

Hepatocellular carcinoma (HCC) is a common cancer, the incidence is rising, and the prognosis remains very poor for the majority. Tumour endothelium is a crucial component of the tumour microenvironment, and my project had 2 broad aims. Firstly, to characterise the presence of CLEC14A in HCC and chronic liver disease and secondly to gain insight into the functional role of CLEC14A. There has been no work previously published looking at CLEC14A in sinusoidal endothelial cells. Promising outcomes with recent immune checkpoint inhibitor trials in hepatocellular carcinoma (HCC) have encouraged the search for novel immunotherapies. The tumour microenvironment in HCC is complex but aggressive tumours are characterised by the accumulation of immunosuppressive cell populations. The endothelium is described as the gatekeeper for immunity, however, the regulation of immune cell/endothelial interaction within HCC is poorly characterised.

Spatial transcriptomics analysis has provided further insight into the heterogenous nature of HCC. The immune environment is far from understood but we know the effector response is highly desirable. A critical step that is poorly understood is the key interaction between immune cells with tumour vasculature during the process of trafficking from the circulation into the tumour microenvironment. Tumour angiogenesis is grossly abnormal, and we see a change from the classical sinusoidal endothelial cell phenotype of the liver to a unique tumour related phenotype. For example, it is widely described that CD34 is not expressed by non-tumour sinusoidal endothelial cells but is expressed in HCC. By increasing our understanding of the endothelium in HCC and how it influences the migration of different immune cell populations we could potentially manipulate this to promote an effector infiltrate while excluding immunosuppressive subsets. In recent years there has been an increasing body of evidence to suggest that the transcriptomic profile of tumour endothelial cells is very different to normal endothelial cells. They have distinctive phenotypic and functional characteristics compared to normal endothelial cells. They are capable of promoting tumour angiogenesis and critical mediators of immune regulation. Studies have shown altered gene expression profiles, including up-regulation of angiogenic genes. It is theorised that this is related partly to cellular hypoxia and that the endothelium contributes to the associated immune suppression we see in many solid organ tumours that advantage the tumour to grow.

9.2 Summary of main findings

The identification of the tumour angiogenic signature CLEC14A-MMRN2-CD248 was an exciting discovery by Khan et al but is still to be fully explored and understood. CLEC14A has been shown previously to be upregulated on tumour endothelium and to have a role in tumour angiogenesis. However, CLEC14A distribution had not previously been described in HCC and the presence in chronic liver disease looked for, this is important because most HCC occurs on the background of liver fibrosis.

The project started with an initial TCGA data interrogation which showed that CLEC14A positivity was associated with improved survival in liver cancer, and this was also the case for MMRN2. Immunohistochemistry studies showed that CLEC14A has minimal expression in the normal liver and where found it is confined to portal vein and hepatic artery branches and there is no staining of sinusoids, hepatocytes, or bile ducts. In chronic liver disease, however, in many cases increased expression at the protein level was found on hepatic artery branches, portal vein branches and in the fibrous septa of alcoholic liver disease, non-alcoholic fatty liver disease and primary biliary cirrhosis. It was noteworthy that sinusoidal staining was seen in and around areas of bridging fibrosis between portal triads and in sinusoids surrounding the portal triads, but no sinusoidal staining around the central veins. I hypothesised that this may be because these areas in a normal liver are comparatively rich in oxygen and in chronic liver disease, where there is an environment of hypoxaemia, these areas may be more sensitive to hypoxaemia and that is why CLEC14A is upregulated. We know that

CLEC14A is associated with angiogenesis and angiogenesis is driven by hypoxaemia. In hepatocellular carcinoma it was clear that CLEC14A is upregulated compared to adjacent tissue however this varied between cases and in some cases CLEC14A was associated with only larger vessels and in some cases where there was sinusoidal positivity it could be patchy and in others diffuse. In some HCC cases there was also strong CLEC14A expression in the tumour capsule and it was noteworthy that in some cases although there was diffuse CLEC14A sinusoidal staining, the periphery of the tumour was spared. Correlating tissue expression at the protein level in our cohort there was no difference in overall survival, however, the survival curves did separate after three years when there was a trend that higher CLEC14A expression was associated with longer survival which is what I found from the TCGA data. CLEC14A expression in tissue was associated with a poorer differentiation of tumour and this was statistically significant so the improved survival in the TCGA data was a curious finding.

For the first time I showed that CLEC14A is expressed by sinusoidal endothelial cells in culture and that MMRN2 is bound to CLEC14A in HSEC, but not all CLEC14A. I also isolated endothelial cells in HCC tissue and could see that the cells isolated from tumours looked distinctly different in that they were elongated and failed to proliferate suggesting they were in a state of senescence in standard HSEC culture media. This finding needs to be explored further perhaps confiming senesence using known markers for this cellular state in the first instance. I was also able to show that CLEC14A, MMRN2 and CD248 co-localise in HCC they are also present in liver colorectal metastases and in neuroendocrine tumour liver

metastases, and therefore are not specific to primary tumours. I confirmed that CD248 does indeed bind MMRN2 and narrowed down the binding site on MMRN2 where this interaction occurs, and I was able to show that it is at a distinct site from where VEGF is known to bind MMRN2.

In view of the high expression of CLEC14A in some solid organ tumours I wanted to see if CLEC14A had a utility as a serum biomarker in cancer. CLEC14A, as described in the introduction, is cleaved from endothelial cells and can be detected in human serum. CLEC14A was not detectable in the serum of 58% of patients with HCC and therefore this is comparable to the number of HCC cases in which we can detect serum AFP. Therefore, using serum CLEC14A as a screening tool would miss some cancers like AFP does. There was no relationship to Barcelona tumour staging and the serum CLEC14A level. I did find, however, that serum CLEC14A is associated with micro rather than macrovascular invasion.

In all cases where serum CLEC14A was detectable, CLEC14A was also highly expressed in the tumour tissue but there was one case where serum CLEC14A was not detectable, but it was highly expressed in the tumour. The main limiting factor for serum CLEC14A as a biomarker is the fact that it is not unique to cancer and the samples collected from patients with liver fibrosis and cirrhosis also had detectable CLEC14A and in some cases at very high levels. This suggested to me there is something about chronic liver disease and HCC microenvironments that promote expression of CLEC14A, for example they both have pathological angiogenesis, areas of low shear stress and are prone to areas of hypoxaemia.

For interest I also looked at TCGA data in other cancers and the effect CLEC14A had on survival, and I found that high expression of CLEC14A in some cancers, for example gastric adenocarcinoma, at the tissue level was associated with a poor outcome; this is the opposite to what the data showed for HCC.

To gain insight into the regulation of CLEC14A I looked at the influence of cytokines and growth factors in HSEC from different donors and the results were inconsistent however in the majority of cases Interferon upregulated CLEC14A and so did BMP9 but this did not reach significance. In response to hypoxaemia CLEC14A was upregulated and MMRN2 down regulated, CD93 was also down regulated which suggests that this angiogenic signature may have a regulatory role. The response to shear stress was that under high shear stress CLEC14A is down regulated and MMRN2 is upregulated. Both hypoxaemia and low shear stress are both features of chronic liver disease and hepatocellular carcinoma.

When exploring the functional role of CLEC14A in HSEC I performed migration and tube formation assays and showed that CLEC14A is important for these processes in keeping with published findings using HUVEC. It was however not known and if CLEC14A promotes the recruitment of leucocytes. I was able to show that low shear stress promotes the adhesion of neutrophils in HSEC and CLEC14A KD reduces neutrophil adhesion. When I looked at some HCC cases with immunohistochemistry, I could find neutrophils localise to areas where there was high CLEC14A expression, but this was not consistent in all cases and there were

cases with high CLEC14A expression and no neutrophils and cases where there were neutrophils but no CLEC14A.

I've shown that PBMCs express MMRN2 by western blotting for MMRN2 but the significance of this is unclear and it is still unknown if neutrophils express MMRN2 at the protein level. I failed to produce monoclonal antibodies that could block the CLEC14A-MMRN2 interaction, and this may be because the antibodies generated were not against the epitope required for this. MMRN2 is a very highly conserved protein between species, and it is likely that areas of high conservation are the ones most functionally significant.

Digital spatial profiling confirmed that there was less CLEC14A at the periphery of tumours and correlation studies showed that CLEC14A correlated with CD34 and CD31 but there was also positive correlation with CD4 and CD8 adding evidence that CLEC14A is involved in the immune landscape in HCC. As expected CLEC14A correlated strongly with genes associated with angiogenesis but also with a neutrophil signature. In CLEC14A high tumours cell abundance scores showed that CLEC14A was associated with natural killer cells which is what I'd also found from TCGA correlations. The clinical data from digital spatial profiling of RNA in tumours confirmed also that CLEC14A was associated with vascular invasion and poorer differentiation of tumours. Pathway analysis revealed that the main biological systems represented in CLEC14A high tumours were the immune system and developmental biology.

9.3 Limitations of studies

Intravital microscopy in murine models would be the next step to look in real time at leucocyte /endothelial interactions. Indeed, this has been done for several decades with inflamed arteries looking at mechanisms of atherosclerosis (Eriksson et al., 2000). The experiments conducted in vitro with endothelial cells, although they are liver sinusoidal cells, they do not reproduce the microenvironment in which leucocytes are recruited via the endothelium in vivo. It has been well documented that there is extensive cross talk that takes place between endothelial cells and other cells found in the liver. For example, the anatomical relationship between Kupffer cells and HSCs which are in close proximity to HSEC is not replicated in my experiments. An experiment using CLEC14A KO mice and a murine model of injury would be interesting to see which immune cell populations are recruited in WT compared to KO.

9.4 Translational aspects of the work

Combination therapies combining immunotherapy with TKIs or VEGF inhibitors to switch cold tumours into hot tumours has already led to increased response rates and improved survival in tumours. If CLEC14A is associated with an abnormal endothelial phenotype, then blockade may promote a 'more normal' phenotype of HSEC. A recent study of CD93 found that CD93 blockade could reduce hypoxia and promote drug delivery by normalising the vasculature (Sun et al., 2021), perhaps CLEC14A blockade could do the same. It has been well described in the literature that hypoxic tumours can be more resistant to cancer therapy and this

raises the question of whether CLEC14A inhibition may sensitise the liver environment to certain cancer treatments like radiotherapy and immunotherapy. The inverse relationship of hypoxia and shear stress to MMRN2 expression was a surprise and is difficult at this point to explain but is noteworthy.

The increased adhesion of neutrophils to HSEC in the presence of CLEC14A is interesting and needs further validation in murine studies to see if the same effect is reproducible. The DSP data also suggest that there may be a link between CLEC14A and natural killer cells.

Thinking more laterally of low flow states in the liver like we see in the portal vein in cirrhosis, if CLEC14A is upregulated it is theoretically possible that CLEC14A may be involved in the development of portal vein thrombosis and this theory should be considered further. It would also be very interesting to see what affect CLEC14A KO has on a liver model of fibrosis.

In summary CLEC14A is clearly an endothelial protein associated with pathological conditions, data suggests it is a key player in low shear stress and hypoxic environments, contributing to pathological angiogenesis and potentially modulating the surrounding immune microenvironment. This makes it a very attractive target for further in vivo studies.

10 APPENDICES

10.1 Appendix 1. Data from volcano plots showing differential gene expression between tumour, non-tumour and peri-tumour regions.

Tumour vs Non Tumour differential gene expression – Upregulated in Tumour
Significance threshold of adjusted P value<0.05.

Target name (T)	Log2	Adjusted pvalue	Target name	Log2	Adjusted pvalue
ABCF1	-0.2123546	1.25E-08	CMTM6	-0.0710807	0.01523041
ACOT12	-0.1459933	0.031622133	COX4I1	-0.3566956	1.19E-10
ACTA2	-0.1557712	0.024717953	COX5B	-0.4453627	9.15E-11
ACVR1B	-0.0943869	9.32E-06	COX6A1	-0.5022117	1.24E-11
ACY1	-0.3341316	2.82E-06	COX6B1	-0.4787075	9.02E-11
AKAP1	-0.2260618	1.39E-11	CPSF7	-0.1623144	1.76E-09
AKR1C4	-0.5570633	6.11E-08	CREB3L3	-0.3488972	5.86E-06
AKT1	-0.2183252	1.25E-09	CRP	-0.6404327	2.07E-06
AKT2	-0.2248929	1.95E-15	CTNNB1	-0.2945791	1.82E-06
ALCAM	-0.080222	0.019023982	CTSH	-0.0751449	0.02581721
ALDOA	-0.264914	0.000156319	CUL1	-0.1405031	3.14E-05
AMBP	-0.657708	0.000991605	CXCL16	-0.0839533	0.03625124
API5	-0.1432659	1.68E-07	CXXC5	-0.0694554	0.00368805
APOA2	-0.9939892	4.40E-05	DAXX	-0.1017531	0.01132722
APOB	-0.4384221	0.022400278	DDIT3	-0.087791	0.00549427
APOC2	-0.9457753	1.67E-05	DGLUCY	-0.0662999	0.00708943
APOL6	-0.1031119	0.043028877	DNAJC14	-0.1029723	0.00359031
APOM	-0.3745605	4.07E-05	DNMT1	-0.1058806	0.00021195
AQP9	-0.4097592	0.011246353	DPP4	-0.1846385	0.00045074
ARNT	-0.1769458	9.25E-11	DSP	-0.2997239	2.72E-11
ASL	-0.1879156	0.038227216	DUSP10	-0.1263921	0.00229469
ATOX1	-0.7067667	1.06E-20	ECSIT	-0.1404769	2.13E-07
ATP2A2	-0.1484894	1.75E-08	EFNA1	-0.2121672	0.00095653
ATP5F1D	-0.3468751	8.18E-09	EGFR	-0.1504754	0.00123075
ATP5ME	-0.242099	7.87E-05	EHHADH	-0.2482675	0.00075107
BAD	-0.08111	0.000169472	EIF4EBP1	-0.1793325	0.00011039
BAP1	-0.1412975	2.19E-07	ELOB	-0.2075103	1.12E-13
BAX	-0.2379307	2.42E-07	ENDOG	-0.1255161	0.0046109
BCL2L1	-0.1522227	0.002148909	EP300	-0.1273426	0.00055776
BRD2	-0.1850031	6.55E-08	ERCC2	-0.1569242	4.84E-05
BRD4	-0.1075929	0.000937646	ERO1A	-0.1029589	1.45E-05
BST2	-0.4227915	9.37E-10	EWSR1	-0.1800842	8.78E-08
C1QBP	-0.1554375	1.01E-06	FEN1	-0.1687329	3.33E-06
C2	-0.5997553	2.27E-07	FGFR4	-0.3930376	1.31E-19
C3	-0.5453799	0.00191728	FH	-0.4166536	4.47E-08
C4B	-0.6719442	3.29E-05	FLNB	-0.1877105	3.85E-08
C4BPA	-0.6323485	0.000264111	FLNC	-0.1906055	0.00596623
C5	-0.2742517	0.004738222	FN1	-0.5227659	8.55E-05
C8G	-0.4671403	7.73E-06	FST	-0.2660314	2.24E-06
CACNA1H	-0.0879697	0.002348399	G6PD	-0.223956	3.83E-05
CCL16	-0.2069621	0.029707337	GNA11	-0.1489152	1.11E-07
CD34	-0.1227461	0.00100118	GNAS	-0.1782871	0.03703263
CD36	-0.1386739	0.006623296	GOT1	-0.1360651	0.03887019
CD46	-0.1172571	0.001946783	GOT2	-0.1607798	0.00410672
CD59	-0.100639	0.020313329	GPI	-0.338785	3.85E-08
CD63	-0.2327442	0.000751074	GPT	-0.2902669	3.29E-07

CD99	-0.1009503	0.015022698	GPX1	-0.2180861	0.00034526
CDC25B	-0.0557716	0.035013591	GPX4	-0.4242543	2.11E-11
CDKN1A	-0.151001	0.000553904	GRB2	-0.1327923	6.75E-07
CEBPA	-0.4159799	2.62E-10	GUSB	-0.1078497	0.00186406
CEBPB	-0.1073578	0.001691483	H2AX	-0.1409788	0.00249215
CFB	-0.6850787	0.000594262	H3-3A	-0.4321917	1.61E-15
CFI	-0.1817559	0.009657658	H3C10	-0.137929	0.01680911
CKLF	-0.0764299	0.031781113	HDAC1	-0.0612196	0.01028194
Target name (T)	Log2	Adjusted pvalue	Target name	Log2	Adjusted pvalue
HDAC3	-0.1533087	1.37E-07	MDM4	-0.0638088	0.03991881
HDAC5	-0.0986186	0.003568314	MEN1	-0.1278855	0.00202885
HHEX	-0.1748426	1.13E-07	MET	-0.1800443	4.26E-05
HLA-A	-0.6872134	3.01E-07	MGMT	-0.1111629	0.00257937
HLA-B	-0.4059101	0.003879378	MIF	-0.4257465	2.63E-10
HLA-C	-0.4402177	5.67E-07	MRM2	-0.0810518	0.01551295
HLA-F	-0.2567318	0.001785255	MRPL19	-0.0836223	0.00612712
HNF1A	-0.2974706	9.63E-12	MSRB2	-0.2828389	5.83E-14
HSD17B8	-0.2555875	1.09E-09	MTOR	-0.1091031	0.00129845
HSP90B1	-0.1914411	0.000498068	NASP	-0.1237984	9.31E-05
HSPA1A	-0.7695658	4.35E-11	NDUFA1	-0.4666146	7.60E-11
HSPB1	-0.7189509	3.65E-12	NDUFA11	-0.2103865	1.75E-06
ICAM1	-0.1038801	0.048897989	NDUFA12	-0.2240246	1.09E-13
ID1	-0.2111645	0.001694403	NDUFA13	-0.530519	1.83E-14
IDH1	-0.3562807	3.45E-06	NDUFA2	-0.0600996	0.04245073
IDH2	-0.2391834	1.55E-06	NDUFA3	-0.4065232	2.88E-14
IFI27	-0.4428082	0.001170141	NDUFA6	-0.20404	1.36E-06
IFI35	-0.0577599	0.027180319	NDUFA7	-0.1055293	5.84E-05
IFITM2	-0.2228009	0.000676773	NDUFB1	-0.3332195	5.53E-09
IGF2R	-0.1767107	2.22E-07	NDUFB10	-0.0518714	0.04575949
IL11RA	-0.1747432	4.63E-08	NDUFB11	-0.218341	3.65E-12
IL13RA1	-0.1489799	0.000477165	NDUFB4	-0.165469	7.15E-08
IL17RB	-0.2498878	6.93E-09	NDUFB7	-0.4400352	1.95E-15
IL32	-0.7194362	9.95E-09	NDUFB8	-0.1650293	7.26E-11
IL6R	-0.2580966	1.71E-08	NDUFS8	-0.2042991	1.27E-08
ILF3	-0.2376575	8.21E-09	NECTIN2	-0.1241209	2.93E-06
INHBB	-0.1128135	0.006195568	NF1	-0.0796016	0.02533359
IRAK1	-0.1174937	0.000264097	NFATC3	-0.1036139	0.04853108
IRF3	-0.08505	0.000320695	NFKB2	-0.0880904	0.04065088
IRS1	-0.1839476	0.000224265	NPM1	-0.1419327	0.0028189
ISG15	-0.2604687	4.50E-05	NR3C1	-0.087293	0.00540845
ITCH	-0.0984309	0.005939514	NRDE2	-0.0694361	0.04329053
ITGB1	-0.2296458	0.001013153	NSD1	-0.0800682	0.0452856
ITPK1	-0.1619119	0.002348399	OAS3	-0.0862842	0.03991881
JUP	-0.1112922	0.000695869	OASL	-0.2214802	0.00409625
KMT2C	-0.1043134	0.001743619	OAT	-0.2371437	0.00107481
KRT10	-0.0644349	0.01705934	OAZ1	-0.3626636	5.09E-07
KRT18	-0.2721368	0.005626977	OPN3	-0.2363436	2.38E-12
KRT5	-0.1899267	0.009703219	OTC	-0.2833945	0.00220995
LAMP1	-0.3570762	1.44E-11	P4HA2	-0.1564853	4.77E-05
LBP	-0.4017978	9.26E-05	PALMD	-0.1086698	0.02948663
LCN2	-0.3202159	0.002232801	PARP9	-0.1714009	2.66E-07
LEPR	-0.181991	0.006452084	PC	-0.1312629	0.01771787
LRP5	-0.1346313	1.27E-05	PEBP1	-0.4544697	0.00034212
MAP2K2	-0.1740674	1.83E-07	PGPEP1	-0.152977	3.18E-06
MAP3K13	-0.1855426	8.16E-05	PIK3R2	-0.3003085	6.25E-13
MAP3K14	-0.0969708	0.020483171	PLA2G2A	-0.2284925	0.01124111
MAPK14	-0.0936408	0.001338997	POLR2A	-0.0938401	0.03711421
MAPKAPK2	-0.1576622	8.12E-06	PPP2R1A	-0.1263187	6.61E-05
MAVS	-0.0674417	0.002109593	PRDX5	-0.1712932	1.89E-06
MBNL3	-0.1346815	0.001884154	PRKACA	-0.1632246	3.28E-07
MCM5	-0.1665831	1.55E-10	PRKAR2A	-0.0648833	0.03569009
MCM7	-0.2039012	5.04E-12	PRKDC	-0.2267911	3.86E-11

MDM2	-0.0811632	0.005948369	PSAT1	-0.1014103	0.04210548

Target name (T)	Log2	Adjusted pvalue	Target name	Log2	Adjusted pvalue
PSEN1	-0.1054131	3.51E-05	SRSF2	-0.1686474	3.48E-06
PSMB5	-0.3040947	1.95E-15	SSX1	-0.5872372	0.00012973
PSMB7	-0.1961915	2.72E-10	ST6GAL1	-0.2361281	0.00319864
PSMB9	-0.1679126	0.000921822	STAT3	-0.1208216	0.00121438
PSMC4	-0.155551	9.69E-10	STK11	-0.1931221	1.40E-12
PSMD7	-0.1298983	2.04E-06	SYT17	-0.1132532	0.0020557
PTPN11	-0.1583485	1.47E-07	TAB1	-0.0990623	0.00515115
PVR	-0.29258	3.04E-11	TAP1	-0.1919182	5.22E-06
RAB7A	-0.1239677	0.000196829	TAP2	-0.1353237	0.00019291
RAC1	-0.104099	1.16E-06	TAPBP	-0.2732168	1.92E-16
RAC3	-0.1197905	0.01050398	TAPBPL	-0.0649727	0.02773961
RAD21	-0.1693428	1.10E-09	TECR	-0.2847839	7.38E-14
RBP4	-0.6903516	0.003611591	TFDP1	-0.1320243	5.99E-05
RBX1	-0.134927	2.17E-07	TFE3	-0.087561	0.00128943
RELA	-0.1351445	8.78E-08	TFRC	-0.1414603	1.93E-05
RFC3	-0.1302642	0.001133226	TMEM45B	-0.2459192	5.20E-07
RHOA	-0.085388	0.00103853	TNFRSF12A	-0.1744667	0.00514344
RNF43	-0.2118795	0.000930037	TOLLIP	-0.1691667	9.27E-07
RNLS	-0.1115537	0.025626423	TPM1	-0.1908239	0.01410538
RORC	-0.26031	1.19E-10	TPR	-0.0666326	0.02761936
RPL23	-0.3024837	0.003802446	TPTE	-0.1243569	0.04437466
RPL7A	-0.3164457	0.001869563	TRAF7	-0.1519932	8.05E-10
RPS27A	-0.2196082	0.000564179	TTPA	-0.2171727	0.00023035
RPTOR	-0.0715313	0.028335992	TUBB	-0.5369272	1.95E-15
RRM2	-0.1770504	2.76E-05	TXN2	-0.1548511	4.78E-06
SAA1	-0.5383432	0.007411659	TYMP	-0.1722596	0.00201388
SDHA	-0.1240273	0.008691336	TYMS	-0.2321108	6.52E-08
SERINC2	-0.1047815	0.009428644	U2AF1	-0.076665	0.00890114
SERINC5	-0.2486999	1.41E-11	UBB	-0.1543217	0.0309266
SERPINA1	-0.3170719	0.040433391	UBC	-0.2017949	0.03562203
SERPINH1	-0.0725433	0.018041872	UBE2C	-0.194501	6.12E-06
SF3A1	-0.0840746	0.000897689	UQCR10	-0.1478297	6.24E-10
SFN	-0.1500647	0.005387342	UQCRQ	-0.447987	1.84E-12
SFXN1	-0.205004	3.48E-06	VEGFA	-0.1281008	0.00141943
SGK2	-0.1347996	0.001530881			
SHC1	-0.3009983	9.10E-19			
SHC2	-0.1933364	7.69E-10			
SKP2	-0.1427432	3.99E-06			
SLC16A1	-0.2571754	2.56E-05			
SLC25A1	-0.4482853	2.43E-15			
SLC39A6	-0.0837152	0.047160966			
SMAD4	-0.0769837	0.020204433			
SMARCA4	-0.1985737	4.88E-09			
SMARCB1	-0.1546807	1.08E-08			
SMC1A	-0.1340567	6.45E-07			
SMO	-0.1734661	1.56E-07			
SOD1	-0.6153034	1.69E-07			
SOD2	-0.7188646	4.05E-08			
SOX9	-0.1367758	0.011327221			
SP1	-0.0753771	0.030926595			
SPINK1	-0.7733455	6.64E-09			
SPOP	-0.1186914	2.61E-05			
SPP1	-1.0178216	7.64E-06			
SRP54	-0.0512002	0.023606769			

Tumour vs Non Tumour differential gene expression – Upregulated in Non-Tumour
Significance threshold of adjusted P value<0.05.

Target name	Log2	Adjusted pvalue	Target name	Log2	Adjusted pvalue
A2M	0.77757658	0.00047906	CXCL14	0.09644504	0.00684451
ABL1	0.17348729	3.85E-08	CXCL2	0.60584782	6.24E-10
ACTR3B	0.15679908	6.24E-05	CXCR3	0.33950864	1.55E-12
ADGRE5	0.21904277	9.17E-08	CXCR4	0.32269462	2.76E-07
ADH4	0.37313226	0.03887019	CYFIP2	0.08080852	0.02533359
ADM	0.23896576	3.85E-10	DDIT4	0.20613429	0.0005539
AMH	0.4412259	8.63E-13	DIPK2B	0.07026924	0.0275935
ANXA1	0.15027265	0.00014349	DLL1	0.12822524	5.34E-05
ATF3	0.13027209	0.00616612	DLL4	0.11001465	0.00063417
ATM	0.06535047	0.0313087	DUSP1	0.60755251	8.60E-12
AXL	0.16724458	1.25E-06	DUSP5	0.12021277	0.00091389
BAIAP3	0.13027261	0.00016753	DUSP6	0.12066394	0.00416035
BCL2	0.10066102	0.00076989	E2F4	0.05421008	0.0199547
BMP5	0.06234016	0.02691273	EFNA2	0.22442878	2.00E-07
BNIP3L	0.14213117	3.93E-06	EFNA3	0.19818009	2.25E-06
C1QA	0.30650139	2.35E-07	EGR1	0.76047331	6.82E-10
C1QB	0.20670955	9.99E-05	EGR2	0.13252662	0.00015456
C1R	0.38936201	0.01975041	ELANE	0.11608241	0.00756757
C7	0.81438768	5.19E-10	ELK1	0.14307915	1.32E-06
C9	0.43070448	0.01127121	ENG	0.30258557	0.00014349
CACNA2D1	0.08439742	0.00110106	ETS2	0.13386941	0.04689295
CALML3	0.2588997	1.33E-06	FBP1	0.41131899	0.00869616
CCL15	0.24123492	0.00073452	FCER1G	0.13291011	0.0008531
CCL18	0.59096827	8.85E-13	FCGRT	0.15146275	0.00201335
CCL19	0.37860876	1.82E-06	FGCR2A/B	0.096948	0.00396199
CCL2	0.08209065	0.04896071	FGF17	0.21289453	3.82E-05
CCL21	0.54958386	9.17E-12	FGF22	0.07924405	0.02732587
CCL25	0.26912687	4.30E-09	FGF8	0.09663702	0.01327161
CCL3/L1	0.45581027	1.37E-15	FGFR1	0.07164507	0.00869408
CCL4	0.1484503	2.42E-05	FOS	1.06182972	1.31E-19
CCL5	0.14715786	1.69E-05	FOXA2	0.43562358	1.67E-12
CCND1	0.13896023	0.00075107	FSTL3	0.26201864	6.03E-07
CCR7	0.25457527	2.76E-11	FYN	0.09556787	0.00025771
CD163	0.26585072	3.36E-10	FZD1	0.27459665	4.71E-14
CD37	0.15205772	0.00018351	GADD45B	0.27847902	7.79E-05
CD4	0.29819192	2.90E-11	GAS1	0.19139027	3.62E-07
CD44	0.30071956	3.85E-08	GIMAP4	0.08958402	0.00143286
CD48	0.10704638	0.0002012	GLI1	0.20371023	1.47E-07
CD53	0.17183845	9.05E-06	GRIN1	0.33925638	6.20E-11
CD74	0.62435178	0.00073522	HAMP	0.84076701	3.85E-08
CD79A	0.25193313	4.53E-11	HES1	0.07855377	0.03551393
CD81	0.20755945	0.00169148	HGF	0.16477977	2.02E-05
CD8A	0.27837454	7.60E-11	HK1	0.05713352	0.03781574
CD9	0.05771122	0.01582836	HLA-DMA	0.1096064	0.01735825
CDKN1C	0.29521952	8.59E-11	HLA-DOA	0.07337081	0.01198286
CHIT1	0.0762668	0.01719955	HLA-DPA1	0.22477768	3.27E-05
COL3A1	0.32707862	0.03185802	HLA-DQA1	0.14553188	2.19E-05
CREB5	0.1501645	1.00E-05	HLA-DQB1	0.07514598	0.00269456
CSF1	0.33954278	1.95E-15	HLA-DRA	0.51946327	5.30E-06
CSF1R	0.16664129	4.21E-05	HLA-DRB	0.42588268	0.00034526
CT45A1	0.12105055	0.00192228	HLA-DRB3	0.25544113	0.00061376
CTAG1B	0.33078868	2.36E-10	HLA-DRB4	0.30116612	0.0001549
CXCL1	0.42668432	8.04E-13	HLA-G	0.0860072	0.00544927
CXCL12	0.56173063	7.38E-14	HMGA1	0.52320571	2.45E-12

Target name	Log2	Adjusted pvalue	Target name	Log2	Adjusted pvalue
HOXA9	0.28106797	1.32E-09	NEIL1	0.10729289	0.00036901
ICAM2	0.25430659	9.36E-11	NGF	0.13068951	0.00593805
ID2	0.24183723	0.00011989	NGFR	0.16369379	4.55E-06
IFITM1	0.32005792	1.44E-11	NOS2	0.14447335	0.00014071
IFNL2	0.14653198	7.79E-05	NR4A1	0.55588866	1.34E-16
IGFBP3	0.71105745	6.36E-15	NUMBL	0.29062211	2.36E-10
IKBKB	0.07015051	0.00149742	NUPR1	0.86154637	9.47E-15
IKBKG	0.0936193	0.00810635	OAS1	0.10070311	0.00206434
IL10RA	0.18369244	5.31E-07	OAS2	0.11680537	0.00026141
IL1R1	0.14897358	5.13E-07	PCK1	0.60453728	0.01804187
IL1RAP	0.13420533	0.00016806	PDCD1	0.25091436	2.83E-08
IL2RA	0.16548448	4.88E-06	PDGFRA	0.24026017	5.45E-08
IL2RB	0.2041643	5.85E-08	PDGFRB	0.14878658	0.01260935
IL7R	0.2005986	4.08E-05	PDZK1IP1	0.23812595	0.00043564
INPP5D	0.06592417	0.00996912	PIK3CD	0.06987497	0.01999478
IRF7	0.16319739	0.0001055	PLAT	0.2425117	2.19E-08
IRF8	0.17590613	6.16E-06	PML	0.14697417	3.14E-06
ITGA3	0.20246843	2.50E-09	POU2AF1	0.30188407	4.86E-14
ITGA9	0.20465188	3.85E-08	PTCRA	0.12059579	0.00288783
ITGAX	0.05945676	0.01726379	PTPRC	0.15939927	2.73E-05
ITGB2	0.15550688	4.30E-05	RAC2	0.26276177	1.37E-10
ITGB4	0.08865234	0.00446242	RASA4	0.07288042	0.00437976
JAG1	0.10350417	0.00094684	RBL2	0.06930536	0.00344873
JAK3	0.09030099	0.00063435	RELB	0.22165662	2.24E-09
JAML	0.12821223	9.96E-05	REN	0.07336958	0.03178111
JUN	0.22352772	6.39E-06	RET	0.24515903	4.30E-08
JUNB	0.37331574	3.86E-11	RHOB	0.16364032	0.02907574
KLF4	0.60804226	1.31E-19	RIN1	0.41061256	2.21E-12
KRT14	0.41096632	7.12E-13	RRAD	0.16097317	3.68E-05
KRT7	0.60832114	1.95E-15	RUNX1T1	0.05145649	0.04499987
LAMC3	0.16311796	3.82E-06	SGK1	0.11493509	0.00191728
LCK	0.23243179	8.78E-11	SH2B2	0.09858754	0.0033553
LCP1	0.10502555	0.00287572	SIGIRR	0.11714409	6.31E-05
LDHB	0.10817643	0.00063315	SMAD9	0.24968543	1.50E-08
LGALS3	0.11874322	0.0001957	SMPD3	0.31691724	2.36E-10
LILRB2	0.09657333	0.03016636	SOCS1	0.17862292	1.93E-06
LTB	0.13392487	1.12E-05	SPIB	0.0991151	0.00258066
LTBP1	0.07024276	0.00300483	SPRED1	0.09559805	0.00016947
LTBR	0.09795919	0.00309064	SPRY2	0.07000164	0.00773835
LY6E	0.62463944	1.88E-12	STING1	0.21086679	6.24E-10
LY86	0.12905801	0.00036901	STK11IP	0.19344824	2.35E-06
MAF	0.07675864	0.00029377	TDO2	0.25821481	0.02777327
MAGEA1	0.10969963	0.00588019	TGFB1	0.23910114	7.60E-10
MAGEA3/A6	0.17421782	1.75E-05	TGFBR2	0.0835461	0.00637107
MAGEA4	0.17806281	0.00047906	THBS1	0.42833447	1.82E-05
MARCO	0.35622217	1.25E-09	TIE1	0.09167477	0.00091258
MBNL1	0.34448947	1.95E-15	TNF	0.16420833	0.0008531
MCL1	0.16608432	0.00262704	TNFRSF1B	0.09008545	0.00093004
MFNG	0.09483154	0.0003411	TNFSF12	0.37588568	1.02E-13
MMP7	0.20906357	0.00045738	TNFSF13	0.25184823	6.55E-09
MNX1	0.23119539	2.59E-06	TNKS	0.05423989	0.03421988
MRC1	0.22614422	5.76E-09	TPI1	0.14673245	2.49E-05
MS4A6A	0.2676247	2.72E-11	TRAC	0.22604731	3.12E-08
NAT8L	0.14891303	0.00021227	TRBC1/2	0.43599871	9.63E-12

Target name	Log2	Adjusted pvalue
TRIM21	0.14378962	1.29E-05
TSC1	0.07201349	0.00346958
TSLP	0.16931387	0.00198965
TSPAN7	0.0989328	0.00071838
TXNIP	0.30680451	5.41E-06
UBA7	0.09778513	5.20E-06
VCAM1	0.12700528	3.51E-05
VCAN	0.1072386	0.00201388
VSIR	0.20950861	3.70E-09
WIPF1	0.23335741	3.29E-10
WNT6	0.26354004	1.57E-09
XCR1	0.49428847	2.63E-13
ZEB2	0.16420097	1.01E-06

Tumour vs Peri-tumoural differential gene expression. Upregulated in Tumour
Significance threshold of adjusted P value<0.05.

Target name	Log2	Adjusted pvalue	Target name	Log2	Adjusted pvalue
ABCB1	-0.1173719	0.03905037	CACNA1H	-0.0714871	0.00716578
ABCF1	-0.1277041	3.86E-05	CCL16	-0.4865888	1.41E-07
ACOT12	-0.3473372	8.66E-08	CD36	-0.1876154	3.92E-05
ACVR1B	-0.103028	4.09E-05	CD46	-0.1687634	1.01E-07
ACY1	-0.7335262	1.86E-19	CDH1	-0.1613081	0.00407855
ADH1A/B/C	-1.0781705	1.81E-05	CDKN1A	-0.2351858	5.18E-05
ADH4	-0.5447573	0.00945214	CEBPA	-0.5517756	1.35E-12
ADH6	-0.4320776	4.44E-09	CEBPB	-0.1870519	2.26E-06
AKAP1	-0.3214071	2.12E-15	CFB	-1.9238751	1.13E-12
AKR1C4	-1.024767	5.00E-16	CFI	-0.6088105	1.60E-10
AKT1	-0.2503078	1.91E-11	CLU	-1.4343173	8.66E-10
AKT2	-0.2552911	1.63E-15	CMTM6	-0.1340398	2.36E-05
ALCAM	-0.1140005	9.67E-05	COX4I1	-0.4246336	8.50E-12
ALDOC	-0.1122153	0.00418517	COX5B	-0.7245912	1.02E-20
AMBP	-2.2938841	2.74E-15	COX6A1	-0.7785623	3.32E-16
ANGPTL4	-0.3361739	5.86E-07	COX6B1	-0.6192556	1.19E-12
API5	-0.1424129	1.81E-06	CPSF7	-0.123019	1.29E-06
APOA1	-1.7958885	2.65E-07	CREB3L3	-0.6308135	2.52E-12
APOA2	-2.7789194	3.21E-16	CRP	-1.1777159	3.59E-09
APOB	-1.8123245	8.73E-13	CTNNB1	-0.2375424	0.00059095
APOC2	-2.4513166	1.65E-15	CTSL	-0.1729964	9.76E-08
APOC3	-1.7504554	3.95E-10	CUL1	-0.138097	9.65E-06
APOL6	-0.195547	0.00011136	CXXC5	-0.1812792	1.17E-09
APOM	-0.8858337	1.24E-12	CYP4A11/22	-0.9040756	3.33E-07
AQP9	-0.8865325	3.37E-08	CYP8B1	-0.5797195	2.62E-06
AR	-0.2669005	9.66E-10	DDIT3	-0.0828797	0.00011563
ARG1	-0.8111927	3.21E-09	DNAJC14	-0.0492864	0.0244726
ARNT	-0.1423133	2.38E-08	DNMT1	-0.066067	0.01324295
ASL	-0.7552814	7.19E-12	DPP4	-0.2434801	1.43E-07
ASPG	-0.2564604	2.35E-06	DSP	-0.3548952	2.69E-13
ATF1	-0.0805189	0.01189035	DUSP10	-0.2566797	1.77E-08
ATF2	-0.0585571	0.02626194	ECSIT	-0.1372766	7.28E-09
ATOX1	-0.8559772	4.29E-22	EFNA1	-0.4642817	2.00E-09
ATP2A2	-0.1489769	8.27E-06	EGFR	-0.3485042	1.03E-07

ATP5F1D	-0.5024487	1.78E-12	EHHADH	-0.5728328	4.44E-12
ATP5ME	-0.4657454	1.64E-09	EIF4EBP1	-0.1738174	1.00E-05
BAD	-0.0869314	8.55E-05	ELOB	-0.2395598	7.51E-13
BAP1	-0.1350248	3.13E-08	ENDOG	-0.1548957	0.00022587
BAX	-0.1428244	0.00392253	EP300	-0.0743779	0.02998241
BRD2	-0.1338689	0.00033509	ERCC2	-0.1206563	0.00023086
BRD4	-0.0998063	0.00509423	ERO1A	-0.1056021	3.92E-06
BST2	-0.4031403	4.23E-08	EWSR1	-0.1221066	0.00702164
C1QBP	-0.2619784	8.21E-11	F12	-0.8522392	3.79E-11
C1S	-0.5425155	0.00365922	FBP1	-0.4108392	0.00143768
C2	-1.06577	1.44E-14	FEN1	-0.0910388	0.00080734
C3	-1.8182559	2.43E-13	FGFR4	-0.4008436	2.29E-15
C4B	-1.7125376	4.44E-15	FH	-0.7221537	2.41E-16
C4BPA	-1.4579071	6.24E-13	FLNB	-0.2229978	1.79E-08
C5	-0.8219722	2.90E-10	FLNC	-0.164957	0.00573266
C6	-0.5923542	4.91E-07	FN1	-1.3473531	2.81E-12
C8A	-0.6054425	5.93E-07	FST	-0.537009	5.26E-13
C8B	-0.8926688	5.88E-11	G6PD	-0.1224128	0.02965216
C8G	-1.0720902	2.04E-14	GADD45A	-0.2484239	2.15E-06
C9	-0.3439181	0.04826461	GADD45G	-0.2656551	3.62E-05

Target name	Log2	Adjusted pvalue	Target name	Log2	Adjusted pvalue
GDF15	-0.1557676	3.83E-05	MAPK14	-0.118993	3.41E-05
GHR	-0.1710167	0.00380347	MASP1	-0.1980073	1.73E-06
GLUD1	-0.1777835	9.16E-05	MASP2	-0.1654981	1.06E-05
GNA11	-0.0707625	0.01000494	MAVS	-0.0355612	0.03477421
GOT1	-0.6552905	1.05E-09	MBL2	-0.3105338	0.00030338
GOT2	-0.5785826	8.80E-12	MBNL3	-0.2798049	1.81E-09
GPI	-0.4886492	5.02E-11	MCM4	-0.1035204	0.00720963
GPT	-0.5441785	6.61E-16	MCM5	-0.1123497	8.08E-07
GPX1	-0.2630627	0.00229948	MCM7	-0.1032742	3.69E-05
GPX4	-0.6694554	2.99E-17	MDM2	-0.1662232	7.67E-06
GRB2	-0.083448	0.00057362	MEN1	-0.0678695	0.02007124
GUSB	-0.2302019	5.63E-08	MERTK	-0.1146396	0.03618579
H3-3A	-0.3342798	3.95E-07	MET	-0.2331928	1.91E-06
H3C2	-0.0715763	0.02669594	MGMT	-0.2973325	4.91E-13
HDAC3	-0.140561	1.42E-08	MIB1	-0.0637923	0.01236383
HDAC6	-0.1580499	2.53E-06	MICA	-0.0860678	0.00681287
HHEX	-0.1970605	2.37E-09	MIF	-0.4279853	1.50E-07
HLA-C	-0.2709535	0.04601701	MRM2	-0.0895186	0.00057671
HNF1A	-0.3010168	6.65E-11	MRPL19	-0.1652795	4.58E-09
HSD11B1	-0.5977952	4.39E-05	MSRB2	-0.3746126	5.14E-19
HSD17B8	-0.3548614	1.56E-15	MTOR	-0.1042747	0.00218317
HSP90B1	-0.2627992	7.91E-05	MXI1	-0.0534261	0.03848582
HSPA1A	-0.7077845	1.72E-08	NASP	-0.1051199	0.00038549
HSPB1	-0.5234486	1.61E-05	NDUFA1	-0.649998	2.02E-15
ID1	-0.1105798	0.04097192	NDUFA11	-0.2447477	1.01E-07
IDH1	-0.6207869	6.18E-13	NDUFA12	-0.2711104	7.95E-15
IDH2	-0.433198	1.41E-10	NDUFA13	-0.6001245	2.24E-15
IFI27	-0.5651059	0.00010025	NDUFA2	-0.1428844	0.00015207
IFI35	-0.0363006	0.04467798	NDUFA3	-0.267185	1.75E-08
IFITM2	-0.2402024	0.01443936	NDUFA6	-0.1944383	5.81E-07
IGF2R	-0.2394795	2.57E-08	NDUFA7	-0.0997953	0.00016051
IL11RA	-0.1416316	7.77E-06	NDUFB1	-0.4923415	4.52E-14
IL13RA1	-0.2681558	2.21E-10	NDUFB10	-0.1522158	7.56E-06
IL17RB	-0.3626721	7.33E-14	NDUFB11	-0.2798108	7.59E-16
IL1RN	-0.1253517	0.00110585	NDUFB4	-0.2154054	6.79E-09
IL32	-0.8088145	1.82E-07	NDUFB7	-0.4441545	7.10E-18
IL6R	-0.359263	9.95E-14	NDUFB8	-0.1423192	2.79E-09
ILF3	-0.1072306	0.02870621	NDUFS7	-0.1128117	2.10E-05
INHBB	-0.062984	0.02160525	NDUFS8	-0.2374827	1.78E-09
IRS1	-0.2132369	3.56E-05	NECTIN2	-0.1936154	6.07E-09

ISG15	-0.3569156	2.43E-05	NF1	-0.0634649	0.01645615
ITCH	-0.1127117	0.00012613	NFE2L2	-0.080832	0.03198878
ITPK1	-0.1754682	7.64E-05	NRDE2	-0.0734511	0.00110243
JUP	-0.0903591	0.03758496	NSD1	-0.0587481	0.04892766
KRT10	-0.0625719	0.00054049	NT5E	-0.1523382	0.00166421
KRT18	-0.530503	8.00E-06	OASL	-0.2469699	0.00066983
LAMP1	-0.4969909	6.09E-16	OAT	-0.2434377	0.00114983
LBP	-0.984653	8.21E-11	OAZ1	-0.3098287	0.00056074
LCN2	-0.2845297	0.03000601	OPN3	-0.2042093	2.57E-10
LEPR	-0.4631538	1.19E-08	OTC	-0.6118081	5.15E-11
LRP1	-0.2107201	0.04432225	P4HA1	-0.1813458	5.94E-05
LRP5	-0.2007755	1.41E-11	P4HA2	-0.0719318	0.03890162
MAP2K2	-0.1234009	0.0004479	PALMD	-0.1893695	1.70E-05
MAP3K13	-0.1868457	2.35E-06	PARP4	-0.059162	0.0422374

Target name	Log2	Adjusted pvalue	Target name	Log2	Adjusted pvalue
PARP9	-0.2227626	1.66E-09	SLC16A1	-0.3412633	2.37E-07
PC	-0.4203292	2.85E-13	SLC16A2	-0.1450806	0.00032204
PCK1	-0.7853037	0.00052488	SLC25A1	-0.5584994	1.23E-19
PCK2	-0.7883797	2.95E-12	SLC39A6	-0.0741109	0.01150916
PEBP1	-1.2672214	1.13E-17	SMAD4	-0.0681695	0.00553367
PGPEP1	-0.2079678	7.54E-11	SMARCA4	-0.0933726	0.00598519
PHGDH	-0.1873447	3.33E-05	SMARCB1	-0.0941617	0.00041653
PIK3R1	-0.1652546	6.64E-08	SMC1A	-0.1022364	8.03E-05
PIK3R2	-0.2412848	3.83E-09	SMO	-0.1761042	2.85E-06
PLA2G2A	-0.5670212	5.08E-05	SOD1	-1.3697795	1.83E-19
PLOD2	-0.1422611	3.40E-06	SOD2	-0.922486	8.56E-08
PPARGC1A	-0.1666052	0.00086766	SPINK1	-0.7391806	2.54E-07
PPP3R1	-0.0581751	0.00578379	SPOP	-0.0901132	0.00315796
PRC1	-0.0625014	0.04448585	SREBF1	-0.2227187	5.89E-09
PRDX5	-0.2710987	8.28E-11	SRP54	-0.1400773	6.70E-09
PRKACA	-0.2444992	1.61E-12	SRSF2	-0.1225619	0.00071526
PRKAR1B	-0.0686344	0.02007545	ST6GAL1	-0.5875618	1.25E-08
PRKAR2A	-0.0568387	0.00359971	STAT3	-0.1981495	2.96E-05
PRKCA	-0.0731193	0.02873718	STK11	-0.1364964	1.07E-07
PRKDC	-0.2030091	2.65E-09	SYT17	-0.1585825	6.62E-06
PSAT1	-0.2437586	7.59E-06	TAB1	-0.0774855	0.00385855
PSMB2	-0.038114	0.01340648	TAP2	-0.1110945	0.00110585
PSMB5	-0.3405226	1.39E-14	TAPBP	-0.1406328	0.00022291
PSMB7	-0.2655549	8.13E-13	TAPBPL	-0.0793746	0.00604172
PSMC4	-0.1802801	1.56E-13	TDO2	-0.2450392	0.02361265
PSMD7	-0.14869	4.33E-07	TECR	-0.2869085	6.91E-12
PTPN11	-0.125465	9.60E-05	TFDP1	-0.0675244	0.02557519
PVR	-0.2902122	1.91E-11	TFRC	-0.2333759	5.35E-10
RAB7A	-0.153872	5.22E-05	TIAM1	-0.0618559	0.01197005
RAC1	-0.094628	0.0006201	TMEM45B	-0.3141364	6.41E-09
RAC3	-0.1223574	6.65E-05	TNFSF14	-0.1272603	0.02870666
RAD21	-0.1851137	1.13E-12	TOLLIP	-0.2098506	6.05E-10
RAF1	-0.0799085	0.00035196	TPR	-0.0517638	0.02216114
RBP4	-2.5177388	2.73E-14	TRAF7	-0.1624607	8.75E-07
RBX1	-0.0935234	0.0004479	TTPA	-0.3934726	1.67E-10
RELN	-0.1104967	0.04396865	TTR	-1.7792233	5.46E-10
RFC3	-0.0863593	0.00451	TUBB	-0.4531276	1.77E-10
RNF43	-0.2088723	0.00051407	TXN2	-0.2090258	8.13E-09
RORA	-0.1470817	0.00547169	TYMS	-0.2391587	2.98E-07
RORC	-0.3951079	2.52E-15	UBB	-0.4995536	1.28E-09
RRM2	-0.1706697	7.65E-07	UBE2C	-0.1714635	0.00181057
SAA1	-1.0462939	0.00021486	UQCR10	-0.24607	1.42E-16
SDHA	-0.3229284	2.55E-08	UQCRQ	-0.7801914	1.65E-22
SERINC2	-0.2060784	5.96E-06	VEGFA	-0.2463884	1.48E-06
SERINC3	-0.0794272	0.00163181			
SERINC5	-0.2674444	2.79E-11			

SERPINA1	-2.1582495	2.57E-10
SERPING1	-0.9684925	2.27E-07
SFN	-0.1270545	0.00410873
SFXN1	-0.4108926	3.32E-17
SGK2	-0.2780251	3.85E-08
SHC1	-0.1918264	7.66E-08
SHC2	-0.2336515	1.41E-10
SKP2	-0.1567012	9.79E-08

Tumour vs Peri-tumour differential gene expression. Upregulated in Peri-tumour
Significance threshold of adjusted P value<0.05.

Target name	Log2	Adjusted pvalue	Target name	Log2	Adjusted pvalue
ABL1	0.23115048	9.29E-12	COL1A2	0.58534478	1.19E-10
ACTA2	0.51217283	3.00E-09	COL3A1	0.95601254	2.75E-12
ACTB	0.15221223	0.00105334	COL5A1	0.45427685	7.82E-10
ACTR3B	0.15613732	0.00268699	COL6A3	0.55085817	7.33E-10
ADGRE5	0.40038667	4.16E-14	CREB5	0.2054004	3.21E-06
ADM	0.21809974	2.56E-06	CSF1	0.38309972	1.25E-17
AMH	0.42893964	1.93E-11	CSF1R	0.33127826	2.28E-11
ANXA1	0.36024348	2.15E-12	CT45A1	0.23316374	0.00025447
APP	0.12585476	0.03890162	CTAG1B	0.33008243	2.70E-08
ASNS	0.10507639	0.04459217	CTSS	0.08629106	0.01722664
ATF3	0.20310733	2.57E-06	CXCL1	0.4109478	2.94E-11
ATM	0.15299592	1.42E-05	CXCL12	0.62517573	4.09E-14
ATRX	0.08716058	0.00602591	CXCL14	0.11383214	0.02160525
AXL	0.2385453	1.26E-08	CXCL2	0.19499759	0.04616441
BCL2	0.23036245	4.24E-08	CXCR3	0.31155708	9.39E-09
BNIP3L	0.16196814	2.06E-06	CXCR4	0.63556037	9.14E-16
C1QA	0.46907138	4.16E-14	DAB2	0.10527075	0.00124533
C1QB	0.29694047	1.45E-10	DDIT4	0.31903946	1.54E-08
C7	1.14979872	6.11E-15	DIPK2B	0.12407187	0.01443835
CACNA2D1	0.11656726	0.0039703	DLL1	0.15870803	4.22E-05
CALML3	0.26733471	2.99E-05	DLL4	0.1619806	0.00016897
CAPN2	0.07937767	0.01130954	DTX3	0.14117155	0.00098908
CASP1	0.15166325	1.19E-06	DUSP1	0.40233637	2.02E-09
CCL15	0.24342376	0.00400257	DUSP5	0.17104355	0.00038549
CCL18	0.62099128	9.14E-14	E2F4	0.09955513	0.0016108
CCL19	0.76018225	5.98E-11	EFNA2	0.19989083	0.0001592
CCL2	0.54520349	1.34E-09	EFNA3	0.18092925	0.00085254
CCL21	0.93265253	2.83E-15	EGR1	0.59588743	7.66E-08
CCL25	0.24195279	3.01E-06	EGR2	0.10311487	0.00953001
CCL3/L1	0.43415354	4.33E-12	ELANE	0.10665986	0.04951462
CCL4	0.23866618	5.02E-08	ELK1	0.12157892	0.00157419
CCL5	0.30386119	3.83E-09	ENG	0.54509184	1.74E-10
CCR7	0.31439216	7.69E-12	ETS1	0.17194876	8.82E-06
CD163	0.26808098	6.23E-10	FCER1G	0.18811941	9.98E-05
CD24	0.15677573	0.00447361	FCGR3A/B	0.08829629	0.03697654
CD37	0.38043962	5.80E-11	FGCR2A/B	0.35055296	1.16E-10
CD3D	0.1223006	0.00214156	FGF17	0.24008195	2.56E-05
CD4	0.34228469	2.66E-13	FGFR1	0.22190142	8.20E-08
CD44	0.55498283	2.99E-14	FGFR2	0.1498753	0.00114983
CD47	0.08053273	0.00788753	FLNA	0.5750603	7.24E-13
CD48	0.2219534	1.65E-07	FOS	0.96428739	1.46E-18
CD53	0.38117093	7.35E-15	FOXA2	0.37405167	1.03E-09
CD59	0.07967084	0.00077945	FSTL3	0.43107274	1.52E-13
CD68	0.10885816	6.03E-05	FUBP1	0.05276035	0.0353133
CD74	1.22744615	1.88E-13	FYN	0.1680184	4.32E-06
CD79A	0.36835265	1.32E-11	FZD1	0.32945384	1.44E-14

CD81	0.1346178	0.00051266	GAS1	0.35086276	4.01E-12
CD8A	0.32021619	3.23E-10	GIMAP4	0.18134023	8.76E-05
CD9	0.19154555	4.63E-09	GLI1	0.23783448	4.91E-07
CDKN1B	0.11301301	7.04E-06	GRIN1	0.32484037	1.21E-08
CDKN1C	0.29824087	2.51E-08	HAMP	0.45108637	0.00073788
CLEC14A	0.10077005	0.01000494	HGF	0.21869732	4.50E-07
CMKLR1	0.12096899	0.00672018	HK1	0.23361912	1.54E-08
COL1A1	0.79165129	2.09E-09	HLA-DMA	0.32463627	4.12E-09

Target name	Log2	Adjusted pvalue	Target name	Log2	Adjusted pvalue
HLA-DMB	0.24448229	2.21E-08	LTB	0.25261461	4.24E-08
HLA-DOA	0.14146071	0.00014138	LTBP1	0.19031216	6.41E-09
HLA-DPA1	0.47787252	1.89E-14	LY6E	0.24181446	1.41E-05
HLA-DQA1	0.24915869	4.14E-10	LY86	0.14933974	0.00094841
HLA-DQB1	0.17219791	2.14E-05	LYZ	0.2665096	0.00255448
HLA-DRA	0.97514897	4.85E-15	MAF	0.04048762	0.04803761
HLA-DRB	0.94805802	1.23E-13	MAGEA3/A6	0.14996107	0.01443835
HLA-DRB3	0.61346223	3.87E-09	MAP3K1	0.08141153	0.00411086
HLA-DRB4	0.5880099	2.95E-09	MAP3K12	0.12214684	0.00605901
HLA-E	0.26852667	1.25E-06	MARCO	0.1434706	0.02249512
HLA-G	0.16675354	0.00026257	MBNL1	0.38452101	1.78E-18
HMGA1	0.50376843	1.96E-11	MCAM	0.15779127	3.25E-06
HOXA9	0.29822254	2.27E-07	MCL1	0.10582227	0.00253916
HSPA6	0.1863268	9.06E-05	MFGE8	0.17500426	2.26E-05
ICAM2	0.31625687	1.42E-11	MFNG	0.16430547	9.63E-06
IER3	0.09335499	0.02285026	MMP7	0.45852219	7.58E-09
IFITM1	0.4609643	5.15E-13	MNX1	0.20368396	0.00046907
IFNGR1	0.04904393	0.04892766	MRC1	0.23153495	1.60E-10
IFNGR2	0.13409986	7.97E-05	MS4A6A	0.28089524	3.24E-11
IFNL2	0.23791266	2.47E-06	MYC	0.10076322	0.00247219
IGFBP3	0.63337615	1.41E-10	NAT8L	0.20683603	0.00100157
IKBKB	0.13161431	2.23E-05	NEIL1	0.1121521	0.01036165
IKBKG	0.12830651	0.00093869	NGF	0.20176611	0.00018919
IL10RA	0.29487526	3.77E-11	NGFR	0.22954758	3.26E-07
IL1R1	0.20561332	9.93E-08	NLRC5	0.1356577	0.00017564
IL2RA	0.18118706	7.81E-05	NOS2	0.13445754	0.01618023
IL2RB	0.20434868	1.86E-06	NOTCH1	0.17695563	9.29E-07
IL2RG	0.15794353	0.00017564	NOTCH2	0.07819787	0.00019518
IL6ST	0.04130841	0.0422374	NOTCH3	0.18662263	0.00016051
IL7R	0.40111458	3.67E-12	NR4A1	0.73709654	3.87E-15
INPP5D	0.20918621	4.18E-08	NUMBL	0.30647719	3.36E-10
IRF7	0.1733932	0.01520076	NUPR1	0.79766716	1.13E-12
IRF8	0.25465465	6.78E-11	OAS2	0.14356752	0.00326824
ITGA3	0.28071026	9.55E-11	PDCD1	0.23456004	3.16E-06
ITGA9	0.26177093	4.25E-09	PDGFB	0.06579942	0.04138335
ITGAV	0.13805686	9.78E-05	PDGFRA	0.3660242	5.16E-11
ITGAX	0.21771339	2.59E-07	PDGFRB	0.37421773	3.77E-11
ITGB2	0.35648635	4.05E-13	PDZK1IP1	0.26684351	1.69E-05
ITGB4	0.13720712	0.00110585	PECAM1	0.28272508	7.78E-10
JAG1	0.20788602	2.59E-06	PIK3CD	0.20739796	7.69E-07
JAK3	0.26613022	7.34E-10	PIM1	0.11189351	0.00117332
JAML	0.22207079	5.25E-07	PKM	0.21643878	2.77E-05
JUN	0.1864287	1.65E-06	PLAT	0.29756163	6.82E-09
JUNB	0.54899279	2.31E-15	PML	0.20091875	2.57E-07
KLF4	0.61969307	6.15E-18	POU2AF1	0.42461888	1.39E-12
KRT14	0.45642802	1.90E-13	PRDM1	0.19224015	1.27E-05
KRT7	0.76470145	9.87E-17	PTCRA	0.14016178	0.01329746
LAMA5	0.13161956	0.00206956	PTPRC	0.34218006	4.34E-12
LAMC3	0.35005867	1.48E-11	RAC2	0.31002614	2.03E-10
LCK	0.25135506	5.25E-08	RASA4	0.21390268	5.48E-10
LCP1	0.19890075	3.56E-06	RBL2	0.10494772	7.31E-06

LDHB	0.23733785	1.19E-08	RELB	0.24204827	7.97E-09
LGALS3	0.15814251	7.41E-05	REN	0.12124136	0.03128396
LILRB2	0.14652471	0.00539779	RET	0.24656457	4.19E-06

Target name	Log2	Adjusted pvalue
RIN1	0.43105477	1.03E-12
RPS6	0.06666061	0.02249512
RRAD	0.22984106	1.12E-06
RUNX1	0.14270188	0.00038335
S100A9	0.1251606	0.00715905
SBNO2	0.06334664	0.00461655
SERPINH1	0.09301651	0.00553628
SF3B1	0.07523781	0.00031912
SFRP4	0.27301006	1.57E-05
SGK1	0.09608573	0.00835774
SH2B2	0.11084293	0.01534744
SIGIRR	0.11690835	0.00049696
SLAMF7	0.09159179	0.04265477
SMAD9	0.24982452	9.25E-07
SMPD3	0.31240604	1.25E-08
SOCS1	0.22354802	4.28E-07
SOCS3	0.23678972	3.68E-06
SPIB	0.14791196	0.00166322
SPRED1	0.17495561	2.18E-08
SPRY2	0.10216646	0.00411086
STING1	0.29774927	1.23E-13
STK11IP	0.22143827	3.38E-06
TGFB1	0.40287589	4.37E-16
TGFBR2	0.23114297	1.37E-10
THBD	0.14781456	0.00022587
THBS1	0.92878995	6.93E-12
THY1	0.19949358	4.19E-06
TIE1	0.16519388	7.31E-06
TNF	0.35678089	9.09E-11
TNFAIP3	0.09953599	0.00889978
TNFRSF14	0.09322958	0.00028007
TNFRSF1B	0.15166418	8.33E-06
TNFSF12	0.42156861	2.09E-14
TNFSF13	0.25769491	2.55E-08
TPI1	0.12442705	0.02610913
TPM1	0.13790577	0.00494728
TPM4	0.58344121	7.69E-12
TPSAB1/B2	0.20389729	0.00012307
TRAC	0.38276444	2.89E-11
TRBC1/2	0.68493722	3.92E-15
TRIM21	0.1699635	6.94E-05
TXNIP	0.54450108	1.31E-14
UBA7	0.12613052	2.57E-05
VCAM1	0.14852394	2.38E-05
VCAN	0.20873865	7.74E-07
VSIR	0.34675223	3.46E-14
WIPF1	0.39766592	1.34E-14
WNT10A	0.11200408	0.02293079
WNT6	0.21815813	4.54E-05
XCR1	0.47150211	2.26E-11
ZEB2	0.27060162	2.69E-10

Non-Tumour vs Peri-tumoural differential gene expression. Upregulated in Peri-tumour
Significance threshold of adjusted P value<0.05.

Target name	Log2	Adjusted pvalue	Target name	Log2	Adjusted pvalue
ACTA2	-0.667944	8.90E-07	DUSP2	-0.1331595	0.0065422
ACTB	-0.2196917	0.008492	ENG	-0.2425063	0.005806
ADGRE5	-0.1813439	0.0005826	ETS1	-0.1212413	0.005806
ALDOA	-0.1367517	0.0073674	EWSR1	-0.0579776	0.0409574
ANXA1	-0.2099708	8.61E-05	FCGR1A	-0.1545187	0.0009416
AXL	-0.0713007	0.0417768	FGCR2A/B	-0.253605	5.74E-05
BAGE	-0.2017884	0.0039247	FGFR1	-0.1502564	0.0020443
BAX	-0.0951063	0.0081518	FGFR3	-0.1497244	0.0033487
BCL2	-0.1297014	0.0086076	FLNA	-0.4521707	1.47E-05
BCL2L1	-0.1484437	0.0055	FSTL3	-0.1690541	0.0088992
C1QA	-0.16257	0.0029476	G6PD	-0.1015432	0.0289756
C7	-0.335411	0.0338227	GAS1	-0.1594725	0.0028578
CAPN2	-0.1106113	0.0046777	GIMAP6	-0.1064157	0.0151742
CASP1	-0.1092029	0.0262796	GNA11	-0.0781527	0.0155137
CBL	-0.0951954	0.0412597	H3-3A	-0.0979119	0.0227705
CCL19	-0.3815735	0.0141103	HDAC1	-0.0845674	0.0082808
CCL2	-0.4631128	1.03E-05	HK1	-0.1764856	2.87E-05
CCL21	-0.3830687	0.0116085	HLA-A	-0.3734333	0.0008594
CCL5	-0.1567033	0.0066834	HLA-B	-0.3690118	0.0040657
CD24	-0.2020477	0.0003056	HLA-C	-0.1692642	0.008821
CD34	-0.1137564	0.0058528	HLA-DMA	-0.2150299	0.0001754
CD37	-0.2283819	0.0010144	HLA-DMB	-0.1977951	0.0001397
CD44	-0.2542633	0.0002791	HLA-DOB	-0.1029298	0.0116085
CD48	-0.114907	0.0070109	HLA-DPA1	-0.2530948	2.87E-05
CD53	-0.2093325	0.0003894	HLA-DQA1	-0.1036268	0.0041634
CD59	-0.1803098	6.68E-05	HLA-DQB1	-0.0970519	0.0338864
CD63	-0.1043351	0.03407	HLA-DRA	-0.4556857	0.0002777
CD68	-0.0676074	0.0354075	HLA-DRB	-0.5221753	8.61E-05
CD74	-0.6030944	0.0003891	HLA-DRB3	-0.3580211	0.000835
CD9	-0.1338343	0.0038173	HLA-DRB4	-0.2868438	0.0067385
CDC25B	-0.0569136	0.0429763	HLA-E	-0.2944658	0.0008271
CDKN1B	-0.0721326	0.0200434	HLA-F	-0.1937802	0.0064342
CKLF	-0.0788343	0.008492	HSPA6	-0.1869483	7.07E-05
CLEC14A	-0.0993651	0.0283947	HSPB1	-0.1955023	0.0034896
COL1A1	-0.8720709	9.51E-08	ICAM1	-0.0859731	0.0276711

COL1A2	-0.446868	1.03E-05	IFITM1	-0.1409064	0.0083983
COL3A1	-0.6289339	1.86E-05	IFNA7/17	-0.0934244	0.0315453
COL5A1	-0.381566	1.47E-05	IFNGR1	-0.0977342	0.0046834
COL6A3	-0.4120946	1.86E-05	IFNGR2	-0.1447461	0.0021496
CREBBP	-0.0673095	0.0303128	IKBKB	-0.0614638	0.0384438
CSF1R	-0.164637	0.0004117	IL10RA	-0.1111828	0.0136996
CSF2RB	-0.1344854	0.0017568	IL2RG	-0.1630211	0.0001865
CTSH	-0.0526076	0.0265288	IL7R	-0.200516	0.0030576
CXCR4	-0.3128658	0.0003285	ILF3	-0.1304268	9.72E-05
DAB2	-0.1321678	0.0015174	INPP5D	-0.143262	0.0005902
DTX3	-0.0902243	0.0165876			

Target name	Log2	Adjusted pvalue	Target name	Log2	Adjusted pvalue
IRAK1	-0.1014911	0.0289856	PTPRC	-0.1827808	0.0013229
IRF3	-0.1060563	0.0003544	RASA4	-0.1410223	0.0054076
IRF9	-0.0628569	0.0209296	RELA	-0.0869458	0.0025879
ITGAV	-0.1799957	0.0008666	RPL7A	-0.3307385	0.0005677
ITGAX	-0.1582566	0.0004259	RPS27A	-0.1692913	0.005666
ITGB1	-0.1418562	0.0273731	S100A9	-0.1433857	0.0111412
ITGB2	-0.2009795	0.0006503	SBNO2	-0.1231552	0.000992
JAK1	-0.0804157	0.0067592	SERPINH1	-0.1655599	1.65E-05
JAK3	-0.1758292	0.000104	SF3A1	-0.0732121	0.023015
JUNB	-0.1756771	0.0001992	SFRP4	-0.2042178	0.003136
KMT2C	-0.0775805	0.0148626	SHC1	-0.1091719	0.0004686
KMT2D	-0.1132859	0.0072595	SLAMF7	-0.0975496	0.0136996
KRT5	-0.1496714	0.0014097	SLC1A5	-0.0848557	0.0325132
LAMA5	-0.1325778	0.0167485	SMAD3	-0.0600257	0.0449989
LAMC3	-0.1869407	0.0016602	SMARCA4	-0.1052011	0.001302
LCP1	-0.0938752	0.0168464	SOCS3	-0.1923537	0.0030148
LDHB	-0.1291614	0.0077448	SOX9	-0.1194467	0.0130836
LTB	-0.1186897	0.0264535	SP1	-0.0955464	0.010414
LTBP1	-0.1200694	0.0032536	SPP1	-0.4667592	2.69E-05
LYZ	-0.2576484	0.0088992	SPRED1	-0.0793576	0.0259008
MAP3K14	-0.0945949	0.0083983	SSX1	-0.5071078	0.0006226
MAPKAPK2	-0.1026811	0.0046834	STK11	-0.0566257	0.0344413
MCAM	-0.1612002	0.0024834	TAP1	-0.138874	0.0008271
MCM7	-0.1006269	0.0010816	TAPBP	-0.132584	0.0005829
MFGE8	-0.1374999	0.001527	TCF3	-0.0839827	0.0429763
MMP7	-0.2494586	0.0061363	TFDP1	-0.0645	0.0403285

NANOG	-0.091119	0.0393196	TGFB1	-0.1637748	0.0004117
NDUFA3	-0.1393382	0.0096704	TGFBR2	-0.1475969	0.001717
NFKB2	-0.0901147	0.0317767	THBD	-0.1199031	0.0018205
NLRC5	-0.1407566	0.0030576	THBS1	-0.5004555	1.97E-05
NOS3	-0.0747409	0.0338709	THY1	-0.2124061	5.28E-05
NOTCH1	-0.1434751	0.0010816	TNFAIP3	-0.1246961	0.014118
NOTCH2	-0.0964125	0.0137704	TPM1	-0.3287296	5.28E-05
NOTCH3	-0.18976	0.0031765	TPM4	-0.4992172	1.12E-06
NRP1	-0.1547051	0.0025879	TPSAB1/B2	-0.1417301	0.0172598
P4HA2	-0.0845535	0.0338709	TRAC	-0.1567171	0.0088517
PDGFRB	-0.2254311	0.0010305	TRBC1/2	-0.2489385	0.0282954
PECAM1	-0.2720667	1.03E-05	TUBB	-0.0837996	0.0081239
PIK3CD	-0.137523	0.0083983	TXNIP	-0.2376966	0.0046959
PKM	-0.2559923	1.51E-05	VCAN	-0.1015001	0.0449989
PPP2R1A	-0.0748752	0.0129285	VSIR	-0.1372436	0.0116311
PRDM1	-0.1275983	0.0209296	WIPF1	-0.1643085	0.0031136
PSEN1	-0.0679599	0.0280007	ZEB2	-0.1064007	0.0166633
PSMB10	-0.0790453	0.0282867			
PSMB9	-0.0804948	0.0388966			

Non-Tumour vs Peri-tumoural differential gene expression. Upregulated in Peri-tumour
Significance threshold of adjusted P value<0.05.

Target name	Log2	Adjusted pvalue	Target name	Log2	Adjusted pvalue
A2M	1.0789484	5.74E-05	CREB3L3	0.2819163	3.92E-05
ACOT12	0.2013439	0.0051195	CRP	0.5372832	0.0008878
ACY1	0.3993946	0.000227	CTSL	0.1973834	0.0004434
ADH1A/B/C	1.2122872	0.0001754	CXCL2	0.4108502	1.88E-05
ADH4	0.9178896	0.000651	CXXC5	0.1118238	0.0024682
ADH6	0.3854712	0.001498	CYP4A11/22	0.8904562	5.28E-05
AKAP1	0.0953452	0.0194724	CYP8B1	0.4682803	3.03E-05
AKR1C4	0.4677037	0.0005957	DUSP10	0.1302877	0.0058271
AMBP	1.6361761	5.11E-05	DUSP6	0.090706	0.0468639
ANGPTL4	0.1939078	0.0085688	EFNA1	0.2521145	1.86E-05
APOA2	1.7849301	9.05E-05	EGFR	0.1980288	5.11E-05
APOB	1.3739024	8.09E-05	EHHADH	0.3245653	0.0005957
APOC2	1.5055412	5.21E-05	ETS2	0.2116636	0.0113927
APOC3	1.550298	1.65E-05	F12	0.6589465	5.05E-05
APOM	0.5112732	0.0001173	FBP1	0.8221582	1.51E-05
AQP9	0.4767733	0.000104	FCGRT	0.1995301	0.0229304

AR	0.2306996	1.03E-05	FH	0.3055001	0.0002069
ARG1	0.7503838	2.72E-05	FN1	0.8245872	0.0046026
ASL	0.5673658	2.69E-05	FST	0.2709776	0.0002543
ASPG	0.2387874	3.92E-05	GADD45A	0.2101323	0.0007532
ATOX1	0.1492104	0.0066729	GADD45B	0.1851996	0.0338709
ATP5F1D	0.1555736	0.000517	GADD45G	0.2777416	0.0010017
ATP5ME	0.2236465	0.0011373	GHR	0.2783194	0.0018205
C1QBP	0.106541	0.0081881	GLUD1	0.227891	0.0042499
C1R	0.6175704	0.0032266	GOT1	0.5192254	5.07E-05
C1S	0.6204839	0.0029533	GOT2	0.4178028	0.0001754
C2	0.4660147	6.34E-05	GPI	0.1498642	0.0085688
C3	1.272876	0.0001289	GPT	0.2539116	3.92E-05
C4B	1.0405934	0.0001832	GPX4	0.2452011	0.0016775
C4BPA	0.8255587	5.40E-05	GUSB	0.1223522	0.0246535
C5	0.5477205	0.0004848	HAMP	0.3896806	0.0229304
C6	0.6405149	1.65E-05	HDAC6	0.0878601	0.0429763
C8A	0.652077	3.92E-05	HSD11B1	0.4928212	7.07E-05
C8B	0.6937256	4.63E-05	HSD17B8	0.0992738	0.0042499
C8G	0.6049498	2.57E-05	ID2	0.2960386	3.11E-05
C9	0.7746226	5.07E-05	IDH1	0.2645062	0.0004297
CCL16	0.2796267	0.0002347	IDH2	0.1940146	0.0034401
CD14	0.250722	0.0001355	IGF2R	0.0627688	0.043699
CEBPA	0.1357957	0.0066983	IL13RA1	0.1191758	0.0135732
CFB	1.2387965	7.07E-05	IL17RB	0.1127844	0.0483706
CFI	0.4270546	0.0003102	IL1RAP	0.1572352	0.0004848
CLU	1.1185855	9.92E-05	IL1RN	0.0979457	0.0429763
COX5B	0.2792285	0.0010305	IL6R	0.1011665	0.0154187
COX6A1	0.2763506	0.0013824	LAMP1	0.1399147	0.0376202
COX6B1	0.1405481	0.0413501	LBP	0.5828552	2.62E-05

Target name	**Log2**	**Adjusted pvalue**	**Target name**	**Log2**	**Adjusted pvalue**
LEPR	0.2811628	0.0001583	RBP4	1.8273872	5.33E-05
LY6E	0.382825	0.0007439	RHOB	0.3390547	0.000517
MARCO	0.2127516	0.0003544	RORA	0.1129137	0.0344413
MASP1	0.1468532	0.0039602	RORC	0.1347979	0.0003615
MBL2	0.3373976	0.0004988	SAA1	0.5079507	0.0033487
MBNL3	0.1451234	0.0050905	SDHA	0.1989011	0.0023663
MGMT	0.1861695	0.0003158	SERINC2	0.1012969	0.0055963
NDUFA1	0.1833833	0.005806	SERPINA1	1.8411776	0.0002202

NDUFA2	0.0827848	0.0152804	SERPING1	0.8256926	0.0003819
NDUFB1	0.159122	0.0004852	SFXN1	0.2058886	0.0006463
NDUFB10	0.1003444	0.0111412	SGK2	0.1432254	0.0003544
NDUFS7	0.0795515	0.0074507	SLC16A1	0.0840879	0.033105
NECTIN2	0.0694945	0.0096053	SLC16A2	0.1811317	0.0002084
NT5E	0.1110802	0.023015	SOD1	0.7544761	0.000142
OTC	0.3284136	0.0010268	SREBF1	0.1715671	0.0073387
PALMD	0.0806998	0.0231276	SRP54	0.0888771	0.012649
PC	0.2890662	0.0001173	ST6GAL1	0.3514337	9.80E-05
PCK1	1.3898409	5.28E-05	TDO2	0.503254	4.23E-05
PCK2	0.620362	5.42E-06	TNFSF14	0.1230141	0.0086812
PEBP1	0.8127517	0.0001152	TSPAN7	0.0564969	0.0287629
PHGDH	0.2107986	9.89E-05	TTPA	0.1762999	0.0027615
PIK3R1	0.1375116	0.0010017	TTR	1.8862976	1.51E-05
PLA2G2A	0.3385288	0.0053872	UBB	0.3452319	0.0012619
PLOD2	0.1279446	0.0040363	UQCR10	0.0982403	0.0080207
PPARGC1A	0.1613045	0.0160776	UQCRQ	0.3322044	0.0003881
PRDX5	0.0998055	0.000992	VEGFA	0.1182876	0.0157196
PSAT1	0.1423483	0.0270036			

10.2 Appendix 2. Data from volcano plot showing differential gene expression for CLEC14A high vs CLEC14A low expressing cases.

Differential gene expression for CLEC14A high vs CLEC14A low expressing cases. Significance threshold of adjusted P value<0.05. – Upregulated in CLEC14A low cases

Target name	Log2	Adjusted pvalue
EFNA1	-0.3681724	5.45E-05
A2M	-1.4717357	0.0291963
APP	-0.6970835	0.0225444
FCGRT	-0.4243995	0.0287912
GADD45B	-0.5119202	0.0135672

Differential gene expression for CLEC14A high vs CLEC14A low expressing cases. Significance threshold of adjusted P value<0.05. – Upregulated in CLEC14A low cases

Target name	Log2	Adjusted pvalue	Target name	Log2	Adjusted pvalue
ALDOC	0.3020552	0.0176197	NECTIN1	0.3111155	0.0191145
ARNT2	0.385226	0.0135672	NFAM1	0.3475627	0.0135672
ATF1	0.2743727	0.0272623	NOS3	0.4087138	0.0135672
BAMBI	0.3186231	0.0135672	NSD1	0.2622927	0.0211887
BMP4	0.3937112	0.0176197	OAS3	0.2475662	0.0135672
BMP5	0.3078439	0.0188195	PARP12	0.2000931	0.0191145
CACNA2D1	0.3044562	0.0216647	PIK3CD	0.2738709	0.0252469
CASP7	0.2931889	0.0211887	PPP3R2	0.3740193	0.0184007
CBL	0.3436881	0.0191145	PRC1	0.3760553	0.0227754
CD209	0.4131266	0.0197073	PRDM1	0.2639204	0.0219806
CD300A	0.3787728	0.0135672	PRKCA	0.2558885	0.0197127
CD34	0.2893892	0.0285356	PRKCD	0.2544842	0.0214572
CD5	0.3360114	0.0176197	PTPN5	0.3162261	0.0144238
CD8B	0.2696316	0.0285356	RAC3	0.3195596	0.0135672
CDC25B	0.1721142	0.0225444	REL	0.3496584	0.0200621
CKLF	0.2537641	0.0211649	RELN	0.4056497	0.0188195
CLEC14A	0.2611259	0.0135672	RGMB	0.3151198	0.0135672
CMKLR1	0.3301624	0.0176197	RNF43	0.3652021	0.0266717
CSF2RB	0.3235528	0.0188195	RNLS	0.3783222	0.0135672
CST2	0.4313893	0.0219806	ROBO4	0.3328882	0.0135672
DTX3	0.2247487	0.0211887	ROPN1	0.2901701	0.0245293
DUSP2	0.360977	0.027692	RPTOR	0.2296048	0.0227754
E2F4	0.165882	0.027692	RRM2	0.3702952	0.0249884
ELMO1	0.2476927	0.0188195	RUNX1	0.2478684	0.0219806
FADD	0.2609715	0.0176197	RUNX1T1	0.307341	0.0149247
FCGR1A	0.3411907	0.0188195	S100A9	0.3861193	0.0135672
FCGR3A/B	0.2624971	0.0226562	SFN	0.3773126	0.0176197
FZD2	0.3191859	0.0271263	SIGLEC1	0.2827126	0.0184007
GATA2	0.3103005	0.0135672	SIRPB2	0.3351811	0.0211887
HLA-DOA	0.2614505	0.0219806	SIX1	0.3686099	0.0135672
HLA-DOB	0.3390974	0.0219806	SLAMF1	0.470456	0.0191145
IFNA7/17	0.4244959	0.0135672	SLC11A1	0.3912792	0.0211649
IL17RA	0.2973097	0.0191145	SLC1A5	0.3599741	0.0216647
IL21R	0.3485865	0.0214572	SLC2A1	0.4317268	0.0219806
IL34	0.3600729	0.0217948	SLC39A6	0.2990623	0.0285356
ITGAX	0.2336191	0.0176197	SMAD2	0.3036303	0.0277402
KRT17	0.3456987	0.0188195	SMO	0.2401634	0.0285356
LEF1	0.376685	0.0027379	TAP2	0.2678237	0.0176197
MAGEC1	0.3670276	0.0176197	TAPBPL	0.1939275	0.0211887
MAP3K13	0.3227917	0.0176197	TCF3	0.3395028	0.0285356

MEN1	0.3324924	0.0176197	TCF7L1	0.2242576	0.0214572
MIA	0.3092732	0.0191145	TNFRSF14	0.1369852	0.0176197
MME	0.3204853	7.767E-09	TPTE	0.385809	0.0176197
MTOR	0.3052969	0.0188195	TRAF2	0.2064477	0.021387
MUC4	0.376451	0.027692	TRAF6	0.2786231	0.0184007
MUTYH	0.2480611	0.0176197	WNT10A	0.3193599	0.0214572
MYCT1	0.3124029	0.0196879	WNT3	0.3117702	0.0140676
MYD88	0.3018324	0.0246484			

11 REFERENCES

ABDEL-MISIH, S. R. & BLOOMSTON, M. 2010. Liver anatomy. *Surg Clin North Am,* 90**,** 643-53.

ADAIR, T. H. & MONTANI, J. P. 2010. *Angiogenesis.* San Rafael (CA).

AFFORD, S. C., AHMED-CHOUDHURY, J., RANDHAWA, S., RUSSELL, C., YOUSTER, J., CROSBY, H. A., ELIOPOULOS, A., HUBSCHER, S. G., YOUNG, L. S. & ADAMS, D. H. 2001. CD40 activation-induced, Fas-dependent apoptosis and NF-kappaB/AP-1 signaling in human intrahepatic biliary epithelial cells. *FASEB J,* 15**,** 2345-54.

AHMADZADEH, M., JOHNSON, L. A., HEEMSKERK, B., WUNDERLICH, J. R., DUDLEY, M. E., WHITE, D. E. & ROSENBERG, S. A. 2009. Tumor antigen-specific CD8 T cells infiltrating the tumor express high levels of PD-1 and are functionally impaired. *Blood,* 114**,** 1537-44.

ALA, A., DHILLON, A. P. & HODGSON, H. J. 2003. Role of cell adhesion molecules in leukocyte recruitment in the liver and gut. *Int J Exp Pathol,* 84**,** 1-16.

ALDRIDGE, D. R., TRANAH, E. J. & SHAWCROSS, D. L. 2015. Pathogenesis of hepatic encephalopathy: role of ammonia and systemic inflammation. *J Clin Exp Hepatol,* 5**,** S7-S20.

ALON, R., FUHLBRIGGE, R. C., FINGER, E. B. & SPRINGER, T. A. 1996. Interactions through L-selectin between leukocytes and adherent leukocytes nucleate rolling adhesions on selectins and VCAM-1 in shear flow. *J Cell Biol,* 135**,** 849-65.

ALON, R., KASSNER, P. D., CARR, M. W., FINGER, E. B., HEMLER, M. E. & SPRINGER, T. A. 1995. The integrin VLA-4 supports tethering and rolling in flow on VCAM-1. *J Cell Biol,* 128**,** 1243-53.

ALTEKRUSE, S. F., MCGLYNN, K. A., DICKIE, L. A. & KLEINER, D. E. 2012. Hepatocellular carcinoma confirmation, treatment, and survival in surveillance, epidemiology, and end results registries, 1992-2008. *Hepatology,* 55**,** 476-82.

BAGLEY, R. G., HONMA, N., WEBER, W., BOUTIN, P., ROULEAU, C., SHANKARA, S., KATAOKA, S., ISHIDA, I., ROBERTS, B. L. & TEICHER, B. A. 2008. Endosialin/TEM 1/CD248 is a pericyte marker of embryonic and tumor neovascularization. *Microvasc Res,* 76**,** 180-8.

BAKIRI, L., HAMACHER, R., GRANA, O., GUIO-CARRION, A., CAMPOS-OLIVAS, R., MARTINEZ, L., DIENES, H. P., THOMSEN, M. K., HASENFUSS, S. C. & WAGNER, E. F. 2017. Liver carcinogenesis by FOS-dependent inflammation and cholesterol dysregulation. *J Exp Med,* 214**,** 1387-1409.

BANDYOPADHYAY, K., MARRERO, I. & KUMAR, V. 2016. NKT cell subsets as key participants in liver physiology and pathology. *Cell Mol Immunol,* 13**,** 337-46.

BARREIRO, O., YANEZ-MO, M., SERRADOR, J. M., MONTOYA, M. C., VICENTE-MANZANARES, M., TEJEDOR, R., FURTHMAYR, H. & SANCHEZ-MADRID, F. 2002. Dynamic interaction of VCAM-1 and ICAM-1 with moesin and ezrin in a novel endothelial docking structure for adherent leukocytes. *J Cell Biol,* 157**,** 1233-45.

BARTHA, A. & GYORFFY, B. 2021. TNMplot.com: A Web Tool for the Comparison of Gene Expression in Normal, Tumor and Metastatic Tissues. *Int J Mol Sci,* 22.

BENJAMINSEN, I. C., GRAFF, B. A., BRURBERG, K. G. & ROFSTAD, E. K. 2004. Assessment of tumor blood perfusion by high-resolution dynamic contrast-enhanced MRI: a preclinical study of human melanoma xenografts. *Magn Reson Med,* 52**,** 269-76.

BERLIN, C., BARGATZE, R. F., CAMPBELL, J. J., VON ANDRIAN, U. H., SZABO, M. C., HASSLEN, S. R., NELSON, R. D., BERG, E. L., ERLANDSEN, S. L. & BUTCHER, E. C. 1995. alpha 4 integrins mediate lymphocyte attachment and rolling under physiologic flow. *Cell,* 80**,** 413-22.

BOCCI, M., SJOLUND, J., KURZEJAMSKA, E., LINDGREN, D., MARZOUKA, N. A., BARTOSCHEK, M., HOGLUND, M. & PIETRAS, K. 2019. Activin receptor-like kinase 1 is associated with immune cell infiltration and regulates CLEC14A transcription in cancer. *Angiogenesis,* 22**,** 117-131.

BOHLSON, S. S., SILVA, R., FONSECA, M. I. & TENNER, A. J. 2005. CD93 is rapidly shed from the surface of human myeloid cells and the soluble form is detected in human plasma. *J Immunol,* 175**,** 1239-47.

BOIRE, A., COVIC, L., AGARWAL, A., JACQUES, S., SHERIFI, S. & KULIOPULOS, A. 2005. PAR1 is a matrix metalloprotease-1 receptor that promotes invasion and tumorigenesis of breast cancer cells. *Cell,* 120**,** 303-13.

BORGSTROM, P., HILLAN, K. J., SRIRAMARAO, P. & FERRARA, N. 1996. Complete inhibition of angiogenesis and growth of microtumors by anti-vascular endothelial growth factor neutralizing antibody: novel concepts of angiostatic therapy from intravital videomicroscopy. *Cancer Res,* 56**,** 4032-9.

BOZWARD, A. G., WARRICKER, F., OO, Y. H. & KHAKOO, S. I. 2021. Natural Killer Cells and Regulatory T Cells Cross Talk in Hepatocellular Carcinoma: Exploring Therapeutic Options for the Next Decade. *Front Immunol,* 12**,** 643310.

BRAY, F., FERLAY, J., SOERJOMATARAM, I., SIEGEL, R. L., TORRE, L. A. & JEMAL, A. 2018. Global cancer statistics 2018: GLOBOCAN estimates of incidence and mortality worldwide for 36 cancers in 185 countries. *CA Cancer J Clin,* 68**,** 394-424.

BRODSKY, S. V., MENDELEV, N., MELAMED, M. & RAMASWAMY, G. 2007. Vascular density and VEGF expression in hepatic lesions. *J Gastrointestin Liver Dis,* 16**,** 373-7.

BUCHBINDER, E. I. & DESAI, A. 2016. CTLA-4 and PD-1 Pathways: Similarities, Differences, and Implications of Their Inhibition. *Am J Clin Oncol,* 39**,** 98-106.

CAI, J., HU, M., CHEN, Z. & LING, Z. 2021. The roles and mechanisms of hypoxia in liver fibrosis. *J Transl Med,* 19**,** 186.

CAI, L., ZHANG, Z., ZHOU, L., WANG, H., FU, J., ZHANG, S., SHI, M., ZHANG, H., YANG, Y., WU, H., TIEN, P. & WANG, F. S. 2008. Functional impairment in circulating and intrahepatic NK cells and relative mechanism in hepatocellular carcinoma patients. *Clin Immunol,* 129**,** 428-37.

CALVENTE, C. J., TAMEDA, M., JOHNSON, C. D., DEL PILAR, H., LIN, Y. C., ADRONIKOU, N., DE MOLLERAT DU JEU, X., LLORENTE, C., BOYER, J. & FELDSTEIN, A. E. 2019. Neutrophils contribute to spontaneous resolution of liver inflammation and fibrosis via microRNA-223. *J Clin Invest,* 129**,** 4091-4109.

CARMELIET, P. & JAIN, R. K. 2000. Angiogenesis in cancer and other diseases. *Nature,* 407**,** 249-57.

CHA, J. H., CHAN, L. C., LI, C. W., HSU, J. L. & HUNG, M. C. 2019. Mechanisms Controlling PD-L1 Expression in Cancer. *Mol Cell,* 76**,** 359-370.

CHEEMERLA, S. & BALAKRISHNAN, M. 2021. Global Epidemiology of Chronic Liver Disease. *Clin Liver Dis (Hoboken),* 17**,** 365-370.

CHEN, C., MA, Y. H., ZHANG, Y. T., ZHANG, F., ZHOU, N., WANG, X., LIU, T. & LI, Y. M. 2018. Effect of dendritic cell-based immunotherapy on hepatocellular carcinoma: A systematic review and meta-analysis. *Cytotherapy,* 20**,** 975-989.

CHEN, P. Y., QIN, L., BAEYENS, N., LI, G., AFOLABI, T., BUDATHA, M., TELLIDES, G., SCHWARTZ, M. A. & SIMONS, M. 2015. Endothelial-to-mesenchymal transition drives atherosclerosis progression. *J Clin Invest,* 125**,** 4514-28.

CHEN, Y. & TIAN, Z. 2021. Innate lymphocytes: pathogenesis and therapeutic targets of liver diseases and cancer. *Cell Mol Immunol,* 18**,** 57-72.

CHENG, A. L., QIN, S., IKEDA, M., GALLE, P. R., DUCREUX, M., KIM, T. Y., LIM, H. Y., KUDO, M., BREDER, V., MERLE, P., KASEB, A. O., LI, D., VERRET, W., MA, N., NICHOLAS, A., WANG, Y., LI, L., ZHU, A. X. & FINN, R. S. 2022. Updated efficacy and safety data from IMbrave150: Atezolizumab plus bevacizumab vs. sorafenib for unresectable hepatocellular carcinoma. *J Hepatol,* 76**,** 862-873.

CHO, Y. & SZABO, G. 2021. Two Faces of Neutrophils in Liver Disease Development and Progression. *Hepatology,* 74**,** 503-512.

CHRISTIAN, S., WINKLER, R., HELFRICH, I., BOOS, A. M., BESEMFELDER, E., SCHADENDORF, D. & AUGUSTIN, H. G. 2008. Endosialin (Tem1) is a marker of tumor-associated myofibroblasts and tumor vessel-associated mural cells. *Am J Pathol,* 172**,** 486-94.

CHU, T. J. & PETERS, D. G. 2008. Serial analysis of the vascular endothelial transcriptome under static and shear stress conditions. *Physiol Genomics,* 34**,** 185-92.

COBLEIGH, M. A. & ROBEK, M. D. 2013. Protective and pathological properties of IL-22 in liver disease: implications for viral hepatitis. *Am J Pathol,* 182**,** 21-8.

COLLADEL, R., PELLICANI, R., ANDREUZZI, E., PAULITTI, A., TARTICCHIO, G., TODARO, F., COLOMBATTI, A. & MONGIAT, M. 2016. MULTIMERIN2 binds VEGF-A primarily via the carbohydrate chains exerting an angiostatic function and impairing tumor growth. *Oncotarget,* 7**,** 2022-37.

CONNOLLY, M. K., BEDROSIAN, A. S., MALLEN-ST CLAIR, J., MITCHELL, A. P., IBRAHIM, J., STROUD, A., PACHTER, H. L., BAR-SAGI, D., FREY, A. B. & MILLER, G. 2009. In liver fibrosis, dendritic cells govern hepatic inflammation in mice via TNF-alpha. *J Clin Invest,* 119**,** 3213-25.

CONWAY, E. M., NOWAKOWSKI, B. & STEINER-MOSONYI, M. 1992. Human neutrophils synthesize thrombomodulin that does not promote thrombin-dependent protein C activation. *Blood,* 80**,** 1254-63.

CONWAY, E. M., VAN DE WOUWER, M., POLLEFEYT, S., JURK, K., VAN AKEN, H., DE VRIESE, A., WEITZ, J. I., WEILER, H., HELLINGS, P. W., SCHAEFFER, P., HERBERT, J. M.,

COLLEN, D. & THEILMEIER, G. 2002. The lectin-like domain of thrombomodulin confers protection from neutrophil-mediated tissue damage by suppressing adhesion molecule expression via nuclear factor kappaB and mitogen-activated protein kinase pathways. *J Exp Med,* 196**,** 565-77.

CRESSMAN, D. E., GREENBAUM, L. E., DEANGELIS, R. A., CILIBERTO, G., FURTH, E. E., POLI, V. & TAUB, R. 1996. Liver failure and defective hepatocyte regeneration in interleukin-6-deficient mice. *Science,* 274**,** 1379-83.

DANAHER, P., KIM, Y., NELSON, B., GRISWOLD, M., YANG, Z., PIAZZA, E. & BEECHEM, J. M. 2022. Advances in mixed cell deconvolution enable quantification of cell types in spatial transcriptomic data. *Nat Commun,* 13**,** 385.

DANIELE, B., BENCIVENGA, A., MEGNA, A. S. & TINESSA, V. 2004. Alpha-fetoprotein and ultrasonography screening for hepatocellular carcinoma. *Gastroenterology,* 127**,** S108-12.

DEGRENDELE, H. C., ESTESS, P., PICKER, L. J. & SIEGELMAN, M. H. 1996. CD44 and its ligand hyaluronate mediate rolling under physiologic flow: a novel lymphocyte-endothelial cell primary adhesion pathway. *J Exp Med,* 183**,** 1119-30.

DELA PAZ, N. G., WALSHE, T. E., LEACH, L. L., SAINT-GENIEZ, M. & D'AMORE, P. A. 2012. Role of shear-stress-induced VEGF expression in endothelial cell survival. *J Cell Sci,* 125**,** 831-43.

DEVAUD, C., ROUSSEAU, B., NETZER, S., PITARD, V., PAROISSIN, C., KHAIRALLAH, C., COSTET, P., MOREAU, J. F., COUILLAUD, F., DECHANET-MERVILLE, J. & CAPONE, M. 2013. Anti-metastatic potential of human Vdelta1(+) gammadelta T cells in an orthotopic mouse xenograft model of colon carcinoma. *Cancer Immunol Immunother,* 62**,** 1199-210.

DHATCHINAMOORTHY, K., COLBERT, J. D. & ROCK, K. L. 2021. Cancer Immune Evasion Through Loss of MHC Class I Antigen Presentation. *Front Immunol,* 12**,** 636568.

DIAZ, L. A., COUGHLIN, C. M., WEIL, S. C., FISHEL, J., GOUNDER, M. M., LAWRENCE, S., AZAD, N., O'SHANNESSY, D. J., GRASSO, L., WUSTNER, J., EBEL, W. & CARVAJAL, R. D. 2015. A first-in-human phase I study of MORAb-004, a monoclonal antibody to endosialin in patients with advanced solid tumors. *Clin Cancer Res,* 21**,** 1281-8.

DIEFENBACH, A., JENSEN, E. R., JAMIESON, A. M. & RAULET, D. H. 2001. Rae1 and H60 ligands of the NKG2D receptor stimulate tumour immunity. *Nature,* 413**,** 165-71.

DING, C., LI, Y., GUO, F., JIANG, Y., YING, W., LI, D., YANG, D., XIA, X., LIU, W., ZHAO, Y., HE, Y., LI, X., SUN, W., LIU, Q., SONG, L., ZHEN, B., ZHANG, P., QIAN, X., QIN, J. & HE, F. 2016. A Cell-type-resolved Liver Proteome. *Mol Cell Proteomics,* 15**,** 3190-3202.

DING, W., XU, X., QIAN, Y., XUE, W., WANG, Y., DU, J., JIN, L. & TAN, Y. 2018. Prognostic value of tumor-infiltrating lymphocytes in hepatocellular carcinoma: A meta-analysis. *Medicine (Baltimore),* 97**,** e13301.

DIRSCHERL, K., SCHLAPFER, M., ROTH Z'GRAGGEN, B., WENGER, R. H., BOOY, C., FLURY-FREI, R., FATZER, R., ALOMAN, C., BARTOSCH, B., PARENT, R., KURTCUOGLU, V., DE ZELICOURT, D., SPAHN, D. R., BECK SCHIMMER, B. & SCHADDE, E. 2020. Hypoxia sensing by hepatic stellate cells leads to VEGF-dependent angiogenesis and may contribute to accelerated liver regeneration. *Sci Rep,* 10**,** 4392.

DOHERTY, D. G. & O'FARRELLY, C. 2000. Innate and adaptive lymphoid cells in the human liver. *Immunol Rev,* 174**,** 5-20.

DONG, N., SHI, X., WANG, S., GAO, Y., KUANG, Z., XIE, Q., LI, Y., DENG, H., WU, Y., LI, M. & LI, J. L. 2019. M2 macrophages mediate sorafenib resistance by secreting HGF in a feed-forward manner in hepatocellular carcinoma. *Br J Cancer,* 121**,** 22-33.

DONNEM, T., HU, J., FERGUSON, M., ADIGHIBE, O., SNELL, C., HARRIS, A. L., GATTER, K. C. & PEZZELLA, F. 2013. Vessel co-option in primary human tumors and metastases: an obstacle to effective anti-angiogenic treatment? *Cancer Med,* 2**,** 427-36.

DRIESSEN, R. C. H., STASSEN, O., SJOQVIST, M., SUAREZ RODRIGUEZ, F., GROLLEMAN, J., BOUTEN, C. V. C. & SAHLGREN, C. M. 2018. Shear stress induces expression, intracellular reorganization and enhanced Notch activation potential of Jagged1. *Integr Biol (Camb),* 10**,** 719-726.

DUARTE, S., BABER, J., FUJII, T. & COITO, A. J. 2015. Matrix metalloproteinases in liver injury, repair and fibrosis. *Matrix Biol,* 44-46**,** 147-56.

DUTROCHET, H. 1824. *Recherches anatomiques et physiologiques sur la structure intime des animaux et des végetaux, et sur leur motilité.*

EASL. 2018. Available: https://www.journal-of-hepatology.eu/action/showPdf?pii=S0168-8278%2818%2930215-0 [Accessed].

EHLING, J., BARTNECK, M., WEI, X., GREMSE, F., FECH, V., MOCKEL, D., BAECK, C., HITTATIYA, K., EULBERG, D., LUEDDE, T., KIESSLING, F., TRAUTWEIN, C., LAMMERS, T. & TACKE, F. 2014. CCL2-dependent infiltrating macrophages promote angiogenesis in progressive liver fibrosis. *Gut,* 63**,** 1960-1971.

EL-SERAG, H. B. & RUDOLPH, K. L. 2007. Hepatocellular carcinoma: epidemiology and molecular carcinogenesis. *Gastroenterology,* 132**,** 2557-76.

ELSEGOOD, C. L., CHAN, C. W., DEGLI-ESPOSTI, M. A., WIKSTROM, M. E., DOMENICHINI, A., LAZARUS, K., VAN ROOIJEN, N., GANSS, R., OLYNYK, J. K. & YEOH, G. C. 2015. Kupffer cell-monocyte communication is essential for initiating murine liver progenitor cell-mediated liver regeneration. *Hepatology,* 62**,** 1272-84.

ENDIG, J., BUITRAGO-MOLINA, L. E., MARHENKE, S., REISINGER, F., SABOROWSKI, A., SCHUTT, J., LIMBOURG, F., KONECKE, C., SCHREDER, A., MICHAEL, A., MISSLITZ, A. C., HEALY, M. E., GEFFERS, R., CLAVEL, T., HALLER, D., UNGER, K., FINEGOLD, M., WEBER, A., MANNS, M. P., LONGERICH, T., HEIKENWALDER, M. & VOGEL, A. 2016. Dual Role of the Adaptive Immune System in Liver Injury and Hepatocellular Carcinoma Development. *Cancer Cell,* 30**,** 308-323.

ERIKSSON, E. E., WERR, J., GUO, Y., THOREN, P. & LINDBOM, L. 2000. Direct observations in vivo on the role of endothelial selectins and alpha(4) integrin in cytokine-induced leukocyte-endothelium interactions in the mouse aorta. *Circ Res,* 86**,** 526-33.

ESTES, C., RAZAVI, H., LOOMBA, R., YOUNOSSI, Z. & SANYAL, A. J. 2018. Modeling the epidemic of nonalcoholic fatty liver disease demonstrates an exponential increase in burden of disease. *Hepatology,* 67**,** 123-133.

FAGERHOLM, S. C., GUENTHER, C., LLORT ASENS, M., SAVINKO, T. & UOTILA, L. M. 2019. Beta2-Integrins and Interacting Proteins in Leukocyte Trafficking, Immune Suppression, and Immunodeficiency Disease. *Front Immunol,* 10**,** 254.

FAGGIOLI, F., PALAGANO, E., DI TOMMASO, L., DONADON, M., MARRELLA, V., RECORDATI, C., MANTERO, S., VILLA, A., VEZZONI, P. & CASSANI, B. 2018. B lymphocytes limit senescence-driven fibrosis resolution and favor hepatocarcinogenesis in mouse liver injury. *Hepatology,* 67**,** 1970-1985.

FALKOWSKI, M., SCHLEDZEWSKI, K., HANSEN, B. & GOERDT, S. 2003. Expression of stabilin-2, a novel fasciclin-like hyaluronan receptor protein, in murine sinusoidal endothelia, avascular tissues, and at solid/liquid interfaces. *Histochem Cell Biol,* 120**,** 361-9.

FAURSCHOU, M. & BORREGAARD, N. 2003. Neutrophil granules and secretory vesicles in inflammation. *Microbes Infect,* 5**,** 1317-27.

FERAY, C. & LOPEZ-LABRADOR, F. X. 2019. Is PD-1 blockade a potential therapy for HBV? *JHEP Rep,* 1**,** 142-144.

FERNANDEZ, M., SEMELA, D., BRUIX, J., COLLE, I., PINZANI, M. & BOSCH, J. 2009. Angiogenesis in liver disease. *J Hepatol,* 50**,** 604-20.

FINGER, E. B., PURI, K. D., ALON, R., LAWRENCE, M. B., VON ANDRIAN, U. H. & SPRINGER, T. A. 1996. Adhesion through L-selectin requires a threshold hydrodynamic shear. *Nature,* 379**,** 266-9.

FINKIN, S., YUAN, D., STEIN, I., TANIGUCHI, K., WEBER, A., UNGER, K., BROWNING, J. L., GOOSSENS, N., NAKAGAWA, S., GUNASEKARAN, G., SCHWARTZ, M. E., KOBAYASHI, M., KUMADA, H., BERGER, M., PAPPO, O., RAJEWSKY, K., HOSHIDA, Y., KARIN, M., HEIKENWALDER, M., BEN-NERIAH, Y. & PIKARSKY, E. 2015. Ectopic lymphoid structures function as microniches for tumor progenitor cells in hepatocellular carcinoma. *Nat Immunol,* 16**,** 1235-44.

FISHER, B., RUSS, C., UPDEGRAFF, H. & FISHER, E. R. 1954. Effect of increased hepatic blood flow upon liver regeneration. *AMA Arch Surg,* 69**,** 263-72.

FOLKMAN, J. 1985. Tumor angiogenesis. *Adv Cancer Res,* 43**,** 175-203.

FREITAS-LOPES, M. A., MAFRA, K., DAVID, B. A., CARVALHO-GONTIJO, R. & MENEZES, G. B. 2017. Differential Location and Distribution of Hepatic Immune Cells. *Cells,* 6.

FRIDMAN, W. H., PAGÈS, F., SAUTÈS-FRIDMAN, C. & GALON, J. 2012. The immune contexture in human tumours: impact on clinical outcome. *Nat Rev Cancer,* 12**,** 298-306.

FU, J., XU, D., LIU, Z., SHI, M., ZHAO, P., FU, B., ZHANG, Z., YANG, H., ZHANG, H., ZHOU, C., YAO, J., JIN, L., WANG, H., YANG, Y., FU, Y. X. & WANG, F. S. 2007. Increased regulatory T cells correlate with CD8 T-cell impairment and poor survival in hepatocellular carcinoma patients. *Gastroenterology,* 132**,** 2328-39.

FU, J., ZHANG, Z., ZHOU, L., QI, Z., XING, S., LV, J., SHI, J., FU, B., LIU, Z., ZHANG, J. Y., JIN, L., ZHAO, Y., LAU, G. K., ZHAO, J. & WANG, F. S. 2013. Impairment of CD4+ cytotoxic T cells predicts poor survival and high recurrence rates in patients with hepatocellular carcinoma. *Hepatology,* 58**,** 139-49.

GABRILOVICH, D. I. & NAGARAJ, S. 2009. Myeloid-derived suppressor cells as regulators of the immune system. *Nat Rev Immunol,* 9**,** 162-74.

GANDHI, C. R. 2012. Oxidative Stress and Hepatic Stellate Cells: A PARADOXICAL RELATIONSHIP. *Trends Cell Mol Biol,* 7**,** 1-10.

GAO, Q., WANG, X. Y., QIU, S. J., YAMATO, I., SHO, M., NAKAJIMA, Y., ZHOU, J., LI, B. Z., SHI, Y. H., XIAO, Y. S., XU, Y. & FAN, J. 2009. Overexpression of PD-L1 significantly associates with tumor aggressiveness and postoperative recurrence in human hepatocellular carcinoma. *Clin Cancer Res,* 15**,** 971-9.

GARNELO, M., TAN, A., HER, Z., YEONG, J., LIM, C. J., CHEN, J., LIM, K. H., WEBER, A., CHOW, P., CHUNG, A., OOI, L. L., TOH, H. C., HEIKENWALDER, M., NG, I. O., NARDIN, A., CHEN, Q., ABASTADO, J. P. & CHEW, V. 2017. Interaction between tumour-infiltrating B cells and T cells controls the progression of hepatocellular carcinoma. *Gut,* 66**,** 342-351.

GERHARDT, H., GOLDING, M., FRUTTIGER, M., RUHRBERG, C., LUNDKVIST, A., ABRAMSSON, A., JELTSCH, M., MITCHELL, C., ALITALO, K., SHIMA, D. & BETSHOLTZ, C. 2003. VEGF guides angiogenic sprouting utilizing endothelial tip cell filopodia. *J Cell Biol,* 161**,** 1163-77.

GHANEM, I., RIVEIRO, M. E., PARADIS, V., FAIVRE, S., DE PARGA, P. M. & RAYMOND, E. 2014. Insights on the CXCL12-CXCR4 axis in hepatocellular carcinoma carcinogenesis. *Am J Transl Res,* 6**,** 340-52.

GHIRINGHELLI, F., MENARD, C., TERME, M., FLAMENT, C., TAIEB, J., CHAPUT, N., PUIG, P. E., NOVAULT, S., ESCUDIER, B., VIVIER, E., LECESNE, A., ROBERT, C., BLAY, J. Y., BERNARD, J., CAILLAT-ZUCMAN, S., FREITAS, A., TURSZ, T., WAGNER-BALLON, O., CAPRON, C., VAINCHENCKER, W., MARTIN, F. & ZITVOGEL, L. 2005. CD4+CD25+ regulatory T cells inhibit natural killer cell functions in a transforming growth factor-beta-dependent manner. *J Exp Med,* 202**,** 1075-85.

GIMBRONE, M. A., JR., LEAPMAN, S. B., COTRAN, R. S. & FOLKMAN, J. 1972. Tumor dormancy in vivo by prevention of neovascularization. *J Exp Med,* 136**,** 261-76.

GLOBAL BURDEN OF DISEASE LIVER CANCER, C., AKINYEMIJU, T., ABERA, S., AHMED, M., ALAM, N., ALEMAYOHU, M. A., ALLEN, C., AL-RADDADI, R., ALVIS-GUZMAN, N., AMOAKO, Y., ARTAMAN, A., AYELE, T. A., BARAC, A., BENSENOR, I., BERHANE, A., BHUTTA, Z., CASTILLO-RIVAS, J., CHITHEER, A., CHOI, J. Y., COWIE, B., DANDONA, L., DANDONA, R., DEY, S., DICKER, D., PHUC, H., EKWUEME, D. U., ZAKI, M. S., FISCHER, F., FURST, T., HANCOCK, J., HAY, S. I., HOTEZ, P., JEE, S. H., KASAEIAN, A., KHADER, Y., KHANG, Y. H., KUMAR, A., KUTZ, M., LARSON, H., LOPEZ, A., LUNEVICIUS, R., MALEKZADEH, R., MCALINDEN, C., MEIER, T., MENDOZA, W., MOKDAD, A., MORADI-LAKEH, M., NAGEL, G., NGUYEN, Q., NGUYEN, G., OGBO, F., PATTON, G., PEREIRA, D. M., POURMALEK, F., QORBANI, M., RADFAR, A., ROSHANDEL, G., SALOMON, J. A., SANABRIA, J., SARTORIUS, B., SATPATHY, M., SAWHNEY, M., SEPANLOU, S., SHACKELFORD, K., SHORE, H., SUN, J., MENGISTU, D. T., TOPOR-MADRY, R., TRAN, B., UKWAJA, K. N., VLASSOV, V., VOLLSET, S. E., VOS, T., WAKAYO, T., WEIDERPASS, E., WERDECKER, A., YONEMOTO, N., YOUNIS, M., YU, C., ZAIDI, Z., ZHU, L., MURRAY, C. J. L., NAGHAVI, M. & FITZMAURICE, C. 2017. The Burden of Primary Liver Cancer and Underlying Etiologies From 1990 to 2015 at the Global, Regional, and National Level: Results From the Global Burden of Disease Study 2015. *JAMA Oncol,* 3**,** 1683-1691.

GOEL, R. & EAPEN, C. E. 2022. Recognizing Dysfunctional Innate and Adaptive Immune Responses Contributing to Liver Damage in Patients With Cirrhosis. *J Clin Exp Hepatol,* 12**,** 993-1002.

GREENLEE-WACKER, M. C., BRISENO, C., GALVAN, M., MORIEL, G., VELAZQUEZ, P. & BOHLSON, S. S. 2011. Membrane-associated CD93 regulates leukocyte migration and C1q-hemolytic activity during murine peritonitis. *J Immunol,* 187**,** 3353-61.

HALDER, R. C., AGUILERA, C., MARICIC, I. & KUMAR, V. 2007. Type II NKT cell-mediated anergy induction in type I NKT cells prevents inflammatory liver disease. *J Clin Invest,* 117**,** 2302-12.

HAMAGUCHI, M., OKAMURA, T., FUKUDA, T., NISHIDA, K., YOSHIMURA, Y., HASHIMOTO, Y., USHIGOME, E., NAKANISHI, N., MAJIMA, S., ASANO, M., YAMAZAKI, M., TAKAKUWA, H., KITA, M. & FUKUI, M. 2021. Group 3 Innate Lymphoid Cells Protect Steatohepatitis From High-Fat Diet Induced Toxicity. *Front Immunol,* 12**,** 648754.

HAMMERICH, L., BANGEN, J. M., GOVAERE, O., ZIMMERMANN, H. W., GASSLER, N., HUSS, S., LIEDTKE, C., PRINZ, I., LIRA, S. A., LUEDDE, T., ROSKAMS, T., TRAUTWEIN, C., HEYMANN, F. & TACKE, F. 2014. Chemokine receptor CCR6-dependent accumulation of gammadelta T cells in injured liver restricts hepatic inflammation and fibrosis. *Hepatology,* 59**,** 630-42.

HAMMERICH, L., HEYMANN, F. & TACKE, F. 2011. Role of IL-17 and Th17 cells in liver diseases. *Clin Dev Immunol,* 2011**,** 345803.

HANAHAN, D. & FOLKMAN, J. 1996. Patterns and emerging mechanisms of the angiogenic switch during tumorigenesis. *Cell,* 86**,** 353-64.

HANAHAN, D. & WEINBERG, R. A. 2011. Hallmarks of cancer: the next generation. *Cell,* 144**,** 646-74.

HAYBAECK, J., ZELLER, N., WOLF, M. J., WEBER, A., WAGNER, U., KURRER, M. O., BREMER, J., IEZZI, G., GRAF, R., CLAVIEN, P. A., THIMME, R., BLUM, H., NEDOSPASOV, S. A., ZATLOUKAL, K., RAMZAN, M., CIESEK, S., PIETSCHMANN, T., MARCHE, P. N., KARIN, M., KOPF, M., BROWNING, J. L., AGUZZI, A. & HEIKENWALDER, M. 2009. A lymphotoxin-driven pathway to hepatocellular carcinoma. *Cancer Cell,* 16**,** 295-308.

HELMLINGER, G., NETTI, P. A., LICHTENBELD, H. C., MELDER, R. J. & JAIN, R. K. 1997. Solid stress inhibits the growth of multicellular tumor spheroids. *Nat Biotechnol,* 15**,** 778-83.

HOU, L., JIE, Z., DESAI, M., LIANG, Y., SOONG, L., WANG, T. & SUN, J. 2013. Early IL-17 production by intrahepatic T cells is important for adaptive immune responses in viral hepatitis. *J Immunol,* 190**,** 621-9.

HUANG, W., HE, W., SHI, X., HE, X., DOU, L. & GAO, Y. 2018. The Role of CD1d and MR1 Restricted T Cells in the Liver. *Front Immunol,* 9**,** 2424.

HUANG, Y., LIAO, H., ZHANG, Y., YUAN, R., WANG, F., GAO, Y., WANG, P. & DU, Z. 2014. Prognostic value of tumor-infiltrating FoxP3+ T cells in gastrointestinal cancers: a meta analysis. *PLoS One,* 9**,** e94376.

HUANG, Y., WANG, F. M., WANG, T., WANG, Y. J., ZHU, Z. Y., GAO, Y. T. & DU, Z. 2012. Tumor-infiltrating FoxP3+ Tregs and CD8+ T cells affect the prognosis of hepatocellular carcinoma patients. *Digestion,* 86**,** 329-37.

HUDSPETH, K., DONADON, M., CIMINO, M., PONTARINI, E., TENTORIO, P., PRETI, M., HONG, M., BERTOLETTI, A., BICCIATO, S., INVERNIZZI, P., LUGLI, E., TORZILLI, G., GERSHWIN, M. E. & MAVILIO, D. 2016. Human liver-resident CD56(bright)/CD16(neg) NK cells are retained within hepatic sinusoids via the engagement of CCR5 and CXCR6 pathways. *J Autoimmun,* 66**,** 40-50.

HUNT, B. J. & JURD, K. M. 1998. Endothelial cell activation. A central pathophysiological process. *BMJ,* 316**,** 1328-9.

IBUSUKI, R., UTO, H., ARIMA, S., MAWATARI, S., SETOGUCHI, Y., IWASHITA, Y., HASHIMOTO, S., MAEDA, T., TANOUE, S., KANMURA, S., OKETANI, M., IDO, A. & TSUBOUCHI, H. 2013. Transgenic expression of human neutrophil peptide-1 enhances hepatic fibrosis in mice fed a choline-deficient, L-amino acid-defined diet. *Liver Int,* 33**,** 1549-56.

IHLING, C., NAUGHTON, B., ZHANG, Y., ROLFE, P. A., FRICK-KRIEGER, E., TERRACCIANO, L. M. & DUSSAULT, I. 2019. Observational Study of PD-L1, TGF-beta, and Immune Cell Infiltrates in Hepatocellular Carcinoma. *Front Med (Lausanne),* 6**,** 15.

JAIN, R. K. 2003. Molecular regulation of vessel maturation. *Nat Med,* 9**,** 685-93.

JAIN, R. K. 2005. Normalization of tumor vasculature: an emerging concept in antiangiogenic therapy. *Science,* 307**,** 58-62.

JENNE, C. N. & KUBES, P. 2013. Immune surveillance by the liver. *Nat Immunol,* 14**,** 996-1006.

JENNE, C. N., WONG, C. H., ZEMP, F. J., MCDONALD, B., RAHMAN, M. M., FORSYTH, P. A., MCFADDEN, G. & KUBES, P. 2013. Neutrophils recruited to sites of infection protect from virus challenge by releasing neutrophil extracellular traps. *Cell Host Microbe,* 13**,** 169-80.

JUENGPANICH, S., SHI, L., IRANMANESH, Y., CHEN, J., CHENG, Z., KHOO, A. K., PAN, L., WANG, Y. & CAI, X. 2019. The role of natural killer cells in hepatocellular carcinoma development and treatment: A narrative review. *Transl Oncol,* 12**,** 1092-1107.

KAKUMU, S., ITO, S., ISHIKAWA, T., MITA, Y., TAGAYA, T., FUKUZAWA, Y. & YOSHIOKA, K. 2000. Decreased function of peripheral blood dendritic cells in patients with hepatocellular carcinoma with hepatitis B and C virus infection. *J Gastroenterol Hepatol,* 15**,** 431-6.

KAWARABAYASHI, N., SEKI, S., HATSUSE, K., OHKAWA, T., KOIKE, Y., AIHARA, T., HABU, Y., NAKAGAWA, R., AMI, K., HIRAIDE, H. & MOCHIZUKI, H. 2000. Decrease of CD56(+)T cells and natural killer cells in cirrhotic livers with hepatitis C may be involved in their susceptibility to hepatocellular carcinoma. *Hepatology,* 32**,** 962-9.

KESSENBROCK, K., PLAKS, V. & WERB, Z. 2010. Matrix metalloproteinases: regulators of the tumor microenvironment. *Cell,* 141**,** 52-67.

KHAN, K. A., NAYLOR, A. J., KHAN, A., NOY, P. J., MAMBRETTI, M., LODHIA, P., ATHWAL, J., KORZYSTKA, A., BUCKLEY, C. D., WILLCOX, B. E., MOHAMMED, F. & BICKNELL, R. 2017. Multimerin-2 is a ligand for group 14 family C-type lectins CLEC14A, CD93 and CD248 spanning the endothelial pericyte interface. *Oncogene,* 36**,** 6097-6108.

KI, S. H., PARK, O., ZHENG, M., MORALES-IBANEZ, O., KOLLS, J. K., BATALLER, R. & GAO, B. 2010. Interleukin-22 treatment ameliorates alcoholic liver injury in a murine model of chronic-binge ethanol feeding: role of signal transducer and activator of transcription 3. *Hepatology,* 52**,** 1291-300.

KIM, C. H., HASHIMOTO-HILL, S. & KIM, M. 2016. Migration and Tissue Tropism of Innate Lymphoid Cells. *Trends Immunol,* 37**,** 68-79.

KNOLLE, P. A. & THIMME, R. 2014. Hepatic immune regulation and its involvement in viral hepatitis infection. *Gastroenterology,* 146**,** 1193-207.

KOCABAYOGLU, P., LADE, A., LEE, Y. A., DRAGOMIR, A. C., SUN, X., FIEL, M. I., THUNG, S., ALOMAN, C., SORIANO, P., HOSHIDA, Y. & FRIEDMAN, S. L. 2015. beta-PDGF receptor expressed by hepatic stellate cells regulates fibrosis in murine liver injury, but not carcinogenesis. *J Hepatol,* 63**,** 141-7.

KOHN, S., NAGY, J. A., DVORAK, H. F. & DVORAK, A. M. 1992. Pathways of macromolecular tracer transport across venules and small veins. Structural basis for the hyperpermeability of tumor blood vessels. *Lab Invest,* 67**,** 596-607.

KOLIOS, G., VALATAS, V. & KOUROUMALIS, E. 2006. Role of Kupffer cells in the pathogenesis of liver disease. *World J Gastroenterol,* 12**,** 7413-20.

KONFORTION, J., COUPLAND, V. H., KOCHER, H. M., ALLUM, W., GROCOCK, M. J. & JACK, R. H. 2014. Time and deprivation trends in incidence of primary liver cancer subtypes in England. *J Eval Clin Pract,* 20**,** 498-504.

KONG, L., ZHOU, Y., BU, H., LV, T., SHI, Y. & YANG, J. 2016. Deletion of interleukin-6 in monocytes/macrophages suppresses the initiation of hepatocellular carcinoma in mice. *J Exp Clin Cancer Res,* 35**,** 131.

KRIZHANOVSKY, V., YON, M., DICKINS, R. A., HEARN, S., SIMON, J., MIETHING, C., YEE, H., ZENDER, L. & LOWE, S. W. 2008. Senescence of activated stellate cells limits liver fibrosis. *Cell,* 134**,** 657-67.

KUANG, D. M., PENG, C., ZHAO, Q., WU, Y., CHEN, M. S. & ZHENG, L. 2010. Activated monocytes in peritumoral stroma of hepatocellular carcinoma promote expansion of memory T helper 17 cells. *Hepatology,* 51**,** 154-64.

KUNKEL, E. J. & LEY, K. 1996. Distinct phenotype of E-selectin-deficient mice. E-selectin is required for slow leukocyte rolling in vivo. *Circ Res,* 79**,** 1196-204.

KURIOKA, A., WALKER, L. J., KLENERMAN, P. & WILLBERG, C. B. 2016. MAIT cells: new guardians of the liver. *Clin Transl Immunology,* 5**,** e98.

LALOR, P. F., SUN, P. J., WESTON, C. J., MARTIN-SANTOS, A., WAKELAM, M. J. & ADAMS, D. H. 2007. Activation of vascular adhesion protein-1 on liver endothelium results in an NF-kappaB-dependent increase in lymphocyte adhesion. *Hepatology,* 45**,** 465-74.

LANGHANS, B., NISCHALKE, H. D., KRAMER, B., DOLD, L., LUTZ, P., MOHR, R., VOGT, A., TOMA, M., EIS-HUBINGER, A. M., NATTERMANN, J., STRASSBURG, C. P., GONZALEZ-CARMONA, M. A. & SPENGLER, U. 2019. Role of regulatory T cells and checkpoint inhibition in hepatocellular carcinoma. *Cancer Immunol Immunother,* 68**,** 2055-2066.

LAWRENCE, M. B., KANSAS, G. S., KUNKEL, E. J. & LEY, K. 1997. Threshold levels of fluid shear promote leukocyte adhesion through selectins (CD62L,P,E). *J Cell Biol,* 136**,** 717-27.

LAX, S., HOU, T. Z., JENKINSON, E., SALMON, M., MACFADYEN, J. R., ISACKE, C. M., ANDERSON, G., CUNNINGHAM, A. F. & BUCKLEY, C. D. 2007. CD248/Endosialin is dynamically expressed on a subset of stromal cells during lymphoid tissue development, splenic remodeling and repair. *FEBS Lett,* 581**,** 3550-6.

LEACH, D. R., KRUMMEL, M. F. & ALLISON, J. P. 1996. Enhancement of antitumor immunity by CTLA-4 blockade. *Science,* 271**,** 1734-6.

LECOT, P., SARABI, M., PEREIRA ABRANTES, M., MUSSARD, J., KOENDERMAN, L., CAUX, C., BENDRISS-VERMARE, N. & MICHALLET, M. C. 2019. Neutrophil Heterogeneity in Cancer: From Biology to Therapies. *Front Immunol,* 10**,** 2155.

LEE, E. S., BOLDO, L. S., FERNANDEZ, B. O., FEELISCH, M. & HARMSEN, M. C. 2017a. Suppression of TAK1 pathway by shear stress counteracts the inflammatory endothelial cell phenotype induced by oxidative stress and TGF-beta1. *Sci Rep,* 7**,** 42487.

LEE, J., AHN, E., KISSICK, H. T. & AHMED, R. 2015. Reinvigorating Exhausted T Cells by Blockade of the PD-1 Pathway. *For Immunopathol Dis Therap,* 6**,** 7-17.

LEE, S., RHO, S. S., PARK, H., PARK, J. A., KIM, J., LEE, I. K., KOH, G. Y., MOCHIZUKI, N., KIM, Y. M. & KWON, Y. G. 2017b. Carbohydrate-binding protein CLEC14A regulates VEGFR-2- and VEGFR-3-dependent signals during angiogenesis and lymphangiogenesis. *J Clin Invest,* 127**,** 457-471.

LEITE-DE-MORAES, M. C., MOREAU, G., ARNOULD, A., MACHAVOINE, F., GARCIA, C., PAPIERNIK, M. & DY, M. 1998. IL-4-producing NK T cells are biased towards IFN-gamma production by IL-12. Influence of the microenvironment on the functional capacities of NK T cells. *Eur J Immunol,* 28**,** 1507-15.

LEY, K., LAUDANNA, C., CYBULSKY, M. I. & NOURSHARGH, S. 2007. Getting to the site of inflammation: the leukocyte adhesion cascade updated. *Nat Rev Immunol,* 7**,** 678-89.

LI, Q., HAN, J., YANG, Y. & CHEN, Y. 2022. PD-1/PD-L1 checkpoint inhibitors in advanced hepatocellular carcinoma immunotherapy. *Front Immunol,* 13**,** 1070961.

LI, X., XING, Y. F., LEI, A. H., XIAO, Q., LIN, Z. H., HONG, Y. F., WU, X. Y. & ZHOU, J. 2017. Neutrophil count is associated with myeloid derived suppressor cell level and presents prognostic value of for hepatocellular carcinoma patients. *Oncotarget,* 8**,** 24380-24388.

LI, X. S., LI, J. W., LI, H. & JIANG, T. 2020. Prognostic value of programmed cell death ligand 1 (PD-L1) for hepatocellular carcinoma: a meta-analysis. *Biosci Rep,* 40.

LIANG, C. M., CHEN, L., HU, H., MA, H. Y., GAO, L. L., QIN, J. & ZHONG, C. P. 2015. Chemokines and their receptors play important roles in the development of hepatocellular carcinoma. *World J Hepatol,* 7**,** 1390-402.

LIN, S. Z., CHEN, K. J., XU, Z. Y., CHEN, H., ZHOU, L., XIE, H. Y. & ZHENG, S. S. 2013. Prediction of recurrence and survival in hepatocellular carcinoma based on two Cox models mainly determined by FoxP3+ regulatory T cells. *Cancer Prev Res (Phila),* 6**,** 594-602.

LING, N. R., BISHOP, S. & JEFFERIS 1977. Use of antibody-coated red cells for the sensitive detection of antigen and in rosette tests for cells bearing surface immunoglobulins. *J Immunol Methods,* 15**,** 279-89.

LIU, J., GHANIM, M., XUE, L., BROWN, C. D., IOSSIFOV, I., ANGELETTI, C., HUA, S., NEGRE, N., LUDWIG, M., STRICKER, T., AL-AHMADIE, H. A., TRETIAKOVA, M., CAMP, R. L., PERERA-ALBERTO, M., RIMM, D. L., XU, T., RZHETSKY, A. & WHITE, K. P. 2009. Analysis of Drosophila segmentation network identifies a JNK pathway factor overexpressed in kidney cancer. *Science,* 323**,** 1218-22.

LIU, Z. X., HAN, D., GUNAWAN, B. & KAPLOWITZ, N. 2006. Neutrophil depletion protects against murine acetaminophen hepatotoxicity. *Hepatology,* 43**,** 1220-30.

LLOVET, J. M., KELLEY, R. K., VILLANUEVA, A., SINGAL, A. G., PIKARSKY, E., ROAYAIE, S., LENCIONI, R., KOIKE, K., ZUCMAN-ROSSI, J. & FINN, R. S. 2021. Hepatocellular carcinoma. *Nat Rev Dis Primers,* 7**,** 6.

LOO, B. M., KREUGER, J., JALKANEN, M., LINDAHL, U. & SALMIVIRTA, M. 2001. Binding of heparin/heparan sulfate to fibroblast growth factor receptor 4. *J Biol Chem,* 276**,** 16868-76.

LORENZON, E., COLLADEL, R., ANDREUZZI, E., MARASTONI, S., TODARO, F., SCHIAPPACASSI, M., LIGRESTI, G., COLOMBATTI, A. & MONGIAT, M. 2012. MULTIMERIN2 impairs tumor angiogenesis and growth by interfering with VEGF-A/VEGFR2 pathway. *Oncogene,* 31**,** 3136-47.

LOUIS, H., LE MOINE, O., PENY, M. O., GULBIS, B., NISOL, F., GOLDMAN, M. & DEVIERE, J. 1997. Hepatoprotective role of interleukin 10 in galactosamine/lipopolysaccharide mouse liver injury. *Gastroenterology,* 112**,** 935-42.

MAHER, J. J. 2001. Interactions between hepatic stellate cells and the immune system. *Semin Liver Dis,* 21**,** 417-26.

MAISONPIERRE, P. C., SURI, C., JONES, P. F., BARTUNKOVA, S., WIEGAND, S. J., RADZIEJEWSKI, C., COMPTON, D., MCCLAIN, J., ALDRICH, T. H., PAPADOPOULOS, N., DALY, T. J., DAVIS, S., SATO, T. N. & YANCOPOULOS, G. D. 1997. Angiopoietin-2, a natural antagonist for Tie2 that disrupts in vivo angiogenesis. *Science,* 277**,** 55-60.

MALARKEY, D. E., JOHNSON, K., RYAN, L., BOORMAN, G. & MARONPOT, R. R. 2005. New insights into functional aspects of liver morphology. *Toxicol Pathol,* 33**,** 27-34.

MANDRYCKY, C., HADLAND, B. & ZHENG, Y. 2020. 3D curvature-instructed endothelial flow response and tissue vascularization. *Sci Adv,* 6.

MARICIC, I., SHENG, H., MARRERO, I., SEKI, E., KISSELEVA, T., CHATURVEDI, S., MOLLE, N., MATHEWS, S. A., GAO, B. & KUMAR, V. 2015. Inhibition of type I natural killer T cells by retinoids or following sulfatide-mediated activation of type II natural killer T cells attenuates alcoholic liver disease in mice. *Hepatology,* 61**,** 1357-69.

MARRA, F. & TACKE, F. 2014. Roles for chemokines in liver disease. *Gastroenterology,* 147**,** 577-594 e1.

MARRERO, J. A., KULIK, L. M., SIRLIN, C. B., ZHU, A. X., FINN, R. S., ABECASSIS, M. M., ROBERTS, L. R. & HEIMBACH, J. K. 2018. Diagnosis, Staging, and Management of Hepatocellular Carcinoma: 2018 Practice Guidance by the American Association for the Study of Liver Diseases. *Hepatology,* 68**,** 723-750.

MASIERO, M., SIMOES, F. C., HAN, H. D., SNELL, C., PETERKIN, T., BRIDGES, E., MANGALA, L. S., WU, S. Y., PRADEEP, S., LI, D., HAN, C., DALTON, H., LOPEZ-BERESTEIN, G., TUYNMAN, J. B., MORTENSEN, N., LI, J. L., PATIENT, R., SOOD, A. K., BANHAM, A. H., HARRIS, A. L. & BUFFA, F. M. 2013. A core human primary tumor angiogenesis signature identifies the endothelial orphan receptor ELTD1 as a key regulator of angiogenesis. *Cancer Cell,* 24**,** 229-41.

MASYUK, A. I., MASYUK, T. V. & LARUSSO, N. F. 2008. Cholangiocyte primary cilia in liver health and disease. *Dev Dyn,* 237**,** 2007-12.

MAZZAFERRO, V., BHOORI, S., SPOSITO, C., BONGINI, M., LANGER, M., MICELI, R. & MARIANI, L. 2011. Milan criteria in liver transplantation for hepatocellular carcinoma: an evidence-based analysis of 15 years of experience. *Liver Transpl,* 17 Suppl 2**,** S44-57.

MCDONALD, B., MCAVOY, E. F., LAM, F., GILL, V., DE LA MOTTE, C., SAVANI, R. C. & KUBES, P. 2008. Interaction of CD44 and hyaluronan is the dominant mechanism for neutrophil sequestration in inflamed liver sinusoids. *J Exp Med,* 205**,** 915-27.

MCDONALD, B., URRUTIA, R., YIPP, B. G., JENNE, C. N. & KUBES, P. 2012. Intravascular neutrophil extracellular traps capture bacteria from the bloodstream during sepsis. *Cell Host Microbe,* 12**,** 324-33.

MCHEDLIDZE, T., WALDNER, M., ZOPF, S., WALKER, J., RANKIN, A. L., SCHUCHMANN, M., VOEHRINGER, D., MCKENZIE, A. N., NEURATH, M. F., PFLANZ, S. & WIRTZ, S. 2013. Interleukin-33-dependent innate lymphoid cells mediate hepatic fibrosis. *Immunity,* 39**,** 357-71.

MCNAB, G., REEVES, J. L., SALMI, M., HUBSCHER, S., JALKANEN, S. & ADAMS, D. H. 1996. Vascular adhesion protein 1 mediates binding of T cells to human hepatic endothelium. *Gastroenterology,* 110**,** 522-8.

MEDINA, J., SANZ-CAMENO, P., GARCIA-BUEY, L., MARTIN-VILCHEZ, S., LOPEZ-CABRERA, M. & MORENO-OTERO, R. 2005. Evidence of angiogenesis in primary biliary cirrhosis: an immunohistochemical descriptive study. *J Hepatol,* 42**,** 124-31.

MENDEZ-SANCHEZ, N., CORDOVA-GALLARDO, J., BARRANCO-FRAGOSO, B. & ESLAM, M. 2021. Hepatic Dendritic Cells in the Development and Progression of Metabolic Steatohepatitis. *Front Immunol,* 12**,** 641240.

MENEZES, G. B., LEE, W. Y., ZHOU, H., WATERHOUSE, C. C., CARA, D. C. & KUBES, P. 2009. Selective down-regulation of neutrophil Mac-1 in endotoxemic hepatic microcirculation via IL-10. *J Immunol,* 183**,** 7557-68.

MENG, F., WANG, K., AOYAMA, T., GRIVENNIKOV, S. I., PAIK, Y., SCHOLTEN, D., CONG, M., IWAISAKO, K., LIU, X., ZHANG, M., OSTERREICHER, C. H., STICKEL, F., LEY, K., BRENNER, D. A. & KISSELEVA, T. 2012. Interleukin-17 signaling in inflammatory, Kupffer cells, and hepatic stellate cells exacerbates liver fibrosis in mice. *Gastroenterology,* 143**,** 765-776 e3.

MENG, Q., LI, X. & XIONG, X. 2022. Identification of Hub Genes Associated With Non-alcoholic Steatohepatitis Using Integrated Bioinformatics Analysis. *Front Genet,* 13**,** 872518.

MENYHART, O., NAGY, A. & GYORFFY, B. 2018. Determining consistent prognostic biomarkers of overall survival and vascular invasion in hepatocellular carcinoma. *R Soc Open Sci,* 5**,** 181006.

MICHALOPOULOS, G. K. 2007. Liver regeneration. *J Cell Physiol,* 213**,** 286-300.

MIKULAK, J., BRUNI, E., ORIOLO, F., DI VITO, C. & MAVILIO, D. 2019. Hepatic Natural Killer Cells: Organ-Specific Sentinels of Liver Immune Homeostasis and Physiopathology. *Front Immunol,* 10**,** 946.

MITROULIS, I., ALEXAKI, V. I., KOURTZELIS, I., ZIOGAS, A., HAJISHENGALLIS, G. & CHAVAKIS, T. 2015. Leukocyte integrins: role in leukocyte recruitment and as therapeutic targets in inflammatory disease. *Pharmacol Ther,* 147**,** 123-135.

MITSUHASHI, N., SHIMIZU, H., OHTSUKA, M., WAKABAYASHI, Y., ITO, H., KIMURA, F., YOSHIDOME, H., KATO, A., NUKUI, Y. & MIYAZAKI, M. 2003. Angiopoietins and Tie-2 expression in angiogenesis and proliferation of human hepatocellular carcinoma. *Hepatology,* 37**,** 1105-13.

MIURA, K., KODAMA, Y., INOKUCHI, S., SCHNABL, B., AOYAMA, T., OHNISHI, H., OLEFSKY, J. M., BRENNER, D. A. & SEKI, E. 2010. Toll-like receptor 9 promotes steatohepatitis by induction of interleukin-1beta in mice. *Gastroenterology,* 139**,** 323-34 e7.

MOAWAD, A. W., SZKLARUK, J., LALL, C., BLAIR, K. J., KASEB, A. O., KAMATH, A., ROHREN, S. A. & ELSAYES, K. M. 2020. Angiogenesis in Hepatocellular Carcinoma; Pathophysiology, Targeted Therapy, and Role of Imaging. *J Hepatocell Carcinoma,* 7**,** 77-89.

MOHAMADZADEH, M., DEGRENDELE, H., ARIZPE, H., ESTESS, P. & SIEGELMAN, M. 1998. Proinflammatory stimuli regulate endothelial hyaluronan expression and CD44/HA-dependent primary adhesion. *J Clin Invest,* 101**,** 97-108.

MOON, W. S., RHYU, K. H., KANG, M. J., LEE, D. G., YU, H. C., YEUM, J. H., KOH, G. Y. & TARNAWSKI, A. S. 2003. Overexpression of VEGF and angiopoietin 2: a key to high vascularity of hepatocellular carcinoma? *Mod Pathol,* 16**,** 552-7.

MORENO, A. H., BURCHELL, A. R., ROUSSELOT, L. M., PANKE, W. F., SLAFSKY, F. & BURKE, J. H. 1967. Portal blood flow in cirrhosis of the liver. *J Clin Invest,* 46**,** 436-45.

MORIGI, M., ZOJA, C., FIGLIUZZI, M., FOPPOLO, M., MICHELETTI, G., BONTEMPELLI, M., SARONNI, M., REMUZZI, G. & REMUZZI, A. 1995. Fluid shear stress modulates surface expression of adhesion molecules by endothelial cells. *Blood,* 85**,** 1696-703.

MORO-SIBILOT, L., BLANC, P., TAILLARDET, M., BARDEL, E., COUILLAULT, C., BOSCHETTI, G., TRAVERSE-GLEHEN, A., DEFRANCE, T., KAISERLIAN, D. & DUBOIS, B. 2016. Mouse and Human Liver Contain Immunoglobulin A-Secreting Cells Originating From Peyer's Patches and Directed Against Intestinal Antigens. *Gastroenterology,* 151**,** 311-23.

MORVAN, M. G. & LANIER, L. L. 2016. NK cells and cancer: you can teach innate cells new tricks. *Nat Rev Cancer,* 16**,** 7-19.

MULLER, W. A. 2011. Mechanisms of leukocyte transendothelial migration. *Annu Rev Pathol,* 6**,** 323-44.

MURA, M., SWAIN, R. K., ZHUANG, X., VORSCHMITT, H., REYNOLDS, G., DURANT, S., BEESLEY, J. F., HERBERT, J. M., SHELDON, H., ANDRE, M., SANDERSON, S., GLEN, K., LUU, N. T., MCGETTRICK, H. M., ANTCZAK, P., FALCIANI, F., NASH, G. B., NAGY, Z. S. & BICKNELL, R. 2012. Identification and angiogenic role of the novel tumor endothelial marker CLEC14A. *Oncogene,* 31**,** 293-305.

NABEKURA, T., RIGGAN, L., HILDRETH, A. D., O'SULLIVAN, T. E. & SHIBUYA, A. 2020. Type 1 Innate Lymphoid Cells Protect Mice from Acute Liver Injury via Interferon-gamma Secretion for Upregulating Bcl-xL Expression in Hepatocytes. *Immunity,* 52**,** 96-108 e9.

NAGARAJ, S., COLLAZO, M., CORZO, C. A., YOUN, J. I., ORTIZ, M., QUICENO, D. & GABRILOVICH, D. I. 2009. Regulatory myeloid suppressor cells in health and disease. *Cancer Res,* 69**,** 7503-6.

NAGEL, T., RESNICK, N., ATKINSON, W. J., DEWEY, C. F., JR. & GIMBRONE, M. A., JR. 1994. Shear stress selectively upregulates intercellular adhesion molecule-1 expression in cultured human vascular endothelial cells. *J Clin Invest,* 94**,** 885-91.

NAKAGAWA, H., SUZUKI, N., HIRATA, Y., HIKIBA, Y., HAYAKAWA, Y., KINOSHITA, H., IHARA, S., UCHINO, K., NISHIKAWA, Y., IJICHI, H., OTSUKA, M., ARITA, J., SAKAMOTO, Y., HASEGAWA, K., KOKUDO, N., TATEISHI, K. & KOIKE, K. 2017. Biliary epithelial injury-induced regenerative response by IL-33 promotes cholangiocarcinogenesis from peribiliary glands. *Proc Natl Acad Sci U S A,* 114**,** E3806-E3815.

NANDA, A., KARIM, B., PENG, Z., LIU, G., QIU, W., GAN, C., VOGELSTEIN, B., ST CROIX, B., KINZLER, K. W. & HUSO, D. L. 2006. Tumor endothelial marker 1 (Tem1) functions in the growth and progression of abdominal tumors. *Proc Natl Acad Sci U S A,* 103**,** 3351-6.

NEUMANN, K., KARIMI, K., MEINERS, J., VOETLAUSE, R., STEINMANN, S., DAMMERMANN, W., LUTH, S., ASGHARI, F., WEGSCHEID, C., HORST, A. K. & TIEGS, G. 2017. A Proinflammatory Role of Type 2 Innate Lymphoid Cells in Murine Immune-Mediated Hepatitis. *J Immunol,* 198**,** 128-137.

NICE. 2017. Available: https://www.nice.org.uk/guidance/qs152/chapter/quality-statement-4-surveillance-for-hepatocellular-carcinoma [Accessed].

NIE, Y., JIANG, M. C., LIU, C., LIU, Q. & ZHU, X. 2021. CXCL5 Has Potential to Be a Marker for Hepatocellular Carcinoma Prognosis and Was Correlating With Immune Infiltrates. *Front Oncol,* 11**,** 637023.

NORRIS, S., COLLINS, C., DOHERTY, D. G., SMITH, F., MCENTEE, G., TRAYNOR, O., NOLAN, N., HEGARTY, J. & O'FARRELLY, C. 1998. Resident human hepatic lymphocytes are phenotypically different from circulating lymphocytes. *J Hepatol,* 28**,** 84-90.

NORRIS, S., DOHERTY, D. G., COLLINS, C., MCENTEE, G., TRAYNOR, O., HEGARTY, J. E. & O'FARRELLY, C. 1999. Natural T cells in the human liver: cytotoxic lymphocytes with dual T cell and natural killer cell phenotype and function are phenotypically heterogenous and include Valpha24-JalphaQ and gammadelta T cell receptor bearing cells. *Hum Immunol,* 60**,** 20-31.

NOVOBRANTSEVA, T. I., MAJEAU, G. R., AMATUCCI, A., KOGAN, S., BRENNER, I., CASOLA, S., SHLOMCHIK, M. J., KOTELIANSKY, V., HOCHMAN, P. S. & IBRAGHIMOV, A. 2005. Attenuated liver fibrosis in the absence of B cells. *J Clin Invest,* 115**,** 3072-82.

NOY, P. J., LODHIA, P., KHAN, K., ZHUANG, X., WARD, D. G., VERISSIMO, A. R., BACON, A. & BICKNELL, R. 2015. Blocking CLEC14A-MMRN2 binding inhibits sprouting angiogenesis and tumour growth. *Oncogene,* 34**,** 5821-31.

NOY, P. J., SWAIN, R. K., KHAN, K., LODHIA, P. & BICKNELL, R. 2016. Sprouting angiogenesis is regulated by shedding of the C-type lectin family 14, member A (CLEC14A) ectodomain, catalyzed by rhomboid-like 2 protein (RHBDL2). *FASEB J,* 30**,** 2311-23.

O'LEARY, K. 2021. T cell drivers in NASH-HCC. *Nat Rev Cancer,* 21**,** 341.

OCHI, M., OHDAN, H., MITSUTA, H., ONOE, T., TOKITA, D., HARA, H., ISHIYAMA, K., ZHOU, W., TANAKA, Y. & ASAHARA, T. 2004. Liver NK cells expressing TRAIL are toxic against self hepatocytes in mice. *Hepatology,* 39**,** 1321-31.

OKEN, M. M., CREECH, R. H., TORMEY, D. C., HORTON, J., DAVIS, T. E., MCFADDEN, E. T. & CARBONE, P. P. 1982. Toxicity and response criteria of the Eastern Cooperative Oncology Group. *Am J Clin Oncol,* 5**,** 649-55.

OO, Y. H., SHETTY, S. & ADAMS, D. H. 2010. The role of chemokines in the recruitment of lymphocytes to the liver. *Dig Dis,* 28**,** 31-44.

OUYANG, F. Z., WU, R. Q., WEI, Y., LIU, R. X., YANG, D., XIAO, X., ZHENG, L., LI, B., LAO, X. M. & KUANG, D. M. 2016. Dendritic cell-elicited B-cell activation fosters immune privilege via IL-10 signals in hepatocellular carcinoma. *Nat Commun,* 7**,** 13453.

PAIN, V. M., GARLICK, P. J. & MCNURLAN, M. A. 1978. Synthesis of albumin and of total plasma proteins by liver of fed and starved rats. *Proc Nutr Soc,* 37**,** 29A.

PALMER, D. H., MIDGLEY, R. S., MIRZA, N., TORR, E. E., AHMED, F., STEELE, J. C., STEVEN, N. M., KERR, D. J., YOUNG, L. S. & ADAMS, D. H. 2009. A phase II study of adoptive immunotherapy using dendritic cells pulsed with tumor lysate in patients with hepatocellular carcinoma. *Hepatology,* 49**,** 124-32.

PAQUIN-PROULX, D., GREENSPUN, B. C., PASQUET, L., STRUNZ, B., ALEMAN, S., FALCONER, K., TERABE, M., BERZOFSKY, J. A., SANDBERG, J. K., MELUM, E., NIXON, D. F. & BJORKSTROM, N. K. 2018. IL13Ralpha2 expression identifies tissue-resident IL-22-producing PLZF(+) innate T cells in the human liver. *Eur J Immunol,* 48**,** 1329-1335.

PARRY, R. V., CHEMNITZ, J. M., FRAUWIRTH, K. A., LANFRANCO, A. R., BRAUNSTEIN, I., KOBAYASHI, S. V., LINSLEY, P. S., THOMPSON, C. B. & RILEY, J. L. 2005. CTLA-4 and PD-1 receptors inhibit T-cell activation by distinct mechanisms. *Mol Cell Biol,* 25**,** 9543-53.

PATEL, A. M., LIU, Y. S., DAVIES, S. P., BROWN, R. M., KELLY, D. A., SCHEEL-TOELLNER, D., REYNOLDS, G. M. & STAMATAKI, Z. 2021. The Role of B Cells in Adult and Paediatric Liver Injury. *Front Immunol,* 12**,** 729143.

PATRICK, A. L., RULLO, J., BEAUDIN, S., LIAW, P. & FOX-ROBICHAUD, A. E. 2007. Hepatic leukocyte recruitment in response to time-limited expression of TNF-alpha and IL-1beta. *Am J Physiol Gastrointest Liver Physiol,* 293**,** G663-72.

PATTEN, D. A. & SHETTY, S. 2018. More Than Just a Removal Service: Scavenger Receptors in Leukocyte Trafficking. *Front Immunol,* 9**,** 2904.

PATTEN, D. A., WILSON, G. K., BAILEY, D., SHAW, R. K., JALKANEN, S., SALMI, M., ROT, A., WESTON, C. J., ADAMS, D. H. & SHETTY, S. 2017. Human liver sinusoidal endothelial cells promote intracellular crawling of lymphocytes during recruitment: A new step in migration. *Hepatology,* 65**,** 294-309.

PAULUSMA, C. C., LAMERS, W. H., BROER, S. & VAN DE GRAAF, S. F. J. 2022. Amino acid metabolism, transport and signalling in the liver revisited. *Biochem Pharmacol,* 201**,** 115074.

PESTANA, R. C., HASSAN, M. M., ABDEL-WAHAB, R., ABUGABAL, Y. I., GIRARD, L. M., LI, D., CHANG, P., RAGHAV, K., MORRIS, J., WOLFF, R. A., RASHID, A., AMIN, H. M. & KASEB, A. 2018. Clinical and prognostic significance of circulating levels of angiopoietin-1 and angiopoietin-2 in hepatocellular carcinoma. *Oncotarget,* 9**,** 37721-37732.

PHILLIPSON, M., HEIT, B., COLARUSSO, P., LIU, L., BALLANTYNE, C. M. & KUBES, P. 2006. Intraluminal crawling of neutrophils to emigration sites: a molecularly distinct process from adhesion in the recruitment cascade. *J Exp Med,* 203**,** 2569-75.

PICCHIO, M., BECK, R., HAUBNER, R., SEIDL, S., MACHULLA, H. J., JOHNSON, T. D., WESTER, H. J., REISCHL, G., SCHWAIGER, M. & PIERT, M. 2008. Intratumoral spatial distribution of hypoxia and angiogenesis assessed by 18F-FAZA and 125I-Gluco-RGD autoradiography. *J Nucl Med,* 49**,** 597-605.

PIETRZYK, Ł. & TORRES, K. 2022. Serum ROBO4 and CLEC14A: preliminary evaluation as diagnostic and progression biomarkers in colorectal cancer patients. *Nowotwory. Journal of Oncology,* 72**,** 1-10.

PILLAY, J., DEN BRABER, I., VRISEKOOP, N., KWAST, L. M., DE BOER, R. J., BORGHANS, J. A., TESSELAAR, K. & KOENDERMAN, L. 2010. In vivo labeling with 2H2O reveals a human neutrophil lifespan of 5.4 days. *Blood,* 116**,** 625-7.

PRICKETT, T. C., MCKENZIE, J. L. & HART, D. N. 1988. Characterization of interstitial dendritic cells in human liver. *Transplantation,* 46**,** 754-61.

RADAEVA, S., SUN, R., JARUGA, B., NGUYEN, V. T., TIAN, Z. & GAO, B. 2006. Natural killer cells ameliorate liver fibrosis by killing activated stellate cells in NKG2D-dependent and tumor necrosis factor-related apoptosis-inducing ligand-dependent manners. *Gastroenterology,* 130**,** 435-52.

RAICA, M. & CIMPEAN, A. M. 2010. Platelet-Derived Growth Factor (PDGF)/PDGF Receptors (PDGFR) Axis as Target for Antitumor and Antiangiogenic Therapy. *Pharmaceuticals (Basel),* 3**,** 572-599.

RAMAKRISHNAN, S., ANAND, V. & ROY, S. 2014. Vascular endothelial growth factor signaling in hypoxia and inflammation. *J Neuroimmune Pharmacol,* 9**,** 142-60.

RAZA, A., FRANKLIN, M. J. & DUDEK, A. Z. 2010. Pericytes and vessel maturation during tumor angiogenesis and metastasis. *Am J Hematol,* 85**,** 593-8.

REIG, M., FORNER, A., RIMOLA, J., FERRER-FABREGA, J., BURREL, M., GARCIA-CRIADO, A., KELLEY, R. K., GALLE, P. R., MAZZAFERRO, V., SALEM, R., SANGRO, B., SINGAL, A. G., VOGEL, A., FUSTER, J., AYUSO, C. & BRUIX, J. 2022. BCLC strategy for prognosis prediction and treatment recommendation: The 2022 update. *J Hepatol,* 76**,** 681-693.

RHO, S. S., CHOI, H. J., MIN, J. K., LEE, H. W., PARK, H., PARK, H., KIM, Y. M. & KWON, Y. G. 2011. Clec14a is specifically expressed in endothelial cells and mediates cell to cell adhesion. *Biochem Biophys Res Commun,* 404**,** 103-8.

ROWELL, D. L., ECKMANN, L., DWINELL, M. B., CARPENTER, S. P., RAUCY, J. L., YANG, S. K. & KAGNOFF, M. F. 1997. Human hepatocytes express an array of proinflammatory cytokines after agonist stimulation or bacterial invasion. *Am J Physiol,* 273**,** G322-32.

RUMGAY, H., ARNOLD, M., FERLAY, J., LESI, O., CABASAG, C. J., VIGNAT, J., LAVERSANNE, M., MCGLYNN, K. A. & SOERJOMATARAM, I. 2022. Global burden of primary liver cancer in 2020 and predictions to 2040. *J Hepatol,* 77**,** 1598-1606.

RYDER, S. D. & BECKINGHAM, I. J. 2001. ABC of diseases of liver, pancreas, and biliary system: Chronic viral hepatitis. *BMJ,* 322**,** 219-21.

SAFADI, R., OHTA, M., ALVAREZ, C. E., FIEL, M. I., BANSAL, M., MEHAL, W. Z. & FRIEDMAN, S. L. 2004. Immune stimulation of hepatic fibrogenesis by CD8 cells and attenuation by transgenic interleukin-10 from hepatocytes. *Gastroenterology,* 127**,** 870-82.

SAIJOU, E., ENOMOTO, Y., MATSUDA, M., YUET-YIN KOK, C., AKIRA, S., TANAKA, M. & MIYAJIMA, A. 2018. Neutrophils alleviate fibrosis in the CCl4-induced mouse chronic liver injury model. *Hepatol Commun,* 2**,** 703-717.

SALCEDO, X., MEDINA, J., SANZ-CAMENO, P., GARCIA-BUEY, L., MARTIN-VILCHEZ, S., BORQUE, M. J., LOPEZ-CABRERA, M. & MORENO-OTERO, R. 2005. The potential of angiogenesis soluble markers in chronic hepatitis C. *Hepatology,* 42**,** 696-701.

SALNIKOVA, O., BREUHAHN, K., HARTMANN, N., SCHMIDT, J. & RYSCHICH, E. 2013. Endothelial plasticity governs the site-specific leukocyte recruitment in hepatocellular cancer. *Int J Cancer,* 133**,** 2372-82.

SANDOVAL, D. R., GOMEZ TOLEDO, A., PAINTER, C. D., TOTA, E. M., SHEIKH, M. O., WEST, A. M. V., FRANK, M. M., WELLS, L., XU, D., BICKNELL, R., CORBETT, K. D. & ESKO, J. D. 2020. Proteomics-based screening of the endothelial heparan sulfate interactome reveals that C-type lectin 14a (CLEC14A) is a heparin-binding protein. *J Biol Chem,* 295**,** 2804-2821.

SAPONARO, C., MALFETTONE, A., RANIERI, G., DANZA, K., SIMONE, G., PARADISO, A. & MANGIA, A. 2013. VEGF, HIF-1alpha expression and MVD as an angiogenic network in familial breast cancer. *PLoS One,* 8**,** e53070.

SCHAEFER, T. J. & JOHN, S. 2022. Acute Hepatitis. *StatPearls.* Treasure Island (FL).

SCHNEEWEISS, B., GRANINGER, W., FERENCI, P., EICHINGER, S., GRIMM, G., SCHNEIDER, B., LAGGNER, A. N., LENZ, K. & KLEINBERGER, G. 1990. Energy metabolism in patients with acute and chronic liver disease. *Hepatology,* 11**,** 387-93.

SEBODE, M., WIGGER, J., FILPE, P., FISCHER, L., WEIDEMANN, S., KRECH, T., WEILER-NORMANN, C., PEISELER, M., HARTL, J., TOLOSA, E., HERKEL, J., SCHRAMM, C., LOHSE, A. W. & ARRENBERG, P. 2019. Inflammatory Phenotype of Intrahepatic Sulfatide-Reactive Type II NKT Cells in Humans With Autoimmune Hepatitis. *Front Immunol,* 10**,** 1065.

SELZNER, N., SELZNER, M., ODERMATT, B., TIAN, Y., VAN ROOIJEN, N. & CLAVIEN, P. A. 2003. ICAM-1 triggers liver regeneration through leukocyte recruitment and Kupffer cell-dependent release of TNF-alpha/IL-6 in mice. *Gastroenterology,* 124**,** 692-700.

SHEIKH, S., RAINGER, G. E., GALE, Z., RAHMAN, M. & NASH, G. B. 2003. Exposure to fluid shear stress modulates the ability of endothelial cells to recruit neutrophils in response to tumor necrosis factor-alpha: a basis for local variations in vascular sensitivity to inflammation. *Blood,* 102**,** 2828-34.

SHERMAN, M. 2010. Hepatocellular carcinoma: epidemiology, surveillance, and diagnosis. *Semin Liver Dis,* 30**,** 3-16.

SHETTY, S., WESTON, C. J., OO, Y. H., WESTERLUND, N., STAMATAKI, Z., YOUSTER, J., HUBSCHER, S. G., SALMI, M., JALKANEN, S., LALOR, P. F. & ADAMS, D. H. 2011. Common lymphatic endothelial and vascular endothelial receptor-1 mediates the transmigration of regulatory T cells across human hepatic sinusoidal endothelium. *J Immunol,* 186**,** 4147-55.

SHUAI, Z., LEUNG, M. W., HE, X., ZHANG, W., YANG, G., LEUNG, P. S. & ERIC GERSHWIN, M. 2016. Adaptive immunity in the liver. *Cell Mol Immunol,* 13**,** 354-68.

SIEVERT, W., TAPIO, S., BREUNINGER, S., GAIPL, U., ANDRATSCHKE, N., TROTT, K. R. & MULTHOFF, G. 2014. Adhesion molecule expression and function of primary endothelial cells in benign and malignant tissues correlates with proliferation. *PLoS One,* 9**,** e91808.

SKANDALAKIS, J. E., SKANDALAKIS, L. J., SKANDALAKIS, P. N. & MIRILAS, P. 2004. Hepatic surgical anatomy. *Surg Clin North Am,* 84**,** 413-35, viii.

SMEDSROD, B., PERTOFT, H., GUSTAFSON, S. & LAURENT, T. C. 1990. Scavenger functions of the liver endothelial cell. *Biochem J,* 266**,** 313-27.

SPITS, H., ARTIS, D., COLONNA, M., DIEFENBACH, A., DI SANTO, J. P., EBERL, G., KOYASU, S., LOCKSLEY, R. M., MCKENZIE, A. N., MEBIUS, R. E., POWRIE, F. & VIVIER, E. 2013. Innate lymphoid cells--a proposal for uniform nomenclature. *Nat Rev Immunol,* 13**,** 145-9.

ST CROIX, B., RAGO, C., VELCULESCU, V., TRAVERSO, G., ROMANS, K. E., MONTGOMERY, E., LAL, A., RIGGINS, G. J., LENGAUER, C., VOGELSTEIN, B. & KINZLER, K. W. 2000. Genes expressed in human tumor endothelium. *Science,* 289**,** 1197-202.

STEEBER, D. A., CAMPBELL, M. A., BASIT, A., LEY, K. & TEDDER, T. F. 1998. Optimal selectin-mediated rolling of leukocytes during inflammation in vivo requires intercellular adhesion molecule-1 expression. *Proc Natl Acad Sci U S A,* 95**,** 7562-7.

STIJLEMANS, B., KORF, H., DE BAETSELIER, P., BRYS, L., VAN GINDERACHTER, J. A., MAGEZ, S. & DE TREZ, C. 2020. Hepatocyte-derived IL-10 plays a crucial role in attenuating pathogenicity during the chronic phase of T. congolense infection. *PLoS Pathog,* 16**,** e1008170.

STRIETER, R. M., BURDICK, M. D., GOMPERTS, B. N., BELPERIO, J. A. & KEANE, M. P. 2005. CXC chemokines in angiogenesis. *Cytokine Growth Factor Rev,* 16**,** 593-609.

SUN, C., XU, J., SONG, J., LIU, C., WANG, J., WENG, C., SUN, H., WEI, H., XIAO, W., SUN, R. & TIAN, Z. 2015. The predictive value of centre tumour CD8(+) T cells in patients with hepatocellular carcinoma: comparison with Immunoscore. *Oncotarget,* 6**,** 35602-15.

SUN, Y., CHEN, W., TORPHY, R. J., YAO, S., ZHU, G., LIN, R., LUGANO, R., MILLER, E. N., FUJIWARA, Y., BIAN, L., ZHENG, L., ANAND, S., GAO, F., ZHANG, W., FERRARA, S. E., GOODSPEED, A. E., DIMBERG, A., WANG, X. J., EDIL, B. H., BARNETT, C. C., SCHULICK, R. D., CHEN, L. & ZHU, Y. 2021. Blockade of the CD93 pathway normalizes tumor vasculature to facilitate drug delivery and immunotherapy. *Sci Transl Med,* 13.

SUND, M., XIE, L. & KALLURI, R. 2004. The contribution of vascular basement membranes and extracellular matrix to the mechanics of tumor angiogenesis. *APMIS,* 112**,** 450-62.

SZABO, G., MANDREKAR, P. & DOLGANIUC, A. 2007. Innate immune response and hepatic inflammation. *Semin Liver Dis,* 27**,** 339-50.

SZAFRANSKA, K., KRUSE, L. D., HOLTE, C. F., MCCOURT, P. & ZAPOTOCZNY, B. 2021. The wHole Story About Fenestrations in LSEC. *Front Physiol,* 12**,** 735573.

TAKEUCHI, A. & SAITO, T. 2017. CD4 CTL, a Cytotoxic Subset of CD4(+) T Cells, Their Differentiation and Function. *Front Immunol,* 8**,** 194.

TANG, L., PENG, H., ZHOU, J., CHEN, Y., WEI, H., SUN, R., YOKOYAMA, W. M. & TIAN, Z. 2016. Differential phenotypic and functional properties of liver-resident NK cells and mucosal ILC1s. *J Autoimmun,* 67**,** 29-35.

TAURA, K., DE MINICIS, S., SEKI, E., HATANO, E., IWAISAKO, K., OSTERREICHER, C. H., KODAMA, Y., MIURA, K., IKAI, I., UEMOTO, S. & BRENNER, D. A. 2008. Hepatic stellate cells secrete angiopoietin 1 that induces angiogenesis in liver fibrosis. *Gastroenterology,* 135**,** 1729-38.

TEN BROEKE, T., WUBBOLTS, R. & STOORVOGEL, W. 2013. MHC class II antigen presentation by dendritic cells regulated through endosomal sorting. *Cold Spring Harb Perspect Biol,* 5**,** a016873.

TIEGS, G. 2007. Cellular and cytokine-mediated mechanisms of inflammation and its modulation in immune-mediated liver injury. *Z Gastroenterol,* 45**,** 63-70.

TREFTS, E., GANNON, M. & WASSERMAN, D. H. 2017. The liver. *Curr Biol,* 27**,** R1147-R1151.

TRINCHET, J. C., CHAFFAUT, C., BOURCIER, V., DEGOS, F., HENRION, J., FONTAINE, H., ROULOT, D., MALLAT, A., HILLAIRE, S., CALES, P., OLLIVIER, I., VINEL, J. P., MATHURIN, P., BRONOWICKI, J. P., VILGRAIN, V., N'KONTCHOU, G., BEAUGRAND, M., CHEVRET, S. & GROUPE D'ETUDE ET DE TRAITEMENT DU CARCINOME, H. 2011. Ultrasonographic surveillance of hepatocellular carcinoma in cirrhosis: a randomized trial comparing 3- and 6-month periodicities. *Hepatology,* 54**,** 1987-97.

TSENG, C. T., MISKOVSKY, E., HOUGHTON, M. & KLIMPEL, G. R. 2001. Characterization of liver T-cell receptor gammadelta T cells obtained from individuals chronically infected with hepatitis C virus (HCV): evidence for these T cells playing a role in the liver pathology associated with HCV infections. *Hepatology,* 33**,** 1312-20.

TZARTZEVA, K., OBI, J., RICH, N. E., PARIKH, N. D., MARRERO, J. A., YOPP, A., WALJEE, A. K. & SINGAL, A. G. 2018. Surveillance Imaging and Alpha Fetoprotein for Early Detection of Hepatocellular Carcinoma in Patients With Cirrhosis: A Meta-analysis. *Gastroenterology,* 154**,** 1706-1718 e1.

VEKEMANS, K. & BRAET, F. 2005. Structural and functional aspects of the liver and liver sinusoidal cells in relation to colon carcinoma metastasis. *World J Gastroenterol,* 11**,** 5095-102.

VISKI, C., KÖNIG, C., KIJEWSKA, M., MOGLER, C., ISACKE, C. M. & AUGUSTIN, H. G. 2016. Endosialin-Expressing Pericytes Promote Metastatic Dissemination. *Cancer Res,* 76**,** 5313-25.

VLODAVSKY, I., ABBOUD-JARROUS, G., ELKIN, M., NAGGI, A., CASU, B., SASISEKHARAN, R. & ILAN, N. 2006. The impact of heparanese and heparin on cancer metastasis and angiogenesis. *Pathophysiol Haemost Thromb,* 35**,** 116-27.

VLODAVSKY, I., ELKIN, M., PAPPO, O., AINGORN, H., ATZMON, R., ISHAI-MICHAELI, R., AVIV, A., PECKER, I. & FRIEDMANN, Y. 2000. Mammalian heparanase as mediator of tumor metastasis and angiogenesis. *Isr Med Assoc J,* 2 Suppl**,** 37-45.

VON MARSCHALL, Z., CRAMER, T., HOCKER, M., FINKENZELLER, G., WIEDENMANN, B. & ROSEWICZ, S. 2001. Dual mechanism of vascular endothelial growth factor upregulation by hypoxia in human hepatocellular carcinoma. *Gut,* 48**,** 87-96.

WADA, Y., NAKASHIMA, O., KUTAMI, R., YAMAMOTO, O. & KOJIRO, M. 1998. Clinicopathological study on hepatocellular carcinoma with lymphocytic infiltration. *Hepatology,* 27**,** 407-14.

WAGNER, R. 1839. *Erlaüterungstafeln zur Physiologie und Entwicklungsgeschichte*.

WAKE, K., DECKER, K., KIRN, A., KNOOK, D. L., MCCUSKEY, R. S., BOUWENS, L. & WISSE, E. 1989. Cell biology and kinetics of Kupffer cells in the liver. *Int Rev Cytol,* 118**,** 173-229.

WALKER, J. A., BARLOW, J. L. & MCKENZIE, A. N. 2013. Innate lymphoid cells--how did we miss them? *Nat Rev Immunol,* 13**,** 75-87.

WANG, C., MA, C., GONG, L., GUO, Y., FU, K., ZHANG, Y., ZHOU, H. & LI, Y. 2021a. Macrophage Polarization and Its Role in Liver Disease. *Front Immunol,* 12**,** 803037.

WANG, J., HAO, F., FEI, X. & CHEN, Y. 2019. SPP1 functions as an enhancer of cell growth in hepatocellular carcinoma targeted by miR-181c. *Am J Transl Res,* 11**,** 6924-6937.

WANG, J., HOSSAIN, M., THANABALASURIAR, A., GUNZER, M., MEININGER, C. & KUBES, P. 2017. Visualizing the function and fate of neutrophils in sterile injury and repair. *Science,* 358**,** 111-116.

WANG, W., GUO, Y., ZHONG, J., WANG, Q., WANG, X., WEI, H., LI, J. & XIU, P. 2021b. The clinical significance of microvascular invasion in the surgical planning and postoperative sequential treatment in hepatocellular carcinoma. *Sci Rep,* 11**,** 2415.

WANG, Y. & ZHANG, C. 2019. The Roles of Liver-Resident Lymphocytes in Liver Diseases. *Front Immunol,* 10**,** 1582.

WEGMANN, F., PETRI, B., KHANDOGA, A. G., MOSER, C., KHANDOGA, A., VOLKERY, S., LI, H., NASDALA, I., BRANDAU, O., FASSLER, R., BUTZ, S., KROMBACH, F. & VESTWEBER, D. 2006. ESAM supports neutrophil extravasation, activation of Rho, and VEGF-induced vascular permeability. *J Exp Med,* 203**,** 1671-7.

WILKINSON, A. L., QURASHI, M. & SHETTY, S. 2020. The Role of Sinusoidal Endothelial Cells in the Axis of Inflammation and Cancer Within the Liver. *Front Physiol,* 11**,** 990.

WISSE, E., LUO, D., VERMIJLEN, D., KANELLOPOULOU, C., DE ZANGER, R. & BRAET, F. 1997. On the function of pit cells, the liver-specific natural killer cells. *Semin Liver Dis,* 17**,** 265-86.

WONG, J., JOHNSTON, B., LEE, S. S., BULLARD, D. C., SMITH, C. W., BEAUDET, A. L. & KUBES, P. 1997. A minimal role for selectins in the recruitment of leukocytes into the inflamed liver microvasculature. *J Clin Invest,* 99**,** 2782-90.

WOO, K. V., QU, X., BABAEV, V. R., LINTON, M. F., GUZMAN, R. J., FAZIO, S. & BALDWIN, H. S. 2011. Tie1 attenuation reduces murine atherosclerosis in a dose-dependent and shear stress-specific manner. *J Clin Invest,* 121**,** 1624-35.

WU, M., MEI, F., LIU, W. & JIANG, J. 2020. Comprehensive characterization of tumor infiltrating natural killer cells and clinical significance in hepatocellular carcinoma based on gene expression profiles. *Biomed Pharmacother,* 121**,** 109637.

WYNN, T. A. 2004. Fibrotic disease and the T(H)1/T(H)2 paradigm. *Nat Rev Immunol,* 4**,** 583-94.

XIAO, N., LI, K., ZHU, X., XU, B., LIU, X., LEI, M. & SUN, H. C. 2022. CD74(+) macrophages are associated with favorable prognosis and immune contexture in hepatocellular carcinoma. *Cancer Immunol Immunother,* 71**,** 57-69.

XIONG, X., LIAO, X., QIU, S., XU, H., ZHANG, S., WANG, S., AI, J. & YANG, L. 2022. CXCL8 in Tumor Biology and Its Implications for Clinical Translation. *Front Mol Biosci,* 9**,** 723846.

XU, F., LIU, C., ZHOU, D. & ZHANG, L. 2016. TGF-beta/SMAD Pathway and Its Regulation in Hepatic Fibrosis. *J Histochem Cytochem,* 64**,** 157-67.

XU, R., HUANG, H., ZHANG, Z. & WANG, F. S. 2014. The role of neutrophils in the development of liver diseases. *Cell Mol Immunol,* 11**,** 224-31.

XU, Z. C., SHEN, H. X., CHEN, C., MA, L., LI, W. Z., WANG, L. & GENG, Z. M. 2018. Neuropilin-1 promotes primary liver cancer progression by potentiating the activity of hepatic stellate cells. *Oncol Lett,* 15**,** 2245-2251.

XUE, D., ZHENG, Y., WEN, J., HAN, J., TUO, H., LIU, Y. & PENG, Y. 2021. Role of chemokines in hepatocellular carcinoma (Review). *Oncol Rep,* 45**,** 809-823.

YAN, L., LI, X. & YUAN, Y. 2022. CLEC14A was up-regulated in hepatocellular carcinoma and may function as a potential diagnostic biomarker. *Clinics (Sao Paulo),* 77**,** 100029.

YANG, W., TAO, Y., WU, Y., ZHAO, X., YE, W., ZHAO, D., FU, L., TIAN, C., YANG, J., HE, F. & TANG, L. 2019. Neutrophils promote the development of reparative macrophages mediated by ROS to orchestrate liver repair. *Nat Commun,* 10**,** 1076.

YAO, W., HE, J. C., YANG, Y., WANG, J. M., QIAN, Y. W., YANG, T. & JI, L. 2017. The Prognostic Value of Tumor-infiltrating Lymphocytes in Hepatocellular Carcinoma: a Systematic Review and Meta-analysis. *Sci Rep,* 7**,** 7525.

YARCHOAN, M., XING, D., LUAN, L., XU, H., SHARMA, R. B., POPOVIC, A., PAWLIK, T. M., KIM, A. K., ZHU, Q., JAFFEE, E. M., TAUBE, J. M. & ANDERS, R. A. 2017. Characterization of the Immune Microenvironment in Hepatocellular Carcinoma. *Clin Cancer Res,* 23**,** 7333-7339.

YOONG, K. F., AFFORD, S. C., JONES, R., AUJLA, P., QIN, S., PRICE, K., HUBSCHER, S. G. & ADAMS, D. H. 1999. Expression and function of CXC and CC chemokines in human malignant liver tumors: a role for human monokine induced by gamma-interferon in lymphocyte recruitment to hepatocellular carcinoma. *Hepatology,* 30**,** 100-11.

YOONG, K. F., MCNAB, G., HUBSCHER, S. G. & ADAMS, D. H. 1998. Vascular adhesion protein-1 and ICAM-1 support the adhesion of tumor-infiltrating lymphocytes to tumor endothelium in human hepatocellular carcinoma. *J Immunol,* 160**,** 3978-88.

YOSHIJI, H., KURIYAMA, S., YOSHII, J., IKENAKA, Y., NOGUCHI, R., HICKLIN, D. J., HUBER, J., NAKATANI, T., TSUJINOUE, H., YANASE, K., IMAZU, H. & FUKUI, H. 2002. Synergistic effect of basic fibroblast growth factor and vascular endothelial growth factor in murine hepatocellular carcinoma. *Hepatology,* 35**,** 834-42.

YOSHIJI, H., KURIYAMA, S., YOSHII, J., IKENAKA, Y., NOGUCHI, R., HICKLIN, D. J., WU, Y., YANASE, K., NAMISAKI, T., YAMAZAKI, M., TSUJINOUE, H., IMAZU, H., MASAKI, T. & FUKUI, H. 2003. Vascular endothelial growth factor and receptor interaction is a prerequisite for murine hepatic fibrogenesis. *Gut,* 52**,** 1347-54.

YUAN, D., HUANG, S., BERGER, E., LIU, L., GROSS, N., HEINZMANN, F., RINGELHAN, M., CONNOR, T. O., STADLER, M., MEISTER, M., WEBER, J., OLLINGER, R., SIMONAVICIUS, N., REISINGER, F., HARTMANN, D., MEYER, R., REICH, M., SEEHAWER, M., LEONE, V., HOCHST, B., WOHLLEBER, D., JORS, S., PRINZ, M., SPALDING, D., PROTZER, U., LUEDDE, T., TERRACCIANO, L., MATTER, M., LONGERICH, T., KNOLLE, P., RIED, T., KEITEL, V., GEISLER, F., UNGER, K., CINNAMON, E., PIKARSKY, E., HUSER, N., DAVIS, R. J., TSCHAHARGANEH, D. F., RAD, R., WEBER, A., ZENDER, L., HALLER, D. & HEIKENWALDER, M. 2017. Kupffer Cell-Derived Tnf Triggers Cholangiocellular Tumorigenesis through JNK due to Chronic Mitochondrial Dysfunction and ROS. *Cancer Cell,* 31**,** 771-789 e6.

YUAN, Y., LIU, J., LIU, Z., HE, Y., ZHANG, Z., JIANG, C. & QIAN, Q. 2010. Chemokine CCL3 facilitates the migration of hepatoma cells by changing the concentration intracellular Ca. *Hepatol Res,* 40**,** 424-31.

YUNUSOVA, N. V., TUGUTOVA, E. A., TAMKOVICH, S. N. & KONDAKOVA, I. V. 2018. [The role of exosomal tetraspanins and proteases in tumor progression]. *Biomed Khim,* 64**,** 123-133.

ZANIVAN, S., MAIONE, F., HEIN, M. Y., HERNANDEZ-FERNAUD, J. R., OSTASIEWICZ, P., GIRAUDO, E. & MANN, M. 2013. SILAC-based proteomics of human primary endothelial cell morphogenesis unveils tumor angiogenic markers. *Mol Cell Proteomics,* 12**,** 3599-611.

ZARBOCK, A., LEY, K., MCEVER, R. P. & HIDALGO, A. 2011. Leukocyte ligands for endothelial selectins: specialized glycoconjugates that mediate rolling and signaling under flow. *Blood,* 118**,** 6743-51.

ZEISSIG, S., PEUKER, K., IYER, S., GENSOLLEN, T., DOUGAN, S. K., OLSZAK, T., KASER, A. & BLUMBERG, R. S. 2017. CD1d-Restricted pathways in hepatocytes control local natural killer T cell homeostasis and hepatic inflammation. *Proc Natl Acad Sci U S A,* 114**,** 10449-10454.

ZELENSKY, A. N. & GREADY, J. E. 2005. The C-type lectin-like domain superfamily. *FEBS J,* 272**,** 6179-217.

ZHANG, D. Y. & FRIEDMAN, S. L. 2012. Fibrosis-dependent mechanisms of hepatocarcinogenesis. *Hepatology,* 56**,** 769-75.

ZHANG, L., ZHANG, L., LI, H., GE, C., ZHAO, F., TIAN, H., CHEN, T., JIANG, G., XIE, H., CUI, Y., YAO, M. & LI, J. 2016. CXCL3 contributes to CD133(+) CSCs maintenance and forms a positive feedback regulation loop with CD133 in HCC via Erk1/2 phosphorylation. *Sci Rep,* 6**,** 27426.

ZHANG, Q. F., YIN, W. W., XIA, Y., YI, Y. Y., HE, Q. F., WANG, X., REN, H. & ZHANG, D. Z. 2017. Liver-infiltrating CD11b(-)CD27(-) NK subsets account for NK-cell dysfunction in patients with hepatocellular carcinoma and are associated with tumor progression. *Cell Mol Immunol,* 14**,** 819-829.

ZHANG, X., FU, X., LI, T. & YAN, H. 2019a. The prognostic value of myeloid derived suppressor cell level in hepatocellular carcinoma: A systematic review and meta-analysis. *PLoS One,* 14**,** e0225327.

ZHANG, Z., MA, L., GOSWAMI, S., MA, J., ZHENG, B., DUAN, M., LIU, L., ZHANG, L., SHI, J., DONG, L., SUN, Y., TIAN, L., GAO, Q. & ZHANG, X. 2019b. Landscape of infiltrating B cells and their clinical significance in human hepatocellular carcinoma. *Oncoimmunology,* 8**,** e1571388.

ZHANG, Z., ZHANG, F., LU, Y. & ZHENG, S. 2015. Update on implications and mechanisms of angiogenesis in liver fibrosis. *Hepatol Res,* 45**,** 162-78.

ZHAO, J., ZHANG, Z., LUAN, Y., ZOU, Z., SUN, Y., LI, Y., JIN, L., ZHOU, C., FU, J., GAO, B., FU, Y. & WANG, F. S. 2014. Pathological functions of interleukin-22 in chronic liver inflammation and fibrosis with hepatitis B virus infection by promoting T helper 17 cell recruitment. *Hepatology,* 59**,** 1331-42.

ZHAO, N., HAO, J., NI, Y., LUO, W., LIANG, R., CAO, G., ZHAO, Y., WANG, P., ZHAO, L., TIAN, Z., FLAVELL, R., HONG, Z., HAN, J., YAO, Z., WU, Z. & YIN, Z. 2011. Vgamma4 gammadelta T cell-derived IL-17A negatively regulates NKT cell function in Con A-induced fulminant hepatitis. *J Immunol,* 187**,** 5007-14.

ZHENG, C., ZHENG, L., YOO, J. K., GUO, H., ZHANG, Y., GUO, X., KANG, B., HU, R., HUANG, J. Y., ZHANG, Q., LIU, Z., DONG, M., HU, X., OUYANG, W., PENG, J. & ZHANG, Z. 2017.

Landscape of Infiltrating T Cells in Liver Cancer Revealed by Single-Cell Sequencing. *Cell,* 169**,** 1342-1356 e16.

ZHOU, S. L., ZHOU, Z. J., HU, Z. Q., HUANG, X. W., WANG, Z., CHEN, E. B., FAN, J., CAO, Y., DAI, Z. & ZHOU, J. 2016. Tumor-Associated Neutrophils Recruit Macrophages and T-Regulatory Cells to Promote Progression of Hepatocellular Carcinoma and Resistance to Sorafenib. *Gastroenterology,* 150**,** 1646-1658 e17.

ZHU, A. X., KANG, Y. K., YEN, C. J., FINN, R. S., GALLE, P. R., LLOVET, J. M., ASSENAT, E., BRANDI, G., PRACHT, M., LIM, H. Y., RAU, K. M., MOTOMURA, K., OHNO, I., MERLE, P., DANIELE, B., SHIN, D. B., GERKEN, G., BORG, C., HIRIART, J. B., OKUSAKA, T., MORIMOTO, M., HSU, Y., ABADA, P. B., KUDO, M. & INVESTIGATORS, R.-S. 2019. Ramucirumab after sorafenib in patients with advanced hepatocellular carcinoma and increased alpha-fetoprotein concentrations (REACH-2): a randomised, double-blind, placebo-controlled, phase 3 trial. *Lancet Oncol,* 20**,** 282-296.

ZHU, X. D., TANG, Z. Y. & SUN, H. C. 2020. Targeting angiogenesis for liver cancer: Past, present, and future. *Genes Dis,* 7**,** 328-335.

ZHUANG, X., CROSS, D., HEATH, V. L. & BICKNELL, R. 2011. Shear stress, tip cells and regulators of endothelial migration. *Biochem Soc Trans,* 39**,** 1571-5.

ZOU, F., WANG, X., HAN, X., ROTHSCHILD, G., ZHENG, S. G., BASU, U. & SUN, J. 2018. Expression and Function of Tetraspanins and Their Interacting Partners in B Cells. *Front Immunol,* 9**,** 1606.

ZOU, Z., LI, B., XU, D., ZHANG, Z., ZHAO, J. M., ZHOU, G., SUN, Y., HUANG, L., FU, J., YANG, Y., JIN, L., ZHANG, W., ZHAO, J., SUN, Y., XIN, S. & WANG, F. S. 2009. Imbalanced intrahepatic cytokine expression of interferon-gamma, tumor necrosis factor-alpha, and interleukin-10 in patients with acute-on-chronic liver failure associated with hepatitis B virus infection. *J Clin Gastroenterol,* 43**,** 182-90.

ZYCINSKA, K., WARDYN, K. A., ZIELONKA, T. M., KRUPA, R. & LUKAS, W. 2009. Clinical implications of serum thrombomodulin in PR3-ANCA-associated vasculitis. *Eur J Med Res,* 14 Suppl 4**,** 268-70.